Université Libre de Bruxelles
Faculté des Sciences

Institut d'Aéronomie
Spatiale de Belgique

Modeling the oxidation of alpha-pinene and the related aerosol formation in laboratory and atmospheric conditions

**Thèse soutenue en vue de l'obtention du grade de
Docteur en Sciences**

Manuel Capouet

Décembre 2005

Au terme de ce travail de thèse, j'aimerais remercier les nombreuses personnes qui ont contribué à son accomplissement. Tout d'abord, mes remerciements vont à Guy Brasseur, directeur de l'Institut Max Planck de Hambourg, et à Jean-François Müller, de l'Institut d'Aéronomie Spatiale de Belgique (IASB) sans qui ce travail n'aurait pu avoir lieu. Alors étudiant-chercheur à l'université de Tokyo, ils me donnèrent la possibilité de revenir en Europe et d'entamer une thèse de doctorat sous leur direction à l'IASB et sous l'égide de l'Université Libre de Bruxelles (ULB). Malgré les nombreuses sollicitations dues à sa renommée internationale, Guy Brasseur s'est toujours montré d'une grande disponibilité. Ses conseils toujours clairs et avisés m'ont beaucoup aidé dans la réalisation de ce travail. Je suis profondément reconnaissant à Jean-François Müller qui a supervisé ma recherche à l'Institut. J'ai pu apprécier sa démarche pragmatique, posée et patiente alliée à un travail soutenu et efficace. Grâce à ses connaissances pointues et à nos discussions régulières, il a guidé la réalisation de cette thèse au fil des années. Je tiens vivement à le remercier pour son soutien et sa persévérance.

La référence "Peeters and co-workers" qui revient régulièrement dans ces pages cache en particulier un duo de choc constitué de Josef Peeters et Luc Vereecken de l'Université de Leuven. La collaboration soutenue avec ces deux experts en calculs théoriques a posé les bases sur lesquelles repose en partie ce travail. J'aimerais aussi mettre en avant les contacts avec Barbara Nozière, de l'Université de Miami. Qu'elle soit remerciée pour les nombreuses données expérimentales qui ont permis en grande partie la validation du modèle développé dans ce travail.

Je suis également reconnaissant à l'ensemble des membres du jury qui ont accepté de rapporter cette thèse malgré les contraintes liées aux agendas : Merci à Maria Kanakidou de l'Université de Crête, grande spécialiste du domaine abordé dans ce travail, à Claudine Buess, ainsi qu'à Jean Vander Auwera et Cécile Moucheron de l'ULB, qui ont également accepté de faire partie de mon comité d'accompagnement et ont montré un vif intérêt durant ces quatre années. Un merci aussi à Jacques Lievin qui m'a donné un cours express sur la chimie théorique avec beaucoup de pédagogie.

Le rôle de mes collègues fut tout aussi important dans l'élaboration de ce travail, puisque leur présence ou leur passage régulier dans le bureau me permirent de ne pas sombrer dans des moments neurasthéniques propres aux périodes difficiles d'une thèse. Je tiens donc à remercier Sabine Wallens, Jenny Stavrakou, Fabien Darrouzet, Karen Jansens, Cindy Senten et bien d'autres pour leur bonne humeur, leur humour et les conversations scientifiques, mais aussi politiques, littéraires et cinématographiques que nous avons eues.

Enfin, il y a les amis qui m'ont toujours soutenu dans ma vie étudiante et professionnelle. Je pense à Stamatis Nicolis et à nos discussions sur ce qui touche à la modélisation (c'est-à-dire à tout) ininterrompues depuis août 1992, à Fabienne

Druant pour son soutien et sa grande écoute depuis tant d'années, ainsi qu'à Yannick Dziechciarek, Catherine Brohée, Fabien Deflorenne, Philippe Verdoolaege et Claude Emmanuelle Robert. Je pense aussi à mes amis plus récents, merci à l'énergique et spontanée Florence Degavre et à Alain Carton. Peut-être est-ce l'occasion de remonter plus loin dans le passé et d'adresser ma gratitude au professeur de chimie de l'Athénée Royal de Nivelles, Myriam Vogels, qui a joué un grand rôle dans le choix de cette voie scientifique. Contre vents et marées, avec un enthousiasme sans égal, elle a réussi, jour après jour, à éveiller et surtout à entretenir une lueur d'intérêt pour les sciences auprès de ses élèves.

Le dernier mot sera pour Marianne, Fabienne, Jean-Christophe, Sylvie, et enfin pour mes parents qui m'ont toujours montré un soutien serein et inconditionnel, et se sont révélés des *consiglieri* hors pairs dans mes moments de doutes. Merci.

Résumé

Modélisation de l'oxydation d'alpha-pinène et de la formation d'aérosols y associée en conditions de laboratoire et atmosphériques

Nous avons développé un modèle décrivant l'oxydation détaillée d'α-pinène par OH et O_3 en phase gazeuse et le partitionnement des produits d'oxydation entre la phase gazeuse et aérosol. Les travaux théoriques menés par le groupe de Peeters sur la cinétique associée aux réactions radicalaires alkoxyles et peroxyles constituent la pierre angulaire du mécanisme en phase gazeuse. Le partitionnement est basé sur la formulation de Pankow et est gouverné largement par la pression de vapeur des produits. Une méthode de prédiction de pression de vapeur destinée à l'ensemble des espèces chimiques générées par l'oxidation d'α-pinene a donc été développée dans ce travail. Un grand nombre d'expériences d'oxydation d'α-pinène ont été simulées afin de valider le modèle d'oxydation et de partitionnement. Le modèle a permis de quantifier la forte dépendance des rendements des produits avec la concentration de NO dans l'oxydation par OH due aux réactions non-traditionnelles identifiées par le groupe de Peeters (décomposition des radicaux α-hydroxy peroxyles et réactions de fermeture de cycle des radicaux peroxyles insaturés). La simulation de la phase aérosol produite par l'oxydation α-pinène montre que l'ozonolyse est la voie privilégiée pour la formation d'aérosols organiques secondaires (AOS). Toutefois, l'oxydation par OH dans des conditions atmosphériques typiques peut former aussi une petite quantité non negligeable d'aérosols composés d'hydroxy hydroperoxydes. Les resultats des simulations indiquent que les acides carboxyliques multifonctionnels produits par l'ozonolyse contribuent grandement à la phase aérosol. Néanmoins, le mécanisme de formation de certains composés importants, comme l'acide pinique et l'acide hydroxy pinonique, nécessite encore des clarifications. Nous avons calculé que la formation d'AOS est renforcée par la dimérisation des acides carboxyliques multifonctionnels. Par conséquent, il est impératif de poursuivre les études théoriques et expérimentales de ces composés de manière à examiner la vitesse de formation ainsi que la pression de vapeur des dimères et des adduits. Les simulations exécutées à l'aide de notre modèle ont mis en relief deux problèmes importants: D'abord, la formation d'AOS mesurée en laboratoire est nettement moins dépendante de la température que prédite par le modèle. D'autre part, le partitionnement des produits carbonyles n'a pu être reproduit comme observé dans les mesures, à cause de leurs hautes pressions de vapeur. L'étude de processus favorisant la production d'AOS, comme l'oligomérisation suggérée par plusieurs groupes, s'avère donc nécessaire. Notre modèle prévoit une production moindre d'aérosols à partir de l'oxydation d'α-pinène que les paramétrisations utilisés dans les modèles globaux récents.

Abstract

Modeling the oxidation of alpha-pinene and the related aerosol formation in laboratory and atmospheric conditions

A model has been developed to describe the detailed gas phase oxidation of α-pinene by OH and O_3 and the partitioning of the oxidation products between the gas and aerosol phases. The theoretical work performed by the group of Peeters on the reaction kinetics of alkoxy and peroxy radical reactions constitutes the cornerstone of the gas phase mechanism. The partitioning follows the Pankow's formulation, and is governed to a large extent by the subcooled vapour pressure of the condensable products. A vapour pressure prediction method has been therefore developed in this work which is applicable to all categories of products generated by the α-pinene oxidation. A large number of α-pinene oxidation experiments have been simulated to validate the gas phase oxidation/partitioning model. The model has been used to quantify the strong dependence of the product yields on the level of NO due to non-traditional reaction sequences in the OH-initiated oxidation of α-pinene identified by Peeters and co-workers (decomposition of α-hydroxy peroxy radicals and ring closure reactions of unsaturated peroxy radicals). Our simulations of the aerosols generated from the oxidation of α-pinene show that ozonolysis is the privileged route for the formation of secondary organic aerosol (SOA). However, in typical atmospheric conditions, the OH-oxidation could provide a small but significant amount of aerosol though the condensation of hydroxy hydroperoxides. Our results show that multifunctional carboxylic acids generated from the ozonolysis contribute largely to the aerosol phase because of their low vapour pressures. Nevertheless, the formation route of important compounds, such as pinic acid and hydroxy pinonic acid, still needs clarification. SOA formation is calculated to be enhanced by the dimerization of these multifunctional acids. Therefore, we stress the need for more experimental and theoretical studies to evaluate the formation rates and the vapour pressure of the dimers and adducts. Our model results raise two important issues: First, the SOA production measured in the laboratory is much less temperature-dependent than predicted by the model. Secondly, the observed partitioning of carbonyl products can not be reproduced by the model because of their high vapour pressures. The investigation of processes favouring SOA production, such as the oligomerization suggested recently by several groups, is therefore necessary. Our oxidation/partitioning mechanism indicates less potential for aerosol formation from α-pinene than the parameterizations which have been adopted in recent global modeling studies.

Contents

List of tables

List of figures

Chapter 1

Introduction

1.1 Context of this study: Global climate change and air quality

As emphasized recently by the latest report of the Intergovernmental Panel on Climate Change, our climate is changing, and human activities appear to be a major driving force for this change (IPCC, 2001). It has been shown that the globally and annually average surface temperature has increased by about 0.6 °C since the 19th century, and model projections indicate that an even stronger positive trend could take place in the future. These temperature variations witness the profound climatic change of the industrial age.

Surface temperature is controlled by the balance between the incoming solar radiation and the outgoing radiation emitted by Earth. An average of 343 W m^{-2} of solar energy radiates the Earth. About 30% of this amount are directly reflected back into space by clouds, by the atmosphere, and by the Earth's surface. The remaining 240 W m^{-2} are absorbed by the Earth/atmosphere system. The fraction absorbed by the Earth's surface is returned to the atmosphere as infrared radiation which, in turn, is partly absorbed by trace gases in the atmosphere, thereby preventing this energy from escaping the system back to space. Without this "greenhouse" effect, the temperature at the Earth's surface would be -20°C. Therefore, despite their relative scarcity in the atmosphere, these "greenhouse" gases play an important role in the regulation of the Earth's energy balance (Seinfeld and Pandis, 1998). Besides water vapour, which is controlled by the hydrological cycle, the main greenhouse gases include methane, nitrous oxide, ozone and carbon dioxide.

Most scientists agree that the rapid increase in surface temperature is for a large part, the result of an enhanced greenhouse effect of anthropogenic origin. Since the industrial revolution, the abundance of greenhouse gases has increased as a consequence of human activities, such as fossil fuel burning and biomass burning (induced mostly by deforestation and agricultural practices). The atmospheric concentration of carbon dioxide, for example, has increased by 30% since the 18th century, whilst

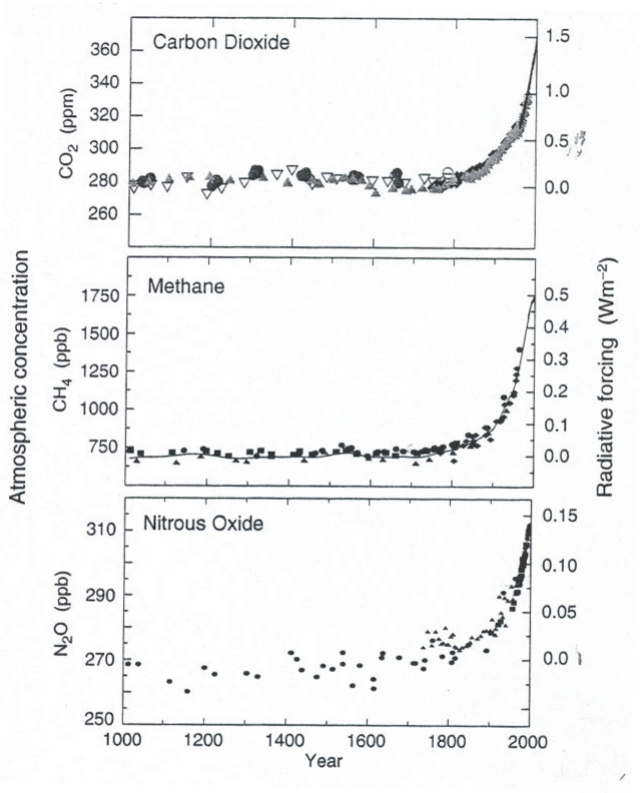

Figure 1.1: Records of change in the atmospheric composition of CO_2, CH_4 and N_2O over the past 1000 years. The estimated radiative forcing of these gases is indicated on the right-hand scale (IPCC, 2001).

the level of methane has more than doubled. The resulting change in the Earth energy budget can be expressed in term of radiative forcing (Fig.1.1). Model projections summarized in the IPCC report predict a temperature increase from 1.4 to 5.8°C by the end of the 21st century. Global warming will be also accompanied by changes in precipitation, sea level, and the frequency and intensity of extreme weather events.

Besides the greenhouses gases, aerosols have been recognized to influence the radiative budget of the Earth/atmosphere (Liao et al., 2004). Aerosols are liquid or solid particles suspended in the air. They are produced by a variety of processes including both natural emissions (vegetation, dust storms, volcanic activities) and anthropogenic emissions (fossil fuel consumption, industry and biomass burning). Primary aerosols are emitted directly, whereas secondary aerosols are generated from the oxidation of precursor gases present in the atmosphere. Aerosols larger than $\mathrm{ca}\ 1\ \mu$m like sea salt particles, pollens, and dust particles are generally of primary origin. Secondary aerosols have both anthropogenic and biogenic origin and they reside mostly in the sub-micron size fraction (Seinfeld and Pandis, 1998). Sulfate and nitrate aerosols constitute important examples of secondary aerosols. The main precursors of sulfate are sulfur dioxide (SO_2) from anthropogenic sources and volcanoes, and dimethyl sulfide ($(CH_3)_2S$) from biogenic sources, especially marine plankton. It

is estimated that a large fraction of nitrate aerosols originates from the use of manure in agriculture (Andreae, 1995). Aerosols can affect the radiative balance in two ways: 1/ the direct effect, whereby aerosols scatter and absorb solar and thermal infrared radiation and, 2/ the indirect effect, whereby aerosols alter warm cloud formation processes by increasing the concentrations of the droplets while decreasing their size. The precipitation efficiency and the albedo of warm clouds are thereby affected, resulting in a negative radiative forcing (i.e. a cooling effect) (Liao et al., 2004).

The main greenhouse gases being well mixed in the atmosphere (particularly the most abundant ones, methane and carbon dioxide), and their absorption properties being well known, their radiative impact can be evaluated to a relatively high degree of confidence. However, the case of the aerosols is more complex. Aerosols undergo chemical and physical processes in the atmosphere and are rapidly removed by precipitation. Their residence time is typically one week. This short atmospheric lifetime, in conjunction with the inhomogeneity of the sources, result in a large spatial and temporal variability of the size, abundance, and composition of the aerosols. The radiative impact depends not only on their spatial distribution, but also on their size, shape, and chemical composition. To date, the quantification of the aerosol sources remains difficult and the fundamental processes governing their physics and chemistry in the atmosphere are poorly understood.

In the last decades, the deterioration of air quality due to the emissions of pollutants by human activities has been identified as another crucial environmental issue. Actually, the concern about air pollution goes back earlier in History than the global warming debate. Records from the seventeenth century indicate smog events in European cities such as London. These air pollution events causing severe health respiratory problems and even excess deaths were caused by the widespread domestic use of high-sulfur coal. In the late 1940's, a new air pollution phenomenon appeared in the Los Angeles area. On hot and bright days, the ambient air of the troposphere (the lowest layer of the atmosphere as described in the next section) was observed to show high concentrations of strongly oxidizing pollutants, in particular ozone (O_3). Studies showed that the L.A. smog was an entirely new form of air pollution due to the oxidation of organics in the atmosphere:

$$\mathrm{Organics} + \mathrm{oxidants} + \mathrm{NO_x} + \mathrm{Sunlight} \rightarrow \mathrm{O_3} + \mathrm{products} \qquad \text{(R1.1)}$$

In presence of sufficiently high levels of sunlight and NO_x (NO_x= NO + NO_2) originating mainly from fossil fuel combustion (e.g. car engines), the oxidation of hydrocarbons produces ozone. Any organic compound emitted from the surface by anthropogenic or biogenic sources, undergoes oxidation processes in the atmosphere. The main oxidants are the hydroxyl radical (OH), the nitrate radical (NO_3) and ozone. They initiate a complex sequence of chemical transformations (represented in a simplified form by the unique reaction R1.1) leading to the formation of stable products, a large fraction of which is ultimately oxidized into carbon dioxide. Until the 1950s, such "polluted" conditions favouring ozone production were restricted to urban areas. Nowadays, high concentrations of ozone are measured in rural regions as well,

due to the transport of pollutants by the wind. In tropical regions, developing countries face also ozone pollution resulting from the oxidation of hydrocarbons originating from biomass burning. Atmospheric pollution has therefore become a phenomenon affecting almost all parts of the world. The World Health Organisation (1994) has reported the damaging effects of the deterioration of air quality on human health (e.g. breathing, cancer). Note that beside being a prominent pollutant, tropospheric ozone presents also an important greenhouse power (Brasseur et al., 1999).

The latest IPCC report has recently summarized our knowledge of the radiative forcing that has occurred since the beginning of the Industrial Era (1750) (Fig. 1.2). The radiative forcing induced by the greenhouse gaseous compounds is now relatively well understood and quantified. The direct radiative forcing has been tentatively estimated for sulfate, biomass-burning, and fossil fuel particles. Carbonaceous particles are usually divided into two fractions, "black carbon" (BC) including elementary carbon species such as soot and charcoal, and "organic aerosols" (OC) representing a mixture of different organic compounds. Black carbon particles show a positive forcing due to their strong absorption capacity. The sign of the radiative forcing due to mineral dust is uncertain. The estimation of the indirect forcing of aerosols (both organic and inorganic) is highly uncertain as well, although it is likely to be a cooling effect of similar magnitude as the direct effect. Note that all the forcing agents reported in Fig. 1.2 have distinct spatial and temporal features, so that the global, annual means appearing in this figure do not represent the complete picture of the radiative perturbation. In particular, the distribution of tropospheric ozone and aerosols is characterized by a high spatial and temporal variability. The uncertainties associated to their impacts, already very large at the global scale, are therefore probably much larger at the regional scale.

Understanding and evaluating the role of aerosols has become a major necessary task in order to predict properly the influence of human activities on the climate and on air quality. Among the different aerosol components, the Secondary Organic Aerosols (SOA), i.e the particles originating from the atmospheric oxidation of organic compounds, are believed to represent a significant fraction in most continental areas. Their production processes are still very poorly understood, however, and they require a better attention.

In the following, our attention will be more focused on the Volatile Organic Compounds (VOC) emitted by the vegetation (the biogenic VOC or BVOC). We will see how the oxidation of BVOC contributes to SOA formation and affects the chemical composition of the atmosphere and in particular the ozone levels. In order to understand these effects, an outline of the structure and composition of the atmosphere will be first given, followed by a description of the main mechanisms of atmospheric chemistry.

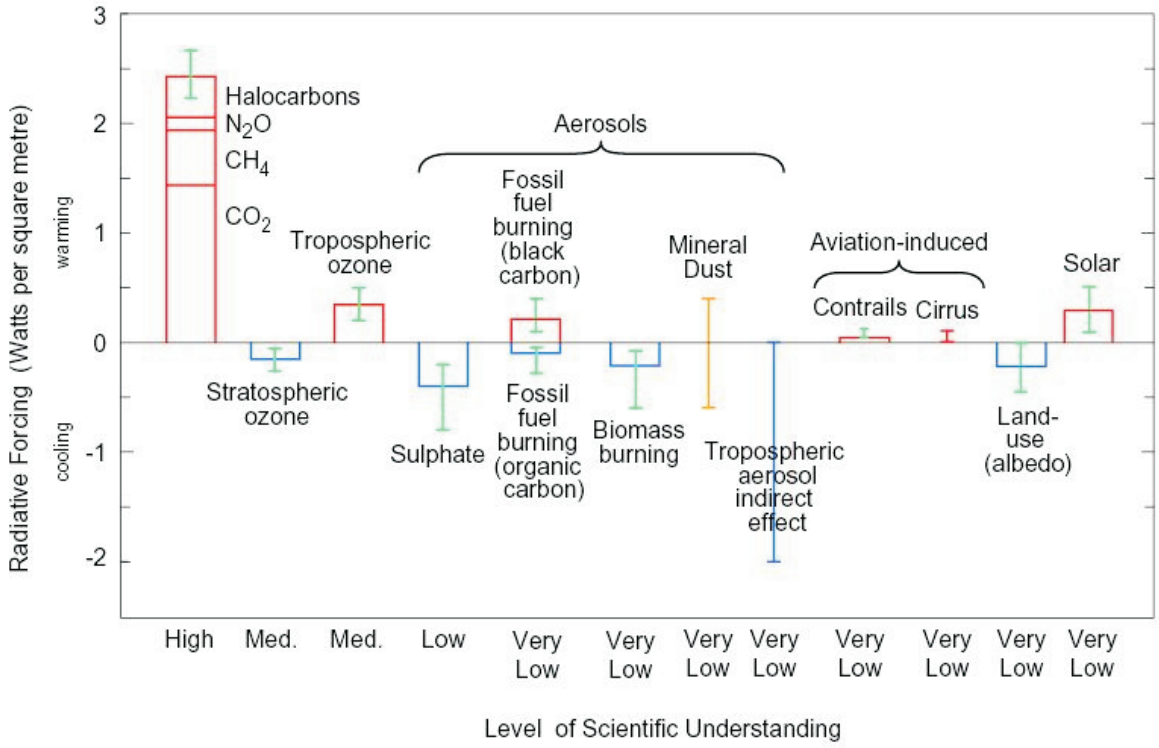

Figure 1.2: IPCC estimates of global annual-mean radiative forcing by a number of agents from the pre-industrial Era (1750) to 2000. Best estimated forcing values and their associated uncertainties are indicated by rectangles and vertical lines respectively (IPCC, 2001).

1.2 Structure and composition of the atmosphere

The Earth's atmosphere is divided into layers according to the variation of temperature (Fig 1.3). The troposphere is the lowest layer of the atmosphere, extending from the Earth's surface up to 10 to 15 km altitude depending on the latitude and time of year. The temperature in the troposphere decreases with increasing distance from the warm Earth's surface which absorbs the largest part of the incoming solar radiation. As a good approximation, atmospheric pressure decreases exponentially with altitude:

$$\frac{p_{(z)}}{p_0} = e^{-z/H}, \tag{1.1}$$

where $H = RT/M_{\text{air}}g$ is called the scale height (varying between 7 and 8.5 km). About 80% of the total mass of the atmosphere is contained in the troposphere. In particular, atmospheric water vapour (including clouds) resides almost exclusively in this region of ceaseless turbulence and mixing (as indicated by the Greek word

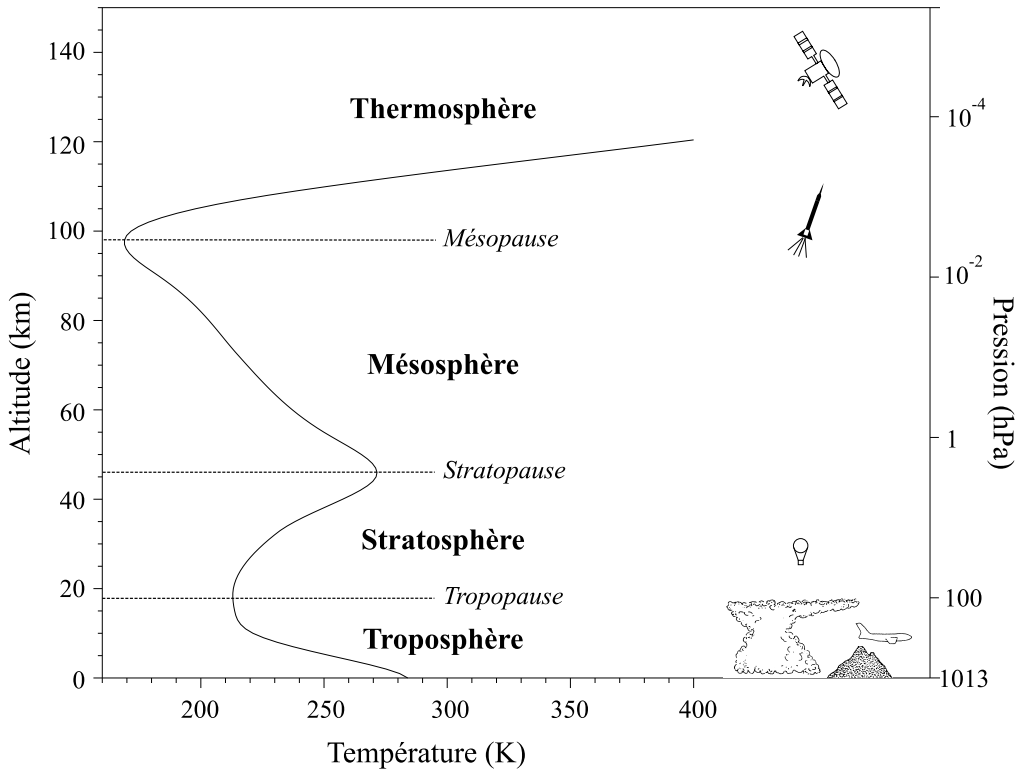

Figure 1.3: Typical temperature profile defined as the "U.S. Standard Atmosphere" (NOAA, 1976)

"tropos"). Above the troposphere lies the stratosphere, extending until 45 km altitude. The change in the sign of the temperature gradient in this region is due to the absorption of solar ultraviolet radiation by ozone. This positive gradient is responsible for the stability of this region, where little vertical mixing occurs. In the mesosphere, the temperature falls again with altitude due to the decrease in O_3 concentration. At about 100 km altitude, the temperature starts to increase again as a result of absorption of short wavelength radiation (<200 nm) by N_2, O_2 and atomic species. This region is known as the thermosphere. The transition zones between the various regions of the atmosphere are known as the tropopause, the stratopause and the mesopause, successively (Finlayson-Pitts and Pitts, 2000; Seinfeld and Pandis, 1998).

The Earth's atmosphere is composed mainly of molecular nitrogen (78.08%), oxygen (20.95%), argon (0.93%) and carbon dioxide (0.03%). Water vapour is present in varying abundances, not exceeding 2-3%. The remaining (0.01%) is a mixture of a multitude of trace gases, as shown in Tab. 1.1. Exchange of air between the troposphere and the stratosphere is much slower than mixing within the troposphere itself. Therefore, only gases possessing a very long lifetime are well mixed throughout the entire atmosphere. This is the case for N_2, O_2, CO_2 and the noble gases. Carbon monoxide (CO) and methane (CH_4) are emitted in large amounts, about 1219 Tg/yr and 469 Tg/yr, respectively (Brasseur et al., 1998). Around 75% of methane emis-

Table 1.1: Chemical composition of the atmosphere (Brasseur et al., 1999)

Constituent	Chemical Formula	Volume Mixing Ratio in Dry Air	Major Sources and Remarks
Nitrogen	N_2	78.084%	Biological
Oxygen	O_2	20.948%	Biological
Argon	Ar	0.934%	Inert
Carbon dioxide	CO_2	350 ppmv	Combustion ocean, biosphere
Neon	Ne	18.18 ppmv	Inert
Helium	He	5.24 ppmv	Inert
Methane	CH_4	1.7 ppmv	Biogenic and anthropogenic
Hydrogen	H_2	0.55 ppmv	Biogenic, anthropogenic, and photochemical
Nitrous oxide	N_2O	0.31 ppmv	Biogenic and anthropogenic
Carbon monoxide	CO	50-200 ppbv	Photochemical and anthropogenic
Ozone (troposphere)	O_3	10-500 ppbv	Photochemical
Ozone (stratosphere)	O_3	0.5-10 ppm	Photochemical
Nonmethane volatile organic compounds		5-20 ppbv	Biogenic and anthropogenic
Halocarbons (as chlorine)		3.8 ppbv	85% anthropogenic
Nitrogen species	$N0_y$	10 ppt-1 ppm	Soils, lightning, anthropogenic
Ammonia	NH_3	10 ppt-1 ppb	Biogenic
Particulate nitrate	NO_3^-	1 ppt-10 ppb	Photochemical, anthropogenic
Particulate ammonium	NH_4^+	10 ppt-10 ppb	Photochemical, anthropogenic
Hydroxyl	OH	0.1 ppt-10 ppt	Photochemical
Hydroperoxyl	HO_2	0.1 ppt-10 ppt	Photochemical
Hydrogen peroxide	H_2O_2	0.1 ppb-l0 ppb	Photochemical
Formaldehyde	CH_2O	0.1-1 ppb	Photochemical
Sulfur dioxide	SO_2	10 ppt-l ppb	Photochemical, volcanic, anthrogenic
Dimethyl sulfide	CH_3SCH_3	10 ppt-100 ppt	Biogenic
Carbon disulfide	CS_2	1 ppt-300 ppt	Biogenic, anthropogenic
Carbonyl sulfide	OCS	500 pptv	Biogenic, volcanic, anthropogenic
Hydrogen sulfide	H_2S	5 ppt-500 ppt	Biogenic, volcanic
Particulate sulfate	SO_4^{-2}	10 ppt-10 ppb	Photochemical, anthropogenic

sions are anthropogenic (particularly in the industrial and agricultural sector). CO direct emissions include biomass burning (50%) and industrial activities (30%). The remainder for these two compounds consist of biogenic emissions. Besides the direct surface emissions, CO is also produced photochemically in the atmosphere, as a by product in the oxidation of methane and the non-methane volatile organic compounds (NMVOC). In general, the NMVOC emitted at the Earth's surface remain confined in the troposphere and are photochemically destroyed in less than a year. The oxidation of methane, which is the dominant hydrocarbon and is quasi uniformly distributed, is ubiquitous in the troposphere. In continental regions, a myriad of nonmethane hydrocarbons of anthropogenic and biogenic origins are oxidized.

The global emissions of anthropogenic NMVOC have been estimated to 103 Tg carbon yr^{-1}. About 60% of these emissions are attributable to fossil fuel use, and

the rest to biomass burning (Brasseur et al., 1999). Guenther et al. (1995) estimated that the emissions of volatile organic compounds released by the vegetation (BVOC) into the atmosphere are on the order of 1150 Tg carbon yr^{-1} worldwide, exceeding by far the anthropogenic emissions. The BVOC include a plethora of compounds of different sizes and structures (Fig. 1.4) (König et al., 1995; Kesselmeier et al., 1997). Isoprene (C_5H_8) accounts for about half of the total biogenic emissions on a mass basis. It is synthesized by less advanced plants (mosses) as well as by trees, in particular by broadleaved trees such as oaks. Monoterpenes ($C_{10}H_{16}$) are another important class of biogenic compounds, and are emitted primarily by conifers. Whereas isoprene emissions by broadleaved trees are sensitive to both leaf temperature and light intensity, with generally little or no emissions at night, the main factor controlling the emissions of monoterpenes by conifers is temperature (Wallens, 2004; Wiedinmyer et al., 2004). Other factors can influence the emissions (leaf age, water or nitrate concentration in the plant, stress conditions) in different proportions in different plants. Beside isoprene and the monoterpenes, other classes of compounds are emitted such as the sesquiterpenes (15-carbon hydrocarbons) and oxygenated hydrocarbons. Their production rates, however, are still poorly characterized. Fig. 1.5 shows the global distribution of monoterpene emissions, as evaluated by Guenther et al. (1995) for the month of July. As expected, the emissions are larger in forested areas. Most of the BVOC are highly reactive in the atmosphere. Their lifetimes under tropospheric conditions are calculated to range from a few minutes to a few hours (Atkinson, 2000).

1.3 Chemistry of the Troposphere

1.3.1 Photochemical cycle of NO_x and HO_x

Key to the chemistry of the troposphere is the "NO_x" family, grouping nitrogen oxide (NO) and nitrogen dioxide (NO_2). Most tropospheric NO_x is emitted as NO, which photochemically equilibrates with NO_2 within a few minutes. The largest emissions of nitric oxide (NO) to the atmosphere results from fossil fuel combustion (14-28 TgN yr^{-1}), biomass burning (4-24 TgN yr^{-1}), and the soils (4-40 TgN yr^{-1}). NO is also formed by lightning (2-20 TgN yr^{-1}) (Brasseur et al., 1999). The nitrogen oxides catalyze tropospheric O_3 formation through a sequence of reactions. At wavelengths < 424 nm, NO_2 photolyzes into NO and atomic oxygen, followed by the rapid formation of an ozone molecule:

$$\mathrm{NO_2} + h\nu \rightarrow \mathrm{NO} + \mathrm{O} \qquad \text{(R1.2)}$$

$$\mathrm{O} + \mathrm{O_2} + \mathrm{M} \rightarrow \mathrm{O_3} + \mathrm{M} \qquad \text{(R1.3)}$$

where M represents N_2, O_2 or another third molecule which can absorb the excess vibrational energy and stabilize the ozone molecule. Once formed, ozone can react with NO to regenerate NO_2,

$$\mathrm{O_3} + \mathrm{NO} \rightarrow \mathrm{NO_2} + \mathrm{O_2}. \qquad \text{(R1.4)}$$

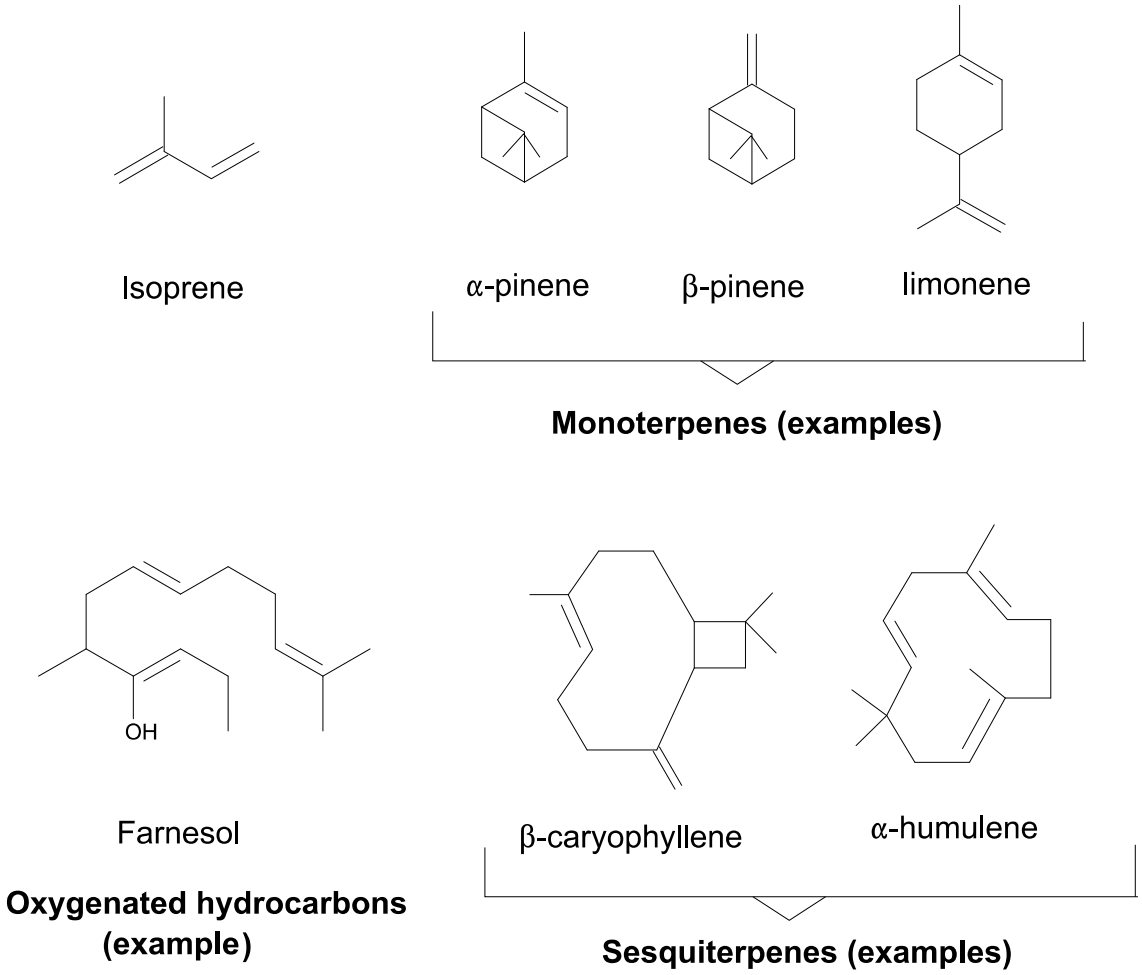

Figure 1.4: Chemical structure and usual name of a variety of biogenic volatile organic compounds (BVOC).

or can photolyze to produce either a ground-state (O) or an excited singlet ($O(^1D)$) oxygen atom:

$$O_3 + h\nu \rightarrow O + O_2 \quad \text{(R1.5)}$$

$$\rightarrow O(^1D) + O_2 \quad \text{(R1.6)}$$

The ground-state O atom combines rapidly with O_2 by reaction R1.3 to reform O_3. In general, $O(^1D)$ loses its excess energy by collision with a third molecule and is quenched back to its ground state. Occasionally, however, $O(^1D)$ collides with H_2O and produces two hydroxyl radicals :

$$O(^1D) + H_2O \rightarrow 2OH. \quad \text{(R1.7)}$$

The major ozone sink represented by reaction R1.6 followed by R1.7 is also the main source of odd hydrogen radicals (HO_x=OH+HO_2) in the atmosphere. Since the production of OH is function of the actinic flux and the water concentration, its concentration shows a diurnal and a seasonal cycle, as well as a dependence to location

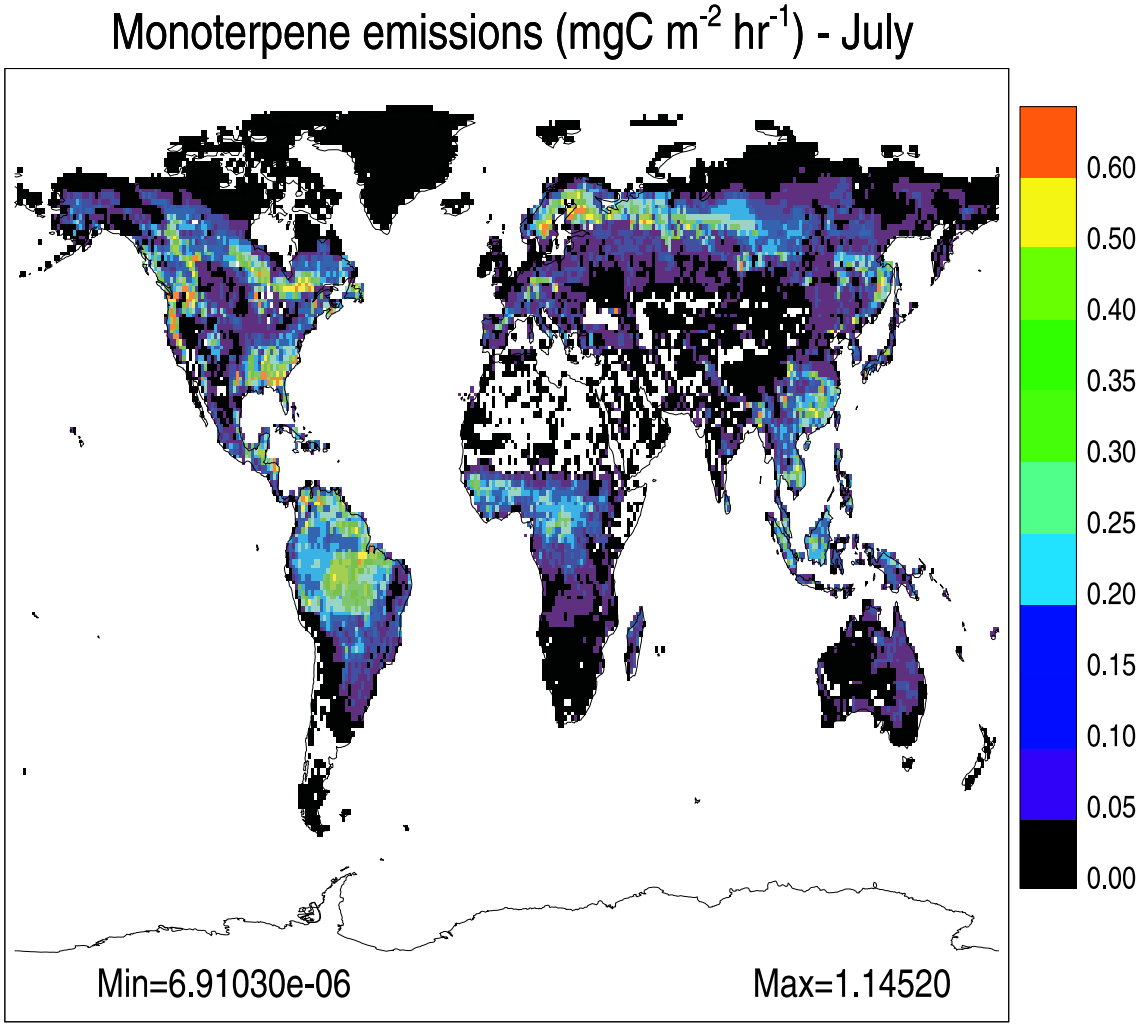

Figure 1.5: Global emission of monoterpenes averaged for the month of July as evaluated by Guenther et al. (1995).

and altitude. Averaged daytime OH levels in the troposphere range from 1-5$\times 10^6$ (winter) to 5-10$\times 10^6$ molecules cm^3 (summer). During the night, it falls below 5$\times 10^5$ molecules cm^{-3} (Seinfeld and Pandis, 1998). OH radical plays a key role in the troposphere due to its high reactivity. Of particular importance is its reaction with carbon monoxide (CO):

$$\mathrm{CO} + \mathrm{OH} + \mathrm{O_2} \rightarrow \mathrm{CO_2} + \mathrm{HO_2}. \qquad \text{(R1.8)}$$

The hydroperoxyl radical HO_2 reacts with NO to generate NO_2, or with O_3 to regenerate the hydroxyl radical:

$$\mathrm{HO_2} + \mathrm{NO} \rightarrow \mathrm{NO_2} + \mathrm{OH} \qquad \text{(R1.9)}$$

$$\mathrm{HO_2} + \mathrm{O_3} \rightarrow \mathrm{OH} + 2\mathrm{O_2} \qquad \text{(R1.10)}$$

When the concentration of NO is high, ozone is formed as a result of reactions R1.8, R1.9, R1.2 and R1.3. This can be represented schematically as:

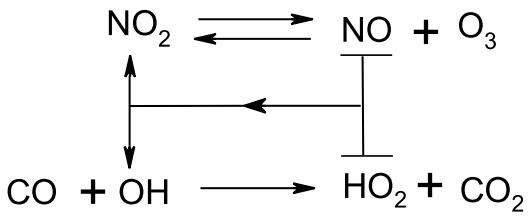

The NO/NO_2 ratio as well as the production of ozone are mainly determined by two interwoven cycles defined by the NO/NO_2 partitioning reactions (R1.2, R1.3 and R1.4) and the HO_x reactions (R1.8, R1.9, R1.10). The effect of the HO_x cycle in presence of NO_x is to convert NO to NO_2 without destroying ozone and therefore to increase the ozone concentration. The production of ozone is therefore dependent on the concentrations of CO and NO_x, and on the presence of sunlight. Besides R1.8, other reactions involving organic compounds can generate peroxy radicals which contribute to ozone formation as described in the following subsections.

1.3.2 Oxidation mechanism of methane

The most abundant hydrocarbon in the atmosphere is methane (CH_4). The hydroxyl radical reacts with CH_4 producing the methyl radical CH_3, which reacts instantaneously with oxygen to yield the methyl peroxy radical, CH_3O_2:

$$\mathrm{CH_4 + OH \rightarrow CH_3 + H_2O} \quad \text{(R1.11)}$$

$$\mathrm{CH_3 + O_2 + M \rightarrow CH_3O_2 + M.} \quad \text{(R1.12)}$$

In the troposphere, the methyl peroxy radical reacts chiefly with NO and HO_2, leading to the formation of the methoxy radical (CH_3O) and methyl hydroperoxide (CH_3OOH), a stable product. The reaction with NO_2 gives an unstable product ($CH_3O_2NO_2$) which decomposes back to the reactants at ambient temperature. CH_3O_2 can also react with other peroxy radicals (RO_2), generated from the degradation of more complex organic compounds, or with other methyl peroxy radicals:

$$\mathrm{CH_3O_2 + NO \rightarrow CH_3O + NO_2} \quad \text{(R1.13)}$$

$$\mathrm{CH_3O_2 + NO_2 \rightleftharpoons CH_3O_2NO_2} \quad \text{(R1.14)}$$

$$\mathrm{CH_3O_2 + HO_2 \rightarrow CH_3OOH + O_2} \quad \text{(R1.15)}$$

$$\mathrm{CH_3O_2 + CH_3O_2 \rightarrow \alpha CH_3O + (1{-}\alpha)products} \quad \text{(R1.16)}$$

$$\mathrm{CH_3O_2 + RO_2 \rightarrow \alpha CH_3O + (1{-}\alpha)products} \quad \text{(R1.17)}$$

Finally, the methoxy radical reacts rapidly with oxygen to form formaldehyde, as a final primary product:

$$\mathrm{CH_3O + O_2 \rightarrow CH_2O + HO_2.} \quad \text{(R1.18)}$$

When the levels of NO_x are sufficiently high, the methane oxidation chain is:

$$
\begin{array}{ll}
k_{R1.11} & \mathrm{CH_4 + OH \rightarrow CH_3O_2 + H_2O} \\
k_{R1.13} & \mathrm{CH_3O_2 + NO \rightarrow CH_3O + NO_2} \\
k_{R1.18} & \mathrm{CH_3O + O_2 \rightarrow CH_2O + HO_2} \\
k_{R1.9} & \mathrm{HO_2 + NO \rightarrow NO_2 + OH} \\
k_{R1.2} & \mathrm{2(NO_2 + h\nu \rightarrow NO + O)} \\
k_{R1.3} & \mathrm{2(O + O_2 + M \rightarrow O_3 + M)} \\
\hline
\text{Net:} & \mathrm{CH_4 + 4O_2 + 2h\nu \rightarrow CH_2O + 2O_3 + H_2O}
\end{array}
$$

In the so-called "high NO_x" regime, CH_3O_2 and HO_2 react dominantly with NO which is converted into NO_2, leading to a production of O_3. In consequence, the oxidation of one molecule of methane down to the first primary product, formaldehyde, yields two molecules of ozone. CH_2O is degraded in the atmosphere by photodissociation and by oxidation by OH (Saunders et al., 2003):

$$\mathrm{CH_2O + OH + O_2 \rightarrow CO + HO_2 + H_2O} \quad \text{(R1.19)}$$

$$\mathrm{CH_2O + h\nu + 2O_2 \rightarrow CO + 2HO_2} \quad \text{(R1.20)}$$

$$\mathrm{CH_2O + h\nu \rightarrow CO + H_2} \quad \text{(R1.21)}$$

Formaldehyde is shown to have an important potential for ozone formation through its production of HO_2 and CO.

When the level of NO is low, the reactions R1.15 to R1.17 become competitive, in particular the reaction with HO_2. Their impact is the removal of CH_3O_2 from the system and a retardation of the rate of ozone production. Furthermore, if the level of NO decreases below a critical threshold, the reaction R1.10 becomes dominant and destroys O_3. However $k_{R1.9}$ being much higher than $k_{R1.10}$, NO levels as low as 10 ppt are sufficient to promote a net production of ozone. NO mixing ratios in the planetary boundary layer over the remote Pacific Ocean are generally lower than 10 ppt, i.e. well below the crossover point. Logan et al. (1981) reported that concentrations of NO exceeding 30 ppt are necessary so that the reaction of the CH_3O_2 radical with NO dominates over that with HO_2. In industrialized countries, the production of ozone is favoured with daytime NO higher than 100 ppt.

At night, the photolytic processes cease and the NO concentration drops near zero. The reaction between O_3 and NO_2 becomes efficient and produces the nitrate radical:

$$\mathrm{NO_2 + O_3 \rightarrow NO_3 + O_2.} \quad \text{(R1.22)}$$

Because of its oxidizing capacity and its relative high nighttime concentrations, the nitrate radical plays an important role in the nighttime oxidation of many VOC (Bey et al., 2001).

1.3.3 Oxidation mechanism of non-methane organic compounds

The oxidation of a NMVOC compound by OH is similar to the oxidation of methane. The attack proceeds via H-atom abstraction from C-H bonds of the organic molecule RH:

$$\mathrm{RH} + \mathrm{OH} \rightarrow \mathrm{R} + \mathrm{H_2O}. \tag{R1.23}$$

In the case of alkenes (as monoterpenes), the initial oxidation step can also occur on the double bond of the molecule. The OH radical adds to the double bond:

$$\mathrm{RC{=}CR'} + \mathrm{OH} \rightarrow \mathrm{RC(OH){-}CR'}. \tag{R1.24}$$

The presence of the double bond renders alkenes reactive also to ozone. The reaction proceeds via initial O_3 addition to the double bond, forming an ozonide which rapidly decomposes:

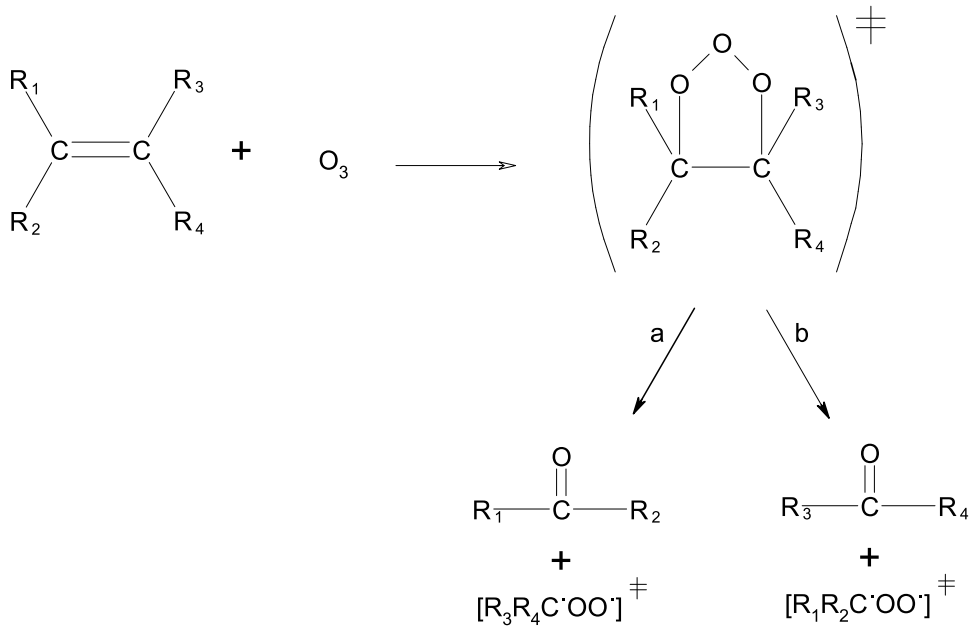

(R1.25)

Different channels are possible for the energy-rich Criegee biradicals $[R_3R_4\dot{C}O\dot{O}]^{\ddagger}$ and $[R_1R_2\dot{C}O\dot{O}]^{\ddagger}$ depending on their structure. In general, the Criegee biradicals can collisionally stabilize or undergo unimolecular decomposition which subsequently produces stable species and alkyl radicals.

The alkyl radical produced in these reactions, R (or RC(OH)-CR'), reacts rapidly with oxygen to form the peroxy radical RO_2 (or RC(OH)-CO_2R'). The subsequent general mechanism is shown in Fig. 1.6. The peroxy radical RO_2 reacts with NO, NO_2,

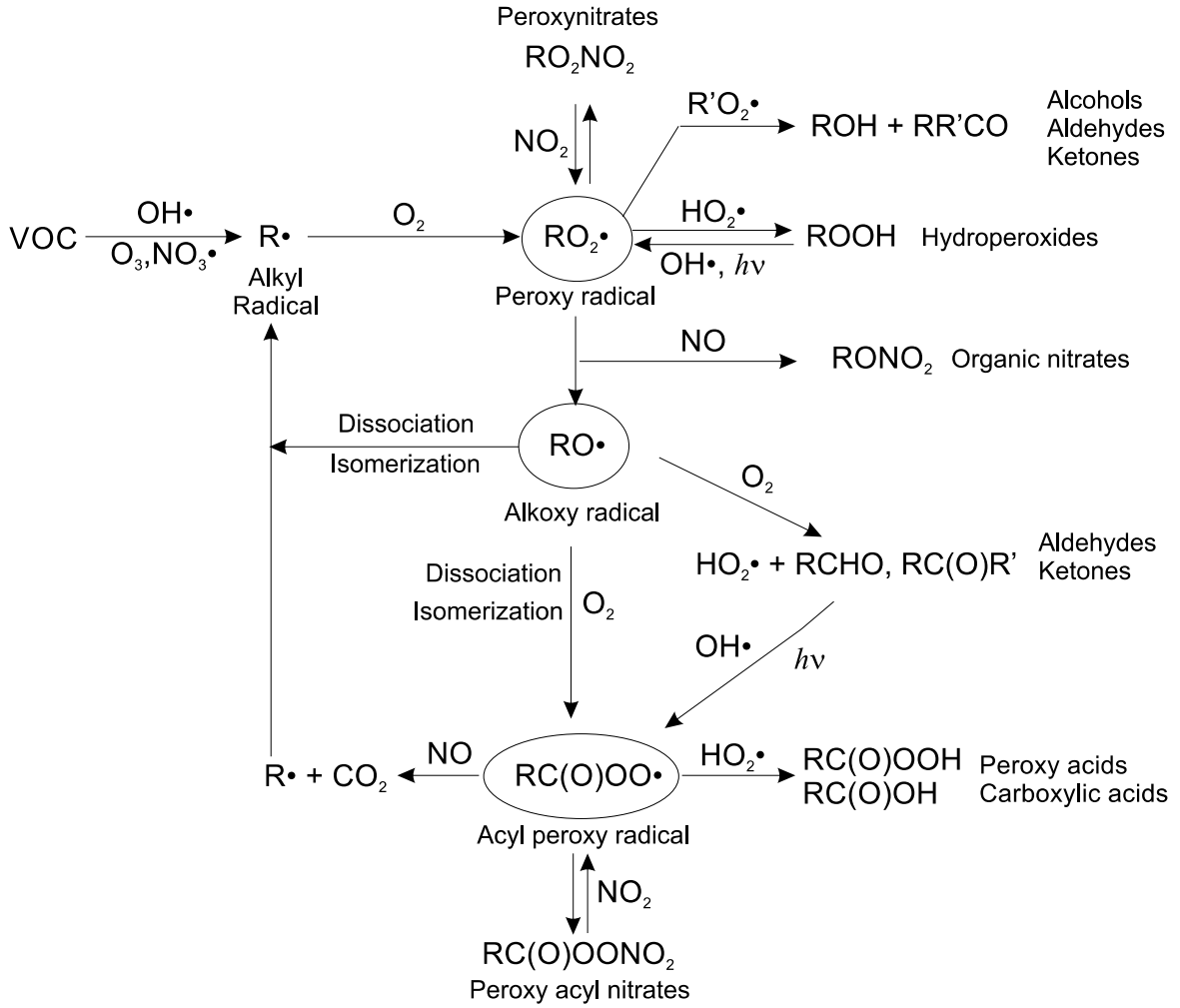

Figure 1.6: General scheme of the photooxidation of an organic molecule

HO_2, and other peroxy radicals similarly to Eqs. R1.13-R1.17. However, depending on the structure of RO_2, the rates and the distribution of the products differ. For example, reaction of higher (>C_2) peroxy radicals with NO have been observed to produce organic nitrates ($RONO_2$). The alkoxy radicals (RO) may undergo a variety of competitive processes under tropospheric conditions: e.g. unimolecular dissociation, unimolecular isomerization, reaction with O_2. The number of possible isomerization/dissociation processes increases with the carbon number and the complexity of the radical. These reactions produce either a stable carbonyl compounds and a hydroperoxyl radical or an alkyl radical R, which reacts with O_2 producing a $R'O_2$ that undergoes a new oxidation step. The radical chain of oxidation propagates until the formation of nonradical products. Reaction with HO_2 terminates the reaction chain by the production of a hydroperoxide (ROOH). The permutation reactions, i.e. the reactions between peroxy radicals RO_2, produce alkoxy radicals as well as alcohol (ROH) and carbonyl compounds (RCHO, RR'CO). These reaction chains lead ultimately to the production of CO_2. As an example, Fig. 1.7 illustrates the photoox-

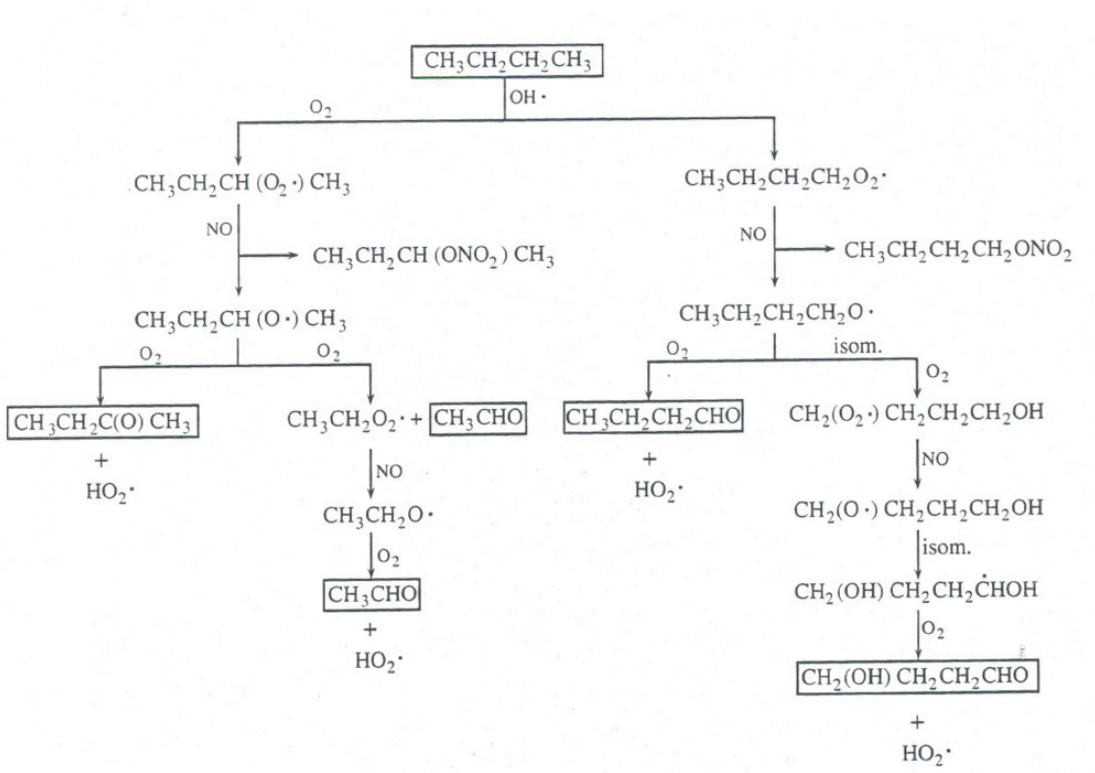

Figure 1.7: Atmospheric photooxidation mechanism of *n*-butane in high NO_x conditions (Seinfeld and Pandis, 1998)

idation mechanism of butane down to the primary products in high NO_x conditions (Reaction RO_2+NO is dominant).

When not removed from the atmosphere by dry or wet deposition, stable products are further oxidized. Moreover, their oxygenated functionalities make them potentially photodissociable. The OH-attack of an aldehyde occurs preferably by abstraction of the hydrogen atom of the aldehydic functionality:

$$\mathrm{RCHO} + \mathrm{OH} \rightarrow \mathrm{RCO} + \mathrm{H_2O} \qquad \text{(R1.26)}$$

$$\mathrm{RCO} + \mathrm{O_2} \rightarrow \mathrm{RC(O)O_2} \qquad \text{(R1.27)}$$

An acyl peroxy radical, of general structure $RC(O)O_2$, is formed after reaction with oxygen. Its reaction with HO_2 produces organic acids (RC(O)OH and RC(O)OOH). In certain cases, as we will see in the α-pinene oxidation mechanism, acyl peroxy radicals are also formed by isomerization (e.g. ring opening, intramolecular shifts of hydrogen atoms) of alkoxy radicals (RO) and reaction with O_2.

As for CO and CH_4, the oxidation of organic compounds yields HO_2 and RO_2 radicals which increase the production of ozone when the NO_x levels are sufficiently high. When the carbon number is large, VOC can undergo several radical reaction cycles before their transformation into stable products. The potential for ozone formation of

a VOC depends on its oxidation mechanism. In general, alkenes yield more ozone than alkanes (Carter, 1990). The oxidation of BVOC generates products of different structures which can interact to some extent with the aerosol phase. The length and the complexity of a degradation mechanism is related to the structure of the VOC compound. Whereas only tens of reactions are required to describe the oxidation of simple alkanes as methane or butane, hundreds of reactions are necessary for the oxidation of isoprene (see molecular structure in Fig. 1.4) (Paulson and Seinfeld, 1992) and thousands of reactions might be required for a monoterpene.

1.4 Modeling the impact of BVOC on tropospheric ozone

The troposphere can be viewed as a chemical reactor cleaning continuously the air polluted by the emissions of the surface. This ability of this atmospheric layer is referred as the oxidizing capacity of the atmosphere. Ozone, being the main precursor of the hydroxyl radical (through R1.6 and R1.7), plays a key role in this respect. Ozone abundance in the troposphere typically varies from less than 10 ppb to over 100 ppb in very polluted metropolitan areas. The source and sink of ozone in the troposphere are difficult to quantify because they require a good knowledge of the emission sources of the ozone precursors, of the photooxidation mechanism of the NMVOC in the atmosphere, and of the dynamic processes. There exists different types of three-dimensional models simulating the formation, transport and sinks of ozone. Global models simulate the zone concentration on Earth scale (Brasseur et al., 1999). Regional and urban models are dedicated to smaller regions and are characterized by a much finer resolution, which makes them more capable to simulate episodic ozone events in great detail (Schmidt et al., 2001). A typical global distribution of ozone simulated by the model IMAGES (Müller and Stavrakou, 2005) at the surface in July is shown in Fig. 1.8. Important photochemical sources of ozone are the oxidation of carbon monoxide (CO) and methane (CH_4) in the presence of nitrogen oxides. Being more reactive in the atmosphere, the effects of the NMVOC on ozone levels are more localized and intense near their emission zones. Wang et al. (1998) and Wang and Shallcross (2000) pointed out substantial effects of the oxidation of anthropogenic and biogenic NMVOC on the concentration of ozone and on the oxidizing capacity of the atmosphere in general. An increase in BVOC emissions is expected in response to the global warming, with potentially significant impacts on ozone. Sanderson et al. (2003) calculated that the increase of isoprene emissions could result in an increase of 5 to 30 ppb of ozone in some continental locations. Since isoprene is estimated to account for about half of the total BVOC emissions, we can expect the effect resulting from the increase in the emissions of other BVOC, among which the monoterpenes, to be of similar amplitude.

The oxidation of simple VOC, e.g. ethane, propane and propene is relatively well represented in models (Brasseur et al., 1998). Experimental studies on the yields of

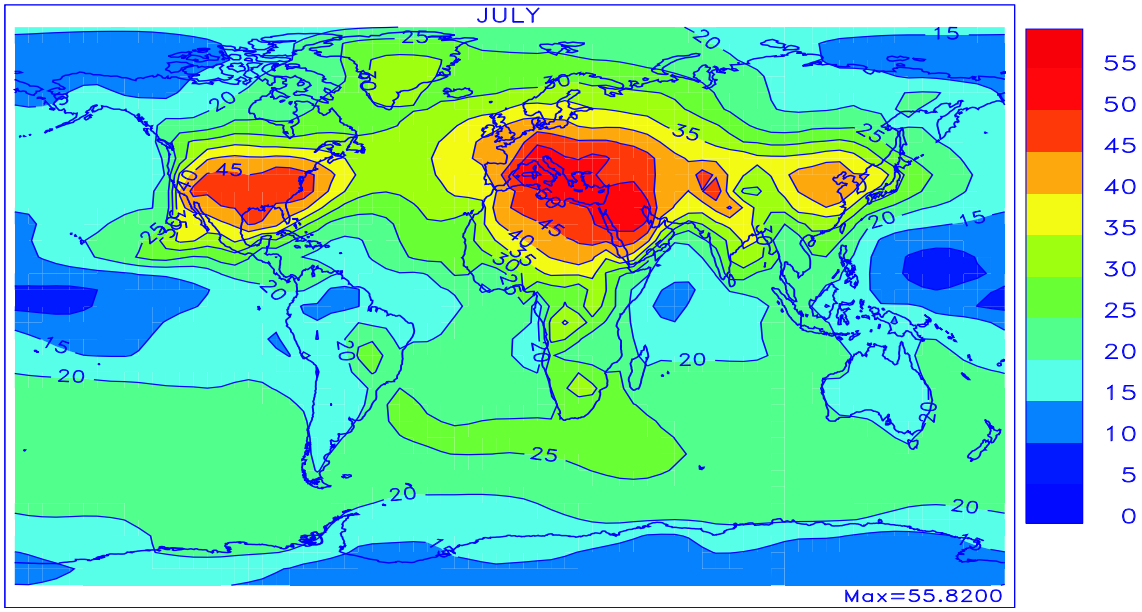

Figure 1.8: Typical surface ozone mixing ratio (ppb) simulated by the global model IMAGES for the month of July (Müller and Stavrakou, 2005)

products and reaction rates provide the basis for developing the oxidation mechanism of these simple hydrocarbons. Over the past two decades, the availability of kinetic and mechanistic data has allowed the development of protocols for VOC degradation. The most known detailed "master" mechanism developed on the basis of these protocols are the NCAR (Madronich and Calvert, 1989) and the MCM (Saunders et al., 2003) mechanisms. They include several thousands of reactions describing the detailed degradation of over 100 VOC that may be relevant in the troposphere. However, the elucidation of the oxidation mechanisms for higher VOC (including most biogenic VOC) is a more difficult task. The number of reactions involved in the oxidation of a biogenic molecule like a monoterpene compound is so large that the information provided from laboratory studies is far from being sufficient to constrain every step in the mechanisms. In order to compensate for the limited contribution of laboratory data, several theoretical tools have been developed to construct the chemical mechanisms of larger VOC. These tools are based on empirical data deduced from the known chemistry of simple compounds and allow predictions of the rate and product distribution of the reactions involving larger VOC. These tools are usually grouped under the generic term "Structure Activity Relationships"(SAR). Several groups (Kwok et al., 1995; Jenkin et al., 1997; Atkinson, 2000; Arey et al., 2001) have developed numerous SAR for application to the mechanistic studies of the gas phase chemistry. However, these methods are inadequate to describe a number of complex reactions appearing in the degradation mechanism of higher carbon number compounds. Since several years, the group of J. Peeters from Leuven University has acquired a world reputation in the development of quantum chemical methods (ab initio/density functional theory) in combination with statistical kinetic theories (TST and RRKM). These

approaches allow a deep understanding of the elementary reaction mechanisms even in absence of direct empirical input. The theoretical calculations require the resolution of the Schrodinger equation which allows to identify and quantify each possible chemical route a reacting system may follow. Uncertainty estimates are provided for the predicted reaction rates and product yields. However, a major drawback of these theoretical analyses is their complexity and their high computational cost. The theoretical approach developed by Peeters and co-workers has already proved to be an essential and complementary tool to the existing laboratory data and SAR methods in the elaboration of gas phase chemical mechanisms.

Due to their large size, explicit mechanisms cannot be implemented as such in global models for computer cost reasons. A reduction of the mechanism to a manageable size is therefore necessary but can lead to oversimplifications and large errors (Kanakidou et al., 2005). For example, although the detailed mechanism of isoprene is largely elucidated (Paulson and Seinfeld, 1992), no standard reduced scheme exists for this compound, with the consequence that different chemical treatments are being used in global models. Recently, a sensitivity study performed by von Kuhlmann et al. (2004) using different reduced schemes of isoprene in global models indicated that the model results can only be seen as first order estimates of its impact in the atmosphere. Monoterpenes are assumed to have the same oxidation products as isoprene in some global models (Brasseur et al., 1998). Other reduced schemes are based on unvalidated detailed mechanisms (Griffin et al., 2002).

1.5 Impact of BVOC on secondary organic aerosols

The observation of a blue haze above forests led Went (1960) to suggest the role of biogenic hydrocarbons as precursors of tropospheric organic aerosols. This hypothesis has been confirmed later by laboratory studies on the photooxidation of BVOC by several groups (Hatakeyama et al., 1989, 1991; Pandis et al., 1991, 1992). They showed that the oxidation of high molecular weight hydrocarbons produces low volatility products which can partition between the gas and the particulate phase. These condensed organic products are referred to as Secondary Organic Aerosols (SOA). Laboratory experiments have indicated that aromatic compounds, representing a small proportion of anthropogenic VOC, are the only anthropogenic sources of SOA (Odum et al., 1997; Stroud et al., 2004). Among the BVOC, the oxidation of isoprene has been observed to yield a negligible production of organic aerosols in laboratory experiments (Pandis et al., 1991) whereas the oxidation of larger compounds generates high SOA yields. In particular, the oxidation of monoterpenes by ozone appears to provide the most efficient routes to the formation of condensable products (Hoffmann et al., 1997). The SOA formation in the troposphere can be summarized as illustrated in Fig. 1.9: Biogenic compounds are emitted from the surface and oxidized. Some of the products, in particular those resulting from the ozonolysis condense completely or partially on a condensed phase which can be made also of

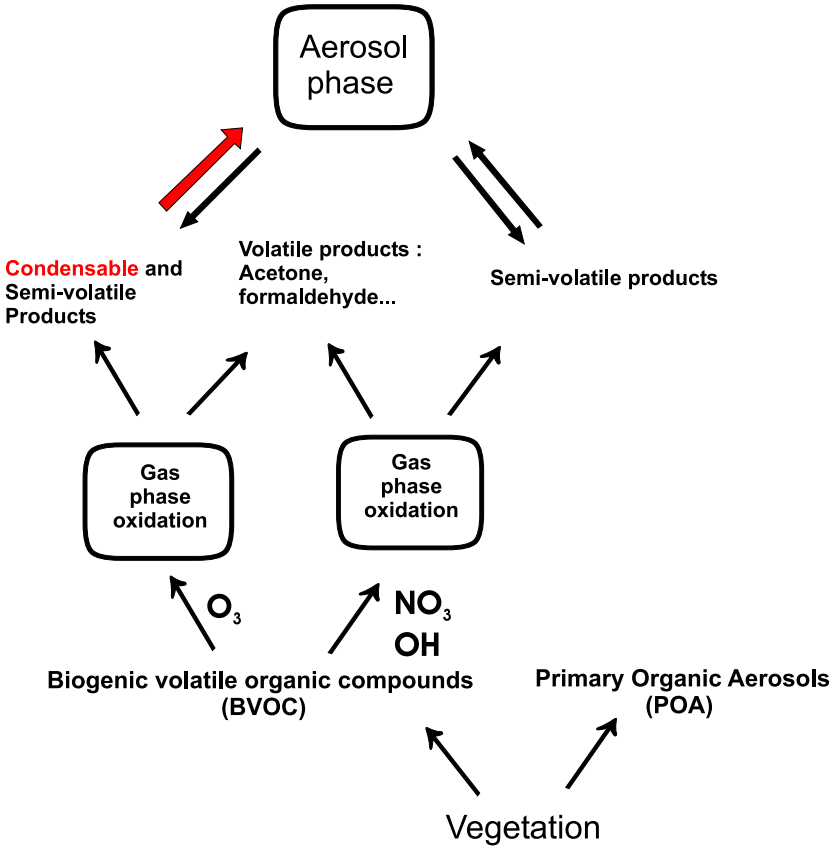

Figure 1.9: Schematic representation of SOA formation from the biogenic volatile organic compounds. The ozonolysis is believed to be responsible for the main production of condensable compounds found in SOA.

Primary Organic Aerosols (POA). The partitioning equilibrium is governed by chemical and physical conditions of the atmosphere. Uptake of water and heterogeneous reactions are believed to occur in the organic aerosol, which alter its chemical composition, but these processes are not well identified so far (Raes et al., 2000).

The experimental SOA yields have been introduced in global transport models using simplified oxidation mechanisms for biogenic compounds. The model assumptions remained crude in these studies: the aerosol yields were assumed to be constant, independent on the chemical conditions. On this quite uncertain basis, the first estimations of the global SOA production have been obtained by several groups among which Liousse et al. (1996), Griffin et al. (1999b) and Kanakidou et al. (2000). Their estimations are summarized in Tab. 1.2. For comparison, estimations for the global sources of POA and anthropogenic SOA are also given (IPCC, 2001). POA emissions are categorized into fossil fuel burning (transportation, energy production and consumption), biomass burning (agricultural waste, savanna and deforestation fires), and biogenic (vegetation fragments, pollens). These primary sources contribute more to the aerosol mass than the production of SOA dominated by the bio-

Table 1.2: Estimates for the global sources (Tg/year) of POA and anthropogenic SOA as reported by IPCC (2001), and comparison with biogenic SOA estimates.

	Northern Hemisphere	**Southern Hemisphere**	**Global**	**Range**
Primary sources				
Organic matter (0-2μm)				
Biomass burning	28	26	54	45-80
Fossil fuel	28	0.4	28	10-30
Biogenic ($>$1μm)			56	0-90
Black Carbon (0-2μm)				
Biomass burning	2.9	2.7	5.7	5-9
Fossil fuel	6.5	0.1	6.6	6-8
Secondary sources				
Anthropogenic	0.15	0.45	0.6	0.3-1.8
Biogenic				
Andreae and Crutzen (1997)			150	30-270
Griffin et al. (1999b)			18.5	13-24
Kanakidou et al. (2000)			70	61-79
Chung and Seinfeld (2002)			11.2	
Derwent et al. (2003)			63	
Tsigaridis and Kanakidou (2003)			23.3	2.5-44.0
Lack et al. (2004)			15.3	
Bonn et al. (2004)			20	

genic sources. However, light scattering by particles in the atmosphere is primarily due to particles in the size range 0.1-1 μm (Finlayson-Pitts and Pitts, 2000). Moreover, cloud condensation nuclei (CCN) are almost exclusively sub-micron particles (Seinfeld and Pandis, 1998). Consequently, the climate relevance of the SOA can be considered of equal or even more important than that of the POA. Kanakidou et al. (2000) predicted that the increase in tropospheric ozone and anthropogenic organic aerosols could have resulted in a possible 3-to 4-fold increase of biogenic SOA since pre-industrial times. Since biogenic SOA are expected to be influenced by anthropogenic activities, their representation in global and regional models is essential in order to quantify the impact of human activities on both air quality and the climate.

On the theoretical level, the work of Pankow (1994a,b) has provided a handy description of the condensation of organic gases onto aerosols which has been commonly accepted. The gas/particle partitioning is governed by an equilibrium law between the concentrations of the organic compounds present in the respective phases. According to this law, the condensation of a gaseous compound on a particle is governed by its vapour pressure and is proportional to the mass of organic aerosol present. This condensation is favoured at low ambient temperature (which leads to a lower equilibrium vapour pressure).

In the first model estimations, the determination of the partitioning coefficients following the parameterization by Pankow was not possible because it requires the knowledge of the exact product distribution in the oxidation of the biogenic precursors as well as the vapour pressure of the products. Further experimental studies were therefore needed to identify the composition of biogenic aerosols. Laboratory experiments were focused in particular on α-pinene, as representative for the monoterpenes, because of its large contribution to the total emissions of monoterpenes (Rinne et al., 2000). They revealed the presence of multifunctional products in the aerosol samples (Christoffersen et al., 1998; Nozière and Barnes, 1998; Jang et al., 1999; Nozière et al., 1999a; Reissel et al., 1999; Yu et al., 1999a; Glasius et al., 2000; Koch et al., 2000; Orlando et al., 2000; Larsen et al., 2001; Wisthaler et al., 2001). Dicarboxylic acids, such as pinic acid and keto-carboxylic acids such as pinonic acid have been identified in the SOA produced from the oxidation of α-pinene, but also (hydroxy-) carbonyl products such as pinonaldehyde and hydroxy pinonaldehyde (the structure of these species is shown in Appendix A). The presence of these compounds in SOA has been corroborated by field measurements performed in forested areas (Kavouras et al., 1998; Yu et al., 1999b; Kubátovátova et al., 2000).

The modeling studies on the partitioning of individual oxidation products between the gas and the particulate phase have highlighted another issue. The compounds identified in the SOA samples present a complex carbon structure and bear several chemical functionalities. Their thermodynamic properties (solubility, boiling point, volatility) have received only little experimental attention. Therefore, the vapour pressure of these compounds necessary to calculate their partitioning coefficient has to be evaluated using prediction methods. Early methods were dedicated to simple monofunctional molecules (e.g. Jensen et al., 1981; Joback and Reid, 1987) and did not allow proper evaluation when applied on more complex compounds. In recent years, experimental studies have been performed to deduce the vapour pressure of several multifunctional compounds found in biogenic SOA (Hallquist et al., 1997; Bilde and Pandis, 2001; Bilde et al., 2003). The measurement of very low vapour pressures requires special experimental set ups and, to date, there exists only few data for these compounds. Several vapour pressure prediction methods have been extended on the basis of these scarce experimental values (e.g. Asher et al., 2002). However, they provide parameterizations for only a few chemical categories among the multifunctional compounds. Moreover, the temperature dependence of the predicted vapour pressure is uncertain. Their current prediction uncertainties can reach one order of magnitude or more.

On the basis of the products identified in the laboratory, several mechanistic studies have attempted to explain the oxidation routes leading to these products. In particular, the general lines in the oxidation mechanisms of α-pinene have been drawn and included in the MCM master mechanism (Jenkin et al., 1997; Saunders et al., 2003).

On the basis of these first simple mechanisms, simulations of laboratory experiments have been carried out by different groups (Kamens et al., 2001; Jenkin et al., 2004). However, many among the proposed routes remain speculative. For example, several routes have been proposed for the formation of pinic acid, a low-volatility product believed to play an important role in condensation and nucleation (Christoffersen et al., 1998; Jang et al., 1999; Koch et al., 2000; Jenkin et al., 2000). However, none of the proposed routes could be substantiated, for the reasons already outlined in the previous section. Moreover, many experimental studies have confirmed the presence of supposedly volatile products such as pinonaldehyde in the aerosol phase, in contradiction with the partitioning theory established by Pankow.

Considering these shortcomings, the representation of the oxidation of BVOC in recent global models (Chung and Seinfeld, 2002; Derwent et al., 2003; Tsigaridis and Kanakidou, 2003; Lack et al., 2004) has not significantly progressed. The chemical schemes of the SOA precursors remain very simplified and the yields and partitioning of the products (sometimes fictitious) are based on regressions of experimental SOA yields obtained in laboratory conditions differing greatly from the conditions found in the atmosphere. However, on the basis of an extensive review of laboratory experiments, Seinfeld and Pankow (2003) have shown the existence of a strong dependence of the SOA yields with the photochemical conditions. They concluded that the use of experimental SOA yields measured in the laboratory may cause large errors when introduced in atmospheric models. Better mechanistic representations of the BVOC oxidation in models are thus required. Pun et al. (2003) have also stressed the importance of errors related to the lack of adequate methods for the prediction of partitioning parameters for the products. These assertions have been confirmed very recently by Griffin et al. (2005) who performed a sensitivity analysis on the impact of the BVOC oxidation mechanism and the vapour pressure predictions on the SOA yields. The uncertainties in the predictions of SOA are also illustrated in Tab. 1.2 by the large discrepancies found between the biogenic SOA production estimates by different global model studies.

1.6 Objectives of the thesis

An important objective of this work is the development of a state-of-the-art near-explicit mechanism for the gas phase oxidation of α-pinene by OH and O_3, based on the theoretical works performed by the group of J. Peeters from University of Leuven which constitute the cornerstone of this mechanism. Another important objective is the implementation of this detailed mechanism in a box model and its confrontation with the results of laboratory experiments. For that purpose, attention will be focused on the model representation of the chemical conditions taking place in laboratory reactors (Chapter 2).

A third major objective is the development of a model describing the formation of SOA, based on the partitioning theory developed by Pankow (1994a,b). The vapour pressure being a key parameter in the partitioning of organic compounds, our goal is to design a prediction method adapted to the α-pinene oxidation products, and to compare our vapour pressure estimates with previous evaluations. The estimation of the uncertainties on the modeled vapour pressures will be performed in order to evaluate the robustness of the partitioning calculations (Chapter 3).

A fourth major objective of this work is to couple the SOA formation model with the gas phase box model, and to confront its results with gas and aerosol phase measurements of the main α-pinene oxidation products in a selection of laboratory experiments. The uncertainties of the model predictions will be also estimated (Chapter 4).

Finally, we aim to reduce the detailed mechanism to a smaller size based on rigorous methods for mechanism reduction. We will verify that the results of the reduced mechanism are reasonably close to the predictions of the detailed mechanism in atmospheric conditions (Chapter 5).

Chapter 2

Modeling the gas phase oxidation of alpha-pinene

2.1 Introduction

This chapter focuses on the development of the gas phase photooxidation mechanism of α-pinene by OH and ozone. This mechanism is largely based on theoretical studies performed by Peeters and coworkers. They have determined the sites of α-pinene where the oxidations are initiated and the resulting main oxidation routes. The elucidation of these routes relies mainly on the determination of the products and rates of the alkoxy radical reactions (isomerizations, decompositions and reactions with O_2). These rates are indeed extremely variable, ranging between $\sim$1 s^{-1} and 10^{11} s^{-1}. Due to the lack of experimental data, theoretical studies are essential to determine which reactions prevail among the set of possible processes. We refer to the publications of this group for the details of their calculations. However, given the importance of theoretical aspects in the development of the α-pinene oxidation mechanism, a brief outline of the methods used is given in the next section.The oxidation routes of α-pinene are presented and briefly discussed in Sec. 2.3.1.

As described in the Introduction, once initiated, we can represent the oxidation routes as reaction chains involving a succession of alkoxy and peroxy radicals until their complete transformation into stable products. The reactions involving peroxy radicals are generally more predictable than those of alkoxy radicals and they do not require case-by-case theoretical studies. Their characterization in the context of the α-pinene mechanism is part of the present work. As it will be described in Sec. 2.3.2, the rates and products of the peroxy radical reactions are estimated on the basis of known reactions. An exception is represented by the reactions involving α-hydroxy peroxy radicals as well as the ring opening reactions of large unsaturated peroxy radicals which have been specifically investigated by Peeters et al. (Sec. 2.3.3).

The primary products formed in the course of the α-pinene oxidation are further oxidized by OH and/or are photolyzed. Among these products, pinonaldehyde is

formed in large amount. Its oxidation mechanism has been treated in details by Peeters and coworkers and will be also discussed in this chapter. However, the explicit representation of the oxidation routes of all the other primary products would be prohibitive, due to the large number (tens of thousands) of reactions involved. Therefore, a simplified representation has been adopted in this work to represent the secondary oxidation routes (Sec. 2.3.4) of every primary product. The OH-reaction rates have been determined using a well-established theoretical method. A more detailed analysis have been performed to determine the parameters (photolytic channels, absorption cross sections and quantum yields) of their photodissociation reactions (Sec. 2.4). As a case study, photolytic rates have been calculated for the laboratory experiments of α-pinene oxidation by OH performed by Nozière et al. (1999a). The simulations of these experiments are discussed in Chapter 4. Further reference to this paper in this chapter and in the next ones will be abbreviated as N99. Photolytic rates calculated for typical atmospheric conditions are also computed.

The gas phase inorganic chemistry of O_x, NO_x, HO_x used in this work is not discussed here and we refer to the review of Atkinson et al. (2003) for more details.

2.2 Methodologies used for the development of the mechanism

2.2.1 Theories of molecular kinetics

The rate of a bimolecular reaction :

$$A + B \rightarrow products \tag{R2.1}$$

generally follows the Arrhenius expression $k(T) = A \exp \frac{-E_a}{RT}$. A is the pre-exponential factor and E_a is the activation energy. The widely accepted Arrhenius equation involves the important concept of an activation barrier to the reaction. This thermodynamic view of activated molecules, produced by molecular collisions, and capable of overcoming the energetic barrier to a reaction leads to the concept of transition state theory (TST). It is based on the assumption of the following sequence (Finlayson-Pitts and Pitts, 2000) :

$$A + B \rightleftharpoons (AB)^\star \rightarrow products. \tag{R2.2}$$

The entity represented as $(AB)^\star$ is called the transition state. The potential energy of the reacting system depends on the molecular orientations, and on the internal geometries of the molecules, and defines a "potential energy surface" (PES) (Fig. 2.1). It is a function of a set of coordinates which define completely the instantaneous relative positions of all atoms in the molecules. This surface possesses one or several saddle point(s). The curve which goes from the bottom of the reactant valley, through the saddle point, and to the bottom of the product valley defines the reaction coordinate. For a particular set of initial conditions of the reactants (initial positions and

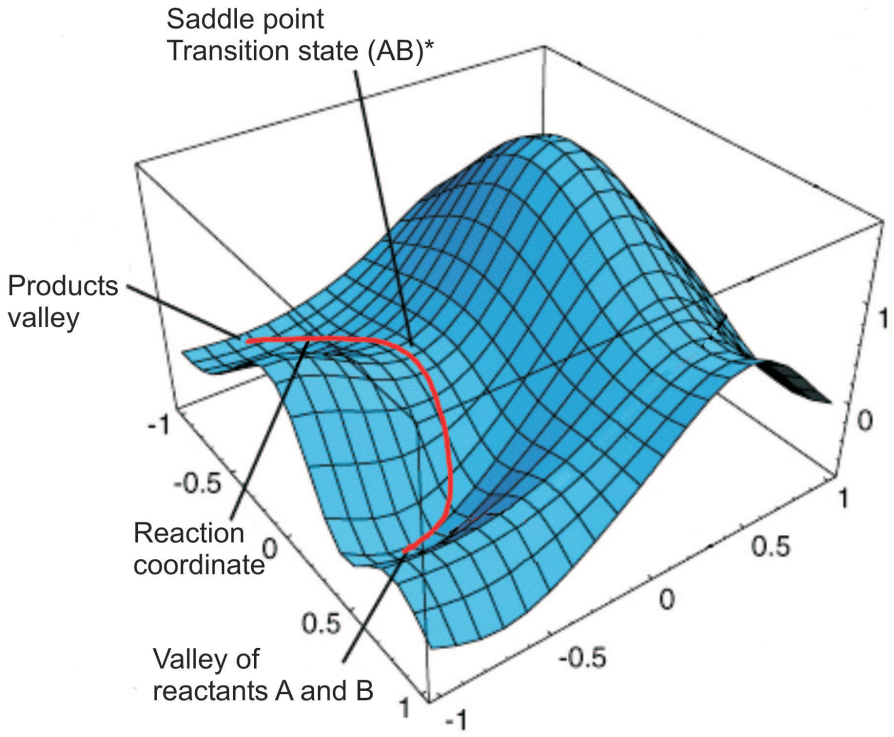

Figure 2.1: Typical potential energy surface in two dimensions showing the reaction path from the reactants to the products, passing by the transition state.

momenta of all atoms), it is in principle possible to calculate a trajectory across the potential energy surface. This trajectory might either end up back in the region of the reactants (case of a non reacting collision), or pass over the saddle to the product region (reactive collision). The activation energy of the reaction is the difference between the energy level of the reactants and the energy level of the transition species (at the saddle point). The reaction rate is defined by the number of molecules in the transition state that cross the activation barrier by second. This rate is equal to the concentration of the transition state multiplied by the frequency at which the barrier is crossed.

In order to determine this concentration, thermal equilibrium is assumed between the reactants and the transition species. The equilibrium constant,

$$K^* = \frac{[(AB)^*]}{[A][B]}, \tag{2.1}$$

is related to the partition functions Q of the species,which take into account the translational, rotational, and vibrational motion of the molecule:

$$K^* = \frac{Q_{(AB^*)}}{Q_A Q_B} e^{-E_0/RT}, \tag{2.2}$$

where E_0 is the height of the potential energy barrier. Using Eq. 2.1 and Eq. 2.2, the rate of the reaction can be written as :

$$v = [(AB)^*]\nu^* = \nu^*[A][B]\frac{Q_{(AB^*)}}{Q_A Q_B}e^{-E_0/RT}, \tag{2.3}$$

where ν^* is the frequency of passage across the barrier. ν^* is calculated based on the partition function of the transition state which represents the motion along the reaction path. The partition functions are determined from the resolution of the Schrodinger equation for the reacting molecules, which allows to construct the Potential Energy Surface. The points on the PES where the energy of the system is minimal correspond to particular arrangements of nuclei which have increased stability, i.e. to stable species (reactants, products and transition states). The calculation of the PES allows therefore to establish the potential reaction path and its activation energy.

The Schrodinger equations are written under the Born-Oppenheimer approximation. It postulates that, the nuclei being much more massive than electrons, the PES can be computed by solving the equations for the electronic wave functions only. The resolution of these equations requires the use of computational chemistry. Methods have been developed since the 1980's when the computers became powerful enough to tackle these issues. The oldest and most popular method is the Hartree-Fock method. It is based on a representation of the molecular system using a linear combination of approximate atomic orbitals. Following this approach, the electrons are subject to an average non-local potential arising from the other electrons. This leads to a poor description of the molecular electronic structure in the case of many-body systems, such as large molecule. This limitation (known as the correlation energy error) leads to an unprecise parameterization of the PES. Fortunately, in the last ten years, new approaches have appeared, known as density functional theories (DFT), which can be applied to much larger systems with good precision and accuracy. The motivation of the DFT is to replace the many-dimensional atomic wave functions by a functional of the density of the electrons $\phi(\rho)$ around the molecule. The most popular functionals used in the literature have been derived by careful comparison with experiments (the BP86, BLYP and B3LYP functionals). The elucidation of the α-pinene mechanism presented in this work is mainly based on B3LYP.

Consider an unimolecular reaction (Billing and Mikkelsen, 1996) :

$$A \Rightarrow products \tag{R2.3}$$

The rate of such a reaction may not be proportional to the concentration of A. If A is a normal stable molecule then there must be some intervention to trigger the reaction. This may be the absorption of light or the effect of molecular collisions between A and species not chemically involved in the reaction. In the last case, the apparent unimolecular mechanism can be described by the following equations proposed by Lindemann-Hinshelwood :

$$\mathrm{A} + \mathrm{M} \rightleftharpoons \mathrm{A}^* + \mathrm{M} \tag{R2.4}$$

$$\mathrm{A}^* \rightarrow products \tag{R2.5}$$

Applying the steady-state approximation to the concentration of A* gives:

$$[A^*] = \frac{k_{R2.4}[A][M]}{k_{-R2.4}[M] + k_{R2.5}}. \tag{2.4}$$

so that the overall rate is :

$$\frac{d[product]}{dt} = k_{R2.5}[A^*] = \frac{k_{R2.5}k_{R2.4}[A][M]}{k_{-R2.4}[M] + k_{R2.5}}. \tag{2.5}$$

The effective first-order rate constant is defined as $k_{eff} = \frac{k_{R2.5}k_{R2.4}[M]}{k_{-R2.4}[M]+k_{R2.5}}$. At high pressures, collisional deactivation of A^* is more likely than unimolecular reaction, k_{eff} reduces to $\frac{k_{R2.5}k_{R2.4}}{k_{-R2.4}}$, and the reaction is truly first order in A. At low pressures, bimolecular excitation is the rate determining step; once formed, A^* is more likely to react than be collisionally deactivated. The rate constant reduces to $k_{eff} = k_{R2.5}[M]$ and the reaction is second order. Although the Lindemann-Hinshelwood mechanism explains the rate behavior of the reaction at high and low pressures, it can not describe properly the reaction rate in the falloff region when the energizing-deenergizing processes of Eq. R2.4 are competing. This is due to the fact that, in reality, A^* is not in equilibrium with A, mainly because A^* has to be in specific energetic modes to react. More precisely, the reaction requires a minimum amount of energy in these specific ("effective") vibrational modes to take place. The RRKM theory addresses this issue. Central to this theory is the introduction of the activated complex A^+. It represents the fraction of A^* which has sufficient energy in its effective mode:

$$A^* \rightleftharpoons A^\dagger \tag{R2.6}$$

$$A^\dagger \rightarrow products. \tag{R2.7}$$

In this theory, it is considered that $k_{R2.6}$ is much smaller than $k_{R2.7}$, and the conversion of A^* to $A^\dagger$ is rate determining. In general, the RRKM theory admits an equilibrium between A^* and $A^\dagger$:

$$k_{R2.6} = k_{R2.7}\frac{[A^\dagger]}{[A^*]}. \tag{2.6}$$

It is possible to determine the proportion of A^+ as well as the rate constant $k_{R2.7}$ using partition functions ($k_{R2.7}$ is treated as a motion along the reaction coordinate as in the TST theory). As in the case of the TST theory, the partition functions are determined by solving the Schrodinger equation of the molecular system.

At high pressure, A^* and A are at equilibrium and they behave as described by transition state theory (which assumes thermal equilibrium between the activated species and the reactants). It follows that at high pressures, both theories can be used and their results coincide. In the framework of the study of α-pinene oxidation, bimolecular reactions, but also thermal unimolecular reactions of alkoxy radicals (e.g. isomerizations, decompositions) are treated on the basis of the TST theory. The rates of the unimolecular reactions which are not in thermal equilibrium, such as prompt decomposition of activated radicals, are calculated using RRKM theory. Examples of prompt decomposition processes are given in Sec .2.3.3.

2.2.2 Structure-Activity Relationships

Another family of prediction methods widely used in the development of the α-pinene mechanism is represented by the Quantitative Structure-Activity Relationships (SAR). These methods designed on empirical or theoretical grounds are much simpler to use than the quantum kinetic theories, and they give usually relatively good results when applied within the limits they have been designed for. The SAR attempt to correlate structural molecular properties (descriptors) with mathematical functions representing a chemical activity of a molecule (i.e. physicochemical properties, biological activities, kinetic rates) for a category of compounds by means of statistical methods. As a result, a simple mathematical relationship is established (Gallegos, 2004):

$$Function = f(structural\ \ descriptors) \tag{2.7}$$

Following this approach, similar compounds have similar activities, and any systematic variation in the chemical structure from one compound to another is reflected by a difference of analogous magnitude in the chemical response. It is important to note that this approach does not seek to identify the particular descriptors causing a particular activity. Although some SAR are based on causal processes clearly identified, the prime objective of a SAR is restricted to the statistical correlation existing between the descriptors and an activity. Applications of SAR are found almost everywhere in chemistry, e.g. in agrochemistry, pharmaceutical chemistry, toxicology and atmospheric chemistry.

To determine the function f, a mathematical model is designed which relates experimental measurements with a set of chemical descriptors characterizing the molecular structure of the compounds in the data set. The selection of the appropriate data set is critical to the predictive capabilities of the SAR model. It defines also the domain of validity of the model. A suitable set requires some degree of chemical similarity between the compounds. Strict structural criterions are therefore essential in the selection of the compounds, which justifies their classification into subgroups. Great care is taken also for the selection of the structural descriptors so that they do not content redundant information. The selection of the descriptors is based on experimental data set. The use of computational methods in the elaboration of the function f allows to optimize the choice of the descriptors.

In the last decade, empirical and theoretical studies have been performed on gas phase reactions involving different types of oxygenated compounds (ethers, esters, ketones, aldehydes, etc.). The data obtained gave rise to numerous structure-activity relationships which can be used to predict the kinetics and mechanisms of oxidation of various families of oxygenated organic compounds. These SAR are widely used in the development of mechanisms of oxidation of VOC, as for example in the MCM mechanism (Saunders et al., 2003). An extensive use of SAR, mostly designed by Peeters and co-workers, has been necessary in the development of the oxidation mechanism of α-pinene. For further details concerning these SAR, we refer to the

published works. The SAR employed in this work comprises :

- Site-specific SAR for addition of OH to polyalkenes (Peeters et al., 2001).
- SAR for H-atom abstraction from (poly)alkenes (Peeters et al., 2001).
- SAR for specific radical stabilization effects in bicyclic terpenic structures (Peeters et al., 2001).
- SAR for barrier heights to dissociation of alkoxy radicals (Peeters et al., 2001).
- SAR for isomerization of alkoxy radicals by 1,5-H shifts (Peeters et al., 2001).
- SAR for the formation of nitrates in reactions of alkyl peroxy radicals with NO (Arey et al., 2001).
- General SAR for OH + hydrocarbon reactions (Kwok et al., 1995).

The predictions of SAR appear to be uncertain when applied to radicals where specific structural effects occur (i.e.(de)stabilization effects due to resonances). In these cases, quantum chemical methods such as those described above may be more adapted to treat these issues.

2.3 Mechanism of α-pinene oxidation by OH and O_3

2.3.1 Outline of mechanism

α-pinene being an alkene, it is highly reactive towards O_3 and OH, with rates of 9.0×10^{-17} cm^3 molecule^{-1} s^{-1} and 5.3×10^{-11} cm^3 molecule^{-1} s^{-1} (Atkinson et al., 2004) at 298 K, respectively. Figures 2.2, 2.3 summarize the main reactions steps of the α-pinene oxidation by OH and O_3.

The main channels (88%) of the reaction between α-pinene and the hydroxy radicals is OH addition on the double bond leading to two activated radicals $R_2^\dagger$ and $R_6^\dagger$ (in Fig. 2.2). About 50% of the activated $R_6^\dagger$ isomerize by cycle opening, whereas 50% stabilize collisionally. In the case of $R_2^\dagger$, collisional stabilization is predicted to be the only possible path. Besides OH-addition, H-abstraction processes account for the remaining $\sim$12% of the reaction flux. Only the major H-abstraction channel ($\sim$9%) is considered in this study. It is assumed to represent the other minor H-abstraction channels (Peeters et al., 2001).

The theoretical study of the oxidation of α-pinene by OH has revealed the existence of "exotic" processes following the OH addition reactions. Peeters et al. (2001)

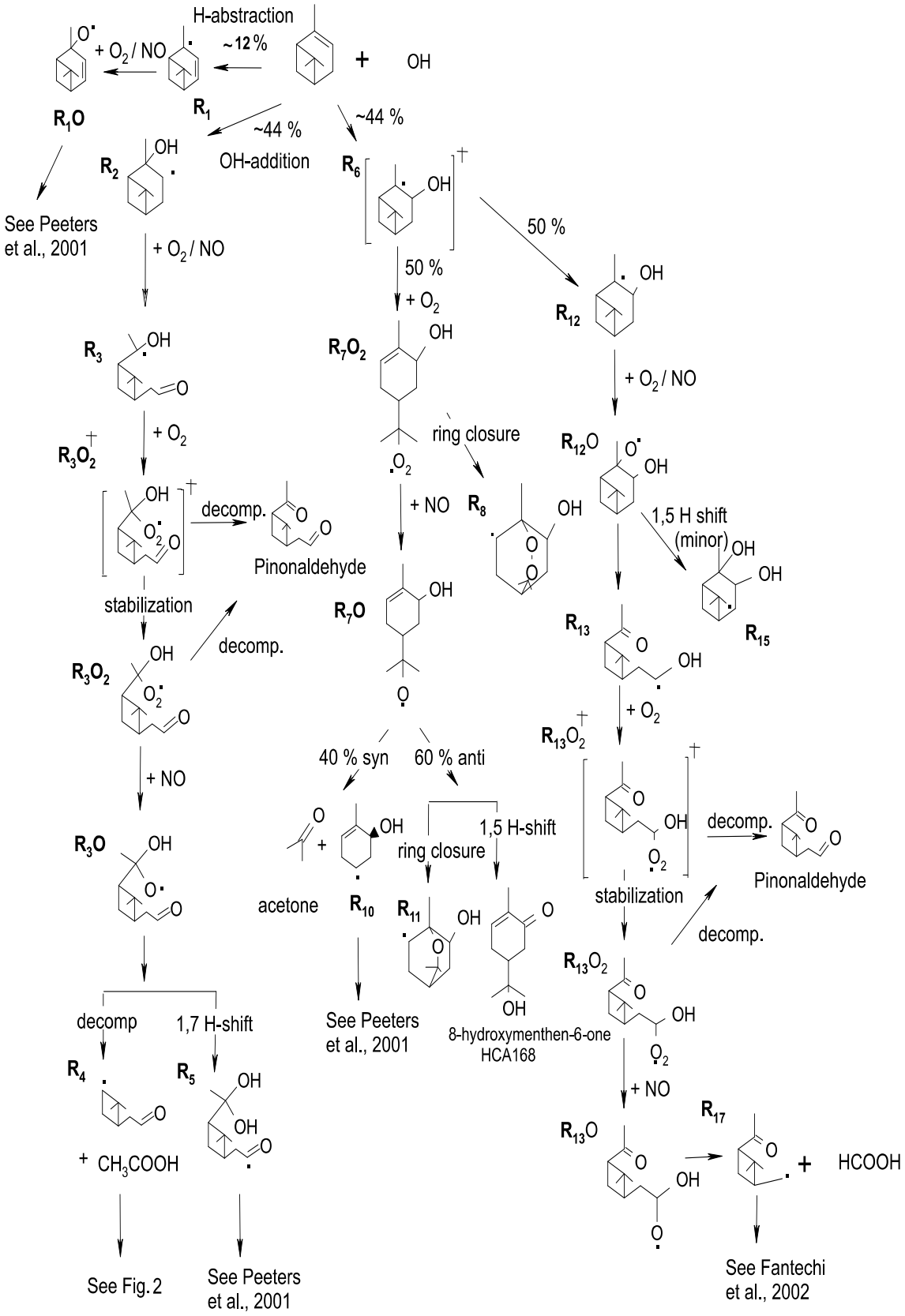

Figure 2.2: Main paths of the α-pinene oxidation by OH.

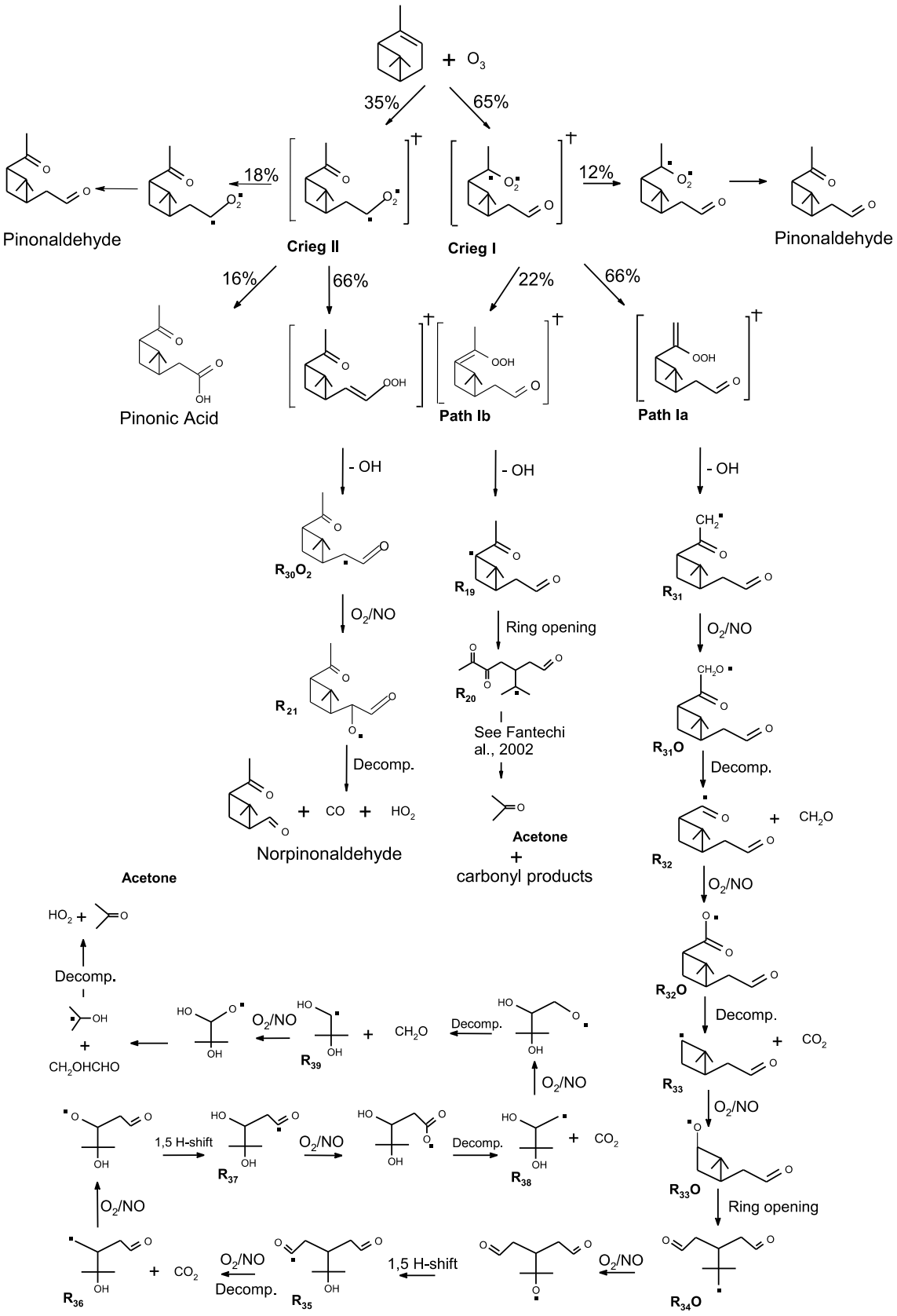

Figure 2.3: Main paths of the α-pinene oxidation by O_3 .

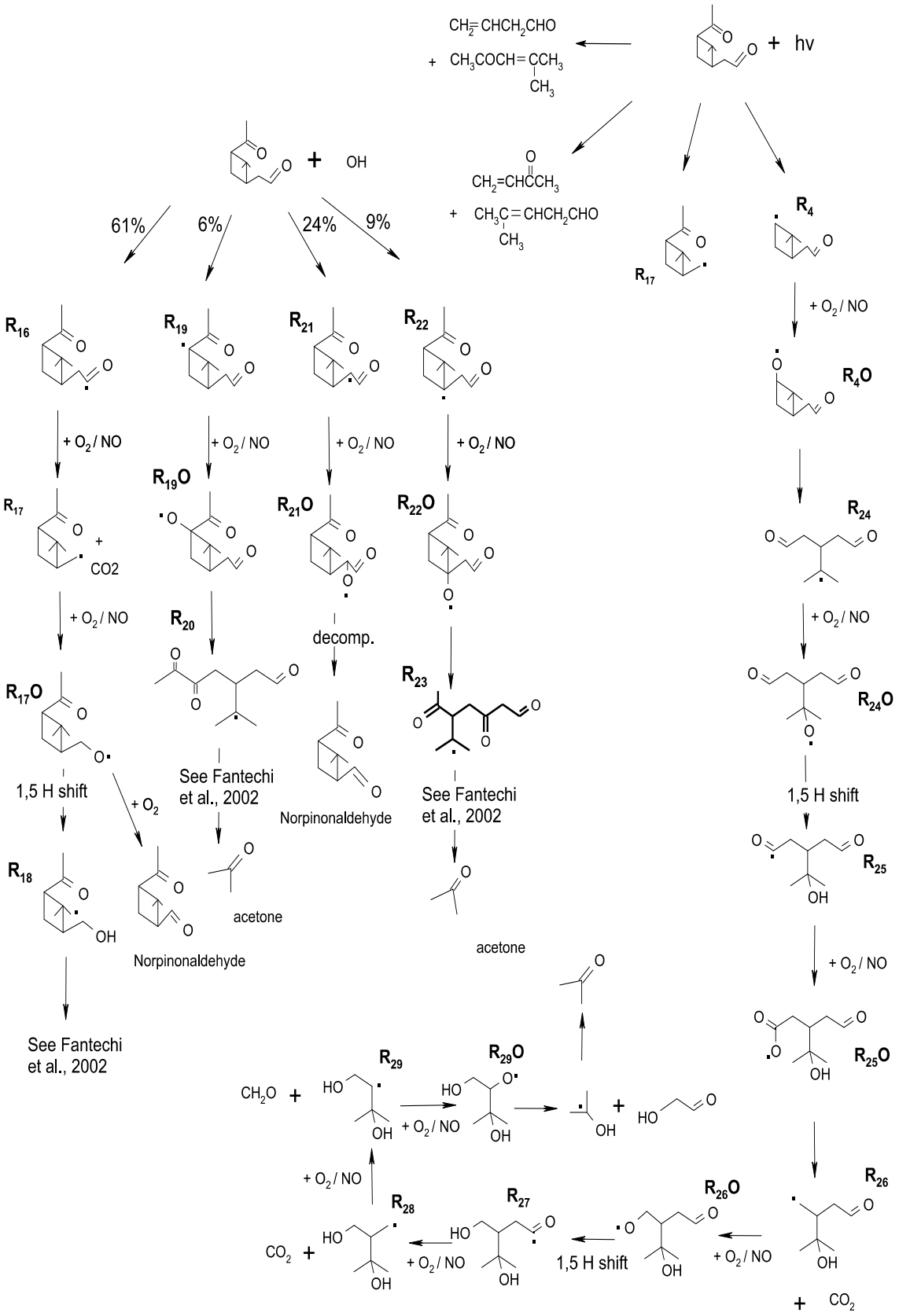

Figure 2.4: Main paths of the OH-oxidation and photolysis of pinonaldehyde.

and Hermans et al. (2005) consider the alkyl radicals R_3 and R_{13} which react with oxygen to produce activated α-hydroxy peroxy radicals (Fig. 2.2). These activated radicals and their subsequent stabilized counterparts can both decompose to pinonaldehyde, a compound which has been observed by several groups (Arey et al., 1990; Hatakeyama et al., 1991; Hakola et al., 1994; Nozière et al., 1999a; Larsen et al., 2001; Wisthaler et al., 2001; Vanhees et al., 2001; Librando et al., 2003). A detailed discussion on the role and rates of these reactions is given in Sec. 2.3.3. In addition, Vereecken and Peeters (2004) demonstrated the importance of ring-closure reactions of unsaturated peroxy radicals formed in the atmospheric oxidation of biogenic VOC. They showed in particular that the radical R_7O_2 formed in the α-pinene oxidation mechanism undergoes a ring closure reaction with a rate of $\sim$2.5 s^{-1}. It should be noted that the chemistry following ring closure has not been studied so far and remains unknown. The NO-reaction of the radical R_7O_2 yields an organic nitrate and an alkoxy radical that promptly decomposes into the alkyl radical R_{10} and acetone. Acetone has been quantified in laboratory experiments of α-pinene oxidation by OH in presence of NO_x with a yield ranging from 5% to 11% by Aschmann et al. (1998), Fantechi (1999), Nozière et al. (1999a), Orlando et al. (2000), Larsen et al. (2001) and Wisthaler et al. (2001).

Depending on the level of NO, the decomposition of α-hydroxy peroxy radicals and the ring closure of large unsatured peroxy radicals can compete with the usual NO-reaction, affecting the yields of pinonaldehyde, acetone, and the semi-volatile aerosol precursors. A detailed discussion of the influence of these reactions on the products yield is given in Sec. 4.2.6.

The ozonolysis of alkenes compounds proceeds by the addition of ozone to the C=C bond to form a "primary ozonide" which rapidly decomposes to two Criegee biradicals intermediates. The branching ratios adopted in this work are based on the review of Atkinson (2000). The production of di-substituted biradical is dominant for alkenes of structure $CR_1H{=}CR_2R_3$ (like α-pinene):

$$\begin{aligned} CR_1H = CR_2R_3 + O_3 \rightarrow \quad & \sim 0.35\ (R_1C(O)C_2 + [R_3\dot{C}H_2O\dot{O}]^*) \\ & \sim 0.65\ (R_3CHO + [R_1R_2\dot{C}O\dot{O}]^*). \end{aligned} \tag{R2.8}$$

The energy-rich biradicals can stabilize collisionally (R2.9) or decompose (R2.10).In the case of $[R_3\dot{C}H_2O\dot{O}]^*$:

$$[R_3\dot{C}H_2O\dot{O}]^* + M \rightarrow R_3\dot{C}H_2O\dot{O} + M \tag{R2.9}$$

$$[R_3\dot{C}H_2O\dot{O}]^* \rightarrow products. \tag{R2.10}$$

The stabilized biradicals can react with a number of species (Seinfeld and Pandis,

1998; Baker et al., 2002):

$$R_3\dot{C}H_2O\dot{O} + H_2O \rightarrow R_3C(O)OH + H_2O \quad \text{(R2.11a)}$$
$$R_3\dot{C}H_2O\dot{O} + H_2O \rightarrow R_3CHO + H_2O_2 \quad \text{(R2.11b)}$$
$$R_3\dot{C}H_2O\dot{O} + NO \rightarrow R_3CHO + NO_2 \quad \text{(R2.12)}$$
$$R_3\dot{C}H_2O\dot{O} + SO_2 \rightarrow R_3CHO + H_2SO_4 \quad \text{(R2.13)}$$
$$R_3\dot{C}H_2O\dot{O} + CO \rightarrow products. \quad \text{(R2.14)}$$

The review by Atkinson (2000) indicates three possible decomposition processes for biradicals which do not stabilize thermally: the O-atom elimination (R2.15a), the ester channel (R2.15b), and the hydroperoxide channel (R2.15c):

$$[R_3\dot{C}H_2O\dot{O}]^* \rightarrow O(^3P) + R_1CH_2C(O)R_2 \quad \text{(R2.15a)}$$
$$[R_3\dot{C}H_2O\dot{O}]^* \rightarrow [R_1CH_2C(O)OR_2]^* \rightarrow decomposition \quad \text{(R2.15b)}$$
$$[R_3\dot{C}H_2O\dot{O}]^* \rightarrow [R_1CH{=}C(OOH)R_2]^* \rightarrow R_1\dot{C}C(O)R_2 + OH \quad \text{(R2.15c)}$$

Early experimental estimates of the yield of OH radicals from the α-pinene-O_3 reaction are 0.70$\pm$0.17 (Paulson et al., 1998), 0.76$\pm$0.11 (Chew and Atkinson, 1996), and 0.83$\pm$0.21 (Rickard et al., 1999). These values suggest that the hydroperoxide channel is the major pathway. Formation of pinonaldehyde has been also observed by several groups using different experimental set ups: Hakola et al. (1994) and Alvarado et al. (1998) used gas chromatography, Ruppert et al. (1999) used in situ Fourier transform infrared absorption spectroscopy, Yu et al. (1999a) used derivatization methods coupled to combined gas chromatography-mass spectroscopy and Baker et al. (2002) used in situ atmospheric pressure ionization tandem mass spectrometry (API-MS). In average, the reported pinonaldehyde yields range from 0.14 to 0.19.

RRKM estimations from by Peeters and Co-workers confirm the dominance of the hydroperoxide formation deduced from the measurements. Calculations indicate that 66% of "Crieg I" (leading to norpinonaldehyde) and 88% of "Crieg II" follow the hydroperoxide channel. Actually, there are two possible hydroperoxide channels for "Crieg I" (Fig. 2.3) depending on where the shift of the hydrogen atom takes place. In the case of the less substituted biradical "Crieg II", an ester channel is expected to occur leading to the formation of pinonic acid, a product of the α-pinene ozonolysis which has been observed by several groups (Hatakeyama et al., 1989; Hoffmann et al., 1997; Christoffersen et al., 1998; Jang et al., 1999; Yu et al., 1999a; Glasius et al., 2000; Koch et al., 2000). Calculations indicate that the remaining fraction of biradicals stabilizes thermally. The dominant pathway for formation of pinonaldehyde is the reaction of the stabilized Criegee intermediates with water vapour. The theoretical fate and fraction of the stabilized biradicals are in good agreement with the experimental yields of pinonaldehyde. The subsequent paths Ia, Ib, IIa of the alkoxy radicals have been determined theoretically by Peeters'group, leading to the mechanism depicted

on Fig. 2.3.

This ozonolysis mechanism does not include the production of pinic acid and hydroxy pinonic acid. However, these two compounds have been identified in the gas and particulate phases in the ozonolysis of alpha-pinene (Christoffersen et al., 1998; Hoffmann et al., 1997; Glasius et al., 2000; Kamens et al., 1999). Observations indicate yields up to 3% in the aerosol phase for each of these products. Several schemes have been proposed in the literature (Fig. 2.5). Jenkin et al. (2000) suggested an isomerization of the radical $R_{31}O$ competing with the decomposition. The 1,8-shift of the aldehydic H atom in $R_{31}O$ leads to an alcohol function. Subsequent reactions with O_2 and HO_2 generate hydroxy pinonic acid (reaction 1). A similar isomerization is also proposed for the formation of pinic acid from the radical R_{32}. According to Jenkin et al. (2000), the loss of CO_2 would represent a minor path (20%) whereas the 1,7 H-shift would be dominant and leads to pinic acid (reaction 2). Winterhalter et al. (2000) proposed also a formation scheme for pinic acid based on the radical R_{32} (reaction 3): Upon reaction with O_2 and HO_2, the peroxo acid $R_{32}OOH$ follows an autoxidation of its aldehydic function and is converted into pinic acid. The reality of this reaction is supported by the autoxidation of acetaldehyde, known to occur in the liquid phase.

However, recent theoretical studies performed by Peeters and co-workers (Peeters and Vereecken, 2005) showed that these isomerization reactions are much slower (by several orders of magnitude) than the decomposition reactions of the radicals. Calculations showed also that autoxidation of the peroxo acid in the gas phase has an activation barrier so high so that the reaction cannot take place.

Pinonaldehyde is a primary product formed in substantial amount in the α-pinene oxidation of both O_3 and OH. With its 10-carbon structure and its two carbonyl functionalities, pinonaldehyde is highly reactive with OH (3.5×10^{-11} molecules cm^{-3} s^{-1}) making this compound a potential precursor for aerosol formation. Consequently, the development of an explicit mechanism for the oxidation of pinonaldehyde is of importance in this work. Fantechi et al. (2002) has calculated that the OH-oxidation of pinonaldehyde proceeds mainly via H-atom abstraction on four carbon sites. The first steps and the relative importance of each abstraction channel are shown in Fig. 2.4. The paths Ib and IIa of α-pinene ozonolysis appear also in the pinonaldehyde+OH mechanism. The photolysis of pinonaldehyde is discussed in Sec. 2.4.3.

2.3.2 Reactions of peroxy radicals RO_2

Peroxy radicals react with NO_x compounds, with HO_2, and with other peroxy radicals. These reactions are slow compared to the reactions of alkoxy radicals. Although their rates depend on the peroxy radical structure, this dependence is much less drastic than in the case of alkoxy radical reactions. In particular, the rates of the reactions

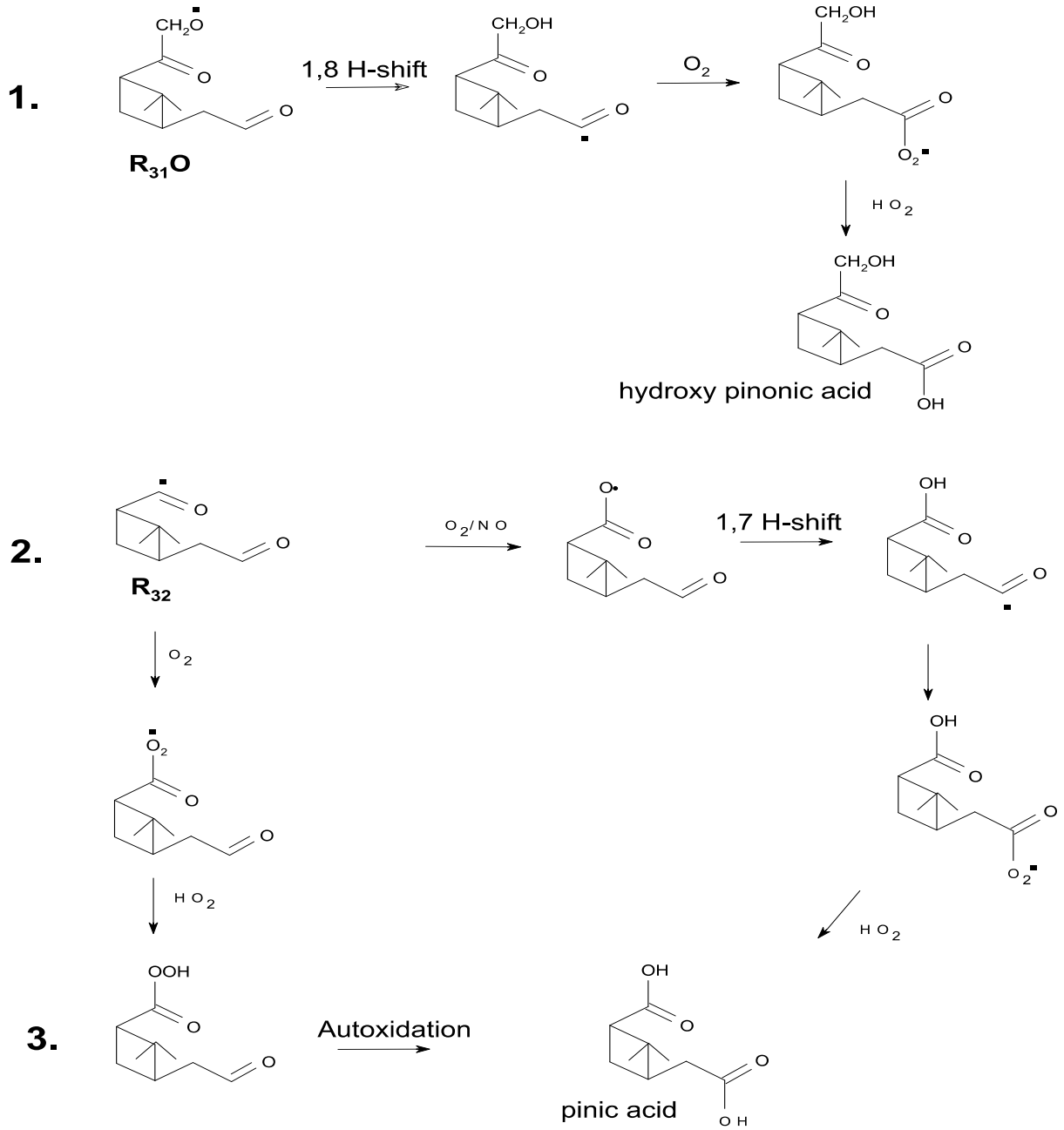

Figure 2.5: Possible formation paths for hydroxy pinonic acid and pinic acid in the ozonolysis of α-pinene proposed by Jenkin et al. (2000) (reaction sequences 1 and 2) and Winterhalter et al. (2000) (reaction 3)

.

of peroxy radicals with NO_x and HO_2 vary by less than an order of magnitude. The rates of the permutation reactions of peroxy radicals can vary by up to 7 order of magnitudes. Such a variation could legitimate the use of theoretical methods, but the tremendous number of possible permutation reactions involved in the α-pinene mechanism makes it unrealistic. Moreover, the relatively minor importance of these reactions in atmospheric conditions does not justify this approach. The rates of the reactions involving the peroxy radicals can therefore be extrapolated from the existing experimental data, in spite of the scarceness of data for large peroxy radicals. As in previous studies (Saunders et al., 2003), simple parameterizations are adopted for the treatment of the peroxy radicals reactions with other radicals. The reactions involving α-hydroxy peroxy radicals and large unsaturated peroxy radicals represent a special case which justifies a theoretical study described further in this section.

Reactions of RO_2 with NO

The reaction of a RO_2 radical with NO leads to the formation of either an alkoxy radical (RO) or an alkyl nitrate ($RONO_2$):

$$\mathrm{RO_2 + NO} \rightarrow \mathrm{RONO_2} \quad \text{(R2.16a)}$$

$$\rightarrow \mathrm{RO + NO_2}. \quad \text{(R2.16b)}$$

The rate coefficients for CH_3O_2, $C_2H_5O_2$, $CH_3C(O)O_2$ and $C_2H_5C(O)O_2$ from the recommendations of Atkinson et al. (2003) are used for all peroxy radicals (RO_2) and acyl peroxy radicals ($RC(O)O_2$) of the same carbon number. For higher ($C_{>2}$) peroxy radicals, the expression 2.54×10^{-12} exp(360/T) cm^3 $molecule^{-1}$ s^{-1} proposed by Saunders et al. (2003) is used. The rate for $C_2H_5C(O)O_2$ + NO, 6.7×10^{-12} exp(340/T) cm^3 $molecule^{-1}$ s^{-1}, is assigned to higher ($C_{>2}$) acyl peroxy radicals. The ratio $k_{R2.16a}/k_{R2.16b}$ for reactions involving CH_3O_2, $C_2H_5O_2$ and $CH_3C(O)O_2$ does not exceed 3% (Tyndall et al., 2001) . The organic nitrate-forming channel is therefore neglected for $C_{\leq 2}$ peroxy and for all acyl peroxy radicals. The organic nitrate yield for other alkyl peroxy radicals is calculated using the SAR of Arey et al. (2001). However theoretical calculations have showed that when the radical is located on the four-membered ring as in the case of $R_{22}O_2$ (Fig. 2.4), the resulting organic nitrate is unsteady and decomposes back to RO_2 + NO. For these specific peroxy radicals, there is no nitrate formation and the yield of the alkoxy radical is unity (Peeters et al., 2001).

Reactions of RO_2 with NO_2

The reaction of RO_2 radicals with NO_2 forms a peroxy nitrate:

$$\mathrm{RO_2 + NO_2 + M} \leftrightharpoons \mathrm{RO_2NO_2 + M}. \quad \text{(R2.17)}$$

The reaction (R2.17) involving peroxy radicals is negligible in the lower atmosphere as well as in laboratory reactors (Atkinson et al., 2003). However $RCO(O)_2$ radicals react with NO_2 to form stable peroxy acyl nitrates (abbreviated as PANs) of general

formula $RC(O)O_2NO_2$. The main loss mechanism of PANs is thermal decomposition back to $RC(O)O_2$ and NO_2. The Troe expression parameterizes the dependence to the pressure and temperature of the rate of the forward termolecular reaction:

$$k_{R2.17} = (\frac{k_0(T)[M]}{1 + \frac{k_0(T)[M]}{k_\infty(T)}}) F_c^{(1+(\log_{10}(\frac{k_0(T)[M]}{k_\infty(T)}))^2)^{-1}} \tag{2.8}$$

$k_0(T)$ and $k_\infty(T)$ represent the rate constants at low and high pressures limits, respectively. Tyndall et al. (2001) determined the low-pressure limit of the forward reaction (R2.17) for $CH_3C(O)O_2$ using F_c = 0.6 :

$$k_{R2.17,0} = 8.5 \times 10^{-29} (T/298)^{-6.5}. \tag{2.9}$$

The high-pressure limit is expressed as :

$$k_{R2.17,\infty} = 1.1 \times 10^{-11} (T/298)^{-1.0}. \tag{2.10}$$

The reverse reaction is obtained from $k_{R2.17}/K_{eq}$, where the equilibrium constant K_{eq} is:

$$K_{eq} = 9.3 \times 10^{-03} \exp(14000/T). \tag{2.11}$$

Due to the lack of additional kinetic data, Atkinson (2000) recommended to set the rate of the forward reaction of higher peroxy acyl radicals to the high-pressure limit of the Troe expression for the $CH_3C(O)O_2$ + NO_2 reaction (Eq. R2.17).

Reactions of RO_2 with NO_3

The reaction of peroxy radicals with NO_3,

$$\mathrm{RO_2 + NO_3 \rightarrow RO + NO_2} \tag{R2.18}$$

proceeds with a rate of 1.1×10^{-12} cm^3 $molecule^{-1}$ s^{-1} for the reaction with CH_3O_2 and 2.3×10^{-12} cm^3 $molecule^{-1}$ s^{-1} for the reaction with $C_2H_5O_2$ (Atkinson et al., 2003). The latter value is also used for the reactions involving $C_{\geq 3}$ peroxy radicals. The rate value of 4.1×10^{-12} cm^3 $molecule^{-1}$ s^{-1} derived by Canosa-Mas et al. (1996) for $CH_3C(O)O_2$ + NO_3 is used for all $RC(O)O_2$ + NO_3 reactions.

Reactions of RO_2 with HO_2

The reaction of the CH_3O_2 radical with HO_2 proceeds through two channels:

$$\mathrm{CH_3O_2 + HO_2} \rightarrow \mathrm{CH_3OOH + O_2} \tag{R2.19a}$$

$$\rightarrow \mathrm{CH_2O + H_2O + O_2}. \tag{R2.19b}$$

Tyndall et al. (2001) recommended a room temperature rate coefficient of 5.2×10^{-12} cm^3 $molecule^{-1}$ s^{-1} for the overall reaction. The relative importance of the CH_2O

branching channel is given by the temperature-dependent equation defined by Elrod et al. (2001):

$$k_{R2.19a}/k_{R2.19b} = \exp(6.21 - 1160/\mathrm{T}). \quad (2.12)$$

At 298 K, the hydroperoxide channel is the main pathway with $k_{R2.19a}/k_{R2.19}$ = 0.91. Experimental evidence indicates that the reaction of most alkyl peroxy radicals with HO_2 proceeds exclusively via the hydroperoxide pathway (Atkinson et al., 2003):

$$\mathrm{RO_2 + HO_2 \rightarrow ROOH + O_2}. \quad (R2.20)$$

The rates reported for CH_3O_2, $C_2H_5O_2$ and $CH_3C(O)CH_2O_2$ are used for all C_1, C_2 and C_3 peroxy radicals respectively. Jenkin et al. (1997) parameterized the RO_2 + HO_2 rates for $C_{\geq 3}$ alkyl peroxy radicals as a function of the carbon number n :

$$k_{R2.20,alkyl} = 3.0 \times 10^{-13} \exp(1250/T) \times [1 - \exp(-0.34n)]. \quad (2.13)$$

This expression is based on the data available for the reactions of alkyl and β-hydroxy RO_2 radicals up to 6 carbons with HO_2. The available data for the reaction $CH_3C(O)O_2$+HO_2 indicate a reaction rate of (Atkinson et al., 2003; Tyndall et al., 2001):

$$k_{R2.20,\mathrm{acyl}} = 5.2 \times 10^{-13} \exp(983/\mathrm{T}). \quad (2.14)$$

Two channels are considered:

$$\begin{aligned} \mathrm{RC(O)O_2 + HO_2} &\rightarrow \mathrm{RC(O)OOH + O_2} && \text{(R2.21a)} \\ &\rightarrow \mathrm{RC(O)OH + O_3}. && \text{(R2.21b)} \end{aligned}$$

The ratio $k_{R2.21a}/k_{R2.21}$ = 0.785 at ambient temperature recommended by Atkinson et al. (2003) for $CH_3C(O)O_2$ is used for all acyl peroxy radicals.

Permutation reactions of RO_2

The permutation reactions of a given RO_2 radical include its self-reaction and the cross reactions of this RO_2 with the other peroxy radicals (Finlayson-Pitts and Pitts, 2000):

$$\begin{aligned} \mathrm{RO_2 + R'O_2} &\rightarrow \mathrm{RO + R'O + O_2} && \text{(R2.22a)} \\ &\rightarrow \mathrm{R_{-H}O + R'OH + O_2} && \text{(R2.22b)} \\ &\rightarrow \mathrm{ROH + R'_{-H}O + O_2}. && \text{(R2.22c)} \end{aligned}$$

The self-reaction of a given RO_2 radical, i.e. RO_2+RO_2, undergoes the same paths. The relative importance of these paths depends on the structure of the radicals reacting with each other. Tab. 2.1 reports the fraction of alkoxy radicals (RO), carbonyls ($R_{-H}O$) and alcohols (ROH) generated from the permutation reactions of a given RO_2 radical. As shown by this table, the degree of substitution and the presence of a cycle

Table 2.1: Branching ratios assigned to the cross reactions of a given $\mathrm{RO_2}$ with other peroxy radicals depending on their respective structure: primary (prim.), secondary (sec.), cyclic (cycl.) and acyl.

For a primary/secondary radical $\mathrm{RO_2}$	Notes
$\mathrm{RO_2}$ + prim.*/sec. $\mathrm{RO_2} \rightarrow 0.50\,\mathrm{RO} + 0.25\,\mathrm{R_{-H}O} + 0.25\,\mathrm{ROH}$	a
$\mathrm{RO_2}$ + cycl. $\mathrm{R'O_2} \rightarrow 0.3\,\mathrm{RO} + 0.35\,\mathrm{R_{-H}O} + 0.35\,\mathrm{ROH}$	e
$\mathrm{RO_2}$ + tert. $\mathrm{R'O_2} \rightarrow 0.7\,\mathrm{RO} + 0.3\,\mathrm{R_{-H}O}$	b
$\mathrm{RO_2}$ + acyl $\mathrm{R'O_2} \rightarrow 0.86\,\mathrm{RO} + 0.14\,\mathrm{R_{-H}O}$	c
For a tertiary radical $\mathrm{RO_2}$	
$\mathrm{RO_2}$ + prim./sec./cycl. $\mathrm{R'O_2} \rightarrow 0.7\,\mathrm{RO} + 0.3\,\mathrm{ROH}$	b
$\mathrm{RO_2}$ + tert. $\mathrm{R'O_2} \rightarrow \mathrm{RO}$	d
$\mathrm{RO_2}$ + acyl $\mathrm{R'O_2} \rightarrow \mathrm{RO}$	d
For an acyl radical $\mathrm{RC(O)O_2}$	
$\mathrm{RO_2}$ + prim./sec./cycl. $\mathrm{R'O_2} \rightarrow 0.86\,\mathrm{RC(O)O}$+ $0.14\,\mathrm{RC(O)OH}$	c
$\mathrm{RO_2}$ + tert. $\mathrm{R'O_2} \rightarrow \mathrm{RC(O)O}$	d
$\mathrm{RO_2}$ + acyl $\mathrm{R'O_2} \rightarrow \mathrm{RC(O)O}$	d
For a cyclic radical $\mathrm{RO_2}$	
$\mathrm{RO_2}$ + prim./sec./cycl. $\mathrm{R'O_2} \rightarrow 0.3\,\mathrm{RO} + 0.35\,\mathrm{R_{-H}O} + 0.35\,\mathrm{ROH}$	e
$\mathrm{RO_2}$ + tert. $\mathrm{R'O_2} \rightarrow 0.7\,\mathrm{RO} + 0.3\,\mathrm{R_{-H}O}$	b
$\mathrm{RO_2}$ + acyl $\mathrm{R'O_2} \rightarrow 0.86\,\mathrm{RO} + 0.14\,\mathrm{R_{-H}O}$	c

[a] For the cross reactions of primary and secondary RO_2 radicals, Atkinson (1994) suggested a constant ratio of 45±20% for the oxy-forming route at 298 K from the few available data of self-reactions. [b] No experimental data. Value assumed. [c] Based on the measurement of Horie and Moortgat (1992) for the reaction of CH_3O_2 with $CH_3C(O)O_2$ at 298 K. [d] Only one reaction path can occur. [e] Based on the measurement of the self-reactions of *c*-$C_6H_{11}O_2$ made by Rowley et al. (1992).

in α are found to influence the branching ratios.

Because of the large number of RO_2 radicals generated in the mechanism, the explicit representation of their permutation reactions would be too demanding in terms of implementation and computational time. A parameterization is required, of the type proposed by Madronich and Calvert (1990) and Jenkin et al. (1997). Following the same approach as in these studies, the RO_2 radicals are grouped into classes according to their structure. Each class is characterized by a self-reaction rate (Tab. 2.2). The permutation reactions of an explicit RO_2 are represented by the reactions of this compound with pseudo-species representing the different classes. The concentration of a pseudo-species is equal to the sum of the explicit peroxy radicals concentrations in the corresponding class. Whenever a particular peroxy radical is produced or destroyed in the mechanism, the pseudo-species representing its class is also produced

Table 2.2: RO_2 classes and self-reaction rate constants (k_{self}) at 298 K.

RO_2 class		Class notation	k_{self} (cm^3 $molec^{-1}$ s^{-1})
Alkyl	primary	R1R	4.0×10^{-12}
	secondary	R2R	4.0×10^{-13}
	tertiary	R3R	1.0×10^{-16}
β-hydroxy	primary	R1H	8.0×10^{-12}
	secondary	R2H	3.0×10^{-12}
	tertiary	R3H	5.0×10^{-14}
α-hydroxy/ β-carbonyl/			
multifunctional	primary	R1M	1.5×10^{-11}
	secondary	R2M	1.0×10^{-11}
	tertiary	R3M	1.0×10^{-13}
acyl peroxy		RO3	1.5×10^{-11}

or destroyed. The rate constant of the reaction between a given RO_2 and a class is estimated as twice the geometric average of the self-reaction rate constants of the class to which the specific RO_2 belongs ($k_{self(RO_2)}$) with the self-reaction rate constant of the class under interest ($k_{self(class)}$):

$$k_{R2.22} = 2 \times (k_{\mathrm{self}(RO_2)} \times k_{\mathrm{self(class)}})^{1/2}. \quad (2.15)$$

An important exception to this rule is the case of the reactions of acyl peroxy radicals with other RO_2, as discussed further below. The classes are defined according to the substitutions and chemical functionalities (hydroxy, carbonyl, or allyl), if any, in α or β position.

Since the photooxidation of α-pinene produces mostly $C_{\geq 7}$ peroxy radicals, the cross reactions involve mostly large radicals in laboratory conditions. In the atmosphere, the reactions of large α-pinene radicals with smaller radicals (e.g. CH_3O_2 and radicals from isoprene) might be important as well. However, since our current focus is mainly on laboratory conditions, we limit our classification to large ($C_{\geq 7}$) radicals. The literature data for the self-reaction rates of peroxy radicals are reported in Tab. 2.3. Based on these values, the self-reaction rates adopted for each class are discussed below. The notations used here for the different classes are as in Tab. 2.2.

Alkyl peroxy radicals (R1R, R2R, R3R)
Experimental data exist for primary alkyl radicals (R1R) of different structures. Lightfoot et al. (1992) and Boyd et al. (1999) measured the self-reaction rate of the linear primary radicals up to *n*-$C_5H_{11}O_2$. However, the presence of a double bond or a substitution in β in a primary radical appears to increase its k_{self} as e.g. for $C(CH_3)_3CH_2O_2$ and $CH_2(OH)C(CH_3)=C(CH_3)CH_2O_2$ (Jenkin et al., 1998). The radicals generated in our mechanism are usually substituted. Therefore we assume that the structure of the neo-pentyl radical ($C(CH_3)_3CH_2O_2$) is representative of the primary peroxy radi-

Table 2.3: Self-reaction rates (k_{self}) of RO_2 radicals measured at 298 K.

RO_2	k_{self}		RO_2	k_{self}	
Primary alkyl/allyl (R1R)			*Secondary hydroxy (R2H)*		
CH_3O_2	$3.7(-13)^\star$	a	$CH_3CH(OH)CH(O_2)CH_3$	$6.9(-13)$	f
$C_2H_5O_2$	$6.6(-14)$	a	*c*$-C_6H_{10}(OH)O_2$	$1.6(-12)$	j,k
n$-C_3H_7O_2$	$3.9(-13)$	a			
n$-C_5H_{11}O_2$	$3.9(-13)$	e	*Tertiary hydroxy (R3H)*		
$C(M)_3CH_2O_2$	$1.2(-12)$	a	$C(M)_2(OH)C(M)_2O_2$	$4.0(-15)$	f
$CH_2{=}CHCH_2O_2$	$6.9(-13)$	b	$C(M)_2O_2CH_2OH$	$1.5(-14)$	j
$CH_2(OH)CH{=}CHCH_2O_2$	$2.8(-12)$	c	*c*$-C_6H_8(M)_2(OH)O_2$	$2.0(-14)$	j,l
$CH_2(OH)C(M){=}C(M)CH_2O_2^{\star\star}$	$3.9(-12)$	c			
			Primary α-hydroxy/		
Secondary alkyl (R2R)			*α-carbonyl/ multifunctional (R1M)*		
i$-C_3H_7O_2$	$1.1(-15)$	a	$CH_2(OH)O_2$	$6.2(-12)$	a
c$-C_5H_9O_2$	$4.5(-14)$	a	$CH_3C(O)CH_2O_2$	$8.3(-12)$	a
c$-C_6H_{11}O_2$	$4.2(-14)$	a			
sec$-C_5H_{11}O_2$	$3.3(-14)$	e	*Secondary α-hydroxy/*		
sec$-C_{10}H_{21}O_2$	$9.4(-14)$	e	*α-carbonyl/ multifunctional (R2M)*		
sec$-C_{12}H_{25}O_2$	$1.4(-13)$	e	$CH_2(OH)CH(O_2)CH{=}CH_2$	$5.7(-12)$	c
Tertiary alkyl (R3R)			*Tertiary α-hydroxy/*		
$(M)_3CO_2$	$3.3(-17)$	a	*α-carbonyl/ multifunctional (R3M)*		
			$CH_2(OH)C(M)(O_2)C(M){=}CH_2$	$6.9(-14)$	c
Primary hydroxy (R1H)					
$CH_2(OH)CH_2O_2$	$2.3(-12)$	f	*Acyl peroxy radicals (RO3)*		
$(M)_2C(OH)CH_2O_2$	$4.8(-12)$	g	$CH_3C(O)O_2$	$1.6(-11)$	h
			$(M)_2CHC(O)O_2$	$1.4(-11)$	i
			$(M)_3CC(O)O_2$	$1.4(-11)$	i

* Notation is $3.7(-13) = 3.7 \times 10^{-13}$ ** M represents the methyl substitution "CH_3" [a]Lightfoot et al. (1992) [b] Boyd et al. (1996a) [c] Jenkin et al. (1998) [e] Boyd et al. (1999) [f]Boyd et al. (1997) [g] Boyd et al. (1996b) [h] Atkinson et al. (2003) [i] Tomas and Lesclaux (2000) [j] Boyd et al. (2003) [k] 2-hydroxycyclohexyl peroxy radical [l] 2-hydroxy-1,2-dimethylcyclohexyl peroxy radical

cals in our model. Since the k_{self} for non-linear alkyl radicals increases slightly with carbon number, we set the self-reaction rate to 4.0×10^{-12} cm^3 molec^{-1} s^{-1} for the R1R class. Boyd et al. (1999) parameterized the self-reaction rates of linear secondary alkyl peroxy radicals (R2R) as a function of the carbon number n:

$$\log k_{(\textit{sec-}RO_2+\textit{sec-}RO_2)} = -13.0 - 3.2\exp\left(-0.64\times(n-2.3)\right). \quad (2.16)$$

Taking $n = 8$ in Eq. 2.16, and assuming that this rate is somewhat higher due to the numerous allyl and substituted secondary radicals present in the mechanism, a k_{self} of 4.0 $\times10^{-13}$ cm^3 molec^{-1} s^{-1} is chosen for the R2R class. Few data exist for the alkyl tertiary radicals (R3R). Lightfoot et al. (1992) reported a very low value of k_{self} for $(CH_3)_3CO_2$. We assume a value of 1.0×10^{-16} cm^{-3} molec^{-1} s^{-1} to represent the R3R class.

β-hydroxy peroxy radicals (R1H, R2H, R3H)

The measurements performed by Lesclaux and coworkers (Boyd et al., 1996b, 1997, 2003) show that the presence of a β-hydroxy functionality on the peroxy radical increases significantly the self-reaction rate. On the basis of their experimental values, the k_{self} of primary radicals (R1H class) is extrapolated to 8.0×10^{-12} cm^{-3} molec^{-1} s^{-1} for R1H radicals generated by the α-pinene oxidation. Following the same approach, the self-reaction rates of β-hydroxy secondary (R2H) and tertiary (R3H) radicals are set to 3.0×10^{-12} cm^{-3} molec^{-1} s^{-1} and 5.0×10^{-14} cm^{-3} molec^{-1} s^{-1}, respectively. Boyd et al. (2003) measured the cross reaction rate between a R2H and a R3H C_7 radical. Using Eq. 2.15 with our estimated self-reaction rates, we calculate a cross reaction rate in fair agreement with their experimental data of 6.2×10^{-13} cm^{-3} molec^{-1} s^{-1}.

α-hydroxy/β-carbonyl/multifunctional peroxy radicals (R1M, R2M, R3M)

Measurements of self-reaction rates for α-hydroxy and β-carbonyl substituted primary alkyl peroxy radicals show high rate values (Lightfoot et al., 1992). A value of 1.5×10^{-11} cm^3 molec^{-1} s^{-1} is chosen for this class (R1M). In absence of more measurement data, we consider this rate as an overall upper limit for the peroxy radicals k_{self}, and compounds containing more than one functionality among hydroxy, carbonyl and allyl substitutions in α or in β are also included in this class. Based on the measurements of Jenkin et al. (1998), rates of 1.0×10^{-11} and 1.0×10^{-13} cm^{-3} molec^{-1} s^{-1} are used for the corresponding secondary (R2M) and tertiary (R3M) classes, respectively.

Acyl peroxy radicals (RO3)

Experimental evidence indicates that the cross reaction rates of acyl peroxy radicals (RO3) with all the other peroxy radicals are of the same order of magnitude (1-1.25×10^{-11} cm^3 molec^{-1} s^{-1}) (Villenave and Lesclaux, 1998; Atkinson et al., 2003). A value of 1×10^{-11} cm^3 molec^{-1} s^{-1} is adopted for these reactions. The rate of the pseudo-reaction between an acyl peroxy radical and the RO3 class is set to 1.5×10^{-11} cm^3 molec^{-1} s^{-1}, based on the measurement of the self-reaction rate constant of $(CH_3)_3CC(O)O_2$ (Tomas and Lesclaux, 2000).

2.3.3 "Exotic" peroxy radical reactions in the oxidation of alpha-pinene

As described in Peeters et al. (2001), the reaction of a large secondary (or tertiary) α-hydroxy alkyl radical with O_2 produces an activated peroxy radical RCH(OH)$O_2^\dagger$ (or R'C(OH)O_2R†). The activated peroxy radical can either stabilize collisionally or decompose thermally in competing reactions. In the case of RCH(OH)$O_2^\dagger$:

$$\mathrm{RCH(OH)O_2}^\dagger \rightarrow \mathrm{RCHO + HO_2} \quad \text{(R2.23a)}$$

$$\mathrm{RCH(OH)O_2}^\dagger \rightarrow \mathrm{RCH(OH)O_2}. \quad \text{(R2.23b)}$$

On the basis of an RRKM analysis, Hermans et al. (2005) estimated the prompt decomposition rates for the nascent chemically activated $HOCH_2O_2^\dagger$, $CH_3CH(OH)O_2^\dagger$ and $C(CH_3)_2(OH)O_2^\dagger$ to be on the order of 10^{10} s^{-1}, and their effective stabilization rates were found to lie in the range 10^4–10^{-1} s^{-1}. These results are in agreement with the available experimental data. For the much larger radicals involved in the oxidation of α-pinene, prompt decomposition and stabilization rates should be more competitive. Using RRKM, the ratio $k_{R2.23a}/k_{R2.23b}$ is estimated to be about 10/90 and 25/75 in the cases of $R_{13}O_2^\dagger$ and $R_3O_2^\dagger$ (Fig. 2.2), respectively . The probable error on these ratios is a factor of 2.5. The stabilized α-hydroxy peroxy radical RCH(OH)O_2 can either decompose or be oxidized via the traditional reactions with NO, HO_2 and RO_2 radicals as described in Sec. 2.3.2. In presence of NO, two reactions compete with each other:

$$\mathrm{RCH(OH)O_2} \rightarrow \mathrm{RCHO + HO_2} \quad \text{(R2.24)}$$

$$\mathrm{RCH(OH)O_2 + NO} \rightarrow \mathrm{RCH(OH)O + NO_2}. \quad \text{(R2.25)}$$

The α-hydroxy alkoxy radical produced in the reaction (R2.25) decomposes and producing HCOOH (or R'C(O)OH in the case of the decomposition of RC(OH)O_2R'†):

$$\mathrm{RCH(OH)O} \rightarrow \mathrm{R + HCOOH}. \quad \text{(R2.26)}$$

The rate of the thermal decomposition reaction (R2.24) is strongly dependent on the degree of substitution of the alpha-hydroxy peroxy radical. Hermans et al. (2005) estimated the decomposition rates of $HOCH_2O_2$ (primary), $CH_3CH(OH)O_2$ (secondary) and $C(CH_3)_2(OH)O_2$ (tertiary) to 201 s^{-1}, 2710 s^{-1} and 29 300 s^{-1} at 300 K, respectively. These results are in good agreement with the available experimental data, although the measured decomposition rate of $CH_3CH(OH)O_2$ is somewhat lower (1870 s^{-1} at 298 K) than the theoretical estimate by Hermans et al. (2005).

In the case of $R_{13}O_2$ and R_3O_2 in the α-pinene+OH mechanism, the fairly strong H-bond between the hydroxyl-H and the carbonyl-O should somewhat slow down the decomposition, but as this bond is entropically disfavored, the thermal decomposition rate $k_{R2.24}$ is reduced by only a factor of 1.5. For $R_{13}O_2$, we adopt the experimental value of 1870 s^{-1} for secondary radicals, but reduced by a factor of 1.5, i.e. $k_{R2.24}$ = 1250 s^{-1}. For R_3O_2, given the absence of experimental data for the tertiary case,

we adopt the estimate by Hermans et al. (2005) again reduced for the hydroxyl-to-aldehyde hydrogen bonding, setting $k_{R2.24}$ to 1.9×10^4 s^{-1} at 298 K. Since HCOOH is mainly produced from reaction R2.26 in our mechanism, the laboratory measurement of the formic acid yield by Orlando et al. (2000) (7% yield for [NO]=$2-22\times10^{14}$ molecules cm^{-3}) partly validates the rates adopted here for $R_{13}O_2^\dagger$ and $R_{13}O_2$. The yield estimated from our mechanism ranges from $\sim$2% at 2 ppm to 16% at 20 ppm NO. The statistical average over the 2–20 ppm range is $\sim$10%, i.e. reasonably close to the measurement. Reaction R2.25 involving $R_{13}O_2$ competes with R2.24 for NO $\gg$ 100 ppb. Because of the faster decomposition rate of R_3O_2, its reaction with NO becomes effective for NO $\gg$ 5 ppm. Under these conditions, the overall product yields in the α-pinene oxidation are dependent on the concentration of NO. In particular, the yields of pinonaldehyde and acetone are determined by the fate of the radicals R_3O_2 and $R_{13}O_2$ (Fig. 2.2).

2.3.4 Chemistry of the primary products

The OH-oxidation rates of the first generation products in the degradation of α-pinene can be estimated using the structure-reactivity approach (SAR) proposed by Kwok et al. (1995). The estimated rates for the compounds present in the mechanism range from 1×10^{-12} to 7×10^{-11} cm^3 $molecule^{-1}$ sec^{-1} depending on the structure of the compound considered. These compounds presenting no double bonds, the reaction with ozone is neglected. The estimation of their photolysis rate is described in the next section. The oxidation mechanism of small organic compounds such as acetone, methyl vinyl ketone, or acrolein is taken from the MCM mechanism (Saunders et al., 2003) or the NCAR master mechanism MM2.1 (Madronich and Calvert, 1989). However there are no published degradation mechanism for larger compounds, to the exception of pinonaldehyde. A detailed investigation of such degradation mechanisms would be beyond the scope of the present study. A simplified representation is therefore adopted. Our aim is to represent the main impact of the oxidation of primary products, i.e. the generation of a chain of peroxy radicals reactions which, in high NO conditions, contribute to NO to NO_2 conversion and to organic nitrate production. We assume here that the unknown chemistry of primary products proceeds in ways similar to the explicit mechanism. Based on this similarity assumption, we estimate to about 4 the average number of successive peroxy radical reactions necessary to generate a stable compound from the oxidation of a typical (C_9 or C_{10}) product in high NO_x conditions, about half of which are $C_{\geq7}$ peroxy radical reactions. Due to the marked dependence of the nitrate yield on the size of the peroxy radicals in RO_2+NO reactions, it is found useful to distinguish between large ($C_{\geq7}$) peroxy radicals produced from the oxidation of primary products, noted LXO2, and smaller ($C_{<7}$) radicals, noted SXO2.

Based on these observations, the oxidation of $C_{\geq7}$ products is represented as a

unique reaction producing generic peroxy radicals:

$$\mathrm{C}_{\geq 7}\ \mathrm{product} + \mathrm{OH} \rightarrow \lambda \sum_{i=1}^{n} \alpha_i\ \mathrm{LXO2}_i, \tag{R2.27}$$

$\mathrm{LXO2}_i$ is a generic peroxy radical $\mathrm{C}_{\geq 7}$ of class i, as defined in Tab. 2.2. λ represents the assumed average number of oxidation steps necessary to obtain a radical of carbon number lower than 7 and is taken equal to 2 based on the above considerations. The distribution of the generic peroxy radicals among the different classes is defined by the stoichiometric coefficients α_i. It is assumed to be similar to the distribution of the different peroxy radicals classes present in the explicit mechanism. The sum of the α_i of the different classes i is equal to unity. Based on a simple count of the number of peroxy radicals in each class in the α-pinene mechanism, the "RxH" and "RxM" (x=1,2 or 3) classes are found to be dominant. The distribution is parameterized as follows: α_{RxR}=0.06, α_{RxH}=0.1, α_{RxM}=0.1, α_{RO3}=0.2.

These LXO2 radicals react with NO, (NO_2 in the case of the acyl peroxy radicals) HO_2 and the other RO_2 radicals, producing stable products and smaller ($\mathrm{C}_{<7}$) generic peroxy radicals SXO2. E.g. for the generic radicals others than the acyl peroxy radicals class:

$$\mathrm{LXO2_i} + \mathrm{NO} \rightarrow \mathrm{NO_2} + \sum_{i=1}^{n} \alpha_i\ \mathrm{SXO2_i} \tag{R2.28a}$$

$$\mathrm{LXO2_i} + \mathrm{NO} \rightarrow \mathrm{LXONO_2} \tag{R2.28b}$$

$$\mathrm{LXO2_i} + \mathrm{HO_2} \rightarrow \mathrm{LXOOH} + \mathrm{O_2} \tag{R2.29}$$

$$\mathrm{LXO2_i} + \mathrm{RO_2} \rightarrow a \sum_{i=1}^{n} \alpha_i\ \mathrm{SXO2_i} + b\ \mathrm{LXOH} + c\ \mathrm{LXCHO}. \tag{R2.30}$$

The SXO2 radicals react in the same manner and terminate the propagation chain:

$$\mathrm{SXO2_i} + \mathrm{NO} \rightarrow \mathrm{NO_2} \tag{R2.31a}$$

$$\mathrm{SXO2_i} + \mathrm{NO} \rightarrow \mathrm{SXONO_2} \tag{R2.31b}$$

$$\mathrm{SXO2_i} + \mathrm{HO_2} \rightarrow \mathrm{SXOOH} + \mathrm{O_2} \tag{R2.32}$$

$$\mathrm{SXO2_i} + \mathrm{RO_2} \rightarrow b\ \mathrm{SXOH} + c\ \mathrm{SXCHO}. \tag{R2.33}$$

The coefficients a, b and c in (R2.30) and (R2.33) depend on the structure of the radicals $\mathrm{LXO2}_i$ and $\mathrm{SXO2}_i$ (see Tab. 2.1). $\mathrm{LXO2}_{RO3}$ and $\mathrm{SXO2}_{RO3}$ produce the generic products LXPAN,LXCOOH and LXCOOOH following the same approach. The $\mathrm{C}_{<7}$ primary products are treated as their $\mathrm{C}_{\geq 7}$ counterparts:

$$\mathrm{C}_{<7}\ \mathrm{products} + \mathrm{OH} \rightarrow \lambda \sum_{i=1}^{n} \alpha_i\ \mathrm{SXO2_i}. \tag{R2.34}$$

The coefficients λ and α_i in Eq. R2.34 are assumed to be the same as in Eq. R2.27.

The subsequent reactions of radicals for which the chemistry is still speculative are also treated following Eq. R2.27 or R2.34, depending on the carbon number of the radical considered. For example, in the case of the R_{11} radical (Fig. 2.2), we write:

$$\mathrm{R_{11}} \rightarrow 2 \sum_{i=1}^{n} \alpha_i \, \mathrm{LXO2_i}. \qquad \text{(R2.35)}$$

2.4 Photodissociation processes

2.4.1 Atmospheric conditions

As already discussed in the Introduction, photodissociation reactions play a crucial role in the atmosphere, in particular for the main oxidants OH and O_3, and consequently for the overall photochemistry in the atmosphere. The photodissociation coefficient (J-value) for a given photolytic process i is calculated as

$$J_i = \int_\lambda I(\lambda) \times \sigma_i(\lambda) \times \phi_i(\lambda) \times d\lambda \tag{2.17}$$

where λ is the wavelength, $I(\lambda)$ is the actinic flux, and $\sigma_i(\lambda)$ and $\phi_i(\lambda)$ are the absorption cross section and the photolysis quantum yield, respectively.

The actinic flux is defined as the radiative flux incident on a given volume of air, from all directions. Light absorption and scattering by atmospheric constituents attenuate solar radiation as it passes through the atmosphere. This attenuation depends on the nature and concentration of the gases and particles, and on the path followed by the light rays. The pathlength is a function of the angle of the Sun, i.e. the latitude and date. The light intensity incident on a given volume of air includes not only the direct solar beam, but also indirect light either reflected by the Earth's surface or by clouds, or scattered into the volume by gases and particles (Fig. 2.6).

Figure 2.7 shows the solar flux I as a function of wavelength outside the atmosphere and at the sea level. The absorption by various atmospheric constituents, mainly O_2, O_3, H_2O and CO_2 is represented by the shaded areas. Mostly because of the presence of oxygen and ozone, only light of $\lambda>$290 nm is available for photochemical reactions in the atmosphere. Water vapour has complex absorption bands, especially for $\lambda>$800 nm. Absorption by atmospheric gases is moderate between 300 and 800 nm, leaving a "window" centered on the visible solar spectrum where the atmosphere can be considered as transparent to the solar energy. The position of the sun relative to a fixed point on the Earth's surface is characterized by the solar zenith angle θ defined as the angle between the direction of the sun and the vertical passing by the point. The larger values of θ in winter, compared to summer, result in a longer path through the atmosphere and hence in a greater reduction in solar intensity by absorption and scattering processes (Seinfeld and Pandis, 1998).

The reduction of the intensity of the direct solar beam can be estimated using the Beer-Lambert law:

$$\frac{I}{I_0} = \exp(-tm). \tag{2.18}$$

I_0 is the light intensity at a given wavelength incident at the top of the atmosphere and I is the intensity of the light transmitted to the earth's surface. m is the air mass parameter, defined as the ratio of the length of path of the direct solar beam though

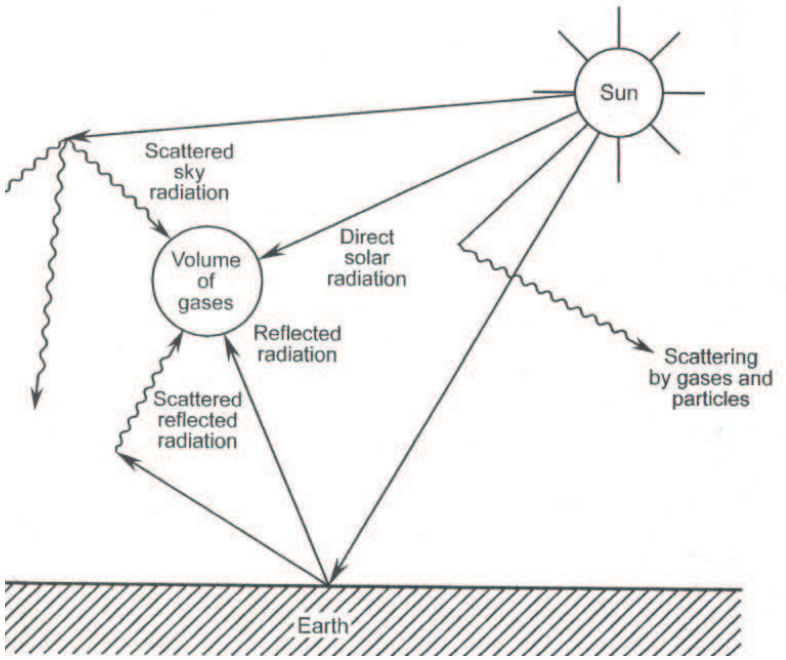

Figure 2.6: Paths followed by solar radiations in the atmosphere (Finlayson-Pitts and Pitts, 2000)

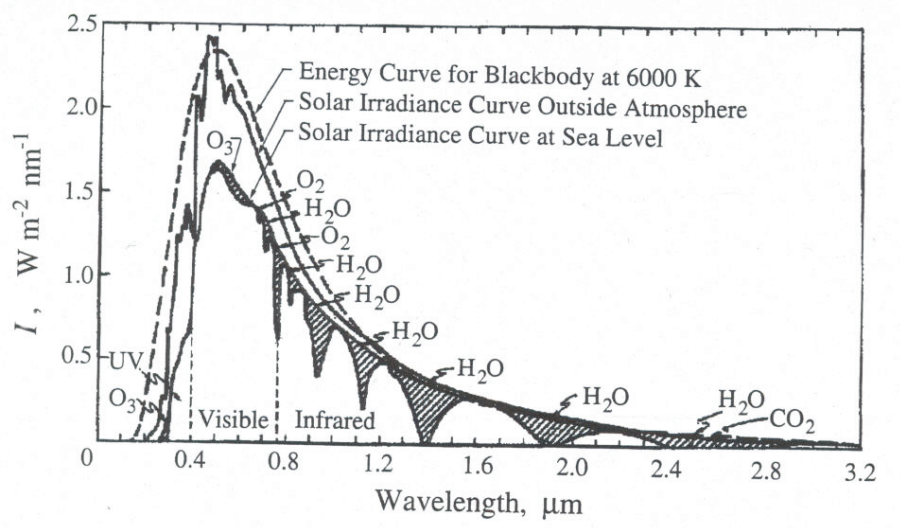

Figure 2.7: Solar spectral irradiance I at the top of the atmosphere and at sea level (overhead sun). The emission of a blackbody at 6000K is also shown for comparison. Shaded regions correspond to absorption by the molecules (Seinfeld and Pandis, 1998).

the atmosphere to a surface point to the length of the vertical path passing by this point. The attenuation coefficient t defined for an overhead sun is a sum of terms :

$$t = t_{ag} + t_{sg} + t_{sp} + t_{ap}, \tag{2.19}$$

where ag represents light absorption by gases, sg, light scattering by gases, sp, light scattering by particles, and ap, light absorption by particles. Scattering by gaseous molecules (Rayleigh scattering) is influenced by a number of factors including the structure of the molecule and the incident angle. However, Rayleigh scattering can be simplified for application to the atmosphere and can be expressed using an averaged index of refraction of air function of temperature, pressure and wavelength. The strong dependence of Rayleigh scattering with wavelength ($\sim \lambda^{-4}$) can be noted in Fig. 2.8.

The Mie theory addresses the problem of light absorption and scattering by a spherical particle. Despite the elegance of this theory, its application to the atmosphere is a complex matter. The size distribution, the chemical composition as well as the concentration of the particles are very important in determining the extent of light scattering. These parameters show large geographical, seasonal and diurnal variations, making difficult to estimate their impact at a particular location at the earth's surface. The literature refers to the term "aerosol extinction" defining the sum of the absorption and light scattering attenuation coefficients. Many standard profiles of aerosol attenuation coefficients based on observations have been proposed in the literature (e.g. Elterman (1968)). One estimate is shown in Fig. 2.8.

The reflection of light by the Earth's surface or by clouds is quantified by the albedo. It represents the fraction of solar energy which is reflected back from Earth to space. Different surface types have different albedos. For example, rain forests have low albedos, which means that they reflect only a small portion of the sun's energy whereas ice and clouds have high albedos. The albedo is parameterized for different surface types, and is a function of wavelength.

2.4.2 Laboratory conditions

The photolysis rates in a laboratory chamber depend on the experimental setup. In the case of laboratory studies aiming at reproducing atmospheric conditions, ambient light can be used, as e.g. in the experiments performed in the EUPHORE chamber (Fig. 2.9). The experimental conditions in these reactors are relatively close to the atmosphere in term of pressure, temperature and photolytic conditions, while the air in the reactor remains isolated from transport and emission effects.

However, it can be desired to study experimentally a particular chemical process as in the case of chemical kinetics studies or investigations of products yields in the oxidation of an hydrocarbon by a specific oxidant. Improved controlled conditions are seeked and smaller indoor smog chambers are preferred in this case (Fig. 2.10).

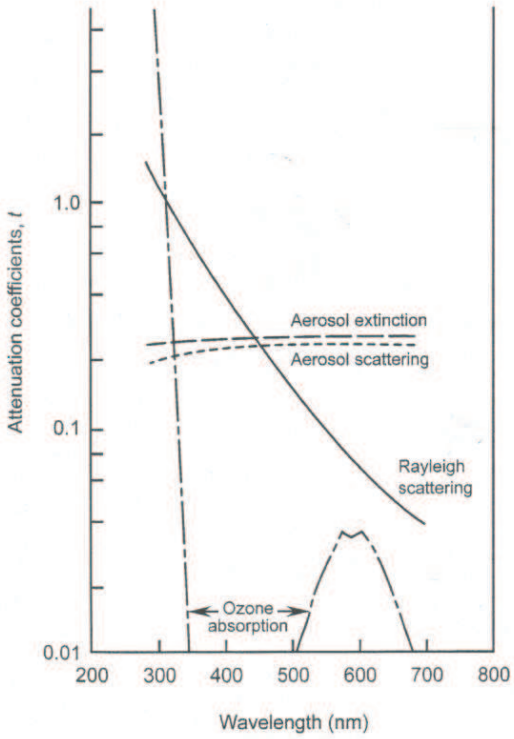

Figure 2.8: Attenuation coefficients t for Rayleigh scattering, ozone absorption, aerosol scattering and extinction (Finlayson-Pitts and Pitts, 2000).

Temperature and light intensity control is made possible by the use of artificial radiation. Additional advantages of the indoor approach include the reduction of thermal gradients and less flow agitation. However, the emission spectrum as well as the intensity of these lamps can differ from solar light, so that the photolytic conditions in the reactor differ markedly from those in the atmosphere. In the case of the study of a VOC+OH reaction, the production of the OH radical is maintained through the photolysis of a OH-precursor. The choice of the lamp(s) used in indoor experiments is thus determined in part by the photolytic parameters of the radical precursor. Due to these factors, the impact of photolysis might differ from one experimental set up to another, affecting the entire chemical regime of the system, e.g. the oxidizing rate of the hydrocarbon studied or the loss of the products by photolysis. Therefore, modeling a photooxidation experiment requires a good parameterization of the light radiating in the reactor and the photodissociation rates of the compounds in the system.

As an example of photolytic conditions in indoor smog chambers, we focus now on the experiments performed by Nozière et al. (1999a) (N99). The simulations of these experiments using a box model will be presented and discussed in Chapter 4. N99 have performed series of experiments of α-pinene oxidation by OH in presence of either visible or UV light.

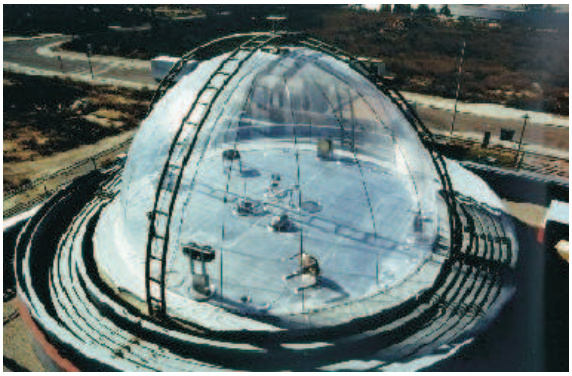

Figure 2.9: The European Photoreactor (EUPHORE) in Valencia/Spain (Brockmann et al., 1996)

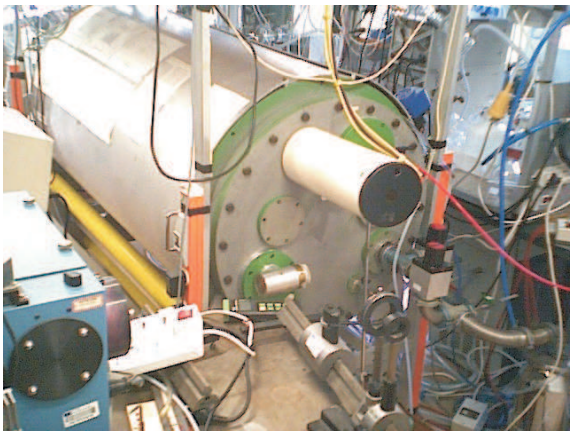

Figure 2.10: A 480 L reaction chamber at the Joint Research Institute, Ispra, Italy (http://carbodat.ei.jrc.it)

As in most experiments dedicated to the OH-photooxidation of VOC, the photochemistry is initiated by the photodissociation of an OH precursor, which is either H_2O_2 :

$$\mathrm{H_2O_2} + h\nu \rightarrow 2\mathrm{OH}, \tag{R2.36}$$

or CH_3ONO :

$$\begin{aligned} \mathrm{CH_3ONO} + h\nu &\rightarrow \mathrm{CH_3O} + \mathrm{NO} && \text{(R2.37)} \\ \mathrm{CH_3O} + \mathrm{O_2} &\rightarrow \mathrm{CH_2O} + \mathrm{HO_2} && \text{(R2.38)} \\ \mathrm{NO} + \mathrm{HO_2} &\rightarrow \mathrm{NO_2} + \mathrm{OH}. && \text{(R2.39)} \end{aligned}$$

CH_3ONO is often used as a source of OH radicals because it photodissociates rapidly under UVA (320-400 nm) light. However, this source yields high concentrations of formaldehyde as a side product, which makes difficult to quantify the direct formaldehyde production from the hydrocarbon oxidation. H_2O_2 can be preferred in order to

avoid this contamination and to allow experimental studies in absence of nitrogen oxides.

In the N99 experiments, both OH-precursors have been used. H_2O_2 is photolyzed by TUV mercury lamps emitting short-wave ultraviolet radiation with a concentrated radiation peak at 253.7 nm. In the second case, TL-05 mercury lamps (Philips, λ_{max} = 360 nm) are used. The lamp spectra are shown in Fig. 2.11 as well as a typical solar spectrum at ground level. The intensity of the lamps reported in the figure are those estimated for the N99 experiments. Because the TL-05 lamps radiate mostly in the 300-480 nm range, they are often considered more appropriate to represent solar radiation in real tropospheric conditions. The experiments performed using TL-05 and TUV lamps will hereafter be referred as "visible" and "UV" experiments, respectively.

The actinic flux $I(\lambda)$ (Eq. 2.17) has not been directly measured in the N99 experiments but it can be related to measurable quantities by writing

$$I(\lambda) = I_0 \times f(\lambda) \tag{2.20}$$

where $f(\lambda)$ is either the TUV or TL-05 normalized lamp spectrum, and I_0 is a scaling factor adjusted so that J(H_2O_2) or J(CH_3ONO) calculated using Eq. 2.17 matches the observed decay rate of H_2O_2 or CH_3ONO in the reactor. The following average photorates are deduced from the observations of H_2O_2 and CH_3ONO in the N99 experiments:
J(H_2O_2) $= 1.0 \times 10^{-3} s^{-1}$
J(CH_3ONO) $= 9.1 \times 10^{-4} s^{-1}$.
These values are corrected for minor effects due to secondary reactions influencing CH_3ONO and H_2O_2. The derivation of I_0 is straightforward, because the photolytic parameters for both precursors are well known. The absorption spectrum of CH_3ONO resembles the one of HNO_2 (Fig. 2.12), which is often used as a surrogate for CH_3ONO. The absorption cross sections spectrum of CH_3ONO is roughly lower by a factor 1.5 and shifted by 16 nm to the shorter wavelengths with respect to the spectrum of HNO_2. The photolytic rates in the N99 experiments can be estimated using these deduced actinic fluxes and the photodissociation parameters of the α-pinene oxidation products, which are discussed in the following subsection.

Note that most experimental studies of the reaction VOC+O_3 are performed in the dark. The absence of light is preferred in ozonolysis studies because it prevents the photolysis of O_3. Furthermore, the loss of products by photodissociation is avoided. The ozonolysis experiments simulated in this work correspond to these conditions.

2.4.3 Determination of the photodissociation rates

The photooxidation of VOC produces organic compounds such as carbonyls, organic nitrates, peroxy acyl nitrates and hydroperoxides which can all photodissociate (photolysis of alcohols or organic acids is negligible in sunlight conditions). The

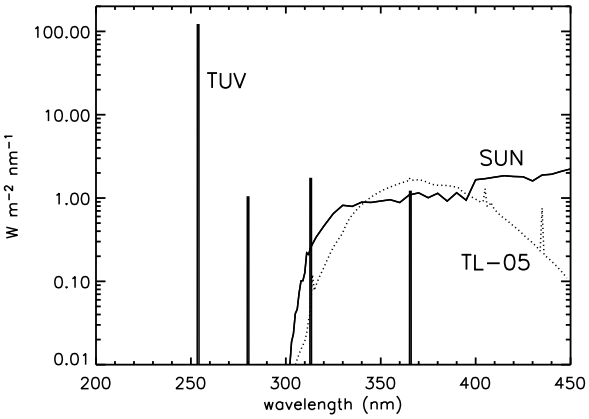

Figure 2.11: Actinic fluxes of the TUV and TL-05 lamps used in N99. A solar spectrum (ground level, standard atmosphere, zenith angle=45°) is also shown for comparison (solid line).

photolysis of inorganic as well as diverse small organic compounds has been investigated in the laboratory (Atkinson et al., 2003) and their photolysis parameters ($\sigma_i(\lambda)$ and $\phi_i(\lambda)$) are well known. The plethora of products generated in the degradation of α-pinene by OH consists mostly of compounds bearing one or several chemical functionalities. To the exception of pinonaldehyde, their photodissociation has not been directly investigated in the laboratory. Therefore, their photolytic parameters are based on those of (smaller) compounds of similar structures.

The photodissociation processes for which the absorption cross sections and the quantum yields are known from laboratory studies are listed in Tab. 2.6 (page 61). The corresponding "J-values" were calculated for both the UV and visible experiments in N99. The photolysis rates for typical tropospheric conditions (ground level, zenith angle of $45°$) given in this table have been estimated using the TUV radiative transfer model (Madronich and Flocke, 1998). Tab. 2.7 (page 62) summarizes the reactions and rates for the compound classes for which the photolysis parameters are deduced. The reference species on which the estimations are based are also indicated in the table. Pinonaldehyde and organic nitrates are important special cases and will be discussed in the next sections.

Pinonaldehyde

The absorption cross sections of pinonaldehyde have been measured by Hallquist et al. (1997) between 275 and 345 nm. Being a keto-aldehyde, it can be expected to photolyze following both aldehydic and ketone dissociation channels. In the first case, by analogy with other aldehydes like *n*-pentanal (Tadic et al., 2001a) and *n*-hexanal (Tadic et al., 2001b), intramolecular rearrangements and fragmentations into free radicals are expected to take place. One radical channel (R2.40a) (Norrish-

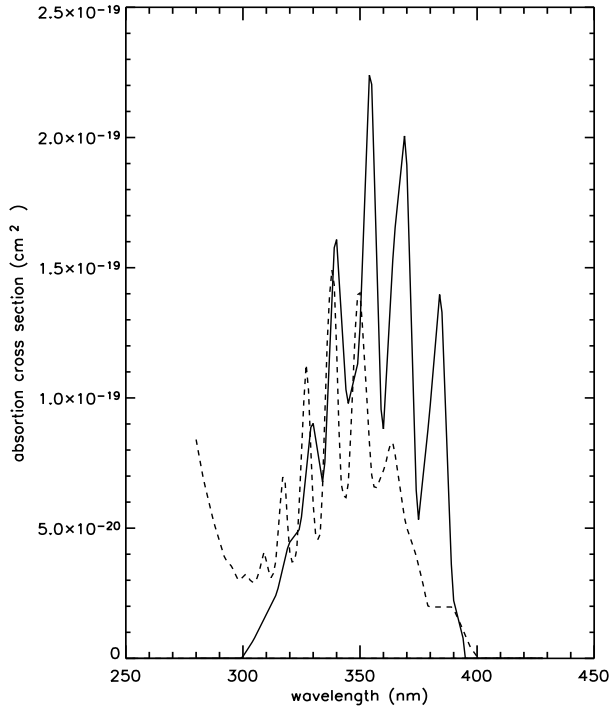

Figure 2.12: CH_3ONO (dotted line) and HNO_2 (solid line) absorption cross sections.

Type I) and two molecular channels (R2.40b) and (R2.40c) (Norrish-Type II) can be considered (PINALD stands for pinonaldehyde) :

$$\mathrm{PINALD} + h\nu \rightarrow \mathrm{CHO} + \mathrm{R}_{17} \quad \text{(R2.40a)}$$

$$\mathrm{PINALD} + h\nu \rightarrow \mathrm{CH_2{=}CHC(O)CH_3} + \mathrm{CH_3C(CH_3){=}CHCH_2CHO} \quad \text{(R2.40b)}$$

$$\mathrm{PINALD} + h\nu \rightarrow \mathrm{CH_3C(O)CH{=}C(CH_3)CH_3} + \mathrm{CH_2{=}CHCH_2CHO}. \quad \text{(R2.40c)}$$

The molecular channels are assumed to proceed through two energetically favored symmetric cleavages of the strained four-membered ring. In absence of experimental data, the two resulting molecular channels are assumed to have the same probability. Chemistry subsequent to R_{17} in Eq. R2.40a is already described in the pinonaldehyde+OH mechanism.

The ketone dissociation channel can be assumed to proceed by cleavage of the CH_3CO-R bond of pinonaldehyde, based on the example of methyl ethyl ketone (Atkinson et al., 2003) :

$$\mathrm{PINALD} + h\nu \rightarrow \mathrm{R}_4 + \mathrm{CH_3CO}. \quad \text{(R2.40d)}$$

This path is shown in Fig. 2.4. Tadic et al. (2001a, 2001b, 2002) measured the relative importance of the different photolysis channels of aldehydes. Their experiments between 275 and 380 nm showed that the contribution of the molecular channel increases slowly with chain length : 70% for *n*-pentanal, 73% for *n*-hexanal and 80% for

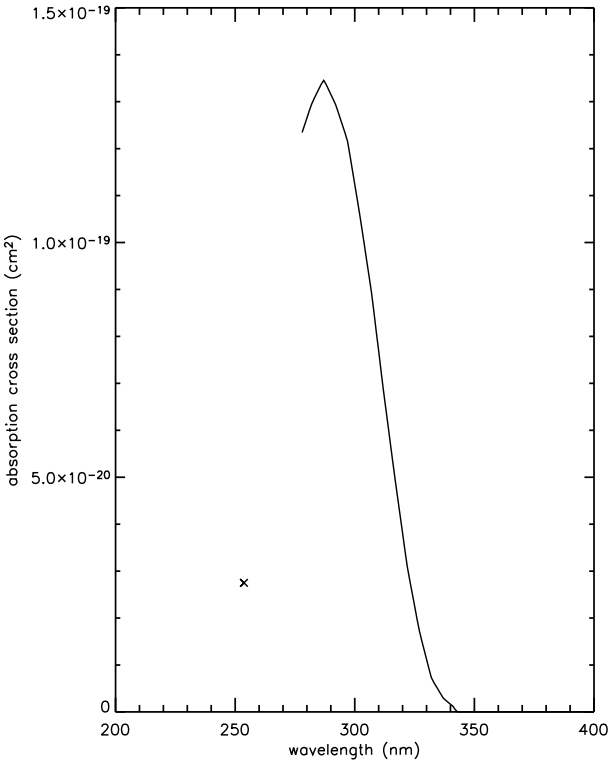

Figure 2.13: Pinonaldehyde absorption cross sections from Hallquist et al. (1997) (solid line). The value at 253.7 nm (cross) is estimated in this study.

n-heptanal. The average quantum yields (averages weighted by the lamp spectrum and the absorption cross sections) were measured to be 0.32, 0.34, 0.38 and 0.31 at 700 Torr for C_4-C_7 alkanals. They all show a similar dependence on total pressure. It should be noted however, that Desai et al. (1986) and Atkinson et al. (2003) reported substantially higher quantum yields for propanal and isobutanal. Based on these studies, we calculate average quantum yields of 0.70 and 0.66 for these two species, respectively (averages weighted by their respective absorption cross sections (Atkinson et al., 2003) and by the spectrum of the lamp used in Tadic et al.). The origins of this difference are unclear.

We assume here that the averaged quantum yield of n-hexanal (0.38) can be used for the aldehydic channels of pinonaldehyde, with probabilities of 27% and 73% for the Norrish-Type I and II, respectively. These yields are assumed to be essentially independent on wavelength. The wavelength-dependent quantum yields of methyl ethyl ketone (MEK) is used for the ketone photodissociation channel. Below 290 nm, the quantum yields are scaled down so that the total quantum yield does not exceed 1. The estimated pinonaldehyde quantum yields are shown in Tab. 2.4. It can be seen that the ketone dissociation channel is expected to be dominant in the UV, while the aldehydic channels are expected to prevail in the visible and therefore in the atmosphere. By using the cross sections of Hallquist et al. (1997) with the quantum yields and the lamp spectrum in Eq. 2.17 described above, a rate of 9.2×10^{-6} s^{-1} is

Table 2.4: Estimated pinonaldehyde photolysis quantum yields. ϕ_1, ϕ_2 and ϕ_3 represent the aldehyde Norrish I, Norrish II and ketone photolysis pathways, respectively.

wavelength / nm	ϕ_1	ϕ_2	ϕ_3	ϕ_{total}
250	0.07	0.20	0.72	1.0
280	0.09	0.23	0.68	1.0
290	0.10	0.28	0.52	0.9
300	0.10	0.28	0.26	0.64
310	0.10	0.28	0.10	0.48
320	0.10	0.28	0.04	0.42
330	0.10	0.28	0.02	0.40
340	0.10	0.28	0.01	0.39

calculated for the visible experiments, i.e. less than the measurement (5.5×10^{-5} s^{-1}) based on a blank pinonaldehyde experiment conducted in the absence of CH_3ONO by N99. Such a discrepancy between the experimental and theoretical J-values cannot be attributed to uncertainties in the pinonaldehyde photolysis parameters. Indeed, even the maximum theoretical quantum yield (unity) would result in a J-value lower than the measured value. In any case, both experimental and theoretical values are very low, making pinonaldehyde photolysis almost negligible in the visible experiments. A similar estimation of the J-value using Eq. 2.17 is not possible for the UV experiments, because the cross sections are unknown at or around the lamp emission peak (253.7 nm). Therefore, the measured photolytic rate of 3.3×10^{-4} s^{-1} reported in N99 for the UV experiments is used in our model. Combining this value with the TUV lamp spectrum, we estimate the cross section of pinonaldehyde to about 2.8×10^{-20} cm^2 at 253.7 nm.

Alkyl Nitrates

The absorption cross sections of organic alkyl nitrates are based on the recommendations of Atkinson et al. (2003). The quantum yield is assumed equal to 1 throughout the visible and UV spectrum. The only channel considered is :

$$\mathrm{RONO_2} + h\nu \rightarrow \mathrm{RO} + \mathrm{NO_2}. \qquad \text{(R2.41)}$$

The calculated photodissociation rates of several organic nitrates investigated in the laboratory are listed in Tab. 2.5. The rates are seen to increase with the number of carbons. They are also higher when a ketone functionality is present. The increase of J(n-alkyl nitrates) with carbon number obeys roughly a logarithmic law. The rate depends also on the position of the nitrate group, as illustrated by the differences between isopropyl nitrate (*i*-$CH_3CH(ONO_2)CH_3$), 2-butyl nitrate ($CH_3CH_2CH(ONO_2)CH_3$) and their n-alkyl counterparts. We group the numerous nitrates generated in the α-pinene photooxidation into 4 families: $C_{<7}$ alkyl nitrates, $C_{\geq 7}$ alkyl nitrates, $C_{<7}$ keto-nitrates and $C_{\geq 7}$ keto-nitrates. The photorate of 2-butyl nitrate is adopted for

the $C_{<7}$ alkyl nitrates. Barnes et al. (1993) reported absorption cross sections of α-nitrooxy acetone, 1-nitrooxy-2-butanone and 3-nitrooxy-2-butanone. The photorate of 3-nitrooxy-2-butanone ($CH_3CH(ONO_2)C(O)CH_3$) is assumed to be representative for the $C_{<7}$ keto-nitrates. The photodissociation rates for $C_{\geq 7}$ alkyl and keto-nitrates compounds are obtained by logarithmic extrapolation. Because of the presence of the carbonyl in the keto-nitrates, the photolytic cleavage of the RCO-$CH(ONO_2)$R bond is another possible pathway for these compounds, in particular in the UV experiments. However, the rupture of the O-NO_2 bond probably dominates. Due to the lack of data, aldehyde-nitrates are assume to photolyze in the same fashion as keto-nitrates.

Table 2.5: Photolysis rates of several alkyl nitrates under the UV and visible conditions in N99.

Species	J(s^{-1}) TUV	J(s^{-1}) TL-05
n-alkyl nitrates		
CH_3ONO_2[a]	5.2×10^{-4}	1.8×10^{-7}
$CH_3CH_2ONO_2$[a]	6.2×10^{-4}	3.1×10^{-7}
n$-C_3H_7ONO_2$[a]	6.9×10^{-4}	4.6×10^{-7}
n$-C_4H_9ONO_2$[a]	7.4×10^{-4}	4.4×10^{-7}
alkyl nitrates		
i$-CH_3CH(ONO_2)CH_3$[a]	7.9×10^{-4}	6.3×10^{-7}
$CH_3CH_2CH(ONO_2)CH_3$[a]	9.0×10^{-4}	1.2×10^{-6}
keto-nitrates		
$CH_3C(O)CH_2(ONO_2)$[b]	2.1×10^{-3}	8.5×10^{-6}
$CH_3CH_2C(O)CH_2(ONO_2)$[b]	3.0×10^{-3}	4.3×10^{-6}
$CH_3CH(ONO_2)C(O)CH_3$[b]	2.7×10^{-3}	1.2×10^{-5}

References for the absorption cross sections: [a] Atkinson et al. (2003). [b] Barnes et al. (1993)

Table 2.6: Photolysis reactions for which the photodissociation parameters (σ = cross section, ϕ=quantum yield) are known from laboratory investigations, and estimated J-values in the N99 reactors and in typical tropospheric conditions (ground level, standard atmosphere, zenith angle = 45 °).

Reactions	$J\,(s^{-1})$ *TUV*	$J\,(s^{-1})$ *TL-05*	$J\,(s^{-1})$ *Tropos.*	*Notes*
$O_3 + h\nu \rightarrow O(^1D) + O_2$	$1.6(-1)^\star$	$4.0(-6)$	$1.7(-5)$	a,b
$O_3 + h\nu \rightarrow O + O_2$	$2.2(-1)$	$9.7(-6)$	$1.4(-5)$	a,b
$NO_3 + h\nu \rightarrow NO_2 + O$	$0.$	$4.0(-4)$	$1.7(-1)$	c,d
$NO_3 + h\nu \rightarrow NO + O_2$	$0.$	$0.$	$2.2(-2)$	c,d
$NO_2 + h\nu \rightarrow NO + O$	$3.7(-4)$	$9.2(-3)$	$8.2(-3)$	c
$N_2O_5 + h\nu \rightarrow NO_3 + NO + O$	$3.2(-3)$	$0.$	$4.1(-10)$	c
$N_2O_5 + h\nu \rightarrow NO_3 + NO_2$	$1.3(-3)$	$1.6(-5)$	$2.8(-5)$	c
$H_2O_2 + h\nu \rightarrow OH + OH$	$1.0(-3)$	$2.7(-6)$	$5.1(-6)$	c
$HONO + h\nu \rightarrow OH + NO$	$2.2(-3)$	$1.8(-3)$	$1.4(-3)$	c
$HNO_3 + h\nu \rightarrow OH + NO_2$	$3.0(-4)$	$1.3(-7)$	$4.1(-7)$	c
$HNO_4 + h\nu \rightarrow HO_2 + NO_2$	$3.3(-3)$	$1.2(-6)$	$2.8(-6)$	c,e
$HNO_4 + h\nu \rightarrow OH + NO_3$	$2.3(-3)$	$8.6(-7)$	$1.9(-6)$	c,e
$CH_2O + h\nu \rightarrow CO + 2HO_2$	$2.0(-5)$	$9.7(-6)$	$2.8(-5)$	c
$CH_2O + h\nu \rightarrow H_2 + CO$	$2.7(-5)$	$3.0(-5)$	$3.8(-5)$	c
$CH_3CHO + h\nu \rightarrow CH_3O_2 + HO_2 + CO$	$5.5(-5)$	$7.7(-7)$	$3.2(-6)$	c
$CH_3CHO + h\nu \rightarrow CH_4 + CO$	$1.4(-4)$	$0.$	$3.0(-11)$	c
$CH_3OOH + h\nu \rightarrow CH_3O + OH$	$5.3(-4)$	$2.5(-6)$	$4.1(-6)$	c
$CHOCHO + h\nu \rightarrow 0.09CH_2O + 1.6CO + 0.6H_2 + 0.31HO_2 + 0.31OH$	$7.1(-5)$	$1.5(-5)$	$6.9(-5)$	c
$CH_3COCH_3 + h\nu \rightarrow CH_3CO_3 + CH_3O_2$	$4.4(-4)$	$9.4(-8)$	$3.6(-7)$	f
$CH_3COC_2H_5 + h\nu \rightarrow CH_3CO + C_2H_5$	$5.1(-4)$	$1.4(-7)$	$5.8(-7)$	c,g
$CH_2OHCHO + h\nu \rightarrow CH_3OH + CO$	$2.7(-4)$	$0.$	$2.8(-11)$	c,h
$CH_2OHCHO + h\nu \rightarrow CH_2O + 2OH + CO$	$1.3(-4)$	$3.9(-7)$	$1.7(-6)$	c,h
$CH_3C(O)CHO + h\nu \rightarrow CH_3CO_3 + CO + HO_2$	$4.4(-4)$	$3.9(-4)$	$6.5(-4)$	c
$CH_2{=}CHC(O)CH_3 + h\nu \rightarrow CH_2{=}CHCO_3 + CH_3O_2$	$0.8(-5)$	$0.4(-6)$	$0.7(-6)$	c,i
$CH_2{=}CHC(O)CH_3 + h\nu \rightarrow CH_2{=}CHCH_3 + CO$	$2.5(-5)$	$1.2(-6)$	$2.0(-6)$	c,i
$CH_2{=}CHC(O)CH_3 + h\nu \rightarrow CH_3CO_3 + CH_2O + CO$	$0.8(-5)$	$0.4(-6)$	$0.7(-6)$	c,i
$CH_2{=}C(CH_3)CHO + h\nu \rightarrow 0.5CH_2{=}C(CH_3) + 0.5HCO + 0.5CH_2{=}CH(CH_3) + 0.5CO$	$2.4(-6)$	$2.1(-5)$	$2.1(-5)$	c,i
$CH_2{=}CHCHO + h\nu \rightarrow 0.5CH_2{=}CH + 0.5HCO + 0.5CH_2{=}CH_2 + 0.5CO$	$4.8(-7)$	$1.9(-6)$	$2.0(-6)$	i,j
$CH_3ONO_2 + h\nu \rightarrow CH_3O + NO_2$	$5.2(-4)$	$1.8(-7)$	$5.8(-7)$	k
$CH_3C(O)CH_2ONO_2 + h\nu \rightarrow CH_3C(O)CH_2O + NO_2$	$2.1(-3)$	$8.5(-6)$	$2.5(-5)$	l,m
$CH_3ONO + h\nu \rightarrow CH_3O + NO$	$5.3(-5)$	$9.1(-4)$	$1.2(-3)$	n
$CH_3C(O)O_2NO_2 + h\nu \rightarrow CH_3C(O)O_2 + NO_2$	$1.3(-3)$	$1.9(-7)$	$4.1(-7)$	c
$CH_3C(O)O_2NO_2 + h\nu \rightarrow CH_3C(O)O + NO_3$	$0.3(-3)$	$0.4(-7)$	$1.0(-7)$	c

* Notation is $1.6(-1) = 1.6 \times 10^{-1}$ ^{a} Sander et al. (2000) ^{b} Molina and Molina (1999) ^{c} Atkinson et al. (2003) ^{d} Johnston et al. (1996) ^{e} Knight et al. (2002) ^{f} Gierczak et al. (1998) and Warneck (2001) ^{g} quantum yield assumed equal to the wavelength-dependent quantum yields of acetone multiplied by a factor 1.2, in order to match the averaged yield measured by Raber et al. (1995) ^{h} assumed equal to the wavelength-dependent quantum yields of CH_3CHO for the different photodissociation paths, adjusted to match the averaged yield reported by Bacher et al. (2001) ^{i} Raber et al. (1995) ^{j} Gardner et al. (1987) ^{k} Talukdar et al. (2001) ^{l} Barnes et al. (1993) ^{m} assumed equal to one ^{n} Hippler et al. (1992)

Table 2.7: Photolysis reactions for the species and classes considered in this work, and estimated rates in the N99 reactors and in typical tropospheric conditions (ground level, standard atmosphere, zenith angle = 45°).

Reaction	*J* (s^{-1}) *TUV*	*J* (s^{-1}) *TL-05*	*J* (s^{-1}) *Tropos.*	*Reference species*
$\mathrm{PINALD} + \mathrm{h}\nu \rightarrow \mathrm{R_{17}} + \mathrm{CHO}$	$2.4(-5)$	$2.2(-6)$	$6.9(-6)$	see text
$\mathrm{PINALD} + \mathrm{h}\nu \rightarrow 0.5\mathrm{CH_2{=}CHC(O)CH_3}$ $+0.5\mathrm{C(CH_3)_2{=}CHCH_2CHO}$	$3.3(-5)$	$3.0(-6)$	$0.9(-5)$	see text
$\mathrm{PINALD} + \mathrm{h}\nu \rightarrow 0.5\mathrm{CH_2{=}CHCH_2CHO}$ $+0.5\mathrm{CH_3C(O)CH{=}C(CH_3)_2}$	$3.3(-5)$	$3.0(-6)$	$0.95(-5)$	see text
$\mathrm{PINALD} + \mathrm{h}\nu \rightarrow \mathrm{R_4} + \mathrm{CH_3CO}$	$2.4(-4)$	$9.4(-7)$	$3.4(-6)$	see text
Keto-aldehydes $\mathrm{C_{<7}} + \mathrm{h}\nu \rightarrow \mathrm{products}$	$4.4(-4)$	$3.9(-4)$	$6.5(-4)$	Methyl glyoxal
Keto-aldehydes $\mathrm{C_{\geq 7}} + \mathrm{h}\nu \rightarrow \mathrm{products}$	$3.3(-4)$	$9.2(-6)$	$2.9(-5)$	PINALD
Aldehydes $+\mathrm{h}\nu \rightarrow \mathrm{products}$	$8.2(-5)$	$5.4(-6)$	$1.5(-5)$	Pentanal
di-aldehydes $+\mathrm{h}\nu \rightarrow \mathrm{products}$	$7.1(-5)$	$1.5(-5)$	$6.9(-5)$	Glyoxal
$\mathrm{RC(O)R'} + \mathrm{h}\nu \rightarrow \mathrm{RC(O)O_2}$	$5.1(-4)$	$1.4(-7)$	$5.8(-7)$	MEK
$\mathrm{ROOH} + \mathrm{h}\nu \rightarrow \mathrm{products}$	$5.3(-4)$	$2.5(-6)$	$4.1(-6)$	$\mathrm{CH_3OOH}$
Unsaturated ketones $+\mathrm{h}\nu \rightarrow \mathrm{products}$	$4.1(-5)$	$1.9(-6)$	$3.4(-6)$	MVK
Unsaturated aldehydes $+\mathrm{h}\nu \rightarrow \mathrm{products}$	$2.4(-6)$	$2.1(-5)$	$2.1(-5)$	MACR
Nitrates $\mathrm{C_{<7}} + \mathrm{h}\nu \rightarrow \mathrm{RO} + \mathrm{NO_2}$	$9.0(-4)$	$1.3(-6)$	$4.5(-6)$	see text
Nitrates $\mathrm{C_{\geq 7}} + \mathrm{h}\nu \rightarrow \mathrm{RO} + \mathrm{NO_2}$	$1.3(-3)$	$2.7(-6)$	$1.1(-5)$	see text
Keto-nitrates $\mathrm{C_{<7}} + \mathrm{h}\nu \rightarrow \mathrm{RO} + \mathrm{NO_2}$	$2.7(-3)$	$1.3(-5)$	$3.6(-5)$	see text
Keto-nitrates $\mathrm{C_{\geq 7}} + \mathrm{h}\nu \rightarrow \mathrm{RO} + \mathrm{NO_2}$	$4.0(-3)$	$2.5(-5)$	$6.3(-5)$	see text
$\mathrm{RC(O)O_2NO_2} + \mathrm{h}\nu \rightarrow \mathrm{RC(O)O_2} + \mathrm{NO_2}$	$1.3(-3)$	$1.9(-7)$	$4.1(-7)$	PAN
$\mathrm{RC(O)O_2NO_2} + \mathrm{h}\nu \rightarrow \mathrm{RC(O)O} + \mathrm{NO_3}$	$0.3(-3)$	$0.4(-7)$	$1.0(-7)$	PAN

Chapter 3

Modeling the aerosol phase

3.1 Introduction

Modeling organic aerosols in the atmosphere would normally require the representation of each of the chemical and physical steps involved in their formation and their transformation. However, due to the lack of detailed knowledge on these processes, oversimplified parameterizations have been designed and used in several global 3-dimensional chemistry/transport models. The earliest and simplest method for parameterizing SOA formation in regional and global models is the bulk method: the aerosol yield (defined as the number of aerosol molecules produced per VOC molecules oxidized) derived in laboratory experiments is applied directly to the emission flux used in the atmospheric model. It is therefore assumed to be independent on the atmospheric photooxidative conditions (Liousse et al., 1996) as well as on the concentrations of organic aerosols and precursor BVOC.

Next in complexity, the two-products model (Odum et al., 1996) allows a simplified representation of the partitioning of BVOC oxidation products between the gas phase and an existing organic aerosol phase. This model represents the BVOC oxidation as:

$$BVOC + oxidant \rightarrow \sum_{i}^{n} \alpha_i P_i + high\ \ volatility\ \ products, \qquad \text{(R3.1)}$$

where α_i is the stoichiometric coefficient of the condensable product P_i. For each of these products P_i, an absorption equilibrium constant $K_{p,i}$ is defined as:

$$K_{p,i} = \frac{C_{p,i}}{C_{g,i} M_o}, \qquad (3.1)$$

where $C_{p,i}$ and $C_{g,i}$ are the gas and the particulate phase concentrations (ng m^{-3}), respectively. M_o is the total organic mass concentration consisting of primary or/and secondary particulates (μg m^{-3}). Using Eq. 3.1, we express the overall SOA yield Y_p in function on the mass of organic matter M_o and the partitioning coefficients of the

oxidation products:

$$Y_p = M_o \sum_i^n (\frac{\alpha_i K_{p,i}}{1 + K_{p,i} M_o}) \tag{3.2}$$

Odum et al. (1997) has shown that the observed dependence of Y_p on M_o in the oxidation of aromatic compounds can be described using only two hypothetical product compounds ($n = 2$). The appropriate values for α_i and $K_{p,i}$ are obtained by fitting the experimental data of SOA yields measured in laboratory conditions. In a similar manner, Hoffmann et al. (1997) derived two-product model parameters for the ozonolysis of α-pinene. This modeling approach and the related empirical parameters have been implemented in global models such as IMAGES (Griffin et al., 1999b), MOGUNTIA (Kanakidou et al., 2000), MOZART-2 (Lack et al., 2004) and TM3 (Tsigaridis and Kanakidou, 2003).

However, these studies ignore the actual complexity of the chemical processes leading to SOA formation. Early laboratory studies of gas phase BVOC oxidation have been conducted to explore this *terra incognita*. They allowed to identify some of the products playing a role in the aerosol partitioning. On the basis of these experimental results and with the help of theoretical studies, oxidation mechanisms have been elaborated. Although these mechanisms remain incomplete and oversimplified, they provide some representation of the SOA formation based on observed products. Consequently, the equation derived by Pankow (1994a,b) relating the partitioning coefficient of a compound i to its thermodynamical properties can be used. This expression is obtained by applying the Raoult's law and the ideal gas law in Eq. 3.1:

$$K_{p,i} = \frac{760 R T f_{om}}{MW_{om} 10^6 \zeta_i p^0_{L,i}}, \tag{3.3}$$

where R is the ideal gas constant; T is temperature; MW_{om} is the mean molecular weight of the absorbing medium; f_{om} is the weight fraction of the total aerosol concentration that constitutes the absorbing om phase; ζ_i is the activity coefficient of compound i in the particulate phase; $p^0_{L,i}$ is the subcooled vapour pressure of compound i at temperature T.

A parameterization based on this formulation (i.e. Eq. 3.3) has been implemented in global models by Griffin et al. (2002) (see also the companion paper of Pun et al. (2002)) and Bonn et al. (2004). They expressed the partitioning of each product from simple gas phase chemical mechanisms for BVOC consisting of tens of reactions. In these global models, the laboratory data on the BVOC photooxidation and methods of vapour pressure predictions are combined to express the K_p of each individual product. However, recent sensitivity studies performed by this group (Griffin et al., 2005) have identified a number of unsolved issues for the representation of SOA formation in global models. First of all, the gas phase chemistry of the SOA potential species remains largely uncertain and the SOA production is dependent on many speculative oxidation pathways. On the other hand, although a mechanism like the

one designed by Griffin et al. (2002) is oversimplified, it is relatively large in view of the currently available computer resources. Therefore, the implementation of detailed reaction schemes (such as the α-pinene oxidation mechanism described in the previous chapter) including thousands of reactions is not feasible. Robust and efficient methods need to be elaborated to reduce such mechanisms to a manageable size for global models.

Additional issues emphasized by Griffin et al. (2005) concern the SOA partitioning model. The parameters of the gas/particle partitioning model (e.g. ζ_i and $p^0_{L,i}$) are very uncertain. Current vapour pressure prediction methods are not applicable to all categories of products found in the oxidation mechanisms of BVOC. Furthermore, early laboratory (Yu et al., 1999a) as well as in situ experimental studies (Kavouras et al., 1998) have revealed the presence of high volatility products in the particulate phase which cannot be explained by the standard partitioning theory (i.e. Eq. 3.3). For example, the experimental vapour pressure of pinonaldehyde (Hallquist et al., 1997) implies a very low theoretical partitioning coefficient preventing its condensation on existing aerosols in typical laboratory and atmospheric conditions. Recently, attention has been drawn on the possible implication of heterogeneous reactions in the aerosol phase, which could explain the observed presence of particulate carbonyl compounds. To date, however, quantitative information on these processes are lacking, and their representation in models cannot be envisaged at this point. Given these uncertainties, model simulations of smog chamber experiments are crucial in order to clarify the gas phase photooxidation mechanisms and the related SOA formation.

In this Chapter, we describe the SOA partitioning model attached to the oxidation mechanism described in Chapter 2. First, we present the kinetic equations governing the partitioning equilibrium implemented in our model. The derivation of Eq. 3.3 requires the prediction of the subcooled vapour pressures. Therefore, a method is described for the prediction of the vapour pressures of all products of our oxidation mechanism. The group contribution principles constituting the basis of our method is also introduced. Next, the performance of our method is compared with the methods used current global models (Bonn et al., 2004; Pun et al., 2002; Griffin et al., 2005), in particular the UNIFAC method (Asher et al., 2002). The second section of this chapter (page 80) gives a brief overview of the possible heterogeneous reactions which have been proposed to occur in secondary organic aerosol.

3.2 The kinetic aerosol model

We have adopted the kinetic representation of the gas/particle partitioning proposed by Kamens et al. (1999):

$$K_{p,i} = K_{on,i}/K_{off,i}. \tag{3.4}$$

The equilibrium between the gas and aerosol phases of a species i is governed by the equilibrium constant $K_{p,i}$, expressed here as the ratio of the adsorption rate ($K_{on,i}$) to the desorption rate ($K_{off,i}$) on an existing aerosol. The adsorption and desorption processes of a species "X" are implemented as chemical reactions in the model:

$$X_g + aerosol \rightarrow X_p + 2 \quad aerosol \tag{R3.2}$$

$$X_p \rightarrow X_g - aerosol. \tag{R3.3}$$

Here, "aerosol" is a counter species representing the sum of all particle phase compounds. X_g and X_p represent the compound X in the gaseous and particulate phases, respectively.

The adsorption rate of a gas by a particle is parameterized as (Lelieveld and Crutzen, 1991):

$$K_{on} = \frac{a^2}{3D_g} + \frac{4a}{3\omega\gamma}, \tag{3.5}$$

where a is the particle radius (cm^2); D_g, the diffusivity in the gas phase, set to 0.06 cm^2 s^{-1} on the basis of the parameterization proposed by Fuller et al. (1969); ω is the mean gas phase molecular speed (cm s^{-1}) and γ is the accommodation coefficient (dimensionless). To the best of our knowledge, there is no experimental data for the accommodation coefficients of organic species on organic aerosols. Here, we assume γ equal to 0.2 for all compounds, based on the value deduced by Bowman et al. (1997) from simulations of smog chamber experiments of *m*-xylene photooxidation.

The desorption rate K^i_{off} is obtained from Eq. 3.3 and Eq. 3.5, which requires the evaluation of the parameters ζ_i, MW_{om} and $p^0_{L,i}$. It is generally assumed that the activity coefficient of VOC oxidation products in particles composed of a mixture of VOC products is close to one (Kamens et al., 1999). MW_{om} is assumed constant and taken equal to 185 g mol^{-1}, based on the molecular weights of the main condensables in the oxidation of α-pinene (between 170 and 200 g mol^{-1}). The vapour pressure of the chemical compounds generated by the oxidation of terpenes range from 10^{-2} to 10^{-7} torr (Hallquist et al., 1997; Hoffmann et al., 1997; Bilde and Pandis, 2001). Given these hypotheses, the ability for a compound i to condense on an aerosol is therefore governed by only one parameter, i.e., its vapour pressure.

The vapour pressure of a compound measures its ability to escape from the condensed phase, which depends on the strength of the intermolecular forces existing

between the condensed molecules. The relatively weak dispersion forces (resulting from temporary dipoles formed in adjacent molecules) are the sole cohesive agent in liquid alkanoic compounds, which explains their high vapour pressures. In oxygenated compounds, cohesion is reinforced by the hydrogen bonds existing between the polar groups of the molecules (Poling et al., 2001). Due to the important role played by these hydrogen bonds, the vapour pressure of an oxygenated organic compound is strongly dependent on the number and type of oxygenated functionalities, as well as on the carbon structure (carbon number, nature and positions of the branchings) of the molecule.

The products of the oxidation of α-pinene by OH and O_3 are generally multifunctional and bear one or several oxygenated groups among the carbonyl, hydroxy, nitrate, hydroperoxide and acid functionalities. Experimental data are lacking for the thermodynamic properties of a large majority of these products. In the following section, we describe a semi empirical extrapolation method for predicting the vapour pressure of the α-pinene oxidation products. Given their large number, this method is meant to be relatively simple and straightforward to apply. It is based on the so-called "group contribution" principles.

3.2.1 Vapour pressure estimation methods

The paradigm of the group contribution methods is basically the same as for the SAR methods (Sec. 2.2.2). Originally, group contribution methods were designed for the prediction of thermodynamic properties whereas SAR methods were used for the estimations of chemical reactivities. A group contribution method expresses the thermodynamic property of a chemical compound such as its vapour pressure as a function of a sum of contributions $\tau_i(T)$ of small groups of atoms i (descriptors) constituting the molecule:

$$p = f(\sum_i \tau_i(T)). \tag{3.6}$$

A large variety of group contribution methods have been designed in the past years, differing in their field of applicability and in the set of experimental data they are based on.

Jensen et al. (1981), Joback and Reid (1987), Tu (1994) and Li et al. (1994) proposed such methods for the prediction of a variety of thermodynamic properties (e.g., vapour pressure, critical temperature, critical pressure, boiling point) of organic compounds. These predictive methods are based on different data sets and provide estimations for specific or various classes of compounds including alkanes, alkenes, aromatics, halogenated hydrocarbons, oxygen-, sulfur- or nitrogen-containing monofunctional compounds. Other approaches have been proposed to estimate the vapour pressure of a component: e.g. Makar (2001) adopted an approach where the vapour pressures are directly estimated from polynomials, functions of the carbon number

and temperature, defined for 39 structural classes. Myrdal and Yalkowsky (1997) proposed a method which requires the knowledge of the normal boiling point as well as structural information related to the molecule flexibility.

In recent years, the experimental identification of multifunctional compounds in secondary organic aerosols has strengthened the need for new prediction methods dedicated to these complex species. Marrero and Gani (2001) and Olsen and Nielsen (2001) developed methods which perform estimations at different levels. While the primary level describes a wide variety of simple, monofunctional groups, the higher levels treat multifunctional structures and allow to differentiate between isomers by considering, to some extent, the interactions among functionalities. Asher et al. (2002) developed a method based on the principles of UNIFAC (Universal Functional Group Activity Coefficients (Fredenslund et al., 1977)). It provides vapour pressure estimates of mono- and multifunctional oxygen-containing species using only 12 group contributions.

Vapour pressure estimates of monofunctional species by current methods are reasonably accurate. An evaluation of several methods performed by Asher et al. (2002) shows that the vapour pressures of volatile compounds having $\log p^0_{L,i} \geq -3$ at ambient temperature are predicted by current methods to within a factor 2 on average. For less volatile compounds (often multifunctional), i.e. $\log_{10} p^0_{L,i} \leq -5$, uncertainties are estimated to a factor 3 for the UNIFAC method and up to an order of magnitude for other methods. This explains the broad use of UNIFAC in SOA models (Griffin et al., 2005). The failure to provide more accurate predictions for low volatile compounds is related in part to experimental difficulties. Measurements of low vapour pressures are easily contaminated by impurities or biased by adsorption of the organic on the reactor walls. The literature reports experimental vapour pressure measurements for only about one hundred multifunctional compounds. The relative uncertainty of their measurements, when known, ranges from 25% to 50% (Hallquist et al., 1997; Bilde and Pandis, 2001; Bilde et al., 2003). Another important cause for the inaccuracy in the predictions for multifunctional compounds is the poorly quantified role of interactions between the chemical functionalities. Although they appear to have a large impact on the vapour pressure, their quantification remains difficult in part because of the scarcity of data for these compounds.

A major drawback of the methods described above is the absence of parameterization for chemical classes believed to play an important role in SOA formation (e.g. organic nitrates). The vapour pressure estimation method described in this work is intended to provide vapour pressure predictions for broad categories of α-pinene degradation products including alcohols, acids and carbonyls (classes which were considered by the methods cited above) as well as nitrates, peroxy acyl nitrates (PANs) and hydroperoxides (which were ignored by these methods).

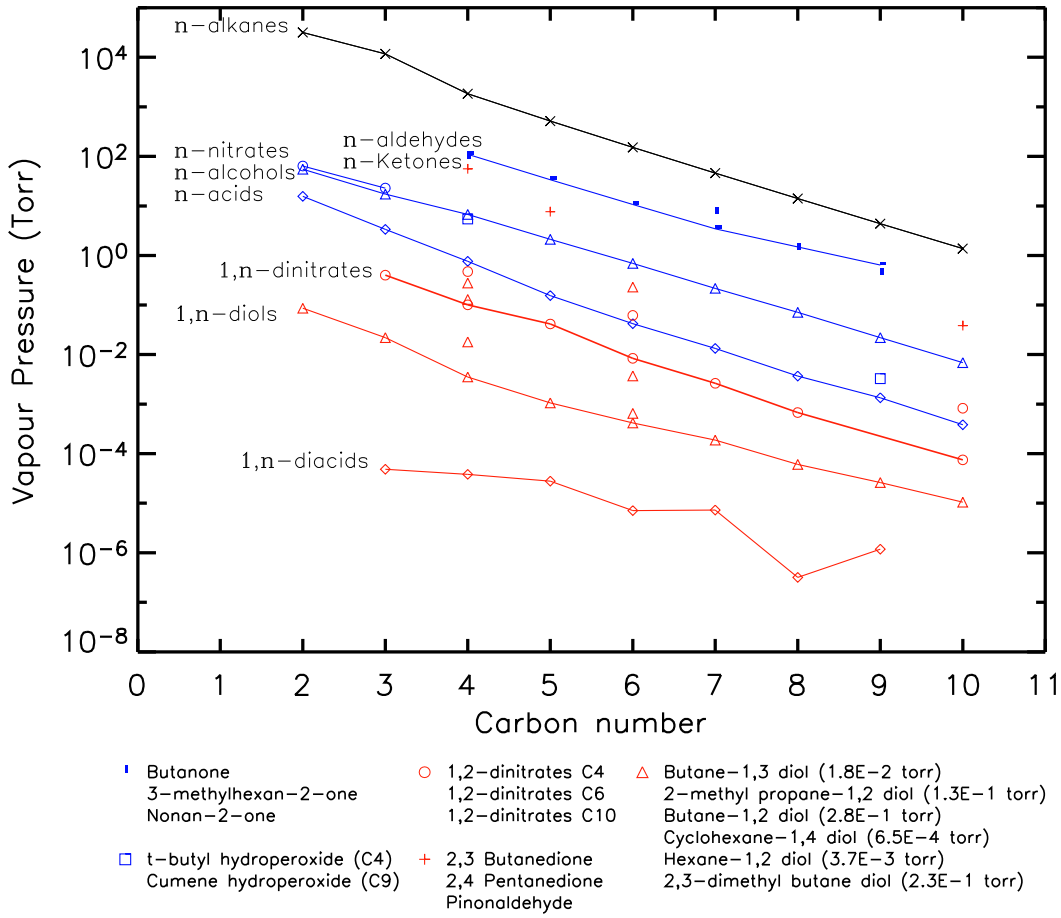

Figure 3.1: Vapour pressures of monofunctional and difunctional compounds at 298 K. Species prefixed by "*n*-" or "*1,n*-" (connected symbols) are of type "$CH_3-(CH_2)_n-X$" or "$X-(CH2)_n-X$", respectively, with X being an oxygenated functionality. Non-connected symbols are used for all other types of compounds.

3.2.2 Vapour pressure prediction method proposed in this work

The literature sources for the vapour pressure data used in this study are listed in Tab. 3.1 (last column). The vapour pressures at 298 K for a selection of compounds are shown as a function of carbon number in Fig. 3.1. As seen on this figure, it is important to distinguish between linear (single-chained) compounds, denoted by the prefix "n-" or "1,n", and the other compounds, including, cyclic, alkyl substituted species and/or species with a functionality not positioned at one extremity of the molecule. The "tri-O-acids"(Tab. 3.1) class follows the definition chosen by Makar (2001). This class represents three-oxygen-acids, i.e., acids with a carbonyl or hydroxy functionality.

Note that all species listed in Tab. 3.1 are either mono- or difunctional. Based on the group contribution principles, and in absence of data for species bearing more than two functionalities, we assume the method to be applicable to all multifunc-

Table 3.1: Literature data used for our vapour pressure parameterization, and standard error (as defined by Eq. 3.10) between the experimental and estimated vapour pressures, using the method developed in this work and using UNIFAC.

Class of compounds	$\sigma(298K)$ This work	$\sigma(298K)$ UNIFAC	$\sigma(320K)$ This work	$\sigma(320K)$ UNIFAC	Sources
Monocarbonyls	0.21	0.36	0.16	0.29	Lide (2001),ESDU (2001)
Dicarbonyls	0.26	0.56	0.15	0.65	HSDB (2004),Lide (2001), Hallquist et al. (1997)
Prim.[d] mononitrates	0.33	-[b]	0.22	-[b]	Lide (2001)
Prim.[d] *n*-monoalcohols	0.34	0.21	0.34	0.18	Poling et al. (2001)
Sec.[d] monoalcohols	0.29	0.29	0.29	0.24	Poling et al. (2001)
Tert.[d] monoalcohols	0.12	0.27	0.06	0.27	Poling et al. (2001)
PAN-like compounds	-[a]	-[b]	-[a]	-[b]	Bruckmann and Willner (1983)
Monohydroperoxydes	0.21	-[b]	-[a]	-[b]	Lide (2001), HSDB (2004)
(prim.)[d] *1,n*-dinitrates	0.11	-[b]	-[c]	-[b]	Fischer and Ballschmiter (1998)
1,2-dinitrates	0.35	-[b]	-[c]	-[b]	Fischer and Ballschmiter (1998)
Sec.[d] dinitrates	0.11	-[b]	-[c]	-[b]	Fischer and Ballschmiter (1998)
(prim.)[d] *1,n*-diols	0.21	0.40	0.23	0.31	ESDU (2001)
Sec.[d] diols	0.20	0.26	0.15	0.22	ESDU (2001)
Tert.[d] diols	0.14	0.89	0.13	0.78	ESDU (2001)
Other[e] diols	0.28	0.38	0.29	0.43	ESDU (2001)
n-carboxylic acid	0.27	0.11	0.04	0.11	Poling et al. (2001)
1,n-dicarboxylic acid	0.26	0.65	0.45	0.48	Bilde et al. (2003)
Hydroxy ketones	0.43	0.58	0.34	0.50	Lide (2001), Asher et al. (2002)
Tri-O-acids[f]	0.42	0.50	0.61	0.60	HSDB (2004), ESDU (2001)

[a] Only one experimental value. [b] Not parameterized. [c] No experimental data. [d] Refers to the degree of substitution of the carbon(s) at which the functionality(ies) is(are) attached. Read "prim." as "primary", "sec." as "secondary", and "tert." as "tertiary". [e] The carbons bearing the functionalities have different degree of substitutions. [f] Acid compounds with a carbonyl or alcohol functionality.

tional species. Figure 3.1 shows that there is a roughly linear relationship between the logarithm of the vapour pressure and the carbon number, with an approximately constant slope for all classes, especially for n $\geq$ 4. A noticeable exception to this pattern is provided by the diacids. Bilde et al. (2003) has shown that the vapour pressures of solid C_3-C_9 dicarboxylic acids depend strongly on the parity of the carbon number. This is due to the increased symmetry of even-numbered molecules, favouring the stability of their crystal structure. Rosenorn et al. (2003) reported that methyl substituted even-numbered diacids have significantly higher vapour pressures than their non-substituted analogues, presumably because of their asymmetry. The vapour pressure of these compounds show no dependence on parity. Note that the *1,n*-diacids and $C_{\geq 7}$ *1,n*-diols are solid at ambient temperature, whereas the other compounds reported in Fig. 3.1 are liquid. The (subcooled) liquid vapour pressures of solid compounds shown in this figure are obtained by converting p_s^0 into p_L^0 using the equation described in Prausnitz (1969):

$$\ln p_s^0(T) = \ln p_L^0(T) - (\frac{\Delta S_{fus}(T_m)}{R}(\frac{T_m}{T} - 1)). \tag{3.7}$$

The melting point T_m and the fusion entropy change Δ $S_{fus}(T_m)$ are provided by NIST (2004) for *1,n*-diacids and $C_{\geq 7}$ *1,n*-diols. Figure 3.1 also shows that the vapour pressures of different isomers of dinitrates and diols sometimes cover several orders of magnitude, with the *1,n*-compounds presenting the lowest values. Our prediction method aims at reproducing to some extent the differences in vapour pressure between different isomers.

Our proposed method to estimate the vapour pressure of a compound i at temperature T has the following form :

$$log\ p^0_{L,i}(T) = log\ p^0_{L,hc}(T) + \sum_k^n \nu_{k,i}\tau_k(T). \tag{3.8}$$

Here $p^0_{L,hc}(T)$ is the vapour pressure of the "parent" alkanoic compound hc, where all oxygenated functionalities in compound i are replaced by hydrogen atoms (e.g. -CH(OH)- is replaced by -CH_2-, etc), $\nu_{k,i}$ is the number of oxygenated functionalities of type k in the compound i, n is the number of defined types of oxygenated functionalities, and τ_k are the group contribution parameters. When no experimental value of the vapour pressure for the parent compound is available, the group contribution method of Marrero and Gani (2001) is used to calculate the boiling point, the critical temperature and the critical pressure of the compound i. $p^0_{L,i}(T)$ is obtained using the Lee and Kesler formulation, function of these properties (Poling et al., 2001). The choice of the method of Marrero and Gani (2001) is motivated by its good performance for alkanoic compounds. A comparison study by these authors shows that their method performs better than the Joback and Reid (1987) method which is commonly used for the prediction of these thermodynamic parameters. We estimate that the error on $p^0_{L,hc}$ predicted using Marrero and Gani (2001) does not exceed 50%, in the case of the most complex structures of VOC.

Table 3.2 lists the temperature dependent contributions optimized in this work. Note that the group contributions for the nitrate and hydroxy functionalities depend on the degree of substitution of the carbon bearing the functionality. The importance of this distinction can be illustrated by the observed lower vapour pressures of 1,6-hexanediol and butane-diol-1,2, compared to their substituted isomers 2,3-dimethyl-2,3-butanediol and 2-methyl propane-diol-1,2 (Fig. 3.1). Only a minor part of this difference is related to the weaker dispersion forces existing in substituted hydrocarbons, as shown by the small difference (30%) observed between the vapour pressures of the corresponding alkane isomers. The rest can be attributed to the interactions produced by the hydroxy functionalities. Their strength depends on the location of the chemical functionalities and the distance between each other in the molecules. This relatively minor influence of the dispersion forces explains the smaller error expected in the prediction of $p^0_{L,hc}(T)$ compared to the second term of Eq. 3.8 representing the influence of the functionalities. The effect of distance between functionalities has been investigated by Knauth and Sabbah (1990a,b,c). They have shown that, when the hydroxy functionalities are positioned close to each other in linear diols, in-

Table 3.2: Optimized group contributions (τ_k), as functions of the temperature (T). The last column reports the number of species for which experimental data are available in each class.

Class of compounds	Abr.	Contribution	Nb. of Species
Carbonyls	τ_{carb}	-0.8937 + 0.0039*(T-298)	16
Primary[a] nitrates	τ_{ONO2p}	-2.0897 + 0.0063*(T-298)	16
Secondary[a] nitrates	τ_{ONO2s}	-1.6711 + 0.0063*(T-298)	14
Tertiary[a] nitrates	τ_{ONO2t}	-1.2793 + 0.0063*(T-298)	0
Hydroperoxides	τ_{OOH}	-2.9942 + 0.0361*(T-298)	3
Primary[a] alcohols	τ_{OHp}	-2.6738 + 0.0171*(T-298)	28
Secondary[a] alcohols	τ_{OHs}	-2.0374 + 0.0124*(T-298)	22
Tertiary[a] alcohols	τ_{OHt}	-1.4418 + 0.0103*(T-298)	7
Acids	τ_{COOH}	-3.2516 + 0.0075*(T-298)	13
PANs	τ_{PAN}	-3.0372 + 0.0133*(T-298)	1

[a] Refers to the degree of substitution of the carbon(s) to which the functionality(ies) is(are) attached.

tramolecular hydrogen bonds between the hydroxy functionalities are favored, resulting in less intermolecular cohesion and therefore in higher vapour pressures. Parameterizing both effects (presence of substitutions and distance between functionalities) simultaneously would require more data than is currently available. Our choice to take into account the effect of alkyl substitutions on the α carbon of the functionalities is motivated by the large number of substitutions in the α-pinene oxidation products. Furthermore, this approach allows to include also some influence of the distance between the functionalities, since this distance is usually larger in primary diols and dinitrates from the data set than in their secondary isomers. An exception to this rule is provided by the case of the *para*-diols and *para*-dinitrates cyclic compounds. As for the linear diols, the effect of intramolecular interactions between two hydroxy groups can be seen in the vapour pressure data for cyclic diols and dinitrates. For example, the vapour pressure of cyclohexanediol isomers is seen to increase when the distance between the hydroxy groups decreases. 1,4-cyclohexanediol and 1,6-hexanediol are found to have similar vapour pressures, reflecting the fact that the hydroxy groups are situated at the respective opposites of the carbon structure in both molecules. Therefore, although the hydroxy groups of 1,4-cyclohexanediol are, strictly speaking, secondary, they are considered as primary in our parameterization of group contributions. Note that, in absence of vapour pressure data for tertiary and secondary (di)nitrates at different temperatures, the temperature dependence of their contributions is derived from the primary dinitrate contribution.

Since linear monoaldehydes and monoketones of same carbon number show very close vapour pressures, both functionalities are treated using a single contribution parameter τ_{carb}. The linear diacids of even carbon number are not taken into account in

the determination of the acid contribution, since their symmetric structure (resulting in abnormally low vapour pressures) is not characteristic of the α-pinene oxidation products. Vapour pressure data are scant for the hydroperoxides and peroxy acyl nitrates (PANs). The contributions shown in Tab. 3.2 for these classes are based on data for only three monofunctional hydroperoxides and one peroxy acyl nitrate (peroxy acetyl nitrate). No adequate data were found to parameterize the contribution of carboxylic peracids. The contribution of the peracid functionality is considered as the same as the acid one.

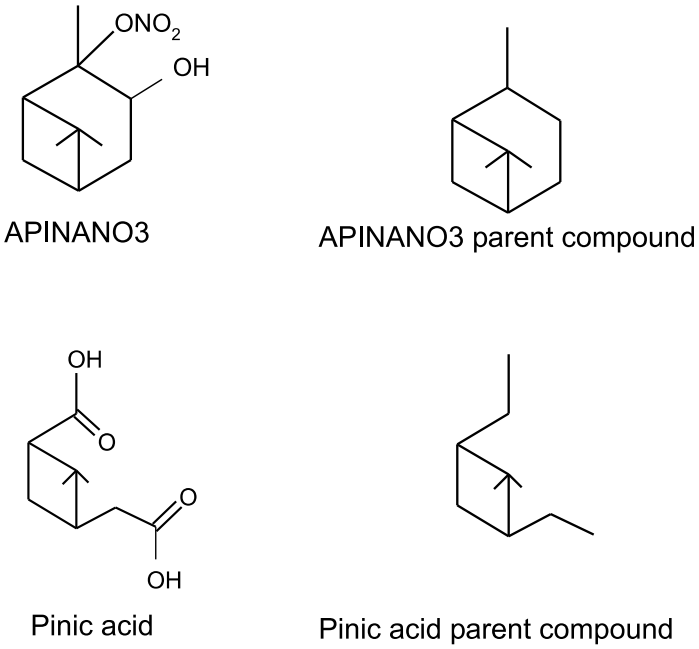

Figure 3.2: Structure of APINANO3 and pinic acid with their respective alkanoic parent compound

The principles of our prediction method are illustrated by the two following examples. In both cases, the Marrero and Gani (2001) method combined with the Lee and Kesler equation is used to predict the vapour pressure of the parent alkanoic compound, whose the structure is shown in Fig. 3.2. Consider first, APINANO3, a hydroxy nitrate produced from the oxidation of α-pinene by OH (from $R_{12}O_2$ + NO, Fig. 2.2). Given the presence of a tertiary nitrate and a secondary hydroxy functionality in APINANO3, its vapour pressure at 298 K is estimated as:

$\log_{10} p^0_{L,hc}$	= 0.4232
$-1 \times \tau_{ONO2t}$	- 1.2793
$-1 \times \tau_{OHs}$	- 2.0374
$\log_{10} p^0_{L,\text{APINANO3}}$	= -2.89351

The second example is provided by pinic acid, a low volatility product formed in the ozonolysis of α-pinene (Saunders et al., 2003). The vapour pressure of pinic acid at

320 K is estimated as:

$\log_{10} p^0_{L,hc}$	= 1.6135
$-2 \times \tau_{COOH}$	- 6.1732
$\log_{10} p^0_{L,\text{pinic acid}}$	= -4.5597

3.2.3 Minimization and comparison with the UNIFAC method

The parameters τ_k are determined by the minimization of a cost function J defined as

$$J = \frac{1}{2} \sum_i^N \frac{(log\, p^{0,mod}_{L,i} - log\, p^{0,exp}_{L,i})^2}{(E_i)^2}. \tag{3.9}$$

The cost function J measures the bias between the model and the entire set of available data (N species) listed in Tab. 3.1. Being a quadratic function of τ_k, its minimization is straightforward. The minimization has been performed at two temperatures (298 K and 320 K). E_i represents the assumed error associated to the data of compound i. It is primarily related to the observational uncertainty, but also to the expected ability of the model to reproduce these data. The measurement uncertainty on the $log\, p^{0,exp}_{L,i}(T)$ is generally of the order of 0.3. Since the less volatile multifunctional compounds are expected to contribute most to organic aerosol formation, the errors E_i are adjusted in order to favour the ability of the method to reproduce their vapour pressures: $E_{mono} = 0.5$ for the monofunctional compounds and $E_{multi} = 0.3$ for the multifunctional compounds. Using these values, we obtain after minimization, $J(298)/N = 0.43$ and $J(320)/N = 0.45$ for both categories, i.e., the modeled vapour pressures fall well within the range of uncertainty adopted for the observations.

The vapour pressures predictions can be approximated by assuming a linear dependence of $\tau_k(T)$ with T, deduced from their values at 298 and 320 K. Comparisons between predictions and experimental data have been conducted at 290 and 310 K. They show that the prediction uncertainty at 310 K is close to the average of their values at 298 K and 320 K. Predictions at 290 K are found to be of similar uncertainty as those at 298 K. Meaningful comparisons at lower temperatures are difficult due to the lack of experimental data for multifunctional compounds at low temperatures.

The measured vapour pressures are compared with the predictions using this method and using UNIFAC (Asher et al., 2002) in Fig. 3.3 and 3.4, respectively. Table 3.1 shows the standard prediction error for both methods and for each compound class calculated as in Asher et al. as

$$\sigma_i(T) = \frac{\sum_i^n |log\, p^{0,exp}_{L,i}(T) - log\, p^{0,mod}_{L,i}(T)|}{n}, \tag{3.10}$$

where n is the number of compounds in class i. The poor performance of UNIFAC for dicarbonyls is due to its large error ($\sigma \sim 0.8$) for pinonaldehyde, pentanedione and

butanedione. Our method performs as well as UNIFAC for monoalcohols. The better performance of our method for diols gives support to the parameterization used to distinguish between isomers. The values of the averaged standard error for alcohols (including monoalcohols and diols) are 0.22 and 0.37 for our method and for UNIFAC, respectively.

The validity of a group contribution method depends on the number and diversity of data it is based on. A drawback of the vapour pressure data set used here is the scarceness of information for heterofunctional species (compounds bearing different oxygenated functionalities): vapour pressure data are known for only 4 hydroxy ketones and 2 tri-O-acids species. Both our method and UNIFAC provide fairly good predictions for hydroxy ketones, with $\sigma \lesssim 0.5$ (Tab. 3.1). However, they both fail to predict the vapour pressures of tri-O-acids. For example, our $p^0_{L,i}$ prediction for pyruvic acid ($CH_3COCOOH$) is excellent at both temperatures, but a bias of one order of magnitude is obtained in the case of levulinic acid ($CH_3CO(CH_2)_2COOH$) at 320 K. A good agreement with the experimental data is obtained with our method for 2-hydroxy propanoic acid at 298 K. Tobias et al. (2000) deduced the subcooled vapour pressure of α-hydroxytridecyl hydroperoxide on the basis of temperature-programmed thermal desorption (TPTD) analysis ($3\times10^{-9\pm1}$ torr). The value predicted by our method for this hydroxy hydroperoxide is two orders of magnitude higher (see Fig. 3.3). This difference being much larger than the standard prediction errors calculated for the compounds containing hydroperoxide and/or hydroxy functionality(ies) (monohydroperoxides, monoalcohols, diols, hydroxy ketones, hydroxy acids), this compound has been omitted from the dataset used for the minimization. The low measured vapour pressure is surprising since, as noted previously, the closeness of functionalities tends to increase the vapour pressure. Experimental artefacts are not excluded. Further studies are required to better quantify the interactions between functionalities, as well as the role of molecular structure (e.g. presence of substitutions, of cycles) in multifunctional compounds in order to provide satisfactory predictions for the products originating from the oxidation of biogenic hydrocarbons.

Figure 3.3 shows that our calculated $log\, p^0_{L,i}$ for monoalcohols are underpredicted by $\sigma = 0.3$, while the predictions for the monocarboxylic acids are roughly overpredicted by $\sigma = 0.2$. These systematic biases for monofunctional classes are related to the oversimplified functional form adopted for parameterizing the vapour pressures. These biases are of little consequence in the context of secondary organic aerosol modeling, however, since the least volatile multifunctional compounds are expected to contribute most to the aerosol mass.

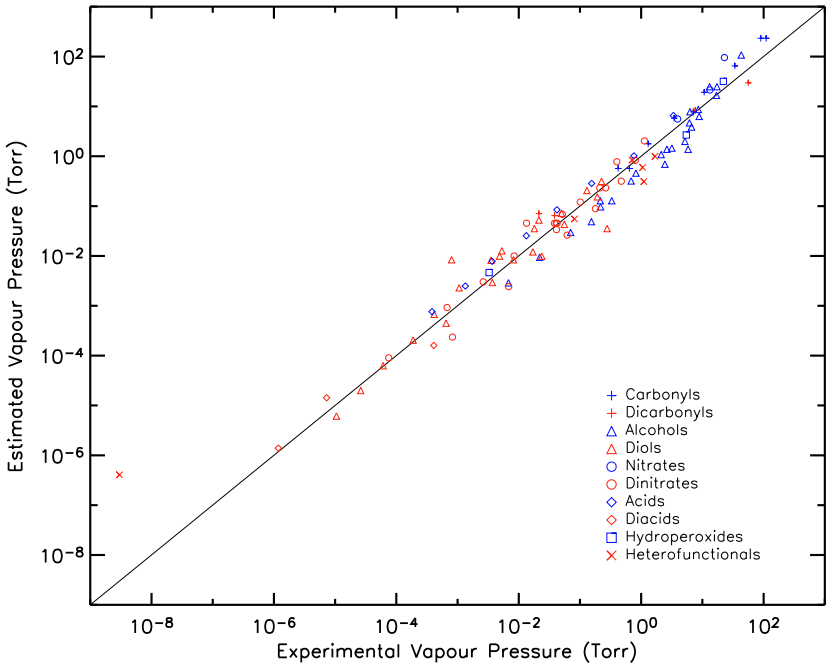

Figure 3.3: Vapour pressures estimated using the prediction method developed in this work against the experimental vapour pressures (sources in Tab. 3.1).

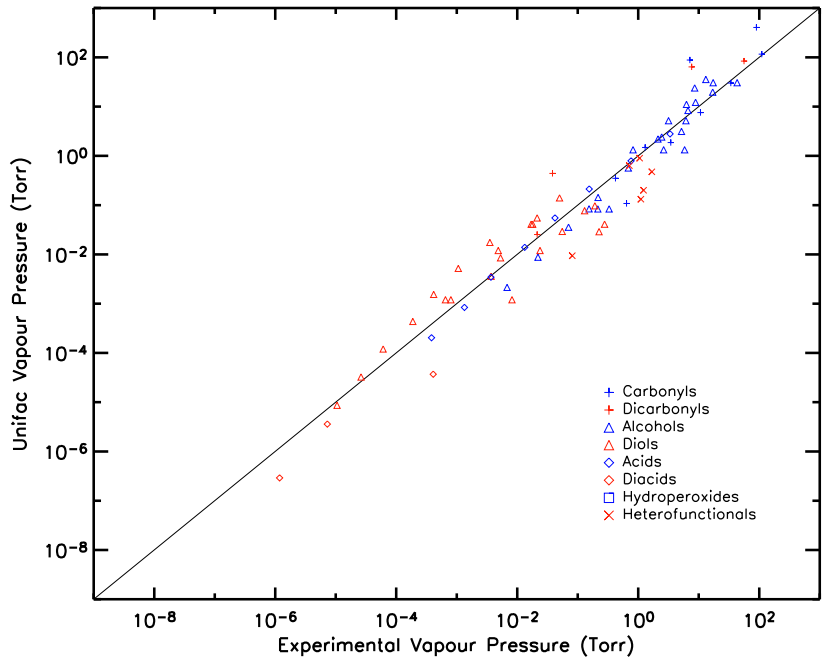

Figure 3.4: Vapour pressures estimated using UNIFAC against the experimental vapour pressures (sources in Tab. 3.1).

3.2.4 Vapour pressure estimations for α-pinene oxidation products

Figure 3.5 shows the variation with temperature of the vapour pressure of several important α-pinene degradation products, as estimated using the method developed in this work. The structure of these compounds is shown in Appendix A. Our predictions are also compared with vapour pressures estimates from previous studies, when available.

Bilde and Pandis (2001) measured the melting point and the evaporation rate of solid pinic acid and deduced its vapour pressure over the range 290-323 K. The fusion entropy change ($\Delta S_{fus}(T_m)$) necessary to deduce the corresponding subcooled vapour pressure is unknown for pinic acid. However, NIST (2004) reported the values for $\Delta S_{fus}(T_m)$ of azelaic acid (86 J mol^{-1} K^{-1}) and nonanoic acid (69 J mol^{-1} K^{-1}). Given the presence of two carboxylic functionalities and the non-linear carbon structure of pinic acid, we can assume that $\Delta S_{fus}(T_m)$ for pinic acid lies between these two values. Introducing their average in Eq. 3.7, we obtain an estimation of the dependence of the subcooled vapour pressure on temperature for this compound (solid line in Fig. 3.5). Both our method and UNIFAC calculate values which are about a factor of 3 higher than this estimation over the range of ambient temperatures. The agreement is fair given the uncertainty of 50% on the measurements performed by Bilde and Pandis. Jenkin et al. (2004) and Yu et al. (1999a) estimated the vapour pressure of the α-pinene oxidation products based on a modified form of the Clausius-Clapeyron equation (Scharzenbach et al., 1993). This equation is function of the boiling point and the molar heat (or entropy) of vaporization. The vapour pressure calculated by Jenkin et al. for pinic acid at 298 K using this equation is about two orders of magnitude higher than the experimentally deduced value at that temperature. This discrepancy could originate from the group contribution method of Joback and Reid (1987) used to estimate the boiling point of pinic acid. This method appears unappropriate for predicting thermodynamical properties of carboxylic diacids. For example, Jenkin et al. estimates the melting point of pinic acid to be 542 K using this method, 200 K above the experimental value (Bilde and Pandis, 2001) .

It is important to note that carboxylic acids are known to form dimers in the gas phase (Singleton et al., 1987; Orlando and Tyndall, 2003). For example, at ambient temperature, the vapour pressure of the dimer represents about 90% of the total vapour pressure of acetic acid in equilibrium with its pure liquid phase (Orlando and Tyndall, 2003). Hoffmann et al. (1998), and more recently Kuckelmann et al. (2000), observed pinic acid dimers as well as adducts of pinonic acid and pinic acid. The dimers of pinic acid were observed to be abundant. The stability of these dicarboxylic acid dimers can be expected to be high, due to the strong hydrogen bonds formed between the acid groups of the monomers. As in the case of acetic acid, we can expect the partial vapour pressure of the dimer form to contribute significantly to the total vapour pressure for many (di)carboxylic acids, and in particular for pinic acid. It follows that the vapour pressure of the dimer should be close to the experimental to-

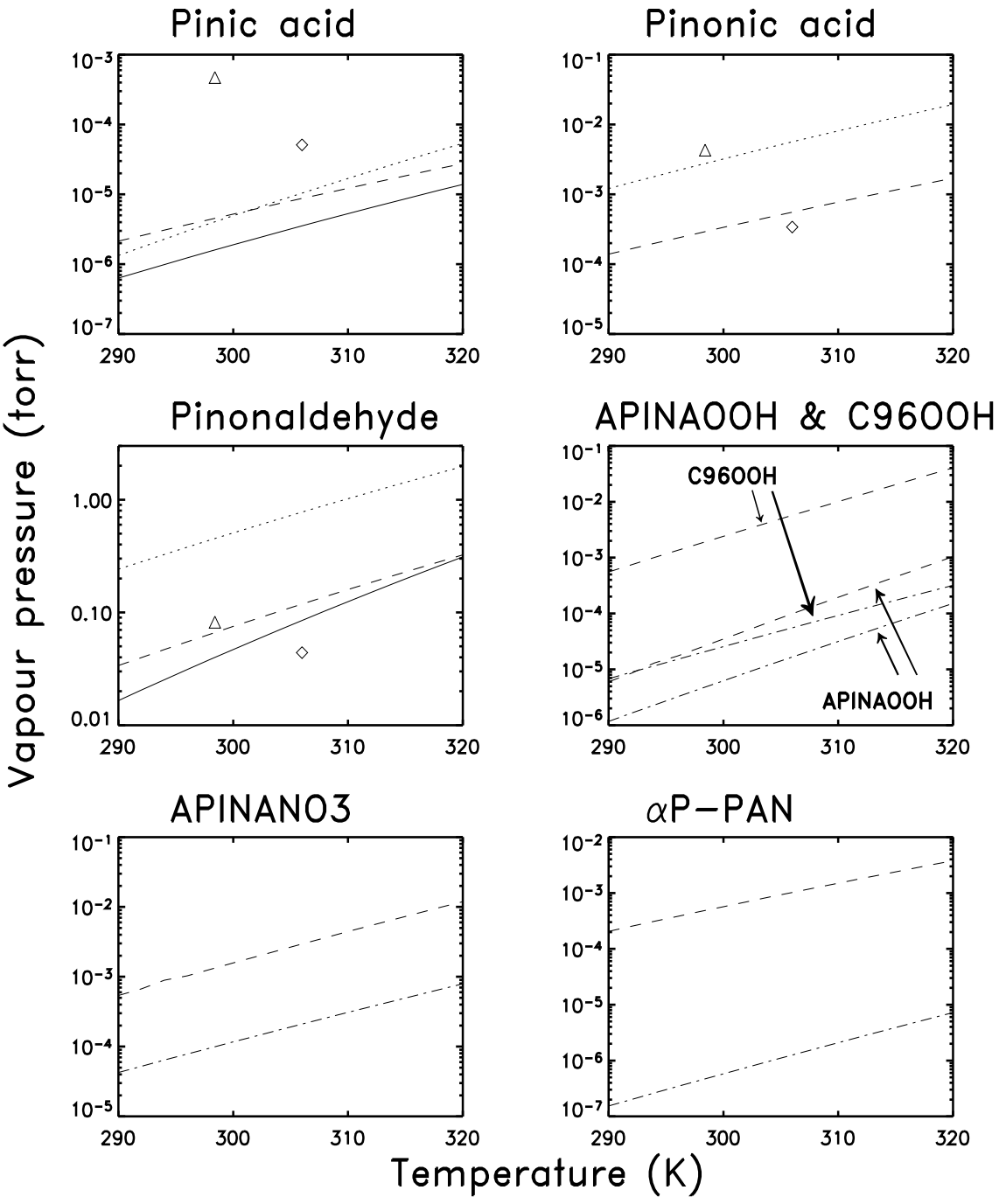

Figure 3.5: Vapor pressure of individual compounds estimated from the measurements (solid line), the method developed in this work (dashed), the UNIFAC method Asher et al. (2002) (dotted), Bonn et al. (2004) (dash dotted), Jenkin et al. (2004) at 298 K (triangles) and Yu et al. (1999a) at 306 K (diamonds).

tal (dimer+monomer) vapour pressure for these compounds. In the pinic acid/pinonic acid adduct, the carbonyl site in one acid group in pinic acid is not H-bonded and able to form an hydrogen bond with another component. Therefore, the vapour pressure of the pinic-pinonic acid adduct should then be on the same order, or even lower, than the vapour pressure of the pinic acid dimer ($\sim 1 \times 10^{-6}$ torr) at ambient temperature.

The vapour pressure estimated by our method for pinonaldehyde agrees well with the measurement of Hallquist et al. (1997). Bilde and Pandis (2001) measured the vapour pressure of pinonic acid to be $\sim$5.3$\times$10^{-7} torr at 296 K, but they did not consider this value as reliable, due to experimental problems. UNIFAC predicts vapour pressure values which are an order of magnitude higher than our estimations for these two compounds.

Bonn et al. (2004) is, to our knowledge, the only previous study providing vapour pressure estimations for hydroperoxides, organic nitrates and PANs generated by the oxidation of α-pinene. They provided temperature dependent estimations for the vapour pressure of APINANO3 (Fig. 3.5). Their estimation uses the group contribution relationship established by Nielsen et al. (1998) which relates the vapour pressure of organic nitrates to their number of carbons and their number of carbonyl, nitrate and hydroxy functionalities. The optimization of the contributions is based on a data set including hydrocarbons, alcohols, diols, carbonyls, alkyl nitrates, small hydroxy nitrates and dinitrates of different structures. The influence of the carbon structure on vapour pressure is not taken into account. For C_{10} hydroxy nitrates, this method calculates a vapour pressure of 2$\times$10^{-4} torr at ambient temperature. The vapour pressures we calculate for such compounds, assuming a moderately substituted carbon structure, are $\sim$5$\times$10^{-5} torr (primary functionalities), $\sim$5$\times$10^{-4} torr (secondary functionalities) and $\sim$7$\times$10^{-3} torr (tertiary functionalities). The value of Nielsen et al. falls therefore well in our range. Our higher values calculated for APINANO3 (Fig. 3.5) result from the tertiary degree of its nitrate functionality and its branched carbon structure. The vapour pressure relationship proposed by Bonn et al. for α-pinonyl peroxynitrate (αP-PAN), a product from the oxidation of pinonaldehyde by OH, is also partly based on the parameterization of Nielsen et al. (1998) for nitrate compounds.

As for the nitrates, our vapour pressure estimates for the hydroperoxides APINAOOH and C96OOH are higher than in Bonn et al.. Bonn et al. based their estimations on UNIFAC and on vapour pressure data for small hydroperoxides and for the C_{13} hydroxy hydroperoxide measured by Tobias et al. (2000). The exceptionally low vapour pressure of the latter compound has not been taken into account in our derivation of the hydroperoxide contribution, which might explain the discrepancy between our method and Bonn et al. for hydroperoxides. As in Bonn et al., however, we predict a lower vapour pressure for APINAOOH than for C96OOH, due to its hydroxy functionality and its higher carbon number. Taking into account the Tobias et al. data in the minimization would increase the magnitude of the hydroperoxide contribution

(τ_{OOH}), with -3.5231 at 298 K (instead of -2.9942, cfr Tab. 3.2). The impact on τ_{OHs} is negligible due to the large amount of data used to constrain this functionality. The vapour pressures of APINAOOH predicted using this alternative value of τ_{OOH} coincide with those determined by Bonn et al.. However, the standard error σ for the hydroperoxide class becomes very large, increasing from 0.2 (Tab. 3.1) to 1.3.

3.3 Heterogeneous reactions

Heterogeneous reactions, in particular those involving carbonyl compounds, have been studied by different groups. The proposed processes include protonation, enolization, hydration, hemiacetal and acetal formation, polymerization and aldol condensation, as summarized by Jang et al. (2002)(Fig. 3.6). Carbonyl compounds dissolved in an acidic aqueous phase may act as weak bases and be protonated. Another process involving carbonyl compounds is enolization. Nozière and Riemer (2003) showed that the keto-enol equilibrium takes place for any carbonyl compound with at least two carbon atoms and a hydrogen atom in α position with respect to the carbonyl group. Larger compounds usually have larger enolization constants than protonation constants because their enol form is stabilized by organic substituents adjacent to the carbonyl group. The uptake of these compounds occurs therefore primarily by enolization.

The impact of these heterogeneous reactions has been highlighted by Jang et al. (2002); Czoschke et al. (2003); Jang et al. (2003). They measured the organic aerosol yields of different aliphatic aldehydes (glyoxal, hexanal, octanal, decanal) in the presence and in the absence of an acid catalyst (H_2SO_4). A marked increase in the organic aerosol yield was observed in the acidic environment in comparison to the neutral system. This group showed that these reactions play a key role in particular in the ozonolysis experiments of small biogenic VOC such as isoprene and acrolein.

Kalberer et al. (2004) measured polymers in the particles generated from the photooxidation of 1,3,5-trimethylbenzene. The suggested mechanism is mainly based on a polymerization of methylglyoxal following the steps described in Fig. 3.6. The hydration of this oxidation product is followed by an acetal polymerization from the carbonyl and its hydrate or other alcohols. Further polymerization processes incorporate carbonyls products of different structure and size as well as carbonyl-containing acids. In contrast with the experiments of Jang et al. (2002), polymerization proceeds here without any seed particle. It is therefore assumed that the organic acids formed in the photooxidation are present in sufficiently high concentrations to catalyze the reactions. Note that this polymerization is a rather slow process and has visible effects only after several hours.

Tolocka et al. (2004), Gao et al. (2004) and Iinuma et al. (2004) observed the pres-

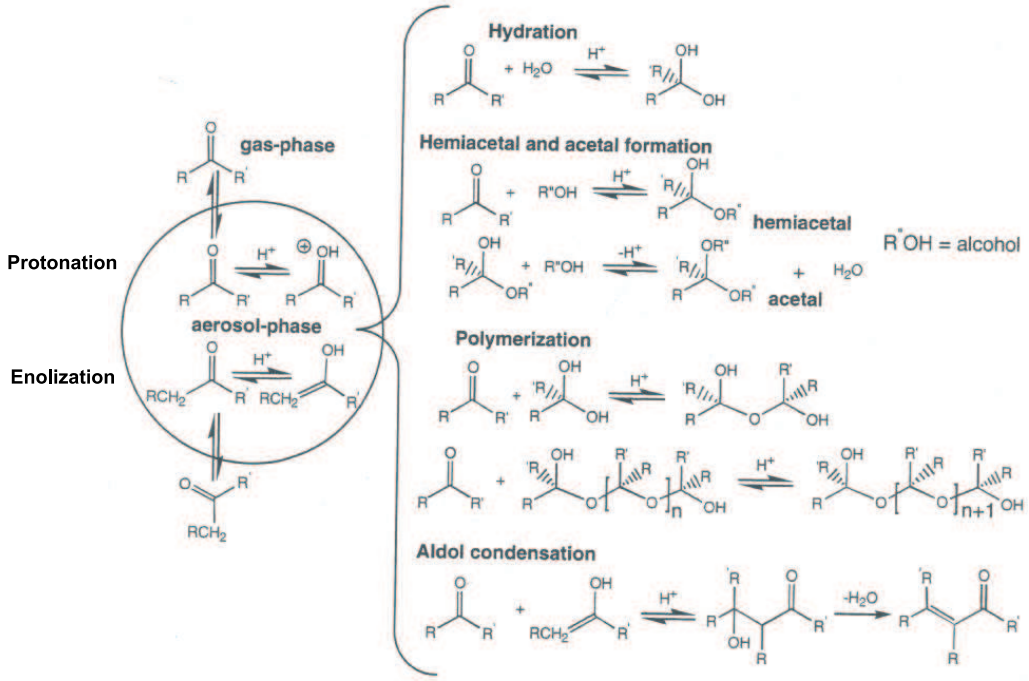

Figure 3.6: Acid-catalyzed heterogeneous reaction mechanism of carbonyls in organic aerosols (Jang et al., 2002).

ence of oligomeric molecules in experiments of α-pinene ozonolysis at relative humidities between 30% and 50%. Gao et al. (2004) reported that oligomers are found regardless of the initial particle acidity. On neutral seed ($MgSO_4$), small oligomers, probably dimers, are the most abundant species. When the seed becomes more acidic (from $(NH_4)_2SO_4$ seed to $MgSO_4$-H_2SO_4 seed), the SOA comprises larger oligomers such as trimers, tetramers and pentamers. The higher the seed acidity, the faster the formation of large oligomers. The presence of oligomers in SOA has been also found in experiments without pre-existing particles. These observations suggest that organic acids produced from the gas phase hydrocarbon oxidation may provide enough acidity to catalyze the reactions.

Tolocka et al. (2004) proposed the oligomer formation mechanism shown in Fig. 3.7. The monomer building blocks in the oxidation of α-pinene are products such as pinonaldehyde, norpinonaldehyde, pinonic acid and hydroxy pinonaldehyde (panel A) but also products resulting from the acid-catalyzed rupture of the cyclopropane moiety (panel B). Panels C and D show the dimerization of pinonaldehyde as an example. The oligomerization process takes place through an enolization and aldol condensation (panel C) or an hydration of the monomer followed by a dimerization process (referred to as *gem*-diol formation) with subsequent dehydration (panel D). Mechanisms similar to this second scheme have been also proposed by Iinuma et al. (2004).

Oligomerization can involve compounds other than large carbonyls. Lightfoot et

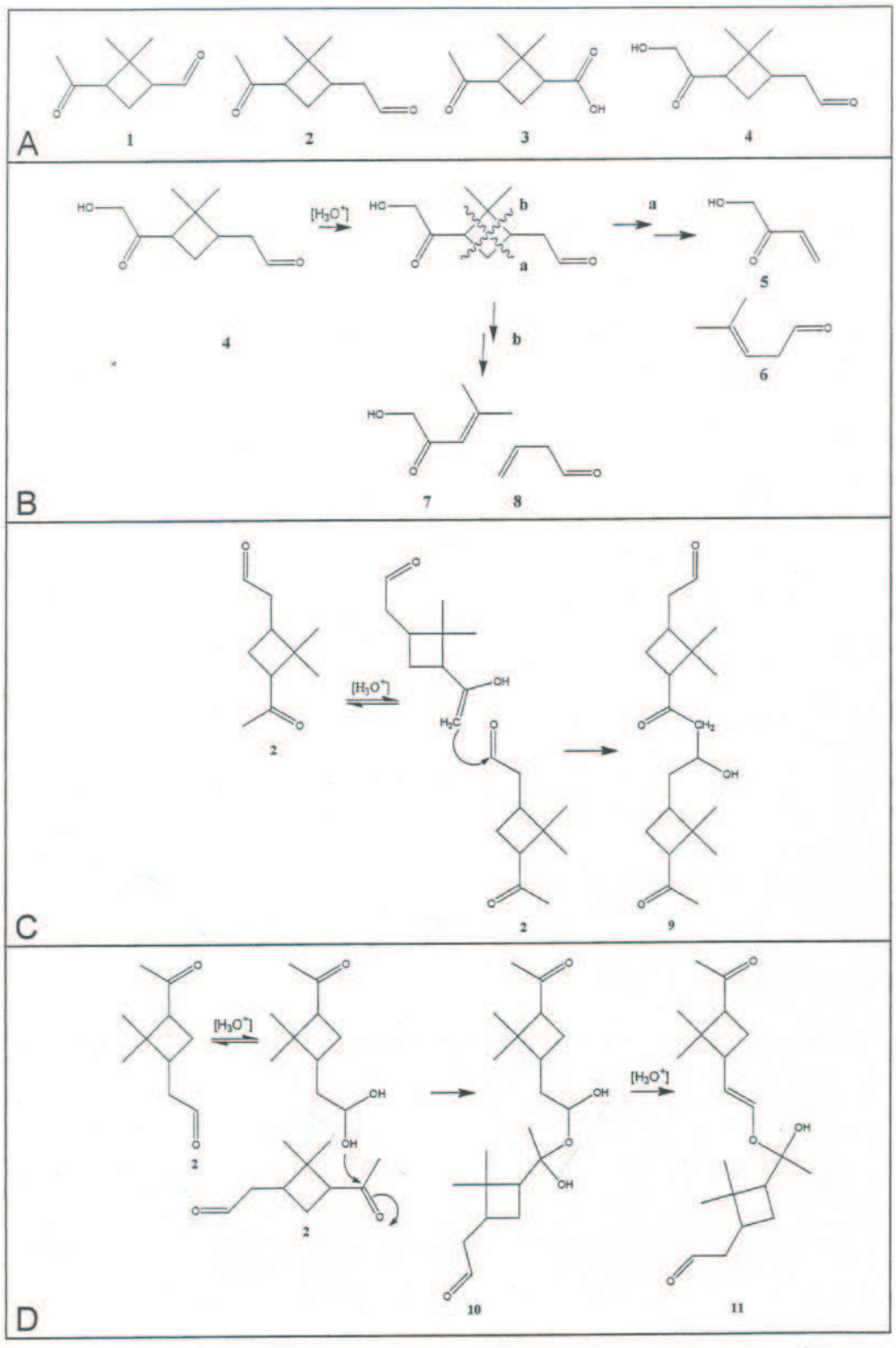

Figure 3.7: (A) Representative monomer products of the reaction of α-pinene with ozone. (B) Possible decomposition products of the monomers using pinonaldehyde as an example. (C) Dimerization of pinonaldehyde via aldol condensation. (D) Dimerization of pinonaldehyde by *gem*-diol formation with subsequent dehydration. (Tolocka et al., 2004)

al. (1992) studied the reactive uptake of glyoxal onto particulate matter in laboratory experiments. Different compositions of inorganic seed particles were used, including NH_4SO_4, $(NH_4)_2SO_4/H_2SO_4$, H_2SO_4, NaCl and $NaNO_3$, while varying the relative humidity and acid concentration. At very low RH (11% and 25%), there is no discernable particle growth. Increasing the RH above 50% dramatically increases the organic mass. The effect of particle acidity on glyoxal uptake is seen to be less pronounced than that of RH. The identification of mass fragments greater than the glyoxal monomer suggests the occurrence of heterogeneous reactions to form glyoxal adducts of low volatility. A reaction mechanism based on gem-diol formation has been proposed to explain the oligomers formation.

Another type of heterogeneous reactions involving carbonyl compounds has been proposed by Tobias and Ziemann (2000) based on the observation of a peroxyhemiacetal in the aerosol produced from the ozonolysis of tetradecene. It is believed to be formed from the reaction of a hydroperoxide with an aldehyde:

$$R_1OOH + R_2CHO \rightarrow R_1OOCH(OH)R_2. \quad \text{(R3.4)}$$

This reaction is proposed to occur at the surface of the aerosol between the condensed hydroperoxide and the aldehyde in the gas phase and possibly by acid catalysis. More experiments are required to identify the factors (acidity and relative humidity) influencing this reaction.

3.4 Conclusions

A model has been developed to describe the gas/aerosol phase partitioning of the products generated in the gas phase oxidation mechanisms of α-pinene. This model is based on Pankow's formulation for the partitioning coefficients of the compounds present in the chemical mechanism. This approach requires the evaluation of the subcooled vapour pressure of these compounds. For this purpose, a semi empirical extrapolation method for predicting the vapour pressure of the α-pinene oxidation products has been developed on the basis of group contribution principles.

Parameterizations have been derived for the influence of the carbonyl, hydroxy, nitrate, peroxy acyl nitrate, acid and hydroperoxide functionalities. The impact of alkyl substitutions is also parameterized for alcohols and nitrates. The predicted vapour pressures are within a factor 2-3 of the experimental values for multifunctional compounds. Further experimental studies are required to investigate 1/ the effect of the substitutions, 2/ the effect of the distance between functionalities on the vapour pressure and 3/ the vapour pressure of heterofunctional compounds.

Our findings support the hypothesis that, among the α-pinene products identified to date, dicarboxylic acids and hydroxy acids such as pinic acid and hydroxy pinonic acid are the least volatile compounds, with estimated vapour pressures of 3×10^{-6}

and 6×10^{-7} torr, respectively. Other primary products can be considered as semi-volatile, with p_L^0 ranging between 1×10^{-5} and 1×10^{-3} torr. Among them, hydroxy hydroperoxides present the lowest vapour pressures. Compounds produced after several oxidation steps in the α-pinene mechanism may have low volatilities due to their increased number of functionalities. However, they are expected to contribute less significantly to the aerosol phase because of their lower yields. Hydroperoxides are expected to contribute more largely to SOA formation at low temperatures due to the strong dependence of the hydroperoxide group contribution with temperature. In any case, the contribution of these semi-volatile products to the aerosol phase is expected to be less important than predicted by Bonn et al. (2004). The dimerization of multifunctional carboxylic acids is believed to take place in laboratory experiments of α-pinene oxidation. Since dimers are expected to contribute largely to the total (dimer+monomer) concentration of multifunctional carboxylic acids in these conditions, their partial vapour pressure is likely to be close to the vapour pressure measured in the laboratory for these compounds. The pinic/pinonic acid adduct is likely to play a significant role in the observed partitioning of pinonic acid (Yu et al., 1999a) between the aerosol and gas phases, due to its low vapour pressure estimated in this study ($\leq1\times10^{-6}$ torr). However, the role of dimers and adducts remains difficult to quantify in absence of kinetic data for their stabilities and formation rates.

Recently, heterogeneous reactions of carbonyls such as oligomerization processes and surface reactions with condensed hydroperoxides, have been proposed to explain the uptake of these compounds in the aerosol phase. The rate of these reactions is dependent on the relative humidity and the acidity of the aerosol. Measurements have shown that the acidity of the acids contained in the aerosol phase could be sufficient to catalyze the oligomerization processes. More experimental studies are required to unravel these observations.

Chapter 4

Simulations of laboratory experiments

4.1 Description of the box model and experiments

In order to simulate laboratory experiments, a comprehensive chemical mechanism has been implemented in a box model, including:

- The gas phase reactions of the α-pinene oxidation by OH and ozone, as well as the photooxidation reactions of the main primary product, pinonaldehyde, as described in Chapter 2.
- The chemistry of inorganic species and small organic compounds, based on the recommendations of Atkinson et al. (2003).
- The partitioning of condensable products between the gas and aerosol phases represented by its adsorption and desorption reactions as described in Chapter 3, (Eq. R3.2 and R3.3).
- The loss of gaseous and particulate compounds on the reactor walls. The rates are specific to the experimental set-up and are based on estimates reported by the authors for the considered experiment.

The complete mechanism includes a total of $\sim$3400 reactions and $\sim$700 species. The box model solves the continuity equations for the chemical species involved in this mechanism. The solver used in this model is based on an embedded Rosenbrock scheme of order 4 (Hairer and Wanner, 1990). A preprocessor called "KPP" (Damian-Iordache et al., 1995) reads text files listing the chemical equations and species involved in the mechanism and generates the FORTRAN code of the solver.

The state-of-the-art α-pinene mechanism developed in this work has been validated by comparison with laboratory experiments performed in diverse conditions. This chapter is divided in three sections. The first part is concerned with the simulations of the experiments of α-pinene+OH in presence and in absence of NO_x. The

experiments performed by Nozière et al. (1999a)(N99) were chosen for the validation of our box model. This group provided concentrations data for numerous compounds measured in a large series of experiments. Some products have been quantified only by this group as for example, α-PPAN (see Appendix A for identification of the structure). The results for the gas phase are first discussed. Based on a methodology described in this section, the measured and simulated concentrations in function of time are compared as well as the experimental and modeled yields. A sensitivity analysis of the simulation results in the gas phase with respect to the less constrained parameters is also included in this part as well as an evaluation of the dependence of the non-traditional reactions (α-hydroxy peroxy radical decompositions and ring closure reactions of unsaturated peroxy radicals) with the NO levels from the laboratory to atmospheric conditions. Next, the SOA formation related to the oxidation of α-pinene by OH is simulated and compared to the data laboratory of N99. The impact of the uncertainties related to the predicted vapour pressures on the SOA production is evaluated. The second section (page 109) is dedicated to the α-pinene ozonolysis. In this work, modeling studies of ozonolysis experiments performed in dark conditions and in absence of NO by Yu et al. (1999a), Hoffmann et al. (1997) and by the "BIOVOC" project (BIOVOC, 1998; Christoffersen et al., 1998) are carried out. Simulations are particularly focused on the Yu et al. (1999a) experiments which provide both gas and aerosol phase yields of products. The influence of the dimerization of multifunctional carboxylic acids, of the temperature and of the use of scavenger on the partitioning is studied. In the third section (page 117), box model simulations have been performed in typical atmospheric conditions. The α-pinene oxidation/partitioning mechanism developed in this work is compared with the treatments used in current global models.

4.2 α-pinene+OH experiments

4.2.1 Description of the experiments

N99 performed α-pinene+OH experiments with and without nitric oxide (NO). In presence of NO, 9 experiments were conducted under UV light and 11 experiments under visible light with H_2O_2 and CH_3ONO as radical precursor, respectively. A few pinonaldehyde+OH experiments were also carried out in presence of NO. A selection of experiments presenting typical features will be discussed in this study. In the following discussion, the experiments are numbered following their appearance number in Tab. 1 (α-pinene+OH in presence of NO: Experiments 1 to 21), Tab. 3 (in absence of NO: Experiments 22 to 31) and Tab. 4 (pinonaldehyde+OH: Experiments 32 to 37) in N99.

The time dependent concentrations of the chemical compounds in the reactor were measured with a Fourier transform infrared (FTIR) spectrometer. The species measured include α-pinene, the OH precursor, pinonaldehyde, acetone and formaldehyde. In addition, organic nitrates, acyl peroxy nitrates (PANs), NO and NO_2 were

also estimated in several experiments. Real-time measurements of the aerosol production were performed in 5 UV experiments in presence of NO_x. The aerosol was measured in real time by a Scanning Mobility Particle Sizer (SMPS) system. No aerosol seeds were used and the SMPS scan of the reactor indicated a negligible background aerosol concentration (3×10^8 nm^3/cm^3). The relative humidity did not exceed 20% in the reactor. A detailed description of the experiments is provided in N99. In the following, the notation "APIN" and "PINALD" will be used for α-pinene and pinonaldehyde, respectively.

4.2.2 Methodology for comparison

A simple way to validate the mechanism could be to compare the primary product yields deduced from the mechanism with the corresponding yields estimated from the laboratory data. However, this simplistic approach ignores the dependence of the yields on photochemical conditions (e.g. concentration of NO) which will be discussed in more detail in Sec. 4.2.6. In addition, the derivation of primary yields from laboratory data is particularly difficult due to the product losses and to the existence of secondary productions. The effect of these processes can be minimized by using the concentrations measured in the early stages of the experiment, and by using the fact that the true primary yield can be approximated as

$$Y(\mathrm{X}) = \lim_{t\to 0} Y_{app}(\mathrm{X}, t) \tag{4.1}$$

where

$$Y_{app}(\mathrm{X}, t) = [\mathrm{X}(t)]/([\mathrm{REACTANT}(0)] - [\mathrm{REACTANT}(t)]). \tag{4.2}$$

$Y_{app}(X, t)$ is the apparent yield of the product X at time t, [X(t)] and [REACTANT(t)] represent the concentration of X and the reactant, (α-pinene or pinonaldehyde) at time t. [REACTANT(0)] is the initial concentration of the reactant. However, it is easy to see that even small errors on the concentrations can lead to large errors on the yields. Also, any delay between the time when [REACTANT(0)] is measured and the actual start of the experiment can have large effects. For larger t values, the relative errors on [X(t)] and on the difference [REACTANT(0)]-[REACTANT(t)] become less important, but the photochemical sink and the secondary production play a larger role, which is difficult to quantify. Therefore, instead of comparing "true" yields, it is more meaningful for the purpose of mechanism validation to compare the observed concentrations [X(t)] with concentrations calculated using a box model.

Let us apply this methodology in the case of the α-pinene+OH experiments. In order to quantify the model/data biases in a systematic way, we average the apparent yields deduced at measurement times t_i comprised between 10% to 60% of α-pinene conversion, i.e. a time interval of typically 10 minutes. Data before 10% of α-pinene conversion are discarded in order to minimize the relative errors on [ΔAPIN(t)] and on the product concentrations, whereas data after 60% of α-pinene conversion are rejected to moderate the influence of product losses and secondary productions. These

processes are taken into account in the model, but to a much lesser degree of detail than the pathways leading to the primary products. For example, the experimental average apparent yield of a product X is calculated as :

$$\bar{Y}_{app}^{obs}(\mathrm{X}) = \frac{\sum_{i=1}^{n} Y_{app}^{obs}(\mathrm{X}, t_i)}{n}, \tag{4.3}$$

where n is the number of samplings between 10% and 60% α-pinene converted. The corresponding model apparent yield ($\bar{Y}_{app}^{mod}(X)$) is deduced in a similar way using the modeled values of X at the same measurement times t_i. Note that the apparent yields deduced from both the model and the observation are calculated using the α-pinene concentrations from the model.

The comparison between experimental and simulated apparent yields is meaningful only if the model is able to reproduce properly the observed variation of α-pinene. This is indeed the case for most experiments. The mean bias between the modeled and measured α-pinene concentrations is below 10% for more than 70% of the experiments. Experiments showing a mean bias higher than 10% are discarded from our analysis. On average, the valid experiments show a mean bias that does not exceed 5%.

Secondary productions of a compound X (Y_{sec}) may result from the photooxidation of other primary products, e.g. pinonaldehyde. The losses (L) of X occur via oxidation by OH, photolysis and, of least importance, by loss on the walls. $\bar{L}(X)$ and $\bar{Y}_{sec}(X)$ are averaged over the n sampling times of X in the same fashion as in Eq. 4.3. The values of $Y(X)$ reported in this study are the theoretical yields obtained following Eq. 4.1. In principle, the yield of X can vary in the course of an experiment, because it is a function of the conditions (e.g. [NO], [NO_2], [HO_2]) which influence the fate of peroxy radicals. In practice, however, these conditions do not vary dramatically in the N99 experiments for the adopted conversion window of α-pinene and $Y(X)$ is almost constant. Therefore, if the samplings of X are made in the early experimental times, we obtain the following relation :

$$Y(\mathrm{X}) \approx \bar{Y}_{app}(\mathrm{X}) + \bar{L}(\mathrm{X}) - \bar{Y}_{sec}(\mathrm{X}). \tag{4.4}$$

The yields $Y(X)$, as well as the average apparent yields, $\bar{Y}_{app}(X)$, the losses $\bar{L}(X)$ and secondary productions $\bar{Y}_{sec}(X)$ are summarized in Tab. 4.1. They are all expressed as molar yields, i.e. as percentages of α-pinene converted. The yields reported by N99 are also shown. The variability in the modeled values are due to 1/ differences in the initial conditions of NO and 2/ differences in the sampling times. The time concentrations calculated by the model are compared with the measured concentrations in Fig. 4.1 (visible, in presence of NO), Fig. 4.2 (UV, in presence of NO) and 4.3 (UV, NO-free).

The same methodology has been used for the pinonaldehyde experiments. However, the strong photolysis of pinonaldehyde in the UV experiments contributes to

Table 4.1: Experimental vs modeled yields of products for the photooxidation of alpha-pinene by OH, expressed as percentages of α-pinene reacted. The numbers given in the table are averages taken over all experiments in each category (high NO_x/UV, high NO_x/visible, NO_x-free). The standard deviations around these means are also given.

$\alpha-$**pinene+OH**		High NO_x/UV		High NO_x/Visible		NO_x Free/UV	
		Model	Exp.	Model	Exp.	Model	Exp
Pinonaldehyde	$\mathbf{Y}^\star$	56±1	(70±12)[a]	55±1	(66±18)[a]	26.4±0.4	(37±7)[a]
	$\bar{\mathbf{L}}_{\mathbf{h}\nu}$	4±1		0.		1.7±0.5	
	$\bar{\mathbf{L}}_{\mathbf{OH}}$	9±1		8±2		4.3±0.7	
	$\bar{\mathbf{Y}}_{\mathbf{app}}$	*44±3*	*44±8*	*47±2*	*45±9*	*20.4±0.6*	*21±1*
Acetone	$\mathbf{Y}$	11.1±0.5	(11±8)[a]	11.0±0.2	(8±7)[a]	0.4±0.1	(6.4 ±2)[a]
	$\bar{\mathbf{Y}}_{\mathbf{sec}}$	3.1±0.9		1.4±0.2		0.1±0.1	
	$\bar{\mathbf{L}}_{\mathbf{h}\nu}$	1.6±0.7		0.		0.	
	$\bar{\mathbf{L}}_{\mathbf{OH}}$	0.		0.		0.	
	$\bar{\mathbf{Y}}_{\mathbf{app}}$	*12.7±0.7*	*12±5*	*11.2±0.1*	*24±14*	*0.5±0.1*	*11±1*[b]
Formaldehyde	$\mathbf{Y}$	12.6±0.4	(23±9)[a]			0.5±0.5	(8.1±1.2)[a]
	$\bar{\mathbf{Y}}_{\mathbf{sec}}$	9 ±2				2.0±0.5	
	$\bar{\mathbf{L}}_{\mathbf{h}\nu}$	0.3±0.2				0.	
	$\bar{\mathbf{L}}_{\mathbf{OH}}$	1.0±0.2				0.2±0.1	
	$\bar{\mathbf{Y}}_{\mathbf{app}}$	*22±4*	*56±25*			*2.6±0.5*	*7±3*
$\sum$Nitrates	$\mathbf{Y}$	14.1±0.4	(26)[a]	14.5±0.5	(17±5)[a]		
	$\bar{\mathbf{Y}}_{\mathbf{sec}}$	2.2±0.5		2.0±0.5			
	$\bar{\mathbf{L}}_{\mathbf{h}\nu}$	5±1		0.			
	$\bar{\mathbf{L}}_{\mathbf{OH}}$	1.7±0.3		1.9±0.5			
	$\bar{\mathbf{Y}}_{\mathbf{app}}$	*9±2*	*13*	*16.3±0.5*	*19±8*		
$\sum$PANs	$\bar{\mathbf{L}}_{\mathbf{h}\nu}$	2±1		0.			
	$\bar{\mathbf{L}}_{\mathbf{OH}}$	0.23±0.07		0.15±0.10			
	$\bar{\mathbf{Y}}_{\mathbf{app}}$	*5±2*	*5±2*	*7±2*	*6±2*		

Pinonaldehyde+OH		High NO_x/UV		High NO_x/Visible	
		Model	Exp.	Model	Exp.
Acetone	$\mathbf{Y}$ [c]	10	(12)[a]	9.0±0.0	(20±6)
	$\bar{\mathbf{L}}_{\mathbf{h}\nu}$	2		0.	
	$\bar{\mathbf{L}}_{\mathbf{OH}}$	0		0.	
	$\bar{\mathbf{Y}}_{\mathbf{app}}$ [d]	*20*	*19*	*9.6±0.1*	*35±2*
Formaldehyde	$\mathbf{Y}$ [c]	29	(157)[a]		
	$\bar{\mathbf{L}}_{\mathbf{h}\nu}$	1			
	$\bar{\mathbf{L}}_{\mathbf{OH}}$	2			
	$\bar{\mathbf{Y}}_{\mathbf{app}}$ [d]	*51*	*167*		
$\sum$PANs	$\bar{\mathbf{L}}_{\mathbf{h}\nu}$	0.3		0.	
	$\bar{\mathbf{L}}_{\mathbf{OH}}$	2.2		1.8±0.2	
	$\bar{\mathbf{Y}}_{\mathbf{app}}$ [d]	*6.0*	*7.5*	*11.1±0.6*	*10.4±0.7*

* Notation: $\mathbf{Y}$ is the primary yield, $\bar{\mathbf{Y}}_{\mathbf{sec}}$ is the secondary yield, $\bar{\mathbf{L}}_{\mathbf{h}\nu}$ is loss by photolysis, $\bar{\mathbf{L}}_{\mathbf{OH}}$ is the loss by OH, and $\bar{\mathbf{Y}}_{\mathbf{app}}$ is the apparent yield. [a] As reported by N99 [b] yields calculated for a conversion from 60 to 90 % and with respect to the measured concentration of alpha-pinene [c] excluding the production from pinonaldehyde photolysis [d] including the production from pinonaldehyde photolysis.

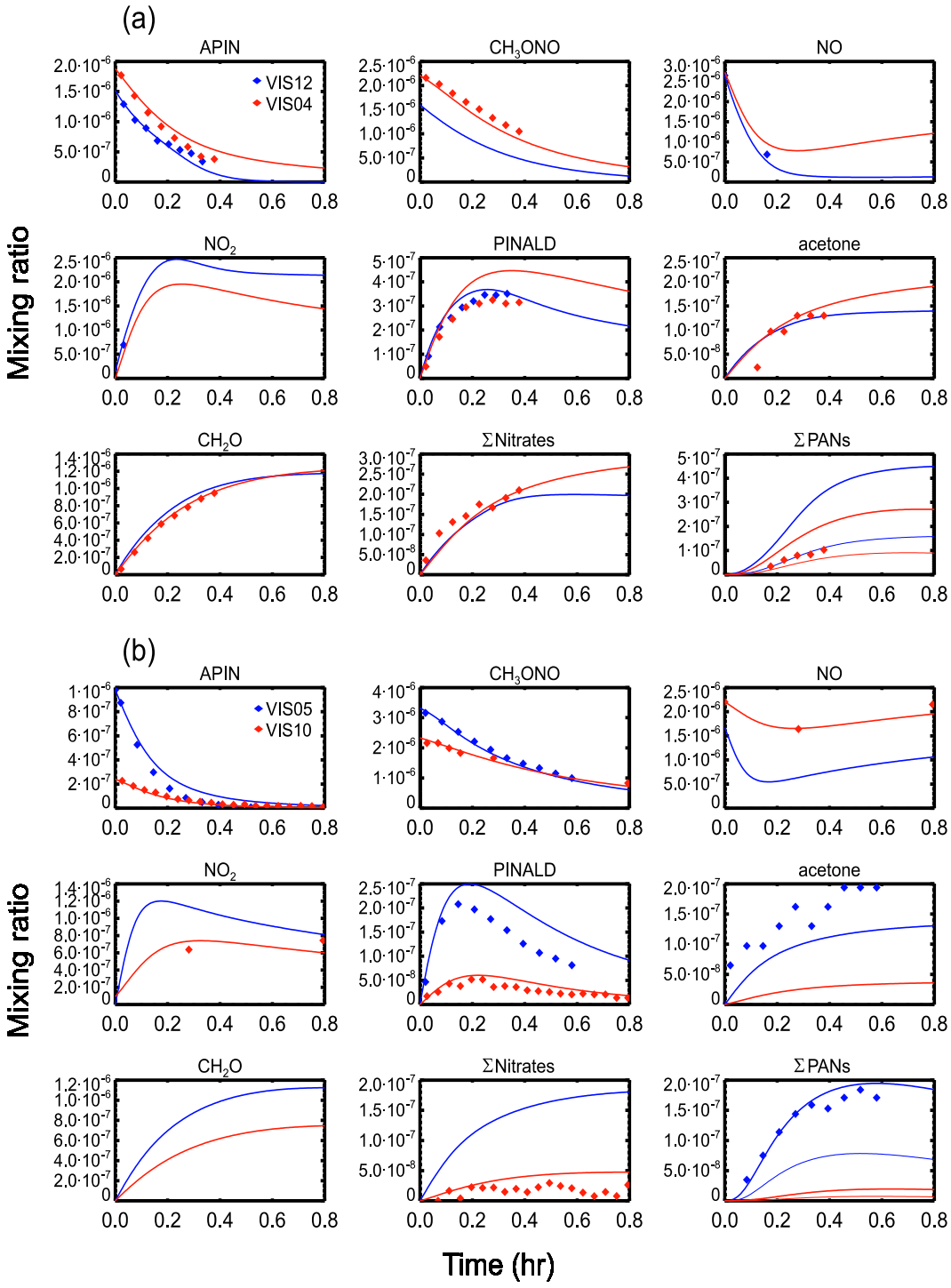

Figure 4.1: Measured (diamonds) vs simulated (curves) concentrations as a function of time for several experiments of α-pinene oxidation in visible conditions in the presence of NO_x: (a) Experiments 12 and 4, (b) Experiments 5 and 10 from N99. Two curves are shown in the modeled $\sum$PANs for each experiment: The lowest curve represents the sum of PAN and α-PPAN and the upper curve is the sum of all PANs.

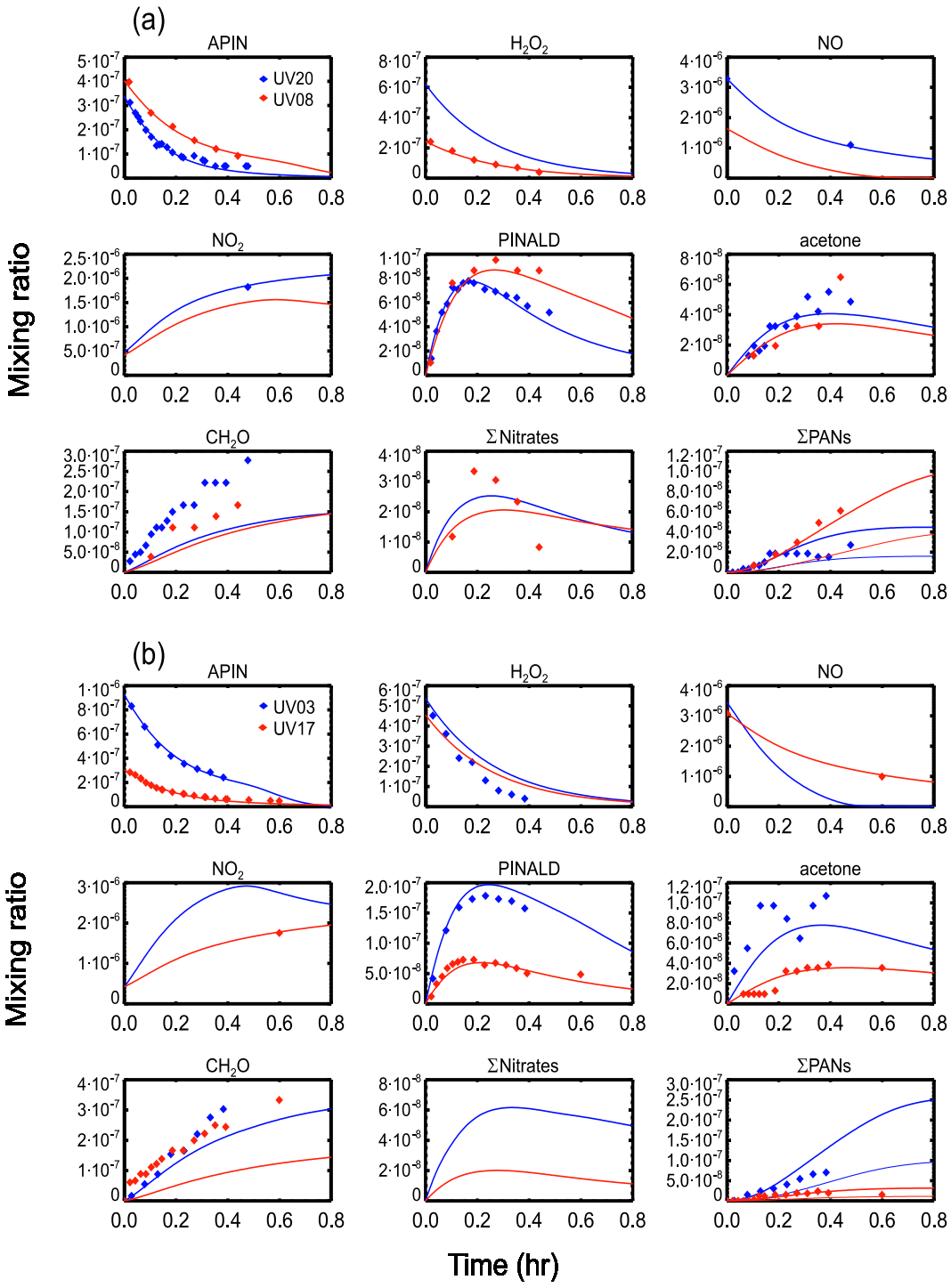

Figure 4.2: Measured (diamonds) vs simulated (curves) concentrations as a function of time for several experiments of α-pinene oxidation in UV conditions in the presence of NO_x: (a) Experiments 20 and 8, (b) Experiments 3 and 17 from N99. Two curves are shown in the modeled $\sum$PANs for each experiment: The lowest curve represents the sum of PAN and α-PPAN and the upper curve is the sum of all PANs.

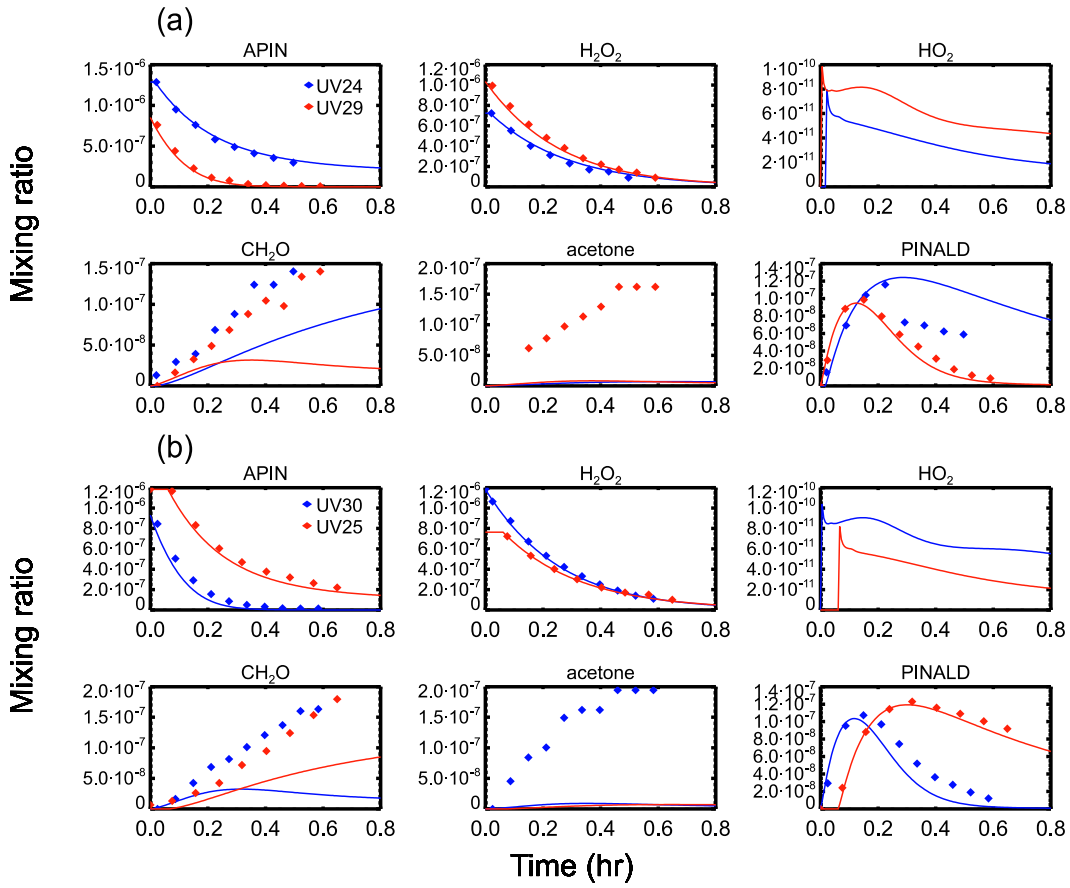

Figure 4.3: Measured (diamonds) vs simulated (curves) concentrations as a function of time for several experiments of α-pinene oxidation in UV conditions in the absence of NO_x: (a) Experiments 24 and 29, (b) Experiments 30 and 25 from N99.

the product concentrations. Therefore $Y(X)$ has to be corrected by retrieving the production from the photolysis and readjusting the yield to the actual [Δ(PINALD)] that has reacted with OH. In the visible conditions, the photolysis of pinonaldehyde is weak, and no correction is needed. Only two pinonaldehyde+OH experiments were performed in UV conditions. The model fails to reproduce the degradation of pinonaldehyde ($>$10% deviation) for one of them. In the visible, the pinonaldehyde decay rate is well caught by the model for the three experiments reported. On average, the mean bias between the modeled and measured pinonaldehyde concentrations is about 5%.

4.2.3 Comparison results for the gas phase products

α-pinene and OH-precursors

As explained in Sec. 2.4, the intensity of the lamps in the model are adjusted on the measured decay rates of the OH-precursors. These rates are found to be essentially constant, demonstrating the stability of the lamps. The degradation of α-pinene is well simulated in the UV conditions in presence as well as in absence of NO, indicating that the processes determining the concentration of OH are well represented by the model. In the visible conditions, the large production of formaldehyde generated through the degradation of CH_3ONO (Eq. R2.37) as well as the concentration of NO are well reproduced. This indicates that the photolysis of CH_3ONO is correctly estimated and so is the primary production of OH (through Eq. R2.39) in the reactor for these conditions. However, discrepancies appear at longer experimental times between the modeled and measured α-pinene degradation rates for about half the experiments simulated in the visible conditions. Examples of this behavior are seen in experiments 4 and 5 in Fig. 4.1. The bias is small ($<$10%) in the first stage of the experiment (before 60% of α-pinene conversion) and it does not influence the estimation of the primary product yields. The discrepancy at later times seems to be independent on the initial concentrations or on the evolution of the photochemical conditions in the course of the experiment (e.g. abrupt decrease of the NO level).

Pinonaldehyde

The pinonaldehyde concentrations are very well reproduced by the model in presence (Fig. 4.1 and Fig. 4.2) as well as in absence (Fig. 4.3) of NO, in particular in the first stage of the experiments ($<$60% α-pinene conversion). This is reflected by the excellent agreement obtained regarding the apparent yields of pinonaldehyde, as defined by Eq. 4.3 (see Tab. 4.1). In presence of NO, the yield of pinonaldehyde (i.e. the yield corrected for its different losses) is calculated to be 56% for an initial concentration of NO around 3 ppm. The strong photolysis of pinonaldehyde in the UV conditions explains the lower apparent yields in the UV compared to the visible conditions, where photolysis plays a negligible role (Tab. 4.1). In both series of experiments, the reaction of pinonaldehyde with OH represents 8-9% of the reacted α-pinene. As much as 10-25% of the pinonaldehyde produced when 60% of α-pinene has reacted is photooxidized in this interval. In the later stages of the experiments, when the oxidation of the primary products plays a more important role in the reactor, pinonaldehyde is overestimated by the model in about half the visible experiments. The reason for this discrepancy might be the oversimplified treatment of the oxidation mechanism of the primary products.

N99 estimated the products yields on the basis of Eq. 4.1 using the measured concentrations at the beginning of the experiments (α-pinene conversion less than 30%). The yields of pinonaldehyde deduced directly from the experiments in presence of NO and published in N99 are shown in Fig. 4.4. The yields for the same experiments

calculated in this work using Eq. 4.4 are shown on the figure for comparison. It appears that the yields calculated by N99 are strongly dependent on the initial α-pinene concentration, increasing from 22 to 89% for α-pinene decreasing from 2.5 ppm to 200 ppb. N99 concluded that this variation of the pinonaldehyde yield results from a partitioning of pinonaldehyde between the gas and condensed phases since the particulate fraction of pinonaldehyde (or of any semi-volatile compound) is expected to increase for increasing initial concentrations of α-pinene. However, since N99 estimated yields using concentrations measured in the early stage of the experiments (i.e. when only a small fraction of the initial α-pinene has reacted), they should be free of condensation processes. In fact, pinonaldehyde yields calculated in this work do not show any significant dependence on the α-pinene concentration. Therefore,we conclude that condensation of pinonaldehyde in the aerosol phase does not seem to occur in the N99 experiments.

In absence of NO_x, pinonaldehyde is produced exclusively from cross reactions of peroxy radicals. About 10% among the 26% pinonaldehyde yield come from reactions of $R_{12}O_2$ (see Fig. 2.2). The low self-reaction rate of this tertiary radical explains that it reacts for about 50% with HO_2, thereby contributing to about 8% among the total 30% of hydroperoxides generated in the system. The remaining 50 % of the $R_{12}O_2$ radicals react mainly with acyl peroxy radicals, then with O_2, producing $R_{13}O_2$. The fast decomposition of $R_{13}O_2$ outruns its reaction with HO_2 and other RO_2s, producing pinonaldehyde. The other channel leading to pinonaldehyde (16%) proceeds via the secondary radical R_2O_2. The high self-reaction rate allows R_2O_2 to react for 90% via the permutation reactions. Among them, the reaction of R_2O_2 with the β-hydroxy secondary radicals (actually mainly composed of R_2O_2) is the preferred pathway ($\sim$40%). The other permutation reactions contribute equally ($\sim$5-10%) to the exception of the cross reactions with the alkyl tertiary radicals R3R which are negligible.

N99 reported yield estimates about 10% higher than reported here although the observed apparent yields of pinonaldehyde are well reproduced by the model in presence as well as in absence of NO_x. Considering the difficulty to retrieve true product yields from the measured concentrations these estimates are in fairly good agreement with our model.

Acetone

The calculated primary yield of acetone for a mean initial concentration of NO of 3 ppm is 11%, in good agreement with N99. The sink of acetone is small: oxidation by OH is negligible, and photolysis plays at most a minor role. The secondary production of acetone originates from the photooxidation of pinonaldehyde. It is more important in the experiments using the UV lamp due to the higher photodissociation rate of pinonaldehyde under these conditions. Considering the large dispersion in the data, the model reproduces quite well the time evolution of acetone.

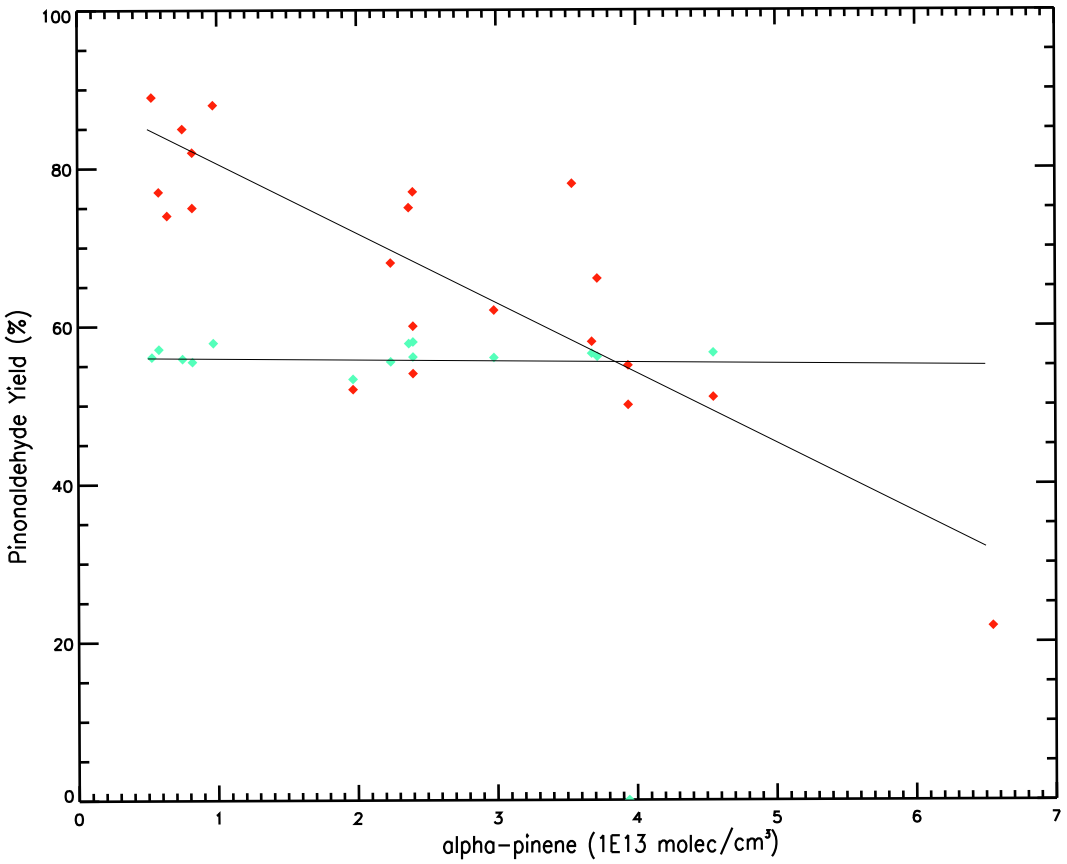

Figure 4.4: Yields of pinonaldehyde in the α-pinene experiments in presence of NO as function of initial α-pinene concentration. Yields estimated by N99 (red diamonds) are compared with the yields calculated in this work (green diamonds). A linear regression is applied on both sets of results.

An important disagreement exists for acetone in the experiments without NO_x. The data show a significant production of acetone ($\approx$11% yield) through primary or/and secondary reactions in these conditions, whereas the model simulates a production close to zero. As explained in Sec. 2.3.1, the ring closure reaction of R_7O_2 outruns the channel leading to the production of acetone in presence of NO. Due to the lack of measurements in the early stages of the experiments, the acetone yields (Tab. 4.1) are calculated using concentration data for α-pinene conversions from 60 to 90%. The observed production of acetone in NO_x-free conditions might have primary as well as secondary origins. In a sensitivity test, turning off the ring closure reactions in the model (thus freeing the path to R_7) results in only 3.5% acetone. This low production is due to the tertiary structure of the peroxy radical R_7O_2 which favours the reaction with HO_2 against the permutation reactions. In the event that ring closure is dominant, we estimate the highest possible (primary) acetone yield to 6%, which is the value obtained by hypothesizing that acetone is produced immediately upon decomposition of R_8O (generated from reactions of R_8 with O_2 and then with other peroxy radicals). Secondary productions are therefore required in order to account for

the high observed yield. This is also suggested by the concentration-time profiles in Fig. 4.3 since acetone is seen to increase even after complete oxidation of α-pinene.

Formaldehyde

The model cannot reproduce the large formaldehyde concentrations measured in the UV experiments. However, the measured production of formaldehyde appears to be constant in time (experiments 3 and 17 in Fig. 4.2) and independent on the photochemical regime (experiments 25 and 30 in Fig. 4.3), suggesting a desorption of this compound from the walls. This effect is not seen in the visible conditions because of the large amount of formaldehyde generated by the photolysis of CH_3ONO (experiment 4 in Fig. 4.1). The modeled primary yield is 12.7% at high NO_x concentrations. Primary production proceeds further in the mechanism, through the reactions of the radicals R_4 and R_{10} (not shown in Fig. 2.2). Secondary productions originate from the photooxidation of pinonaldehyde (6%) and other smaller organic compounds (3%). Yield values are not reported for the visible experiments, since methyl nitrite photolysis generates large quantities of formaldehyde. The formaldehyde yield is very low in the NO_x-free experiments. This is due to the fast decomposition of the radicals R_3O_2 and $R_{13}O_2$ to pinonaldehyde, outrunning the formation of formaldehyde through these pathways. The other channel (via R_6 and R_7O_2) leads to R_8 for which we have no explicit mechanism. Therefore we can assume that, as for acetone, formaldehyde is underestimated in the model in absence of NO.

Nitrates

The total concentration of organic nitrates (mainly made of $C_{\geq 7}$ compounds) generated by the α-pinene oxidation were quantified by N99 on the basis of the integrated cross sections (σ_{int}) of 2-hydroxypinane-3-nitrate and 3-oxopinane-2-nitrate in the range 1635-1700 cm^{-1}. The first compound represents 20% of the total amount of nitrates produced according to the mechanism, whereas the latter is not produced. However, the great majority of the nitrates generated in the α-pinene mechanism have a structure comparable to 2-hydroxypinane-3-nitrate (presence of a cycle, presence of an alcohol function, and similar number of carbons), so that we can consider plausible that they absorb in a similar fashion as 2-hydroxypinane-3-nitrate and 3-oxopinane-2-nitrate.

The model reproduces quite well the observed apparent yields for both actinic conditions. The nitrates were quantified in only one experiment in the UV series. In that case, the data at longer times show a sharp increase of the nitrates concentration that could not be reproduced by the model.

The experiments in the visible conditions were performed at different pressures of O_2: Experiments 5 and 10 at P_{O_2}=10 mbar, experiment 4 at P_{O_2}=26 mbar and

experiment 12 at P_{O_2}=200 mbar. Varying the pressure of O_2 affects the decay rate of CH_3ONO. This is due to the main reactions involving CH_3O, which is produced by reaction (R2.37):

$$\mathrm{CH_3O} + \mathrm{O_2} \rightarrow \mathrm{CH_2O} + \mathrm{HO_2} \quad \text{(R4.1)}$$

$$\mathrm{CH_3O} + \mathrm{NO} + \mathrm{M} \rightarrow \mathrm{CH_3ONO} \quad \text{(R4.2)}$$

$$\mathrm{CH_3O} + \mathrm{NO_2} + \mathrm{M} \rightarrow \mathrm{CH_3ONO_2}. \quad \text{(R4.3)}$$

Reactions R4.2 and R4.3 are negligible at standard pressure but they compete with reaction R4.1 at low oxygen pressure, resulting in CH_3ONO reformation and in a large production of methyl nitrate. Experiment 4, 5 and 10 produce 15, 20 and 50% of CH_3ONO_2, respectively, whereas the yield of CH_3ONO_2 is only 3% in experiment 12. In Fig. 4.1, 4.2, 4.5, and in Tab. 4.1, "ΣNitrates" represents the total nitrates excluding CH_3ONO_2.

PANs

Measurements of peroxy acetyl nitrate (PAN) and α-pinonyl peroxy nitrate (α-PPAN) were carried out for almost all UV experiments. α-PPAN is the main PAN analogue produced in the pinonaldehyde oxidation by OH (Fantechi et al., 2002). These measurements should be considered with caution, since many other PAN analogues are produced in the mechanism, which can be expected to have very similar IR spectra (Nozière and Barnes, 1998). For example, alkyled PAN analogues (e.g. benzoyl peroxy nitrate and peroxy methacryloyl nitrate) show a peak within 1 cm^{-1} of PAN in the main band of their spectra (at 1741 cm^{-1}). It follows that the spectroscopic measurements of PAN and α-PPAN in N99 experiments cover all PAN analogues similar to PAN and α-PPAN in the reactor. Therefore, we make the assumption that the sum of the measured concentrations of PAN and α-PPAN should be close to the sum of all PANs in the system (ΣPANs). Figures 4.1 and 4.2 display also the sum of PAN and α-PPAN (lower curve) as calculated by the model for illustration purposes (the upper curve representing ΣPANs). In general, the model agrees well with the measurements in both UV and visible conditions.

4.2.4 Pinonaldehyde+OH comparison results

It is more difficult to draw precise conclusions regarding the product yields in the pinonaldehyde+OH experiments, due to their small number. The experiment in the UV indicates an acetone apparent yield around 20% (Tab. 4.1 and Fig. 4.5) which is well reproduced by the model. In these conditions, 30% of the pinonaldehyde present in the reactor photolyze while 8% are lost by adsorption on the walls, leaving only 62% reacting with OH. This explains the large amount of acetone produced in the experiment, whereas the primary yield from pinonaldehyde+OH only is actually twice

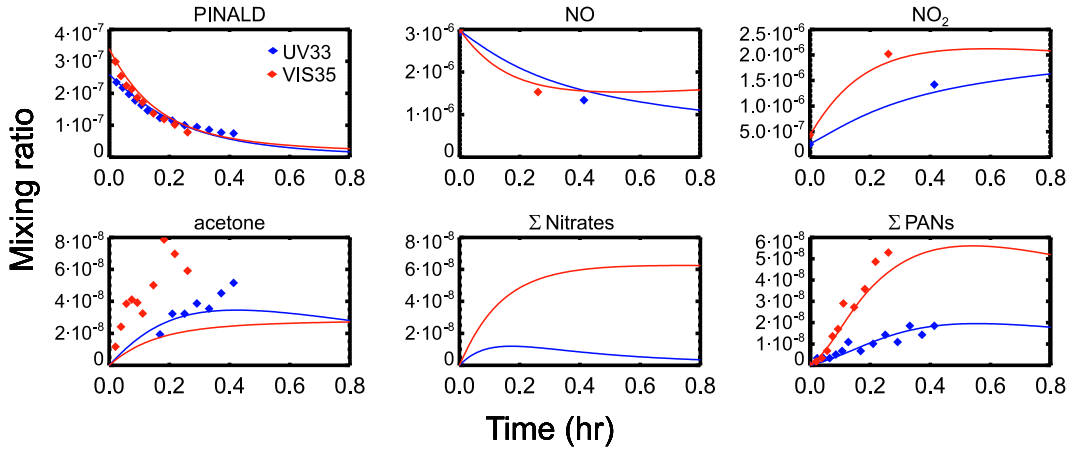

Figure 4.5: Measured (diamonds) vs simulated (curves) concentrations as a function of time for pinonaldehyde oxidation experiments in UV (experiment 33, blue lines), and in visible conditions (experiment 35, red lines) in the presence of NO_x from N99.

lower. Photolysis of pinonaldehyde is assumed to occur mainly around the ketone function in the UV (Sec. 2.4.3). The bond breaking produces the R_4 radical (see Fig. 2.4) leading to acetone. The model calculates that photolysis yields as much as 50% of acetone in these conditions. The apparent yield as well as the primary yield of acetone are in good agreement with the estimations of N99 for the UV conditions. The modeled apparent yield of acetone is lower in the experiments conducted under visible light because photolysis is negligible in these conditions. However the data show the opposite, with a twice higher apparent yield in the visible experiments. The causes of these differences are unclear.

4.2.5 Sensitivity studies

We evaluate the sensitivity of the model results to three sources of uncertainties. The first and probably most important of all is the incompleteness of the mechanism. As discussed in Sec. 2.3.4, the reactions of many primary products and radicals are treated in a crude way in the model. In order to assess the impact of these reactions, the standard model results are compared with simulations where the reactions of the generic peroxy radicals LXO2 and SXO2 (Eq. R2.28a to Eq. R2.33) are switched off. Figure 4.6 shows typical simulation results in presence and in absence of NO. When NO is present, the influence of the generic peroxy radicals is small in the first stage of the experiment, because the conversion of NO to NO_2 are due to radicals generated in the first reactions in the oxidation of α-pinene. Later on, the chemistry of the primary products becomes more important. When α-pinene is almost entirely oxidized, the NO to NO_2 conversion is mainly due to LXO2 and SXO2. The importance of these radicals is also noticeable for the total PANs concentrations, which are lowered by about 35% when this chemistry is omitted.

In absence of NO, the pinonaldehyde yield is significantly reduced (to 17%) when the chemistry of the generic radicals is switched off. This is due to the fact that the ring closure of R_7O_2 promoted by the absence of NO produces large amounts of LXO2 in the first steps of the oxidation process. These radicals contribute largely to the cross reactions producing pinonaldehyde.

Although the use of generic radicals allows us to simulate NO to NO_2 conversions and permutation reactions missing in our mechanism, it should be considered with caution, especially in NO_x-free conditions. The values of λ and the α_i in Eq. R2.27, R2.30 and R2.34 are indeed based on the high-NO assumption. In spite of this apparent limitation, however, the use of generic radicals provides satisfactory results for the simulations presented in this study. For example, the simulated concentrations of total PANs as well as of pinonaldehyde in absence of NO (both largely dependent on the chemistry of the generic radicals) reproduce well the measurements. The other products are not much influenced by this chemistry: e.g., the total peroxide yield in NO_x-free conditions goes down by only 5% (from the standard case of 30%) and the total organic nitrate yield decreases only from 14% to 12% in the experiments in presence of NO_x.

A similar sensitivity test performed in typical atmospheric conditions (Sec. 4.2.6), shows that the chemistry of the generic radicals has little influence on the primary yields of pinonaldehyde and acetone. Our representation of the missing chemistry in the mechanism can therefore be considered as reasonably accurate for predicting the product concentrations in the first stages of the oxidation of α-pinene.

In another sensitivity test, the uncertainties related to the rates of the reactions of inorganic and small organic ($C_{\leq 3}$) compounds have been investigated. For that purpose, the rates proposed by Atkinson et al. (2003) (IUPAC) for these reactions are replaced by those proposed by DeMore et al. (1997) and Sander et al. (2000) (JPL). This substitution affects the levels of OH and, therefore, the oxidation rate of α-pinene. As seen in Fig. 4.7, this rate is slightly higher when the JPL set is used. This difference is mainly due to two reactions :

$$\mathrm{OH + OH + M \rightarrow H_2O_2 + M} \qquad \text{(R4.4)}$$

and,

$$\mathrm{OH + NO + M \rightarrow HONO + M.} \qquad \text{(R4.5)}$$

Atkinson et al. (2003) report rates of 5.26×10^{-12} and 9.71×10^{-12} cm^3 molec^{-1} s^{-1} for reaction R4.4 and R4.5, respectively, whereas DeMore et al. (1997) gives 5.98×10^{-12} and 7.39×10^{-12} cm^3 molec^{-1} s^{-1}, respectively. When the JPL set is used in the visible simulations, the modeled apparent yield of pinonaldehyde is overestimated by 5%, a larger discrepancy than when the IUPAC set is used (2%). These changes remain reasonably small.

The rate of 3.5×10^{-11} cm^3 molec^{-1} s^{-1} proposed by Fantechi et al. (2002) is used in the model for the reaction of pinonaldehyde with OH. This value based on

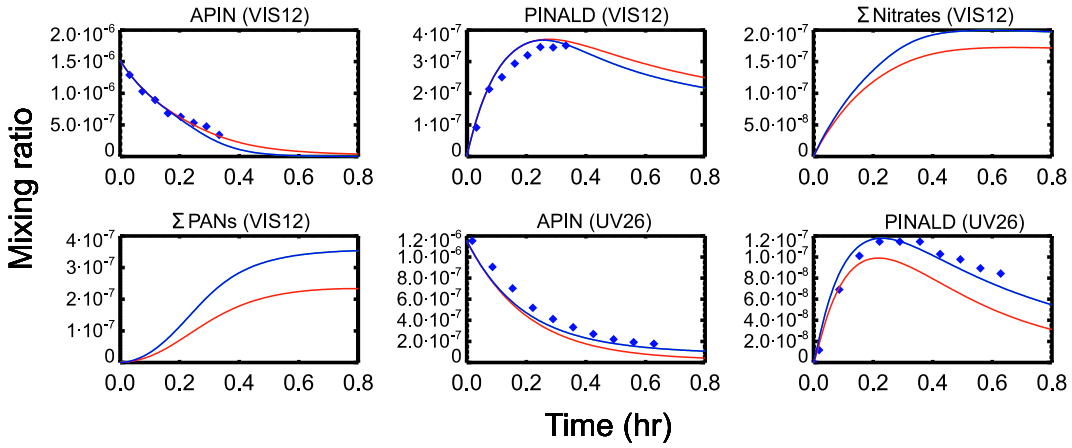

Figure 4.6: Modeled concentrations when the chemistry of the generic radicals LXO2 and SXO2 (see Sec.2.3.4) is omitted (red lines), and comparison with the standard case (blue lines). Effects in presence and absence of NO_x are represented by experiments VIS12 and UV26, respectively.

theoretical calculations is in fair agreement with the two most recent experimental values of 4-5$\times 10^{-11}$ cm^3 molec^{-1} s^{-1} (Alvarado et al., 1998; Nozière et al., 1999b). Setting the rate to the higher limit of 5×10^{-11} cm^3 molec^{-1} s^{-1} in the model leads to a slightly better match with the data for pinonaldehyde in visible conditions (Fig. 4.7). However in the UV conditions, pinonaldehyde is underestimated, with a calculated apparent yield of 41%.

4.2.6 Influence of the photochemical conditions on the modeled pinonaldehyde and acetone yields

The yield of pinonaldehyde is determined by the reactions of peroxy radicals: the reactions of R_2O_2 and $R_{12}O_2$ with NO, with HO_2 and with the other peroxy radicals, and the reaction with NO and the decomposition reaction of the α-hydroxy peroxy radicals R_3O_2, $R_3O_2^\dagger$, $R_{13}O_2$, $R_{13}O_2^\dagger$ (Fig. 2.2). Consequently, as already noted in Sec. 2.3.3, the yield depends on the photochemical conditions. Figure 4.8 represents the yield of pinonaldehyde as a function of NO and α-pinene. The solid blue line is the yield calculated by the model with an initial concentration of α-pinene of 400 ppb (1×10^{13} cm^3 molecule^{-1}), typical of the N99 experiments (standard case). In the chemical regime (A) (a "low NO_x" regime), the permutation reactions of the peroxy radicals are dominant and the decomposition reaction R2.23a and R2.24 are the only reactions of the α-hydroxy peroxy radicals. The pinonaldehyde yield is limited by the alkoxy channel ratio in the permutation reactions of R_2O_2 and $R_{12}O_2$. The regime B is characterized by a transition where the NO-reaction of R_2O_2 and $R_{12}O_2$ compete with the permutation reactions. This transition takes place at higher NO levels when the concentration of α-pinene is augmented, as shown by the dotted blue line in Fig. 4.8 calculated using a higher α-pinene level. The highest yield (61%) is reached when the

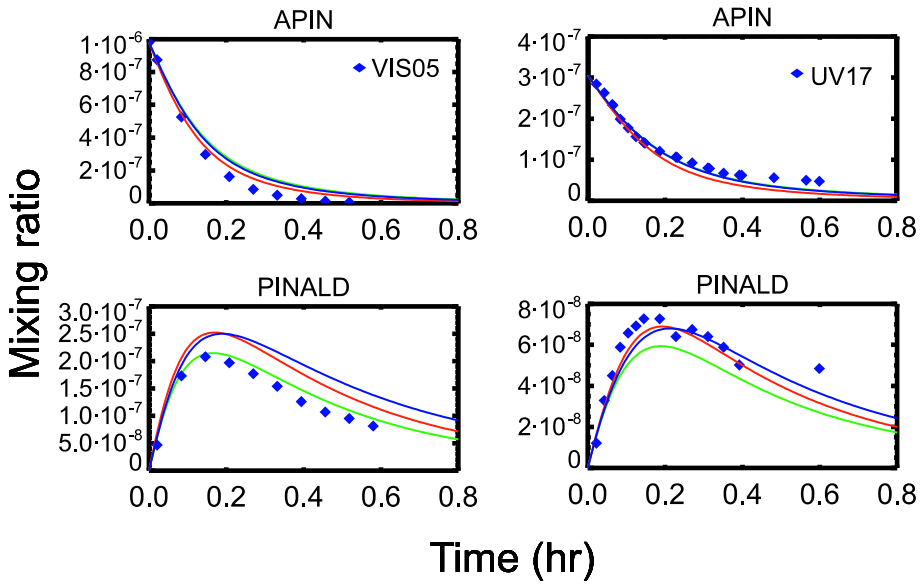

Figure 4.7: Modeled concentrations when the rates from DeMore et al. (1997) and Sander et al. (2000) are used (red lines) instead of the corresponding rates from Atkinson et al. (2003) (standard case, blue lines). The results using k(pinald+OH)=5$\times$10^{-11} cm^{-3} molec^{-1} s^{-1} are also shown (green lines).

NO-reaction is the only reaction for the radicals R_2O_2 and $R_{12}O_2$, and is still negligible compared to decomposition for the α-hydroxy peroxy radicals (Eq. R2.24, regime C). For NO $>$ 100 ppb (regime D) $k_{R2.25}$ becomes effective and reduces the production of pinonaldehyde. However the reaction of the tertiary radical R_3O_2 with NO plays only a minor role for NO concentrations below 10 ppm.

Besides the N99 experiments, other α-pinene+OH experiments have been performed at similar NO levels: Among these studies, Hatakeyama et al. (1991) derived a pinonaldehyde yield of 78.5 % (value adjusted by N99), whereas Wisthaler et al. (2001) deduced a yield of 34$\pm$9 %. A few experiments were made at higher concentrations of NO. Arey et al. (1990) and Hakola et al. (1994), with about 10 ppm of NO derived yields of 28$\pm$5% and 29$\pm$5% respectively. These results are in fair agreement with the modeled yield considering the uncertainty on the rates $k_{R2.23a}$, $k_{R2.23b}$ and $k_{R2.24}$. They tend to confirm the predicted decrease of the pinonaldehyde yield for NO concentrations higher than 100 ppb.

The yield of acetone is also dependent of NO. For NO $<$ 1 ppb, the ring closure reaction of radicals R_7O_2 outruns the other reactions and the acetone production pathway proceeding through the reaction of R_7O_2 with NO or RO_2 is negligible. The ring closure products being unknown, it is unfortunately not possible to provide theoretical estimates of the acetone yield at low NO_x (regime A and B). In regime C (NO $\geq$ 100 ppb), the ring closure reaction becomes negligible and the acetone yield is estimated to be about 10%. In regime D, the channel promoted by R_3O_2+NO brings

an additional contribution to the primary yield of acetone which reaches 17% for 100 ppm of NO.

In the atmosphere, the abundances of α-pinene and NO are usually much lower than in the reactor. Typical atmospheric concentrations of [NO] range from several ppt to several hundreds of ppt. It follows that the α-hydroxy peroxy radicals R_3 and R_{13} decompose entirely to pinonaldehyde. The influence of the reaction with NO (Eq. R2.25) is restricted to laboratory conditions when [NO]$\geq$100 ppb. The other usual reactions of peroxy radicals compete with each other in the atmosphere. In particular, we can expect HO_2, CH_3O_2, and the peroxy radicals produced by the oxidation of isoprene and the other VOC to play a significant role.

The dependence of the pinonaldehyde yield on NO concentration in the atmosphere is illustrated by the black curves in Fig. 4.8. They represent the yield calculated with the box model in relatively typical atmospheric conditions, with [CH_4]=1.7 ppm, [CO]=300 ppb (a higher than usual mixing ratio in order to represent the effect of other VOC), [O_3]=30 ppb, T=298 K, relative humidity=50%, and [α-pinene]=100 ppt (solid line) or 500 ppt (dash dotted line). The photolysis rates are those reported in Tab. 2.6 and 2.7. In these conditions, [OH] and [HO_2] are calculated to range between 4 and 6 $\times$ 10^6 and 3 and 4 $\times$ 10^8 molecules cm^{-3}, respectively.

The pinonaldehyde yield varies significantly with the level of NO from about 10% (NO$\sim$5 ppt) in clean conditions to more than 50% for NO$\geq$200 ppt. This variation results almost exclusively from a competition between NO- and HO_2-reactions of the peroxy radicals. The permutation reactions bring only a minor contribution to pinonaldehyde production. The α-pinene concentration has therefore little influence on the product distribution. Note that the chemical interactions with other VOC and in particular the biogenic compounds are not taken into account in these calculations. The photooxidation of isoprene, the most abundant biogenic VOC (Guenther et al., 1995), generates peroxy radicals bearing alcoholic and allyl functionalities (Paulson and Seinfeld, 1992). Half of them have self-reaction rates typical of the R1H or R2M classes (see Tab. 2.2). We can expect the cross reactions between these radicals and those from α-pinene to occur in the canopy and to offer an additional channel to the production of pinonaldehyde.

The dependence of the total primary nitrate and hydroperoxide yields with NO has also been calculated for typical atmospheric conditions, with [α-pinene]=500 ppt. As seen in Fig.4.9, the production of hydroperoxides is expected to be important in the atmosphere, with a yield close to 90% at very low NOx (1 ppt NO), and as high as 30% at 100 ppt of NO. Hydroxy hydroperoxides represent the majority of these hydroperoxides. They have low vapor pressures and high solubilities and may therefore have a strong impact on SOA formation (Bonn et al., 2004).

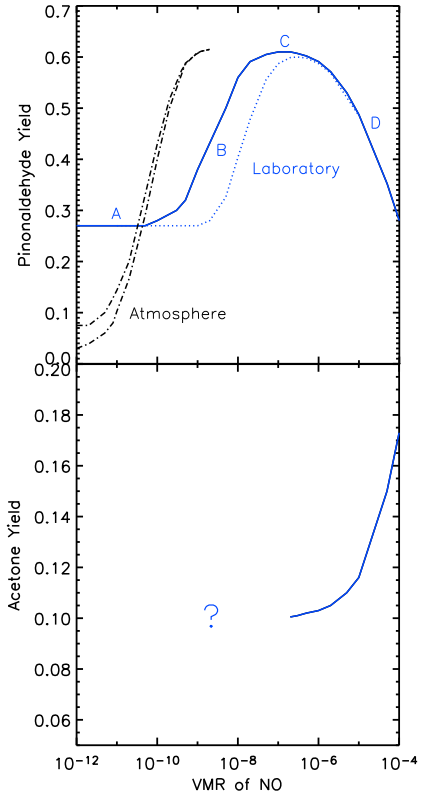

Figure 4.8: Yields of pinonaldehyde (upper panel) and acetone (lower panel) as a function of the NO volume mixing ratio (VMR). The blue curves correspond to laboratory conditions, with [α-pinene]=400 ppb (solid lines) or [α-pinene] = 20 ppm (dotted lines). The black curves correspond to atmospheric conditions, with [α-pinene] = 100 ppt or [α-pinene] = 500 ppt (dash dotted lines).

4.2.7 Comparison results for aerosol formation

In addition to the gas phase products, the production and composition of secondary organic aerosols in the N99 experiments has been estimated, based on the partitioning model described in the preceding chapter. This aerosol model relies on the vapour pressure prediction method described in Sec. 3.2.2. It has been noted that the relative uncertainty on the estimated vapour pressures of multifunctional organic compounds can reach a factor of three, in particular, in the case of heterofunctional compounds (e.g. hydroxy ketones and tri-O-acids, see Tab. 3.1). Such a large uncertainty can have significant effects on the calculation of the partitioning coefficients and consequently on the production of particulate compounds. The impact of this uncertainty on the results has been estimated by using the following approach. Instead of performing only one simulation for each N99 experiment, a series of 30 simulations

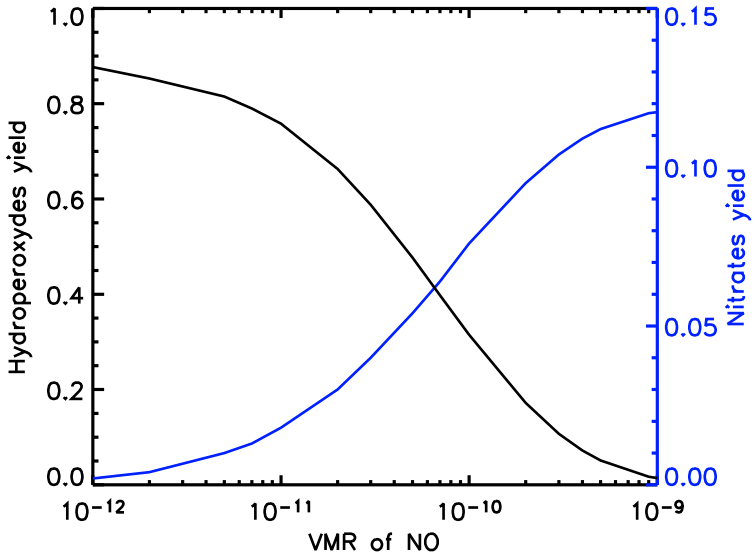

Figure 4.9: Primary yields of total hydroperoxide (black curve) and total nitrate (blue curve) as a function of the NO volume mixing ratio (VMR) in atmospheric conditions, with [α-pinene] = 500 ppt.

has been performed using randomly perturbed sets of vapour pressures:

$$log\ p_{L,i}^{0,pert} = log\ p_{L,i}^{0,mod} + \Delta_i, \tag{4.5}$$

where the index i denotes the compound. $p_{L,i}^{0,mod}$ is the best estimate of the vapour pressure of compound i as obtained using our prediction method, whereas $p_{L,i}^{0,pert}$ is the perturbed vapour pressure actually used in the model. The set of Δ_i are random numbers normally distributed with $\sigma = 0.5$, reflecting the bias between the model and the measurements for low-volatile compounds. For each run, a new set of Δ_i is selected for all compounds i. The normal distribution of Δ_i reproduces similarly the distribution of the differences between the measured and the estimated vapour pressures (Fig. 3.3).

The degradation of α-pinene is successfully simulated by our model for four out of the five experiments providing aerosol-phase measurements. Experiments 19 and 21 are discarded from the analysis because they show a mean bias between the modeled and measured α-pinene concentrations higher than 10%. For each of the three experiments remaining, 30 series of simulations were performed with different sets of $p_{L,i}^{0,pert}$. Results of this sensitivity test are shown in Fig. 4.10, 4.11 and 4.12 .

The simulations of the aerosol in the three experiments show a systematic bias. The measurements indicate that aerosol production starts as soon as the photooxidation is initiated, whereas aerosol production starts 5 to 10 minutes after the beginning of the experiment according to the model. The slow aerosol production in the model is due to the semi-volatility of the hydroxy nitrates and, hydroxy peroxy acyl nitrates

constituting the aerosol in high NO_x conditions. The vapour pressures of these products are higher than 10^{-4} torr. Therefore an accumulation of these compounds in the gas phase is necessary to trigger the aerosol production. Note that pinonaldehyde does not contribute to the aerosol phase, confirming our analysis of the gas phase. In any case, uncertainties on the estimated vapour pressures cannot explain this systematic difference between the model and the data. To date, no reason could be found to explain the observed fast aerosol production, particularly in absence of seed particles. A lower volatility product is possibly formed in the gas phase in the first steps of the OH-oxidation, which is not currently taken into account in the model.

Experiments "UV17" and "UV20" performed with the same initial concentration of α-pinene ($\sim$300 ppb) give both an aerosol yield between 2 and 5%. The higher yield of 20% in Experiment "UV18" results in part from the larger initial concentration of the precursor hydrocarbon (1.5 ppm). Furthermore, the model predicts a complete conversion of NO occurring before α-pinene is completely oxidized. The absence of NO results in an increase of hydroxy PANs and hydroxy hydroperoxides compounds contributing to the particulate phase.

In presence of NO_x, LXONO2 and LXPAN are the main products of the generic peroxy radicals $LXO2_i$. Their vapour pressures are estimated on the basis of the structures of the explicit products generated in the oxidation mechanism. LXONO2 and LXPAN are not produced in large amounts (their total yield does not exceed 2%) and although these products are multifunctional, their carbon number is assumed equal to 8, which makes them rather volatile. For these reasons, these products are found to contribute little to the aerosol phase at high NO_x.

Although the model does not reproduce the observed timing for aerosol production, the different simulations reproduce the correct order of magnitude of the total aerosol yield in the three experiments. Other experimental studies have been conducted to quantify the production of aerosols in the α-pinene/OH/NO_x system. Hatakeyama et al. (1991) and Bonn and Moortgat (2002) used 1.3 ppm and 500 ppb of initial α-pinene, respectively. On the basis of the measured volume concentration of aerosols, we estimate molar aerosol yields of the order of 20% and 2-3% for these studies, respectively, in good agreement with the yields of N99 obtained at similar concentrations of α-pinene. Note, however, that the actinic conditions in both experiments are different than in N99 due to the choice of different lamps.

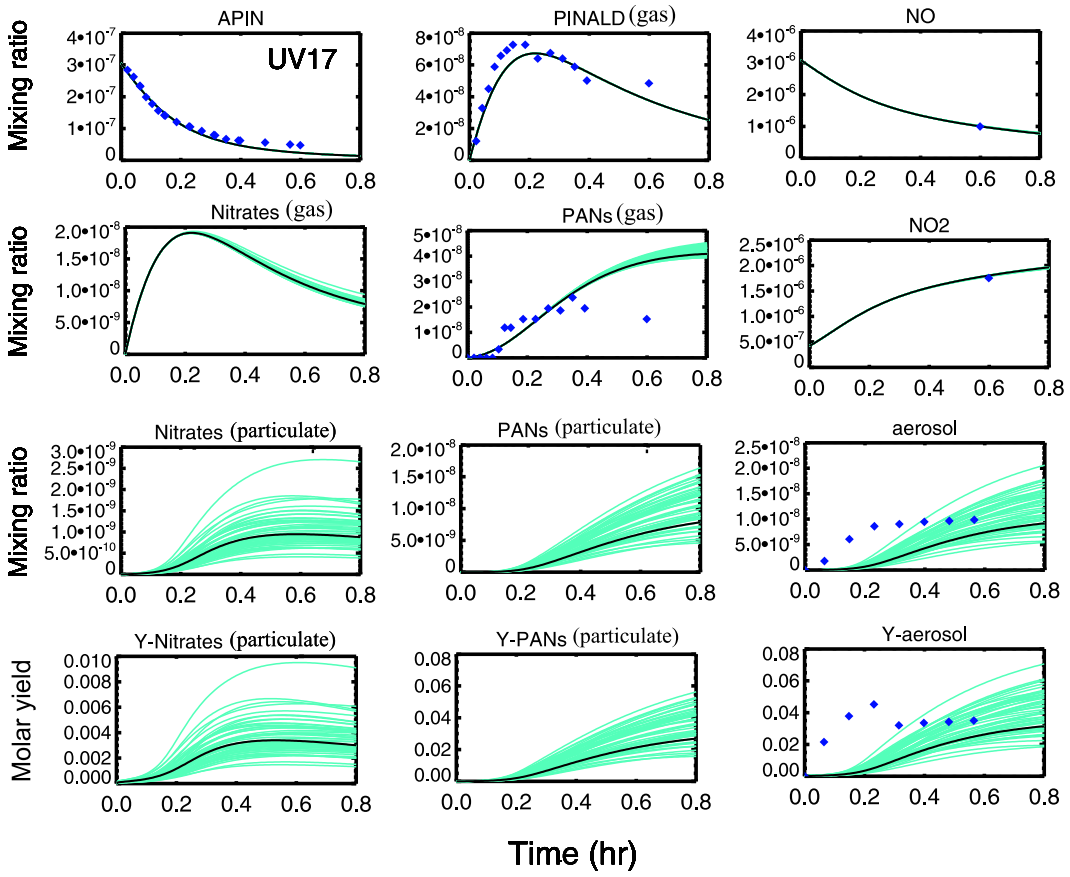

Figure 4.10: Simulations of experiment 17 from N99. Each run (green curves) corresponds to different choices of Δ_i (Eq. 4.5). Black curves correspond to Δ_i=0 for all compounds. Experimental data are represented by the diamonds. Compound names preceded by "Y-" denote the molar yield of this (class of) compound(s)

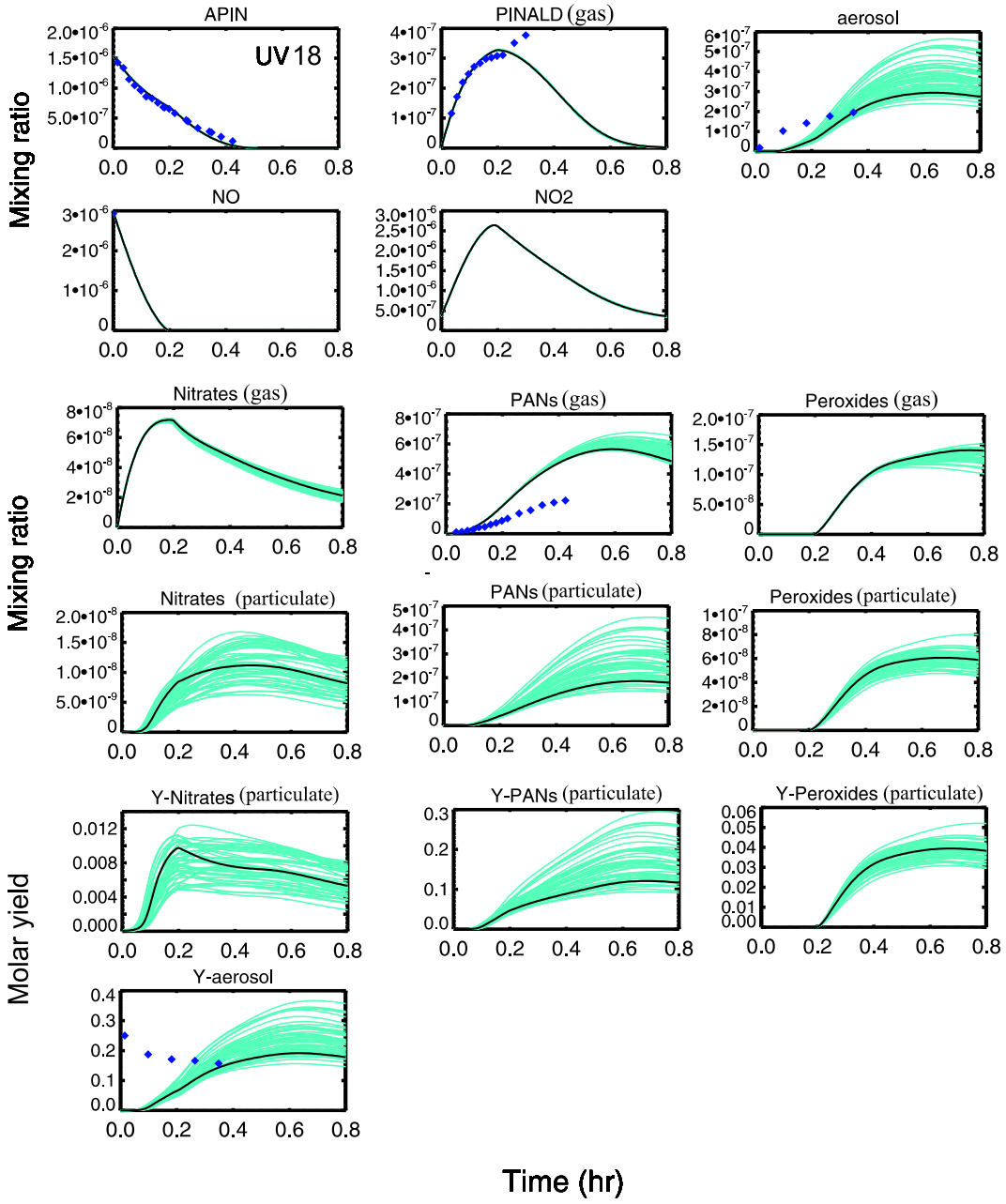

Figure 4.11: Simulations of experiment 18 from N99. Each run (green curves) corresponds to different choices of Δ_i (Eq. 4.5). Black curves correspond to Δ_i=0 for all compounds. Experimental data are represented by the diamonds. Compound names preceded by "Y-" denote the molar yield of this (class of) compound(s)

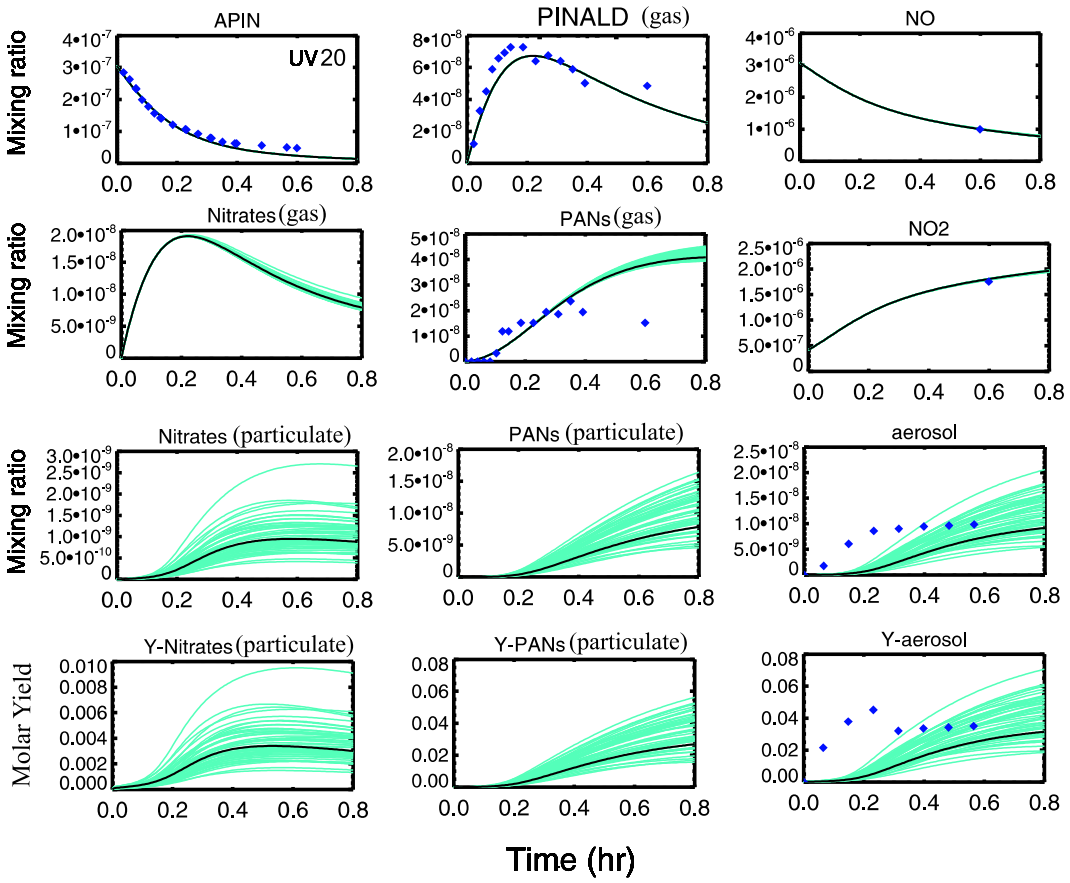

Figure 4.12: Simulations of experiment 20 from N99. Each run (green curves) corresponds to different choices of Δ_i (Eq. 4.5). Black curves correspond to Δ_i=0 for all compounds. Experimental data are represented by the diamonds. Compound names preceded by "Y-" denote the molar yield of this (class of) compound(s).

4.3 α-pinene+O_3 experiments

4.3.1 Description of the experiments

Table 4.2 summarizes the conditions of the experiments studied in this work. In general, experiments are performed around 290 K, 308 K or 320 K, with initial concentrations of α-pinene between 10 and 150 ppb. The relative humidity does not exceed 20% in the three series of experiments. These dry conditions are expected to result in a negligible role for aqueous processes in the aerosol phase since these relative humidities are well below the deliquescence relative humidities of usual organic aerosols (Marcolli et al., 2004).

Yu et al. (1999a) performed the most detailed qualitative and quantitative analysis of the products. Besides the total aerosol mass measurements, they also provided concentrations of individual products in both the gas and particulate phase. Samples were treated by gas chromatography/Mass spectrometry (GC/MS). Yu et al. (1999a) deduced the partitioning coefficients for these compounds from their measured gas and aerosol phase concentrations.

Hoffmann et al. (1997) investigated the formation of aerosols during the ozonolysis of biogenic hydrocarbons in the dark. The instrumentation included two scanning electrical mobility spectrometer (SEMS) and two condensation nucleus counters (CNC). α-pinene experiments were carried out at different initial concentrations and without OH scavenger. Experiments performed in the framework of the "BIOVOC" project (BIOVOC, 1998; Christoffersen et al., 1998) included measurements of the aerosol mass produced in the ozonolysis of α-pinene at different temperatures, with and without OH scavenger. The aerosol yields were calculated on the basis of the aerosol volume, measured by a Differential Mobility Analyser (DMA). Note that neutral seed particles ($(NH_4)_2SO_4$) were injected prior to each experiment in Yu et al. and Hoffmann et al.. No seeds were used in the BIOVOC experiments.

Many parameters influencing the chemical conditions differ from one experiment to one another (temperature, initial concentrations, type of scavenger, relative humidity, addition of seeds, sampling time) which makes the comparisons between experimental yields difficult. Moreover, the three groups used different experimental set ups (e.g. measurement methods, reactor volumes). Therefore, measurement biases, wall losses and possible wall desorptions might differ in the three series of experiments. Yu et al. estimated the experimental uncertainty associated to the product yields to $\sim$50%. Neither Hoffmann et al. nor BIOVOC provided uncertainty estimates. However, the comparison of the yields from experiments performed in close conditions (e.g. Hof_F vs. Bio_I,Bio_A vs Bio_B) reveals differences of a factor 2-3 on the aerosol yield, suggesting the existence of large uncertainties in the BIOVOC results.

Table 4.2: Ozonolysis experiments investigated using the box model. ΔM_o is the aerosol mass produced from the oxidation (directly measured or calculated from volume measured)

References	Experiments	T K	$\Delta(\alpha$-pinene) ppb	RH %	OH scavenger	ΔM_o $\mu g\ m^{-3}$
Yu et al. (1999a)	Yu_A	308	57.0	5	2-butanol	54.2
Yu et al. (1999a)	Yu_B	308	65.1	5	2-butanol	65.1
Yu et al. (1999a)	Yu_C	306	45.1	5	2-butanol	38.8
Hoffmann et al. (1997)	Hof_A	322	38.0	5	none	29.9
Hoffmann et al. (1997)	Hof_B	321	88.0	5	none	82.0
Hoffmann et al. (1997)	Hof_C	320	101.9	5	none	80.4
Hoffmann et al. (1997)	Hof_D	319	132.9	5	none	94.9
Hoffmann et al. (1997)	Hof_E	321	154.1	5	none	183.5
Hoffmann et al. (1997)	Hof_F	289	88.5	5	none	341.0
BIOVOC-project	Bio_A	293$\pm$2	745	1	cyclohexane	967.8
BIOVOC-project	Bio_B	297.5$\pm$1.5	684	1	cyclohexane	1699.8
BIOVOC-project	Bio_C	290.5$\pm$1.5	790	20	cyclohexane	2364.8
BIOVOC-project	Bio_D	292$\pm$1	74	20	cyclohexane	62.7
BIOVOC-project	Bio_E	291$\pm$1	55	1	none	62.1
BIOVOC-project	Bio_F	293$\pm$3	10	1	none	2.3
BIOVOC-project	Bio_G	289$\pm$3	66.6	1	cyclohexane	56.4
BIOVOC-project	Bio_H	292$\pm$2	63.7	1	cyclohexane	68.4
BIOVOC-project	Bio_I	289.5$\pm$1	85	20	none	105.6

4.3.2 Mechanism for the formation of condensable products

Very small aerosol yields are predicted by the box model simulations of Yu et al. experiments using the gas phase mechanism described in Sec. 2.3 ($\sim$1%). The reason is the relatively high volatility of the products. As mentioned is Sec. 2.3, although pinic acid and hydroxy pinonic acid are known products resulting from the ozonolysis of α-pinene, their formation processes remain so far unknown and are therefore missing in our gas phase mechanism. These two compounds are expected to be very condensable (p_L^0= 3$\times$10^{-6} torr and p_L^0=6$\times$10^{-7} torr for pinic acid and hydroxy pinonic acid, respectively) and to adsorb promptly on the aerosol seeds. Their presence would lead to an increase in the aerosol mass M_o, thereby allowing more volatile compounds to condense according to Eq. 3.1. Therefore these two compounds play an essential role in the formation of aerosol, and they need to be taken into account somehow.

A simplified reaction path has therefore been adopted to represent the formation of these two compounds, on the basis of the Yu et al. experimental results. Given that the use of the OH scavenger, 2-butanol, by Yu et al. leads to a large production of HO_2 (as simulated using the MCM mechanism of Saunders et al. (2003)) and therefore to a large production of hydroperoxides and acids in the reactions of (acyl) peroxy radicals, pinic acid and hydroxy pinonic acid must be produced in the early steps of the

oxidation mechanism after one peroxy radical reaction or less. We adopted a prompt formation of both acids from the radical Crieg II. Their overall yield (gas and aerosol phase) in the ozonolysis of α-pinene are taken to be 3% for each of them, based on laboratory observations (Christoffersen et al., 1998; Hoffmann et al., 1997; Glasius et al., 2000; Kamens et al., 1999; Yu et al., 1999a). The ratio of the hydroperoxide channel of Crieg II has been reduced correspondingly. The reduction remains within the uncertainty of the channel ratio.

The dimerization of carboxylic acids in the gas phase has been introduced in Sec. 3.2.4. The equilibrium reaction on the form:

$$acid + acid \rightleftharpoons dimer, \tag{R4.6}$$

has been observed to produce large amounts of dimers and adducts of pinic acid and pinonic acid in smog chambers (Hoffmann et al., 1998; Kuckelmann et al., 2000). Theoretical estimations by Peeters and Vereecken (2005) for pinic acid dimer leads to an equilibrium constant K_{eq} = 2×10^{-29} exp(15400/T) cm^3 $molecule^{-1}$ and a dimerization rate k = 1×10^{-12} exp(1000/T) cm^3 $molecule^{-1}$ sec^{-1}. In absence of estimations for other multifunctional carboxylic acids dimers, these kinetic constants are adopted in our box model for all dimers/adducts equilibrium reactions involving pinic, pinonic and pinalic acid. As discussed in Sec. 3.2.4, the vapour pressures of the dimers formed in the α-pinene oxidation mechanism are assumed to be equal to the vapour pressure of pinic acid (with the same temperature dependence).

4.3.3 Total yield of products

Two of the three experiments by Yu et al., Yu_A and Yu_B were performed in excess of ozone and sampled after 4 hours, whereas α-pinene was in excess in experiment Yu_C and the sampling was made before one hour of experiment. The experiments being performed in presence of a scavenger and without light, the losses of the products by secondary reactions in the gas phase can be neglected. The compounds identified by Yu et al. can be considered as primary products. The losses on the walls are small compared to the experimental uncertainty and the apparent yields can be assumed equal to the true yields (Sec.4.2.2). Table 4.3 reports the averaged total yield (gas+aerosol phase) of the products measured. The yields of hydroxy pinonaldehyde (&isomers), pinonaldehyde and pinonic acid (see Appendix A for identification of the products) are well reproduced by the box model. However, the yields of hydroxy pinonaldehydes and pinonic acid are lower by a factor 3-4 in both samples taken after 4 hours (Yu_A and Yu_B) compared to the sample taken after one hour (Yu_C). No reason has been found that could explain this difference. Model and measurements disagree for the yields of norpinonaldehyde and norpinonic acid (&isomers). Causes may include the uncertainty in the branching ratios of the Criegee reactions, and the uncertainty in the rates and product ratios of the permutation reactions of peroxy radicals, since these reactions are responsible for the propagation of the oxidation chain

Table 4.3: Experimental and modeled yields of products in the experiments performed by Yu et al. (1999a)

	Molar Yield (%)				
Species	Exp.	Model	Species	Exp.	Model
Pinic acid*	4.8±1.3	3.2	Pinonaldehyde	11.8±5.4	12.8
Hydroxy pinonic acid*	2.7±0.9	2.7	Norpinonaldehyde	1.8±0.6	6.5
Pinonic acid	4.2±2.6	6.3	Hydroxy pinonaldehyde	5.6±4.0	9.8
Norpinonic&Isom.	9.0±3.5	3.2			

* Using adjusted mechanism (See Sec. 4.3.2)

in absence of NO_x.

Several studies have reported the production of acetone from experiments of α-pinene ozonolysis performed in the dark (BIOVOC, 1998; Reissel et al., 1999; Orlando et al., 2000). The experimental molar yields range between 3% and 9%. Simulations in the same conditions indicate a negligible primary yield ($<$1%). This low value is explained by the fact that acetone is produced in the ultimate steps of the oxidation paths Ia and Ib of the ozonolysis mechanism (Fig. 2.3). In absence of NO_x, the permutation reactions of RO_2 compete with the reactions with HO_2. Due to the high levels of HO_2, low yields are predicted for the products generated after the first oxidation steps. The missing fraction of acetone reveals the existence of missing routes in our ozonolysis mechanism.

4.3.4 Aerosol phase simulations

Table 4.4 reports the distribution of the products between the gas and the aerosol phase modeled for typical experiments. The box model reproduces well the equal distribution of the carboxylic acids between both phases in experiment Yu_B. However the model underestimates the particulate matter concentration by 10-20% (Tab. 4.5) in the three experiments of Yu et al.. This underestimation might be due to the absence of carbonyl compounds in the simulated aerosol phase. Yu et al. reported indeed that an equivalent fraction of the aerosol phase is made mainly of pinonaldehyde and hydroxy pinonaldehyde. The low partitioning coefficients calculated in the model for carbonyl compounds result from their high volatility. Heterogeneous reactions, such as oligomerization processes described in Sec. 3.3 are believed to explain their partitioning. The oligomeric products were not identified in the experiments used in this study because the detection and characterization methods used to study SOA induce back decomposition of the oligomers to the primary monomers (Tolocka et al., 2004). The oligomerization reactions are not included in the box model, because they remain so far unclear. Many factors, such as the relative humidity and the acidity of the aerosol, seem to influence the formation of oligomers. However, although heterogeneous reactions are not modeled, the time dependence of the aerosol is well

Table 4.4: Modeled gaseous and particulate yields of the main products generated from the ozonolysis of α-pinene in the experiments Yu_B, Bio_C, Bio_G, Bio_E (see Tab. 4.2)

Species	Yu_B		Bio_G		Bio_C		Bio_E	
	Y_{gas}	$Y_{part.}$	Y_{gas}	$Y_{part.}$	Y_{gas}	$Y_{part.}$	Y_{gas}	$Y_{part.}$
Pinonic acid	2.6	3.8	0.2	6.1	0.	6.1	0.3	3.9
Pinalic acid	1.4	1.8	0.1	3.9	0.	4.1	0.1	1.5
Pinic acid	1.3	1.9	0.1	3.1	0.	2.4	0.1	1.8
Perpinalic acid	11.0	0.	13.2	0.8	6.3	7.2	5.2	0.2
Hydroxy pinonic acid	0.7	1.9	0.	2.9	0.	2.7	0.	1.9
Hydroperoxides	35.5	0.7	3.4	7.5	0.	9.8	4.3	2.9
Hydroxy pinonaldehyde&Isom.	9.3	0.	11.4	1.1	4.2	7.2	6.0	0.3

Table 4.5: Modeled vs experimental yields for the ozonolysis experiments listed in Tab. 4.2

Experiments	Y_{SOA} (%)		Experiments	Y_{SOA} (%)	
	Exp.	Model		Exp.	Model
Yu_A	11.5	9.4	Bio_A	15.64	40.1
Yu_B	12.0	10.1	Bio_B	29.9	37.1
Yu_C	10.4	9.5	Bio_C	36.0	43.9
Hof_A	9.5	0.	Bio_D	10.2	23.0
Hof_B	11.2	0.4	Bio_E	13.6	15.7
Hof_C	9.5	0.8	Bio_F	2.72	3.9
Hof_D	8.6	2.3	Bio_G	10.2	26.1
Hof_E	14.3	1.8	Bio_H	12.9	22.0
Hof_F	46.1	17.9	Bio_I	15.0	15.9

reproduced by the model for the Yu et al. experiments, as shown in Fig. 4.13.

The acid dimer formation affects significantly the aerosol formation. Figure 4.14 shows the impact of dimerization as a function of the reacted α-pinene at different temperatures (290 K, 308 K, 320 K). The modeled yields shown in the figure are based on simulations of typical ozonolysis experiments after two hours, in presence of cyclohexane as scavenger. Experimental yields from Yu et al. and BIOVOC performed in similar conditions are also shown. Simulations performed without accounting for the dimerization process show a lower production of aerosols. Almost no particulate matter is formed at 308 and 320 K for $\Delta\alpha$-pinene $<$ 100 ppb. Due to the fast rate of the forward reaction (Eq. R4.6), the three acids involved in the dimerization are under the form of dimers in the range of ambient temperatures. Therefore, pinonic acid which does not condense significantly as monomer (p_L^0=3$\times$10^{-3} torr at 298K), is incorporated in the aerosol phase through dimerization processes ($p_L^0 \leq$3$\times$10^{-6} torr

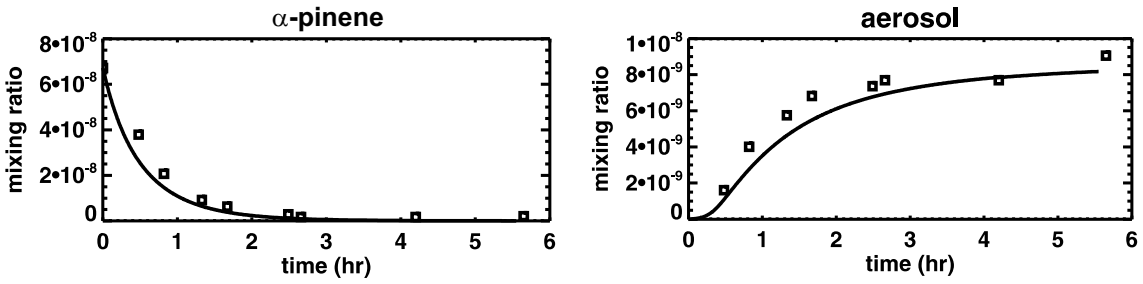

Figure 4.13: Time-dependent concentrations of α-pinene and SOA in experiments Yu_B from Yu et al. (1999a)

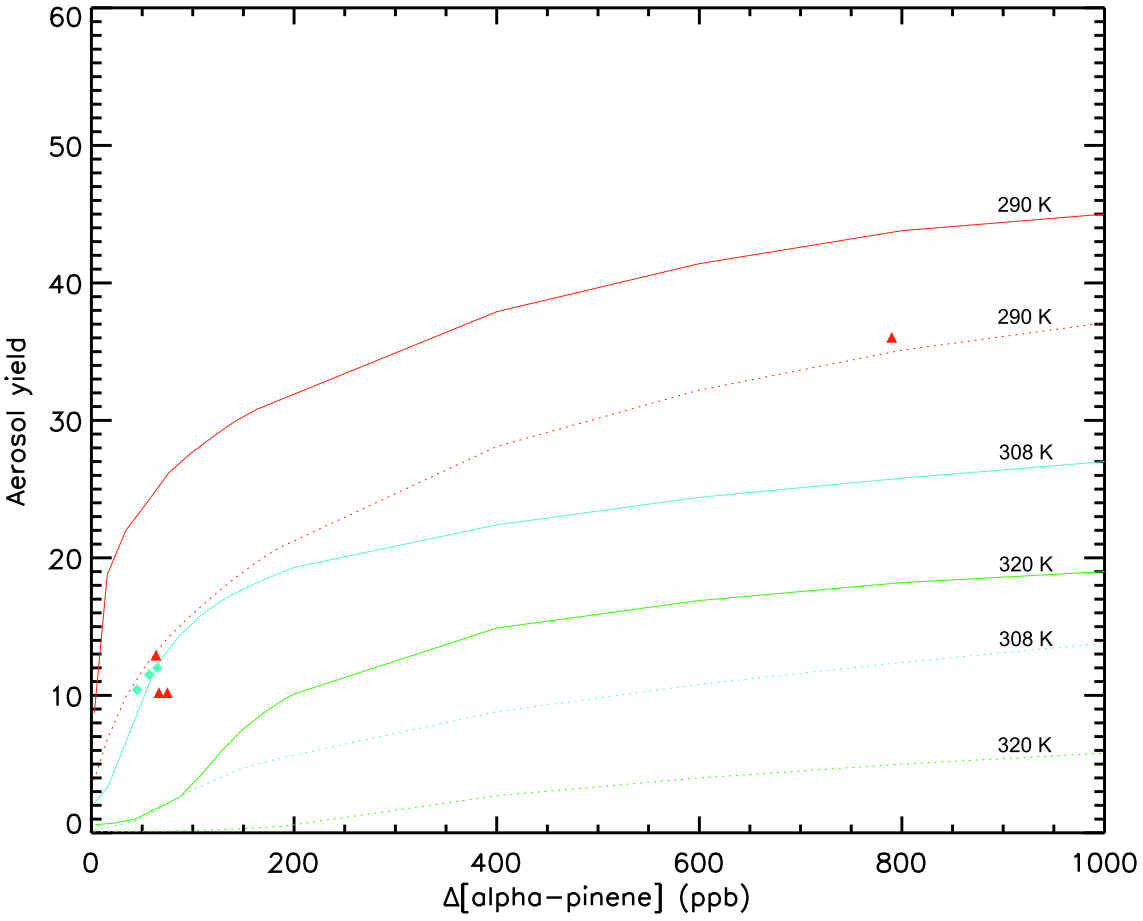

Figure 4.14: Aerosol yield as a function of the concentration of α-pinene oxidized by O_3, in presence of a scavenger (cyclohexane). Experimental yields are represented by triangles (Bio_H, Bio_G, Bio_D, Bio_C) and diamonds (Yu_A, Yu_B, Yu_C). Model simulations with (solid lines) and without (dotted lines) the acid dimerization reactions are also shown. Colors characterize temperature of interest: Red for 290 K, blue for 308K, and green for 320 K.

at 298 K for the dimers and adducts of pinonic acid). However, due to the adopted temperature dependency of the vapour pressures, the dimers are too volatile at 320K.

A sensitivity test on the SOA yields has been performed using a different approach for the vapour pressures of the dimers and adducts. The dimers were assumed to have the same volatility as their corresponding monomers. Following an hypothesis outlined in Sec. 3.2.4, the adducts formed by pinonic acid (or pinalic acid) with pinic acid were supposed to have a low volatility because of the free carbonyl site. Their vapour pressures have been calculated using the vapour pressure of pinic acid reinforced by the carbonyl contribution as:

$$log\ p^0_{L,\text{adduct}}(T) = log\ p^0_{L,\text{pinic acid}}(T) + \tau_{carb}(T). \quad (4.6)$$

As a consequence, the dimers of pinic acid and the adducts pinonic acid (pinalic acid)/pinic acid (4.9×10^{-7} torr) are the only dimeric forms which condense at ambient temperature. Simulations of the Yu et al. experiments with these vapour pressures indicate that the proportion of dimers/adducts in the aerosol decreases only from $\sim$11% to $\sim$7%.

Experiments BIO_D, BIO_G, BIO_H used a similar amount of α-pinene as in Yu et al., but at $\sim$ 290 K. The model simulates a yield of $\sim$ 24%, whereas the measurements indicate yields close to those of Yu et al. (10-13%) despite a difference of 18 K between both experiments. These similar yields are difficult to explain since, according to the strong temperature dependence of the partitioning coefficient (via the vapour pressure), such a marked decrease of the temperature should favour an increase in SOA production. At higher concentration of converted α-pinene (BIO_C), the model and the measurements are in fair agreement. At lower temperatures, the hydroperoxide compounds contribute more to the aerosol phase. Due to the stronger temperature dependence of their vapour pressures with respect to other compounds, they represent about 30% of the aerosol in experiment Bio_G, to be compared with the small fraction (7%) predicted in experiment Yu_B (Tab. 4.5). Small amounts of semi-volatile hydroxy carbonyls are also found in the aerosol. Note that for all conditions, perpinalic acid is an important primary product although it has not been identified so far in experimental studies.

The series of experiments by Hoffmann et al. as well as several BIOVOC experiments were performed without any OH scavenger. The BIOVOC experiments (BIO_E and BIO_I) are in good agreement with the box model. However, the simulations of the Hoffmann et al. experiments predict a negligible production of aerosol contrasting with the averaged experimental yield of 10%. The unability to model SOA concentrations at low and particularly at high temperature may be due to the simplified kinetic scheme adopted for the formation of dimers and the crude estimation of their temperature dependent vapour pressures.

The sensitivity tests performed with the model highlight the influence of the scavenger (Fig. 4.15). In the simulations without OH scavenger, about one third of α-

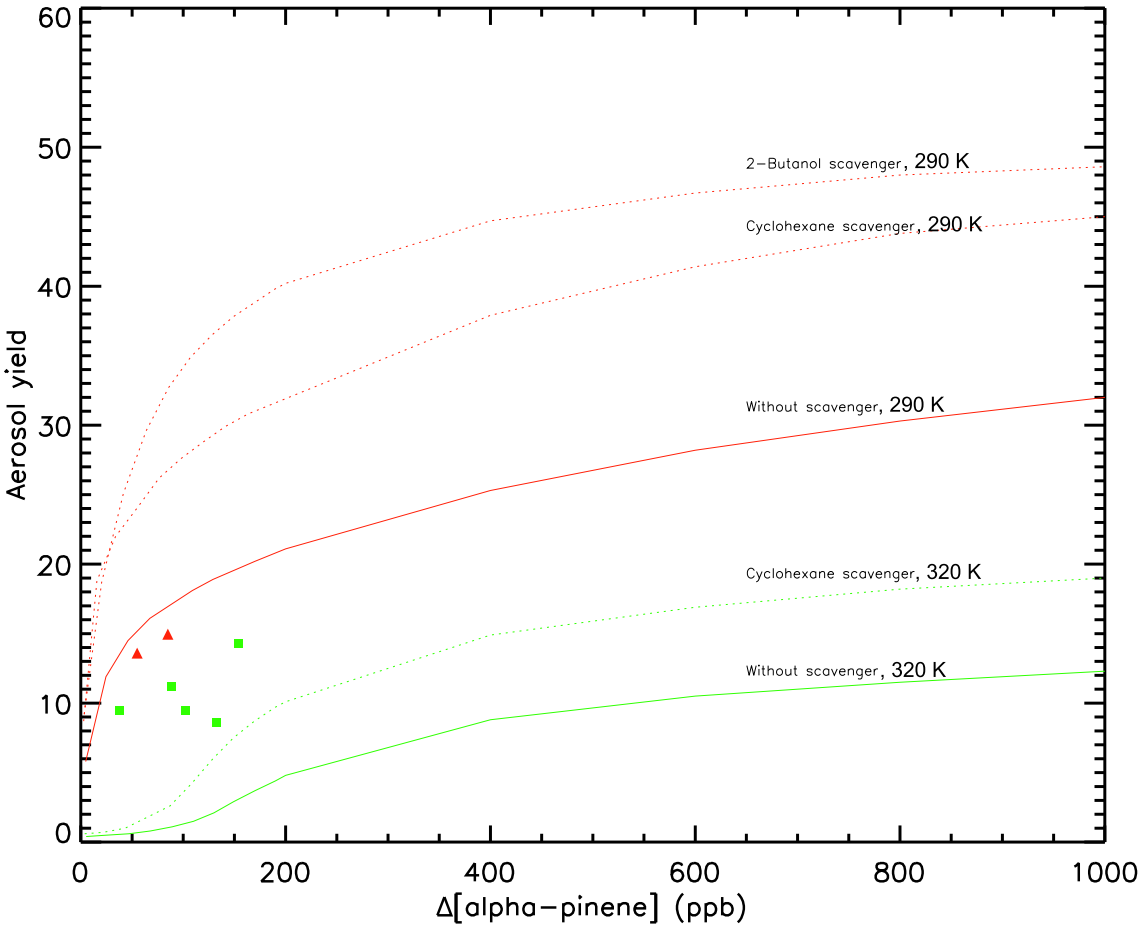

Figure 4.15: Aerosol yield as a function of the concentrations of α-pinene oxidized. Symbols represent the yields in experiments performed without scavenger: Squares and triangles are used for Hoffmann et al. (1997) and BIOVOC experiments (Bio_E and Bio_I), respectively. The effect of the scavenger is shown by model simulations (solid lines). Colors characterize temperature of interest: Red for 290 K, and green for 320 K.

pinene is oxidized by OH. Scavenging the hydroxyl radical is found to increase the SOA production in similar proportions. This confirms the view that ozonolysis is the major oxidation path for the generation of condensables. Interestingly, the chemical conditions are affected by the choice of the scavenger. The oxidation of 2-butanol by OH generates an important amount of HO_2 (Saunders et al., 2003). Consequently, a more important production of hydroperoxides is seen in the Yu et al. (1999a) experiments (Tab. 4.5) where 2-butanol is used as scavenger, compared to the BIOVOC experiments using cyclohexane. This effect is almost negligible regarding aerosol formation at 308 K. However, the sensitivity test shows that at 290K, the amount of particulate products increases when 2-butanol is used instead of cyclohexane due to the condensation of a larger amount of hydroperoxides.

4.4 Modeling SOA production in atmospheric conditions

Box model simulations have been performed in daytime atmospheric conditions to evaluate the production of SOA from the photooxidation of α-pinene. The photochemical conditions used in these simulations are comparable to those adopted in Sec. 4.2.6 for the forested areas where the emissions of α-pinene are particularly intense: [α-pinene]=500 ppt, [CH_4]=1.7 ppm, [CO]=400 ppb, [NO]=50 ppt, [O_3]=30 ppb, T=293 K, and relative humidity=50%. M_o is initially set to 8 μg/m^3 (Eq. 3.3, page 64), representing a typical concentration of organic aerosols as observed in forested areas (Kanakidou et al., 2000).

20-hour simulations have been performed in these conditions, keeping α-pinene and NO constant. After 10 hour of simulation, the SOA yield reaches a constant value of approximatively 5% (simulations results are shown in Fig. 5.7 of Chapter 5, page 138). Under these conditions, the aerosol phase is dominated by multifunctional acids and to a lesser extent by hydroxy hydroperoxides. Interestingly, a major fraction of pinonic, pinalic and pinic acids are under the dimer form. The dimerization is favoured by the rapidity of this process combined to the slow oxidation by OH calculated using the SAR of Kwok et al. (1995) for acid compounds. The ozonolysis remains the privileged path for aerosol formation in atmospheric conditions. However, the oxidation by OH is not negligible, as shown by the presence of particulate hydroxy hydroperoxides which originate mainly from this oxidation route. It is not possible to compare these box model results with the simulations of a global model in which the emissions, transport and deposition processes are taken into account. However, it is possible to compare the chemical schemes and the partitioning coefficients adopted in the most recent global models (Tab. 1.2, page 20) with those used in this work.

Tsigaridis and Kanakidou (2003) have used the global 3-dimensional chemistry/transport model, TM3, in order to simulate the temporal and spatial distribution of primary and secondary organic aerosols from both anthropogenic and biogenic origins. They estimated the global annual SOA production from biogenic sources at 23.2 Tg/year. The chemical mechanism for the oxidation of α-pinene is represented by a temperature-dependent two-product model (Eq. 3.2, page 64). The partitioning ($K_{p,i}$) and stoichiometric (α_i) coefficients have been deduced by Griffin et al. (1999a) on the basis of their ozonolysis experiments of α-pinene performed in presence of a scavenger and at an average temperature of 307 K. The dependence of the aerosol yields to the organic aerosol concentration M_o are shown in Fig. 4.16 (green dashed curves). The aerosol production from the oxidation by OH and NO_3 is considered as negligible by Tsigaridis and Kanakidou (2003). The SOA yields simulated using our box model (discussed in the previous section) are lower than the model results of Griffin et al. (1999a). In TM3, the temperature dependence of the partitioning coefficients is based on an estimation of the enthalpy of vaporization assumed to be representative of the mixture of products. Due to the exponential dependence of the

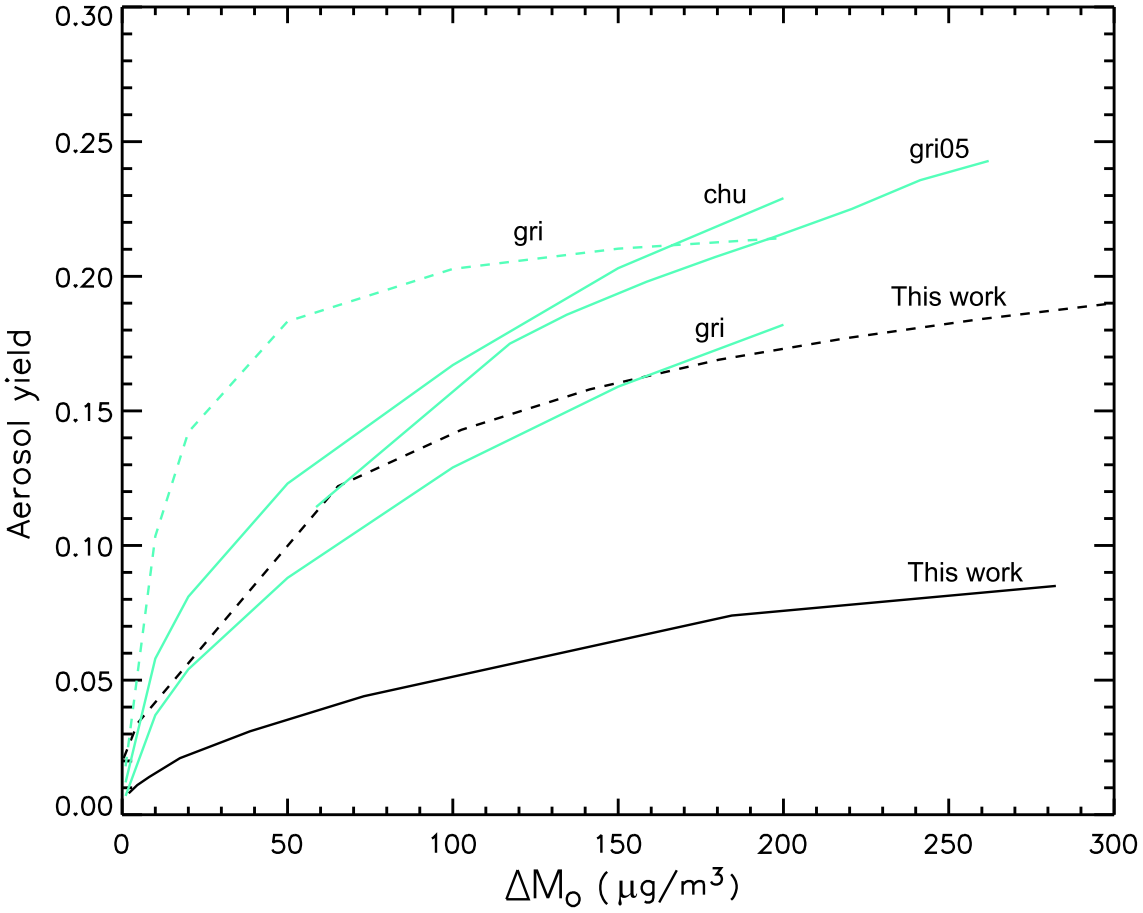

Figure 4.16: SOA yields from the α-pinene oxidation as a function of organic mass concentration between 308 and 320 K, calculated using the two-product models of Griffin et al. (1999a) (gri) and Chung and Seinfeld (2002) (chu), and using the CACM/MPMPO model of Griffin et al. (2005) (gri05). Dashed and solid lines represent yields calculated for the ozonolysis and the photooxidation, respectively. The yields calculated using the box model developed in this work are represented by the black curves.

vapour pressure to the enthalpy of vaporization, uncertainties of a factor 2 for the enthalpy are evaluated to translate into tremendous differences up to 150% on the predicted global annual SOA production.

The biogenic SOA formation has been also simulated in the global models GISS GCM II-prime (Chung and Seinfeld, 2002, 11.2 Tg/year) and MOZART (Lack et al., 2004, 15.3 Tg/year). The 2-product mechanism used in both models is assumed to represent the chemistry of all monoterpenes. The parameters used in Chung and Seinfeld (2002) to model the partitioning have been obtained from an average of the experimental K_p deduced from photooxidation experiments of Hoffmann et al. (1997) and Griffin et al. (1999a) on a series of monoterpenes. In MOZART, these parameters are taken from Griffin et al. (1999a) and are based on the photooxidation experiments

of α-pinene only. In contrast with Tsigaridis and Kanakidou (2003), both OH- and O_3 oxidation routes are considered to produce SOA in these global models. The SOA yields calculated by the 2-product models used in both global simulations are shown in Fig. 4.16. They are significantly higher than the yields obtained from the simulations using our box model for similar photooxidation experiments.

A more complex chemical mechanism describing the photooxidation of VOC has been elaborated by Griffin et al. (2002). The CACM mechanism includes a total of 191 species and 361 reactions. Among them, 40 reactions, leading to about 10 products, describe the oxidation of "BIOH" which is representative of 7 monoterpenes (including α-pinene) known to produce high SOA yields in laboratory. The gas phase module has been coupled to the MPMPO module which describes the partitioning of the organic products between the gas phase and a condensed phase consisting of an aerosol and an aqueous phase (Griffin et al., 2003). In a recent version of the CACM/MPMPO model (Griffin et al., 2005), the vapour pressures and stoichiometric coefficients of the condensable products have been adjusted in order to match chamber experiments (Odum et al., 1996, 1997; Hoffmann et al., 1997; Griffin et al., 1999a). Simulations of SOA formation from the photooxidation of a "BIOH" compound in laboratory conditions using the CACM/MPMPO model is shown in Fig. 4.16.

Another alternative to the 2-product model has been proposed in Bonn et al. (2004). A reduced scheme of the α-pinene oxidation described in the MCM mechanism (Saunders et al., 2003) has been implemented in a global model. The vapour pressure of the condensable products is estimated on the basis of the UNIFAC method and experimental data (see Sec. 3.2.4, page 79). This approach allows to model the distribution of individual products in the particulate phase. A production of 20 Tg/year of aerosol is simulated, consisting of hydroperoxides (63%), carboxylic acids (26%) and PANs (11%). This distribution differs from ours calculated for a typical atmosphere, due mainly to the choice of the vapour prediction method and the chemical mechanism. The vapour pressures predicted by Bonn et al. (2004) for the oxidation products are much lower than our estimations (see Fig. 3.5). Our treatment of the α-pinene oxidation has therefore less potential for aerosol formation than in the Bonn et al. (2004) model.

Figure 4.16 illustrates the large differences existing in the treatment of the chemical mechanism of the SOA precursors and the partitioning of their oxidation products between the gas and aerosol phase in the current global models. In any case, our oxidation mechanism and SOA formation module based on the vapour pressure prediction method developed in this work should imply a much lower prediction of SOA production than the recent estimations.

4.5 Conclusions

An exhaustive mechanism of both the OH- and O_3 initiated oxidation of α-pinene and pinonaldehyde developed by Peeters and co-workers has been implemented in a box model and validated against series of experiments performed in different conditions.

The experiments of oxidation by OH in presence of NO performed by N99 are well reproduced by the model. A good agreement is obtained for the yields of pinonaldehyde, acetone, total nitrates and total peroxy acyl nitrates in the gas phase. Pinonaldehyde production appears to be fairly well described. The concentrations of NO used in the experiments are relatively high ($\geq$1 ppm) so that the α-hydroxy peroxy radicals can react with NO or decompose to pinonaldehyde in competing processes. In these conditions, the pinonaldehyde yields vary between 50% to 60%. In absence of NO, this yield falls to about 26% in the measurements as well as in the model simulations. The model fails, however, to reproduce the production of acetone in absence of NO, presumably because the chemistry following the ring closure reaction of R_7O_2 and the oxidation of the primary products (except pinonaldehyde) is not treated explicitly in the model.

In the atmosphere, where the NO levels lie in the range 1 ppt-1 ppb, the decomposition of the α-hydroxy peroxy radicals is dominant. Due to the competition between the reactions of the other peroxy radicals with NO, HO_2 and other RO_2s, the yield of pinonaldehyde is predicted to vary from 10% in clean conditions to 60% in the most polluted areas. Further theoretical or laboratory studies will be required to elucidate the acetone formation channels in low NO_x (i.e. atmospheric) conditions.

The OH-oxidation is found to produce particulate products in small amounts (2-5% for 300 ppb of α-pinene) in laboratory conditions. The aerosol production is observed to start as soon as the α-pinene oxidation is initiated. Although the total aerosol yield calculated by the box model is in good agreement with the measurements, it is not possible to reproduce the aerosol production in the early times of the experiments. Sensitivity tests show that the uncertainties related to the vapour pressure estimations are not the cause of these discrepancies. To date, neither gas phase, nor heterogeneous processes can explain the rapid condensation of products in the OH-oxidation in high NO_x conditions. Box model simulations indicate that hydroxy nitrates and hydroxy peroxy acyl nitrates are the main constituents of the aerosol phase. Carbonyl products, such as pinonaldehyde are calculated to remain in the gas phase, contradicting the hypothesis made by N99.

As far as the ozonolysis is concerned, we have seen that box model simulations of the ozonolysis mechanism described in Sec. 2.3 largely underestimate aerosol production due to the lack of formation routes for two important condensables, pinic acid and hydroxy pinonic acid. A simple hypothetical route for their formation has therefore

been adopted in the mechanism in order to model the aerosol phase.

The adjusted mechanism has been implemented in the box model in order to simulate a number of ozonolysis experiments. A good agreement is obtained regarding hydroxy pinonaldehyde (&Isomers), pinonic acid and pinonaldehyde. Some differences are found for norpinonaldehye and for norpinonic acid (&isomers), possibly related to the uncertainties on the rates and product ratios of the permutation reactions of peroxy radicals. However, box model simulations underestimate the production of acetone in comparison with several experimental studies. Similarly to the OH-oxidation, the origin of the observed acetone yield has not been elucidated so far. However, the observed acetone is believed to be only primary in the ozonolysis experiments, given the absence of secondary reactions.

Simulations of the aerosol phase shows that the oxidation by ozone is the dominant oxidation process for SOA formation. Large amounts of multifunctional carboxylic acids are present in the aerosol formed from the ozonolysis. Model simulations confirm the experimental observations suggesting that dimerization of multifunctional carboxylic acids occur in smog chambers. Furthermore, since these dimers are supposed to have a low vapour pressure, the simulations indicate that they play an important role in SOA production. The observed partitioning of carbonyl products could not be reproduced by the box model due to their high vapour pressure. Oligomerization processes mentioned in Sec. 3.3 could be responsible for the presence of these compounds in the particulate phase. Given the large experimental uncertainties (on the order of 50%), the total aerosol yield is usually well reproduced by the model in the cases of the Yu et al. (1999a) and BIOVOC experiments. However, modeled yields are overestimated for the BIOVOC experiments using $\sim$50 ppb of α-pinene in presence of a scavenger. The box model calculates a negligible production of aerosols for the Hoffmann et al. (1997) experiments at 320 K. This could be due to the temperature dependence of the vapour pressures of the α-pinene oxidation products and, in particular, the carboxylic acid dimers/adducts. The origin of this large aerosol production at high temperature is not clarified. Further work on the role of heterogeneous reactions and on the vapour pressure and stability of the dimers/adducts of multifunctional carboxylic acids are required in order to elucidate the mechanisms responsible for aerosol production in the ozonolysis of α-pinene.

Although the crude representation adopted in this study for the oxidation of the primary products (other than pinonaldehyde) appears to be sufficient in the simulations of the early stages in the oxidation of α-pinene, it is likely to be unrealistic in general conditions. Thousands of reactions will probably have to be carefully examined before the impact of these processes in the atmosphere can be assessed to a good degree of confidence. Since a rigorous evaluation of every possible oxidation step is not possible in a realistic time frame, focus should be given to the main oxidation pathways and to the formation of critical compounds, e.g., acetone and SOA precursors.

Box model simulations in typical atmospheric conditions suggest that the biogenic SOA from the oxidation of α-pinene are mainly made of multifunctional carboxylic acids and hydroperoxides. Furthermore, model results indicate that the dimerization of acids could be important in atmospheric conditions. Further work will be needed to better constrain the kinetic rates associated to dimerization. Our α-pinene oxidation mechanism and its related SOA partitioning model has less potential for SOA formation than the treatments which have been adopted in recent modeling studies.

Chapter 5

Mechanism reduction for global modeling

5.1 Introduction

The development of detailed oxidation mechanisms for hydrocarbons has raised an important technical issue: the chemistry of all organic species present in the atmosphere involves hundreds of thousands of reactions which cannot be considered explicitly in multi-dimensional atmospheric models. Thousands of reactions are considered in current "master" mechanisms (Madronich and Calvert, 1989; Saunders et al., 2003) which describe only a small fraction of the complete picture. Since computer resources allow the representation of several hundreds of reactions at most in 3D models, it follows that the chemical mechanisms must be simplified in order to be implementable in models. In fact, reduced chemical mechanisms have been elaborated as soon as the 1980's to alleviate the computational burden. The basis principle generally used to condense the chemistry and minimize the number of species is to combine ("to lump") the organic species with similar chemistry. Species are partitioned in categories according to their reactivities and oxidation products. The categories are determined through the use of structural reactivity analyses and depend on the processes to be represented and the desired level of accuracy. Earlier condensed mechanisms such as the carbon bond mechanism (Whitten et al., 1980) or the ALW mechanisms (Atkinson et al., 1982) were relatively simple (fifty reactions at most). The carbon bond mechanism relies on the so-called structure-oriented lumping approach, where organic species are grouped according to bond type (e.g. carbon single bonds, carbon double bonds, or carbonyl bonds). An organic compound is therefore represented by surrogates describing the different types of carbon bonds found in its chemical structure. The main advantage of this approach is that only few surrogate categories are needed, and that the carbon number is conserved. Structure-oriented lumping approaches have found applications in modeling studies of the chemistry of complex petroleum mixtures. The molecule-oriented approach adopted in the ALW mechanism relies on categories defined in terms of chemical families (e.g. alkanes, alkenes, carbonyls, aromatics). The categories are subdivided

according to the carbon number if necessary. All species in a category are represented by only one species which is explicitly represented in the mechanism. The carbon number of the explicit structure of the organic compounds is not conserved in this approach. This approach is particularly suitable for simulations of photochemical ozone formation.

Further methods have been shown to be useful to condense chemical mechanisms: e.g the hypothesis of the quasi-steady state approximation (QSSA, described further in this chapter) allowing to remove fast reacting species, and the use of pseudo-reactions (Sec. 2.3.2). These reduction methods combined with sensitivity analyses to identify negligible species and reactions have allowed to design condensed mechanisms for specific atmospheric conditions: for example, the SAPRC mechanism developed by Carter (1990) to describe photochemical smokes in urban areas or the MIM mechanism (Pöschl et al., 2000) dedicated specifically to the oxidation of isoprene. Versions of the Carbon Bond mechanism have been elaborated for global (Houweling et al., 1998) and regional modeling (Morris and Myers, 1990). Recently, Whitehouse et al. (2004a,b) proposed a reduced version of the fully explicit MCM master mechanism (counting 3487 species and 10763 reactions) suitable for polluted tropospheric UK conditions. As a result of lumping, the reduced mechanism contains 35% of the number of species and 40% of the number of reactions of the full mechanism.

However, the chemical calculations still consume a large fraction of the CPU time in typical simulations of global chemical transport models. The situation can worsen in the future, since new generations of mechanisms will incorporate heterogeneous reactions in order to model the formation and aging of aerosols. Lumping techniques will therefore remain critical in the future. The α-pinene oxidation mechanism developed in this work includes ca. 700 species involved in ca. 2300 gas phase reactions. ca. 250 condensed species involved in ca. 500 reactions of adsorption and desorption are included in the partitioning mechanism. In order to provide a condensed version for global modeling, we propose to reduce this mechanism (both the gas phase and the partitioning) using a combination of techniques, as described further below in this Chapter. An innovative aspect of our reduction work is the consideration of impacts in the gas phase as well as in the aerosol phase.

5.2 Objectives and outline of the mechanism reduction

The major requirement for the reduced mechanism is that it must be able to represent the impact of α-pinene on the levels of inorganic compounds playing a role in the oxidizing capacity of the atmosphere (OH, NO_x and ozone), as well as on the production of SOA. Several products specific to the α-pinene degradation play an important role and need to be represented explicitly in the mechanism. This is the case for pinonaldehyde, due to its high molar yield, and for pinic acid, pinonic acid, and hydroxy pinonic acid due to their importance in SOA production. Small organic species like CO, CH_2O and acetone should also be described explicitly in the condensed mechanism, since these compounds play a key role in atmospheric chemistry. The other species can be lumped in order to represent their general and averaged effects. We have seen that the oxygenated functionalities determine the reactivity of organic compounds in the gas phase (e.g. photodissociation, peroxy radical reactions) as well as their partitioning properties (through the vapour pressure). Therefore, lumping should be performed according to the chemical functionalities, (e.g. acids, hydroperoxides, nitrates). The list of the compounds and the reactions of the reduced mechanism is presented in Appendix B.

The reduction is performed in successive steps. Sensitivity tests using the box model with the detailed and the intermediate reduced mechanism are performed to evaluate the impact of each reduction step. For this purpose, one-hour simulations have been performed using the box model. The photochemical conditions used in these simulations are comparable to those adopted in Sec. 4.4 for the forested areas ([α-pinene]=500 ppt, [CH_4]=1.7 ppm, [CO]=400 ppb, T=293 K, M_o=8 μg/m^3, and relative humidity=50%). Simulations are performed for levels of NO ranging from 10 to 100 ppt, and ozone from 30 to 80 ppb. In the following, we will describe the different steps of the reduction procedure. Next, the comparison results between box model simulations using the reduced and detailed mechanisms will be discussed.

5.3 Procedure

5.3.1 Identification of negligible reactions in atmospheric conditions

The first step is to remove the reactions which have a negligible impact in atmospheric conditions. These reactions are identified using sensitivity analyses. Are considered as negligible, minor reaction paths affecting negligibly the yields of the inorganic species, the explicit products, and the chemical families. An example is provided by the route leading to radical R_{15} (Fig. 2.2, page 32). The dominance of the "exotic" peroxy radical reactions in atmospheric conditions discussed in Sec. 2.3.3 should be noted: the decomposition of the α-hydroxy peroxy radicals R_3O_2 and $R_{13}O_2$

to pinonaldehyde as well as the ring closure reaction of R_7O_2 outrun all other reactions involving these peroxy radicals in atmospheric conditions. The oxidation channels from R_3O, $R_{13}O$ and R_7O radicals can be therefore removed, which simplifies significantly the mechanism. As a whole, cutting off the minor routes results in a relative change inferior to 2% on the products yields, whereas the number of reactions in the mechanism is reduced by 15%.

5.3.2 Reduction of the length of the oxidation routes

The alkyl and alkoxy radicals can react with O_2, decompose or isomerize. Compared to the peroxy radicals, these radicals react very rapidly and their rates of production and consumption can be considered as equal. The Quasi-Steady-State Approximation (QSSA) defines the assumption of equilibrium for short-lived species:

$$\frac{dC_i}{dt} = 0, \tag{5.1}$$

where C_i is the concentration of the QSSA species. This hypothesis allows to remove the alkyl and alkoxy radical species and their related reactions by adjusting the stoichiometric coefficients of the peroxy radicals produced through these reactions. For example, typical radical reactions, of respective rates k_1, k_2, k_3, of the explicit mechanism such as:

$$\mathrm{RO_2 + NO \rightarrow RO + NO_2} \tag{R5.7}$$
$$\mathrm{RO \rightarrow 0.5\,Product + 0.5\,R'O} \tag{R5.8}$$
$$\mathrm{R'O + O_2 \rightarrow R'O_2} \tag{R5.9}$$

can be reduced to

$$\mathrm{RO_2 + NO\ (+O_2) \rightarrow 0.5\,Product + 0.5\,R'O_2 + NO_2,} \tag{R5.10}$$

because the lifetime of the alkoxy radicals RO and R'O is much smaller than that of RO_2. Based on this reduction technique, alkyl and alkoxy radicals, and their related reactions are removed from the intermediate reduced mechanism.

Any further reduction is more delicate because it requires the lumping of RO_2 which have different fates in different regions of the atmosphere. In high NO conditions (NO $\geq$ 100 ppt), the RO_2+NO reactions are dominant. When decreasing NO, the reactions of the peroxy radicals with HO_2 and, to a lesser extent, with other peroxy radicals become more important. For NO of the order of 10 ppt, the HO_2-reaction outruns the reaction with NO. In median conditions (10 ppt<NO<100 ppt) , both reactions are competing. The dependence of the nitrate and hydroperoxide yields on the NO levels has been discussed in Sec. 4.2.6 and is illustrated in Fig. 4.9, page 104. On this basis, the strategy adopted in this work consists in designing two reduced mechanisms, each representing one "extreme" condition of NO (NO=500 ppt, and

NO=10 ppt). Both reduced mechanisms are developed for their specific NO conditions. These two reduced mechanisms will then be merged into a mechanism representing intermediate NO conditions (10$\leq$NO$\leq$500 ppt) which are the most common in the atmosphere.

The development of two separate mechanisms for specific NO levels allows to decrease further the length of the oxidation routes by reducing the number of peroxy radicals in each oxidation route. The peroxy radicals generated in the first oxidation steps are kept explicit in both schemes because of the high yields of the primary products generated from these radicals. However, after three oxidation steps, or even less, the products have yields below 10%, and their influence is smaller. Consequently, these reactions can be lumped and represented by only one "condensed" reaction. The explicit NO- and HO_2-reactions are represented in the condensed reaction by using the generic radicals described in Sec. 2.3.4 (page 47). Two types of generic radicals are used: a peroxy radical "LXO2" and an acyl peroxy radical "LXO3". The properties (i.e. the structure) of the generic LXO2 (LXO3) are adapted to represent the average chemical effect of the (acyl) peroxy radicals being replaced, by means of sensitivity analyses. The organic nitrate and hydroperoxide yields are adjusted in each intermediate reduced mechanism. LXO2 is assumed to belong to the R2R class (cfr. Sec. 2.3.2) as far as the permutation reactions are concerned. Its structure presents a carbon chain bearing a carbonyl and a secondary hydroxy functionality, similar to the structure of the explicit radicals replaced which show in general at least two functionalities among the hydroxy and the carbonyl functionalities. The vapour pressures and the reactivities towards OH of the corresponding generic products (e.g. LXOOH, LXONO2) are also determined for both mechanisms. Since the reactivity of acyl peroxy radicals does not depend on details of its structure, no adjustment is required for LXO3. Note that the use of generic radicals is not necessary for all oxidation routes. The OH-addition routes leading to pinonaldehyde, or those leading to norpinonaldehyde and pinonic acid in the ozonolysis mechanism are kept explicit because they involve at most one peroxy radical.

The treatment of the acyl peroxy radicals in high NO conditions is difficult due to the variable relative importance of their reactions with NO_2. Therefore it is preferred to represent explicitly the most important acyl peroxy radicals produced in the mechanism. For that reason, the acyl peroxy radical $R_{32}O_2$ of the ozonolysis path Ia is kept explicit (represented as APINCO3 in the final reduced mechanism). APINCO3 is the precursor of pinalic acid, which plays a role in aerosol formation.

An example illustrating the reduction operated in the mechanisms for high and low NO conditions is shown in Fig. 5.1 for a path from pinonaldehyde+OH (Fig. 2.4, page 34). In high NO conditions, the number of NO to NO_2 conversions in the entire path is equal to 1 (for $R_{23}O_2$)+0.8 (for $R_{41}O_2$), which is represented by the stoichiometric coefficient of 1.8 for LXO2 in the reduced mechanism. More generally, the stoichiometric coefficients in the condensed reaction corresponds to the yields of the

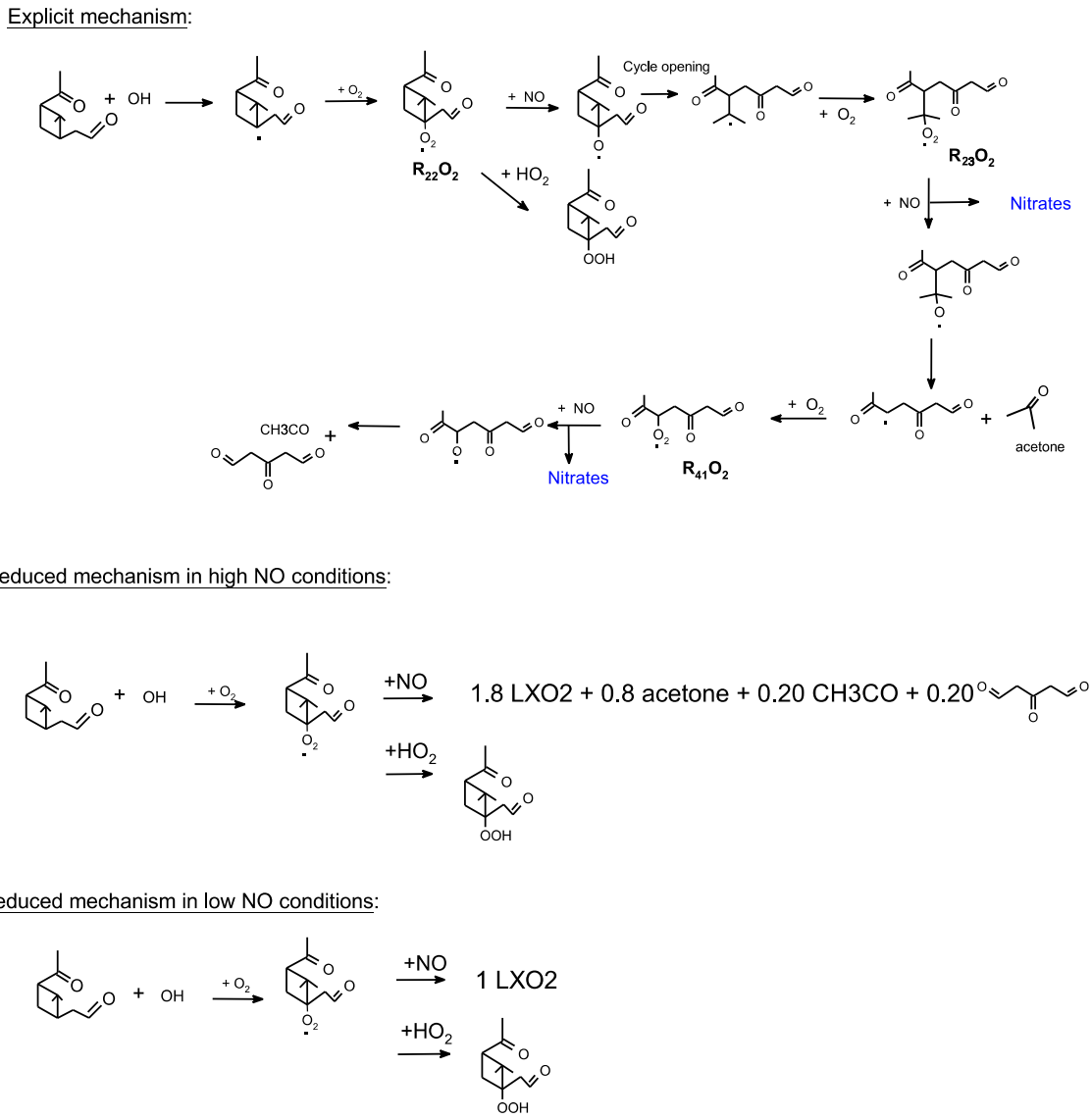

Figure 5.1: Example illustrating the reduction of the length of an oxidation route (here, from pinonaldehyde+OH). From the detailed mechanism, two reduced mechanisms are designed, for high and low NO conditions. The oxidation chain subsequent to the first oxidation step is represented by a "condensed" reaction in both reduced mechanisms.

products generated along the explicit oxidation path calculated by the box model for NO=500 ppt. The acetyl peroxy radical is treated explicitly in the reduced mechanism. In low NO conditions (NO=10 ppt), the reaction with HO2 is dominant. The alkoxy radical yield is very small ($\sim$10%) after the first oxidation path. Therefore, the condensed reaction for the reaction with NO generates only one LXO2 radical.

5.3.3 Reaction paths and product merging

The third stage of the reduction process is based on the similarities identified between different reaction paths with respect to the radical reactivities and the structure of the stable products formed. When two oxidation paths present similarities, sensitivity studies are performed to adjust the kinetic rates and the product yields of the reaction resulting from their merging in the reduced mechanism. The stable compounds produced in the explicit oxidation paths are lumped according to their functionalities: Carbonyl, hydroxy, acid, hydroperoxide, nitrate and PAN. The carbon number and the group contributions for vapour pressure prediction (as parameterized in Tab. 3.2, page 72) defining their structure are shown in Tab. B.1 in Appendix B.

The most striking example of similar oxidation paths are the two routes leading to the formation of pinonaldehyde in the α-pinene OH-oxidation mechanism (Fig. 2.2, page 32). Both routes involve only one peroxy radical, R_2O_2 and $R_{12}O_2$ respectively. R_2O_2 being a secondary radical whereas $R_{12}O_2$ is tertiary, their organic nitrate yields and their permutation reactions differ significantly. Therefore, it is necessary to adjust the products yields and the kinetic rates of the surrogate (represented as "OHAPIN2HO2") in both reduced mechanisms. The hydroperoxide and nitrate products generated in both routes have similar volatilities, due to the presence of the hydroxy functionality. They are represented by OHAPINOOH and OHAPINONO2, respectively.

A second important merging example concerns the minor abstraction route of the α-pinene OH-oxidation, the path Ib in the ozonolysis and two OH-oxidation routes of pinonaldehyde (via R_{19} and R_{22}). The four routes are initiated via a tertiary alkyl peroxy radical bearing carbonyl functionality(ies), and generate semi-volatile products (e.g. APINONO2, APINOOH). The next oxidation step leads to the opening of the C_4 cycle, producing again tertiary peroxy radicals of similar structures (e.g. $R_{20}O_2$, $R_{23}O_2$). These radicals are lumped and represented as APIN3RO2 in the reduced mechanism. Further oxidation of the tertiary radical is represented by generic radicals. Eventually these routes produce volatile carbonyls in the detailed mechanism. Some among them bear several carbonyl functionalities (e.g. Path Ib of the ozonolysis). Methylglyoxal is used to represent these multicarbonyls. A channel of the pinonaldehyde photolysis (through R_4) is also included in this reduced route.

The major OH-oxidation route of pinonaldehyde produces an acyl peroxy radical ($R_{16}O_2$) showing resemblance with $R_{32}O_2$. This route can therefore be merged with the route producing APINCO3. The route leading to norpinonaldehyde (ozonolysis path IIa, and pinonaldehyde+OH) is not modified: R_{21} is represented by APIN2OO2.

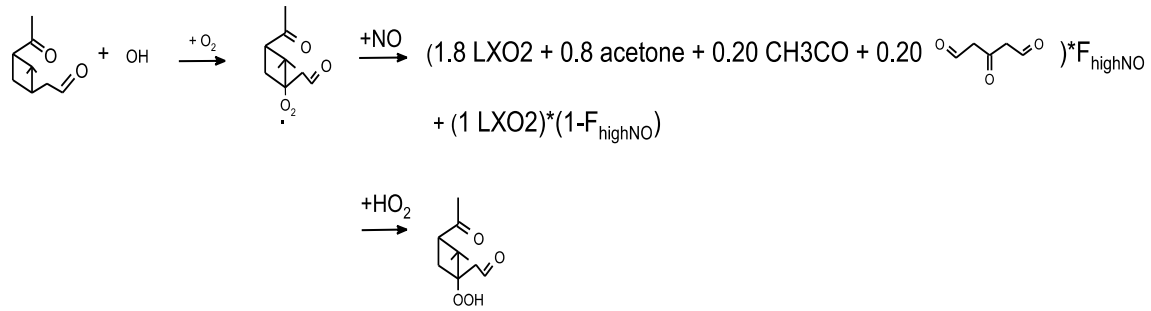

Figure 5.2: Example of a condensed reaction (here for pinonaldehyde+OH) obtained as a linear combination of the condensed reactions from the reduced mechanisms for "high NO" and "low NO" conditions.

5.3.4 Optimization for atmospheric conditions

At this development stage, two reduced mechanisms have been created, one for low NO and one for high NO conditions. From these two mechanisms, one unique reduced mechanism capable of representing intermediate chemical conditions is developed. For this purpose, the condensed reactions of the final reduced mechanism are obtained as linear combinations of the condensed reactions from the reduced mechanism for high NO and low NO conditions. This is illustrated in Fig. 5.2 with the example of a pinonaldehyde OH-oxidation route (route already discussed in Fig. 5.1). For clarity, the pinonaldehyde reaction route used for illustration has not been merged with other routes according to the procedure described in the previous section.

Depending on the levels of NO, the relative importance of each condensed reaction is determined through the parameter $F_{High\ NO}$. The optimal combination of the condensed reactions for the median atmospheric conditions (NO=50 ppt) is obtained with $F_{High\ NO}$=0.6.

Next, sensitivity studies performed at low NO concentrations allow to eliminate negligible permutation reactions. In particular, permutation reactions involving tertiary radicals are very slow and can be removed without any effect on the other compounds.

5.4 Results

Simulations results for atmospheric NO levels of 50 ppt using the detailed and the reduced mechanisms are shown in Fig. 5.3 and Fig. 5.4. The relative importance of each oxidant is shown in Fig. 5.3. Under these conditions, OH contributes to about 75% of the total oxidation of α-pinene. The oxidation reaction of α-pinene by NO_3 has been introduced in the model based on the rate proposed by Atkinson et al. (2004), but this reaction appears negligible under day light and can be ignored. Model simulations using the reduced mechanism reproduce almost perfectly the concentrations

predicted using the detailed mechanism for the inorganic compounds. This agreement is also excellent for NO levels ranging from 10 to 500 ppt (not shown in this work). As an example of the excellent agreement of the peroxy radicals, the total acyl peroxy radicals are also shown in Fig. 5.3 (represented as "RO3").

Fig. 5.4, Fig. 5.5 and Fig. 5.6 shows the comparison between the yields of organic products obtained using both mechanisms for NO levels equal to 50, 10 and 100 ppt, respectively. The yields are simply calculated as Δ[Product]/Δ[α-pinene] in function of time and are given for the total concentration (gas and particulate phase) and for the particulate phase (represented by "p"). Pinonaldehyde and acid dimers present an excellent agreement in all NO conditions since they are represented explicitly in the reduced mechanism. However, differences are observed for acetone. Acetone is generated via primary reactions (α-pinene ozonolysis), and via secondary reactions (oxidation and photolysis of pinonaldehyde). At least five oxidation steps are required in each of these routes. The representation of the yields generated after so many steps is more unprecise in the condensed route. Furthermore, most of these routes involve acyl peroxy radicals. These radicals reacting also with NO_2, the subsequent products yields are dependent on the NO_2 concentration. This dependence is not represented by the condensed reactions, resulting in larger uncertainties. Generally speaking, any product generated late in the oxidation shows a complex dependence to the chemical conditions, which is poorly represented by the reduced mechanism. However, the yields of these products being small, their impact in the atmosphere is limited. Moreover, in the case of acetone, it should be reminded that the mechanism used in this work is believed to strongly underestimate its production at low as well as high NO (Chapter 4). Therefore, a good agreement between the detailed and reduced mechanisms is not relevant at this stage for this compound.

A difference of less than 10% is found between the two mechanisms for the total yields (gas+particulate phase) of nitrates, hydroperoxides and PANs, between 10 and 100 ppt of NO. The total hydroxy nitrates and the total hydroxy hydroperoxides are also well reproduced by the reduced mechanism. A less good agreement is obtained for hydroxy PANs at 100 ppt. These products are generated after numerous oxidation steps and their production involves LXO3 (which generates LXPAN after reaction with NO_2) in the condensed reactions. The concentration of APINPAN being larger and well reproduced by the reduced mechanism, the total PANs (grouping APINPAN and LXPAN) are well described from 10 to 100 ppt.

The SOA yield after one hour varies between 3% (when [NO]=50 or 100 ppt) and 4% (when [NO]=10 ppt). The total SOA includes mainly acid dimers, hydroxy pinonic acid (acid monomers), and hydroxy hydroperoxides. The larger yield in low NO conditions is due to the larger production of hydroperoxides as well as to the increased importance of ozonolysis in this case. In general, over the studied range of NO level, the total aerosol concentrations predicted by the model using the detailed and the reduced mechanism agree to within 10%. Sensitivity tests with only 2 μg/m^3 of POA

(causing a decrease of the SOA concentration, as described by Eq. 3.3, page 64) have been also performed, which confirm the capacity of the reduced mechanism to mimic the detailed representation for different atmospheric conditions. Note that OHAPINONO2 and OHAPINOOH, produced in the OH-oxidation of α-pinene, have vapour pressures of the same order as APINONO2 and APINOOH, which are mainly produced from the ozonolysis. The "hydroxy" compounds contribute more to the aerosol yield because of their higher yield.

Simulations using the reduced mechanism show positive and negative biases for the "hydroxy" compounds (i.e. hydroxy nitrates, hydroxy PANs and hydroxy hydroperoxides) in the aerosol phase at 10 and 100 ppt of NO, respectively, compared to the simulations using the detailed mechanism. These deviations are due to the impact of the structure adopted for the generic compounds in the reduced mechanism on the partitioning. When the chemical conditions change (concentration of NO, fraction of α-pinene oxidized by OH and O_3), the structure and the yields of the products represented by the generic products vary. For example, at NO=100 ppt, simulations using the detailed mechanism indicate that the hydroxy nitrates family contains more low-volatility compounds than at 50 ppt because the oxidation routes are longer. The oxidation reactions of a radical tend to increase its number of chemical functionalities, and contribute also to transform the carbonyl functionalities into (less volatile) hydroxy functionalities (via hydrogen shifts). An example of this trend is shown in the reaction route Ia of the ozonolysis (Fig. 2.3, page 33). In the course of the oxidation, the carbon number of the radicals decreases, which increases the vapour pressure of the associated products. However, the net result of these two opposite effects in the NO conditions studied here, is a decrease of the vapour pressure. The structure, and therefore the vapour pressure, of the generic products being deduced from simulations at conditions NO=50 ppt, less hydroxy nitrates are simulated in the condensed phase at higher NO concentrations when the reduced mechanism is used.

In typical NO conditions, the peroxy radical reactions with NO and HO_2 account for approximatively 60% and 40% of their total sink, respectively, making the permutation reactions almost negligible. At NO=10 ppt, the importance of the permutation reactions remains small, representing at most 10% of the total sink of peroxy radicals. Their minor importance in atmospheric conditions questions the usefulness of their large number in the reduced mechanism (34 reactions out of 160).

A 20 hour simulation has been also performed to evaluate the behavior of both mechanisms at longer times (Fig. 5.7) at [NO]=50 ppt. The gas phase remains very well simulated, whereas deviations between the simulations using the reduced and the detailed mechanism increase for all chemical families in the aerosol phase after 10 hours, except for the dimer acids which are represented explicitly in the reduced mechanism. Despite these biases, the SOA concentration is well simulated by the reduced mechanism after 20 hours (deviation less than 5%).

5.5 Conclusions

The detailed mechanism of α-pinene oxidation by OH and O_3 has been reduced to a manageable size for global modeling. The molecule-lumping approach of the oxidation routes has allowed us to reduce the mechanism to 43 species and ca. 160 reactions (including the partitioning reactions). The box model using the reduced mechanism reproduces very well the total concentrations of the chemical families for NO ranging between 10 and 100 ppt. The total SOA yield (3-4% after one hour, about 5% after 20 hours) is well reproduced with the reduced mechanism, although with significant discrepancies regarding the precise composition of SOA, in particular at very high or very low NO. The reason is that the yield and the partitioning properties of the mixture of compounds represented by the generic products of the reduced mechanism varies with the level of NO.

A possible future improvement in order to obtain a better agreement over a large range of conditions could be the use of a parameter $F_{\text{High NO}}$ expressed as a function of NO and possibly O_3. Moreover, it is possible to create an additional condensed path dedicated to very high NO conditions since the average oxidation chain becomes longer in such conditions and generates a large number of primary products. A linear combination of three condensed paths instead of two would allow a better parameterization of the condensed phase.

The mechanism has been significantly reduced and is implementable in the chemistry transport models IMAGES for global modeling (Müller and Brasseur, 1995). More work should be performed to reduce further its size allowing its use in other chemistry transport models (e.g. by reducing the number of permutation reactions of peroxy radicals).

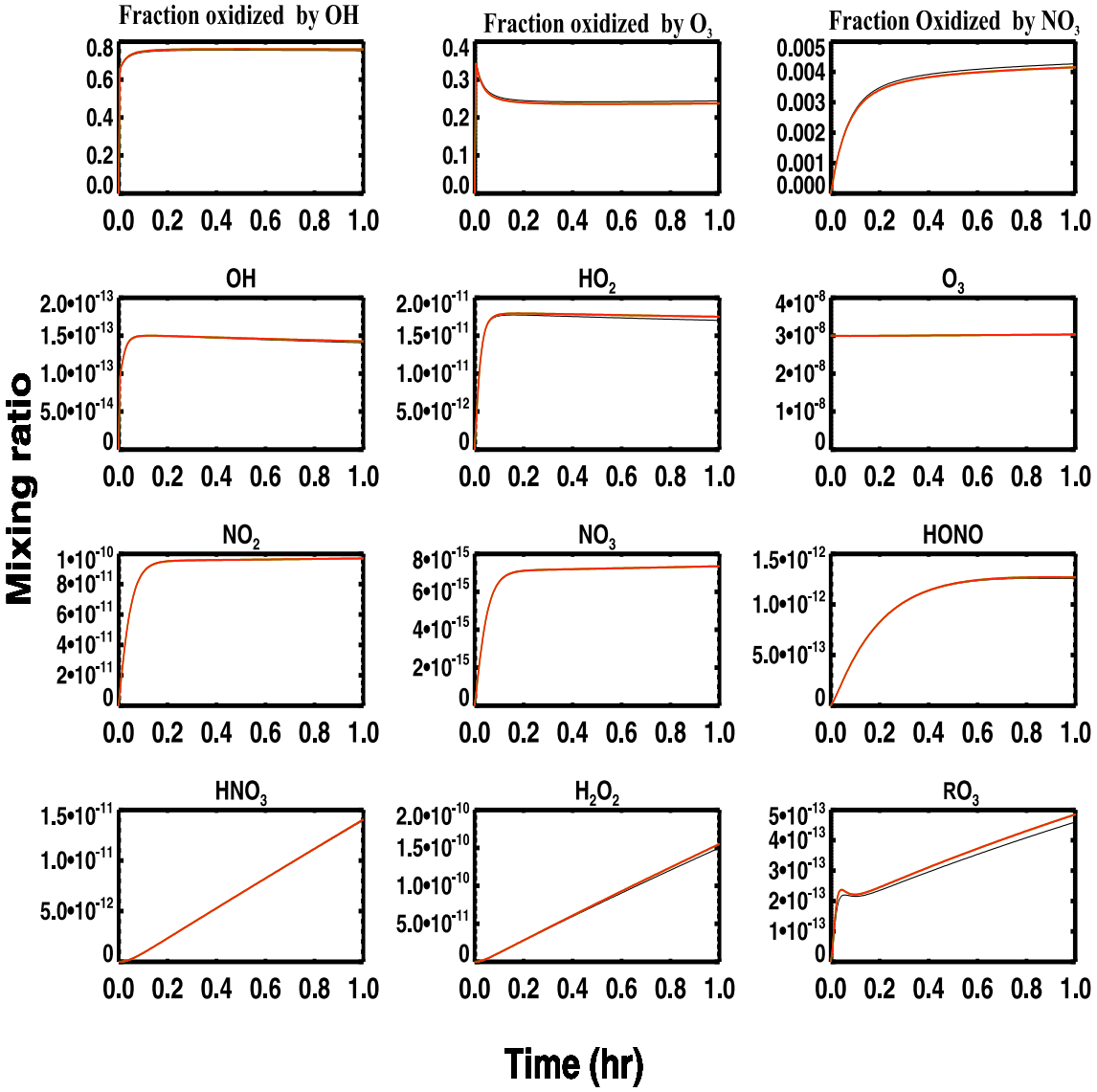

Figure 5.3: Concentrations of inorganic compounds and acyl peroxy radicals (RO_3) in the α-pinene oxidation simulations using the detailed mechanism (black curve) and the reduced mechanism (red curve) for typical atmospheric conditions, with [NO]=50 ppt. The relative importance of each oxidant is also calculated.

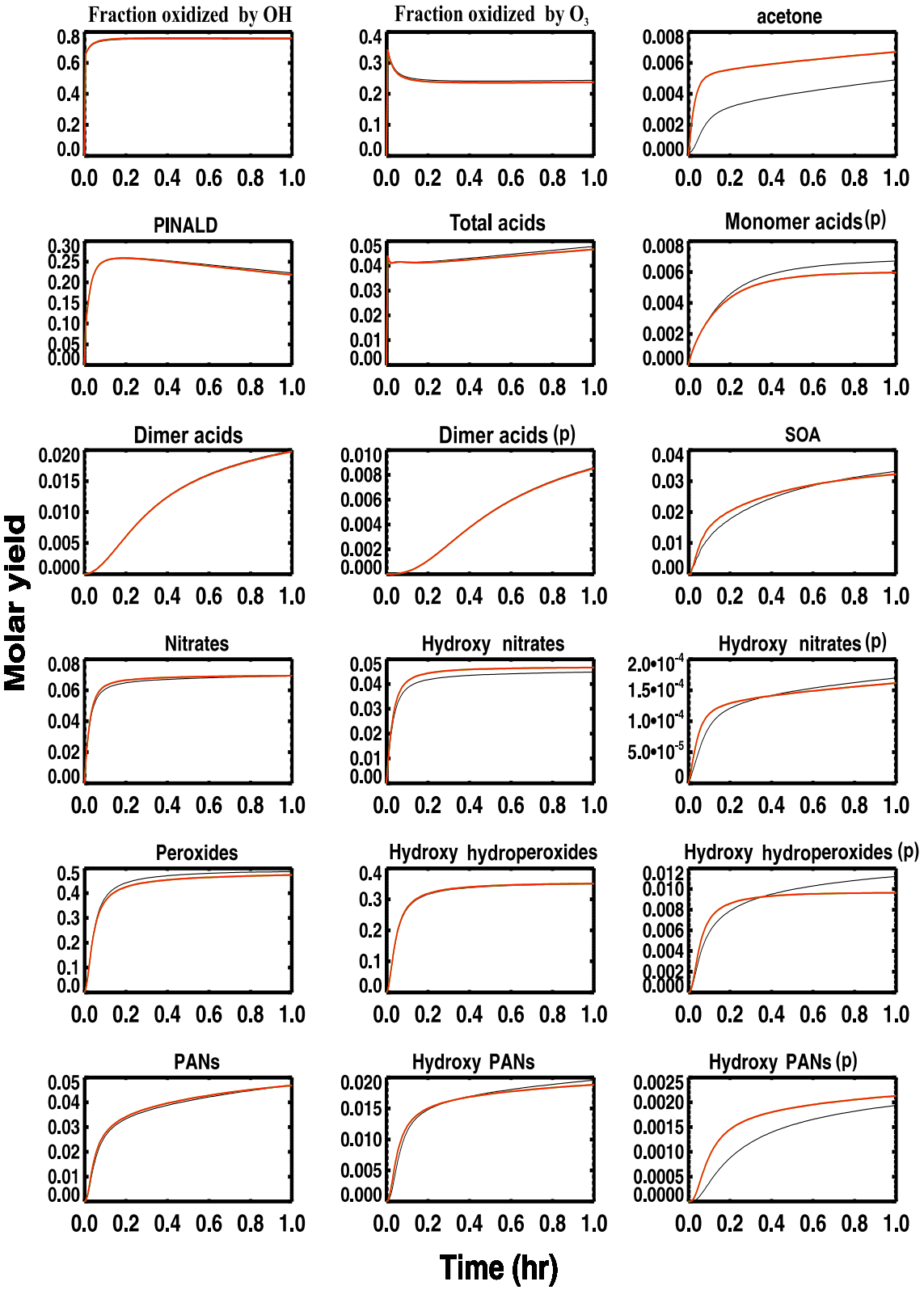

Figure 5.4: Yields of organic compounds in the α-pinene oxidation simulations using the detailed mechanism (black curve) and the reduced mechanism (red curve) for typical atmospheric conditions, with [NO]=50 ppt. The notation "(p)" refers to the particulate phase. In absence of this suffix, the yield is calculated from the total (gas + particulate) concentration.

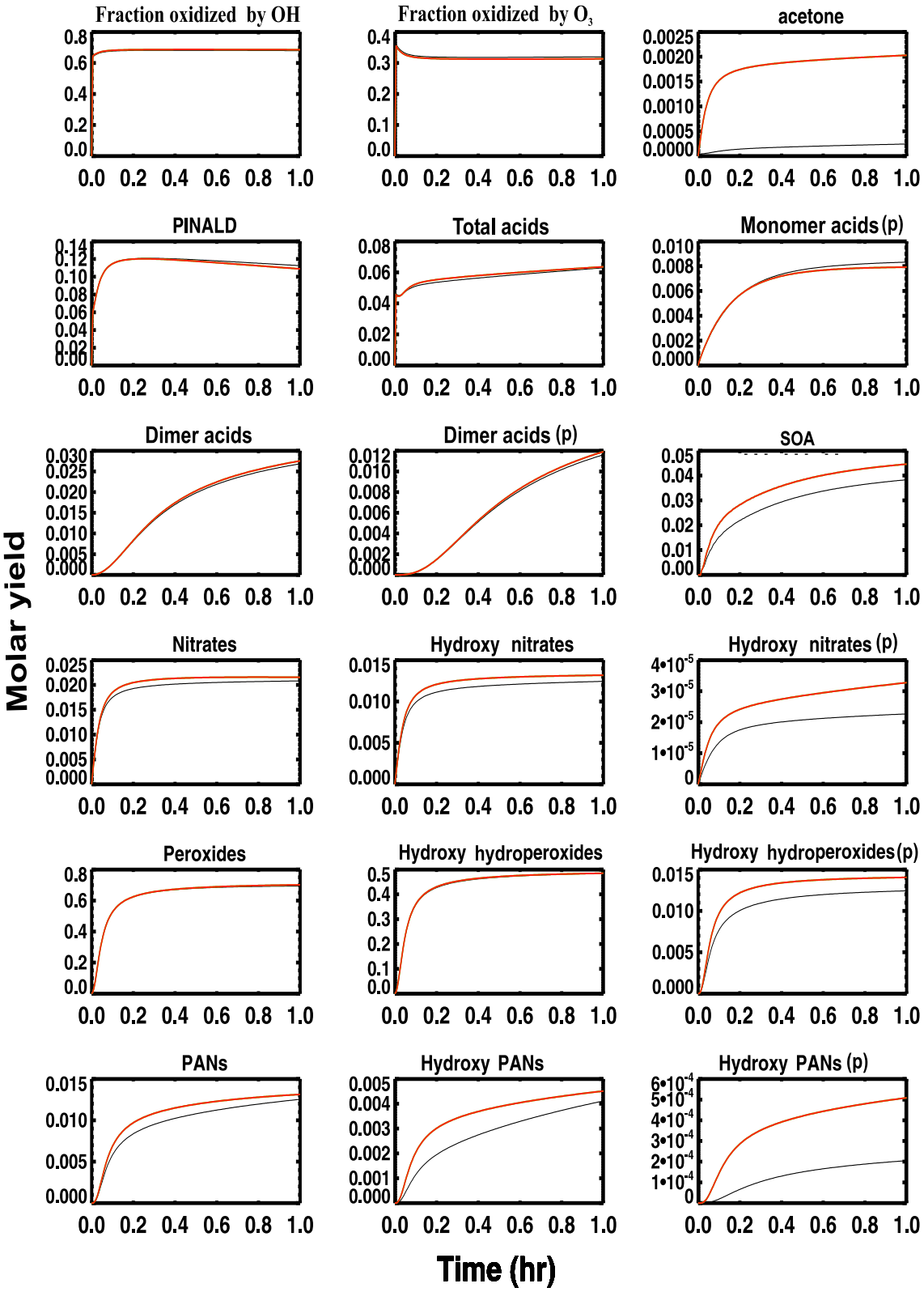

Figure 5.5: Yields of organic compounds in the α-pinene oxidation simulations using the detailed mechanism (black curve) and the reduced mechanism (red curve) for typical atmospheric conditions, with [NO]=10 ppt. The notation "(p)" refers to the particulate phase. In absence of this suffix, the yield is calculated from the total (gas + particulate) concentration.

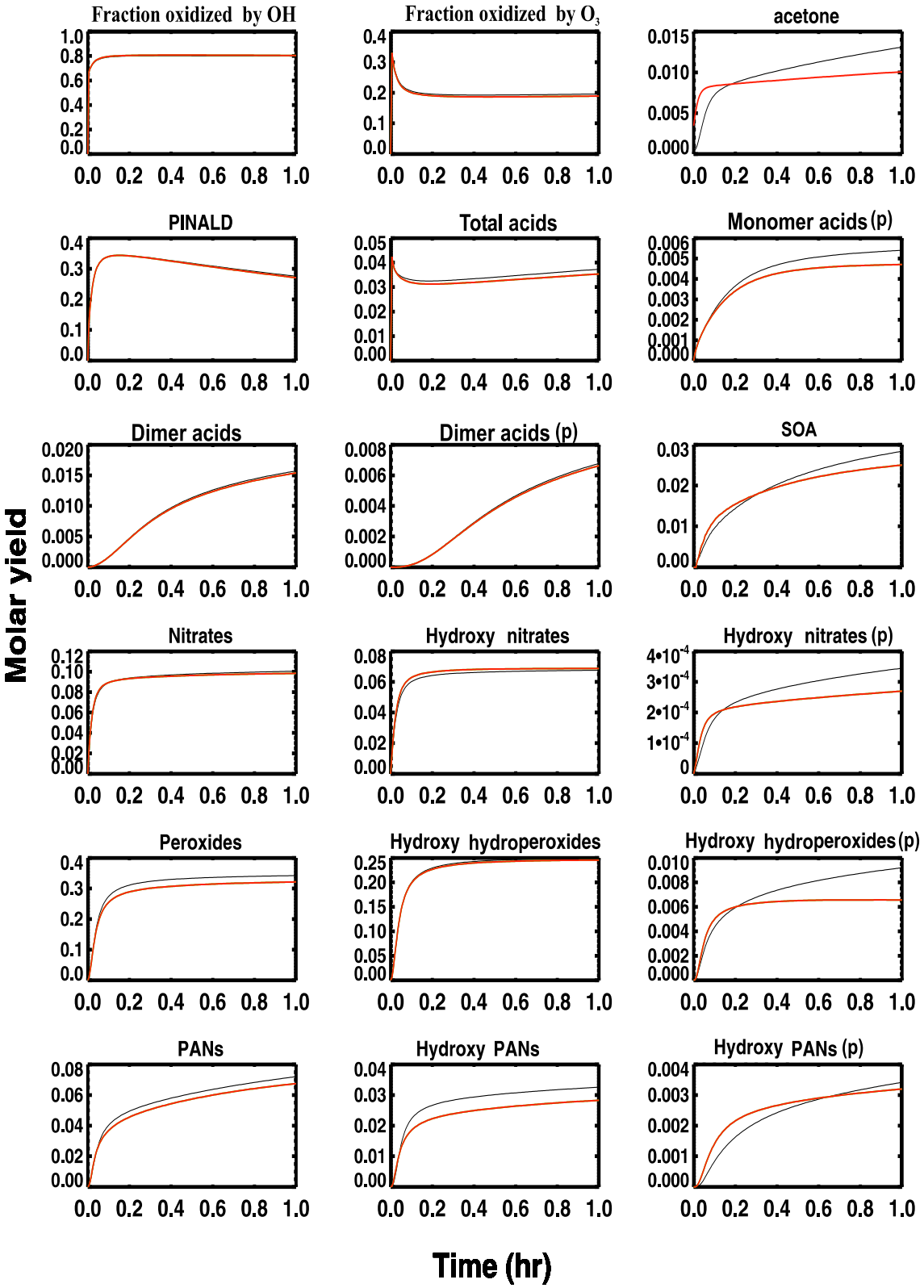

Figure 5.6: Yields of organic compounds in the α-pinene oxidation simulations using the detailed mechanism (black curve) and the reduced mechanism (red curve) for typical atmospheric conditions, with [NO]=100 ppt. The notation "(p)" refers to the particulate phase. In absence of this suffix, the yield is calculated from the total (gas + particulate) concentration.

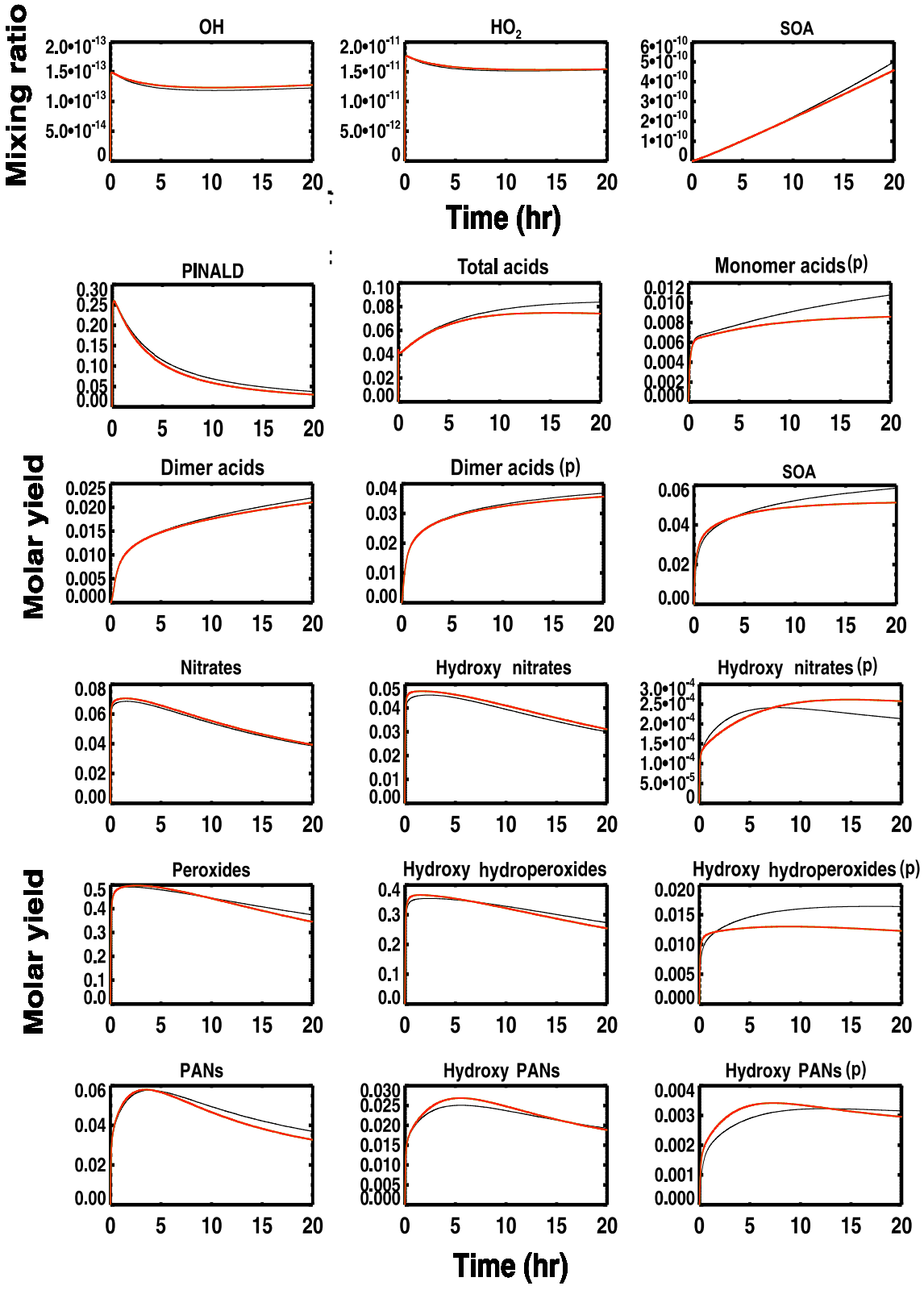

Figure 5.7: Mixing ratios of OH, HO_2, SOA, and yields of organic compounds in a 20-hours simulation of α-pinene oxidation using the detailed mechanism (black curve) and the reduced mechanism (red curve) for typical atmospheric conditions, with [NO]=50 ppt. The notation "(p)" refers to the particulate phase. In absence of this suffix, the yield is calculated over the total (gas + particulate) concentration.

Chapter 6

General conclusions

A mechanism describing the oxidation of α-pinene by OH and O_3 and the partitioning of the products between the gas and aerosol phase has been implemented in a box model for simulations of laboratory experiments. This mechanism of unprecedented degree of detail is chosen to be as explicit as possible, given the current knowledge of the individual reaction steps. The gas phase chemical mechanism is based on the theoretical work of Peeters and co-workers. They estimated the products and rates of the key reactions controlling the general lines of the mechanism: the reactions of alkoxy radicals, the ring closure reactions of large unsaturated peroxy radicals and the decomposition reactions of α-hydroxy peroxy radicals. The classical reactions of peroxy radicals (reactions with NO_x, HO_2 and other peroxy radicals) have been characterized in this work and a formalism has been proposed and implemented to represent the effect of their numerous permutation reactions. The sinks of the stable oxidation products -carbonyls, nitrates, hydroperoxides,etc- have been determined by a careful review and generalization of experimental photolysis parameters and by the application of existing Structure Activity Relationships for their OH-reaction. A general formalism has been also proposed for the oxidation mechanism of the products for which the chemistry is not explicitly known.

The partitioning model is based on the equation of Pankow (1994a,b) which relates the partitioning of the condensable products to their vapour pressures. In order to provide the best possible estimates of these vapour pressures, we have developed a prediction method based on group contribution principles which, for the first time to our knowledge, is applicable to all categories of species found in the oxidation mechanism of α-pinene. Parameterization is provided for alcohols, acids, carbonyls, nitrates, peroxy acyl nitrates (PANs) and hydroperoxides. Our method shows a better performance than the well-known UNIFAC method (Asher et al., 2002). The uncertainties of the predicted vapour pressures for the oxidation products are within a factor 2-3. The least volatile compounds are calculated to be pinic acid (3×10^{-6} torr) and hydroxy pinonic acid (6×10^{-7} torr). Recent calculations indicate that pinic acid dimerizes to a large extent in laboratory conditions. This process is believed to concern also other multifunctional carboxylic acids. Since dimers contribute to the total (monomer+dimer) concentrations measured in the laboratory, and are predicted in

this work to contribute to the formation of SOA, estimating their vapour pressures by experimental and theoretical means appears to be a necessary task for future studies.

Simulations of laboratory experiments of the OH-oxidation of α-pinene indicate that the model reproduces well the concentrations of pinonaldehyde and of the chemical families (e.g. nitrates, PANs). The existence of "exotic" reactions pointed out by the group of Peeters induces a large dependence of the product yields, in particular acetone and pinonaldehyde, on the concentration of NO. Consequently, the yields obtained at ppm-levels of NO in the laboratory can not be extrapolated to the atmosphere, where the concentrations of NO are usually lower than 1 ppb. A striking example is provided by the case of acetone: its yield reaches 10% or more in the laboratory, for NO$\geq$1 ppm, but falls to zero according to the model calculations for atmospheric conditions because of the ring closure reaction. It is important to stress that, to date, theoretical calculations fail to identify formation routes for important constituents of SOA (hydroxy pinonic acid and pinic acid) in the ozonolysis mechanism, and for acetone in both the ozone and OH-oxidation in low NO conditions. Further theoretical and experimental studies are required to elucidate these processes.

The total yield of SOA from the oxidation of OH in laboratory conditions is well simulated by the model. This result provides some validation for the partitioning module based on the vapour pressure prediction method developed in this work. The SOA production generated by the OH oxidation at high NO is relatively small (2-5% for 300 ppt α-pinene). However, the temporal behavior of the observed SOA cannot be reproduced by the box model. Sensitivity analyses have been performed, which show that the discrepancies between data and model for SOA are not related to the uncertainties of the predicted vapour pressures.

Box model simulations of ozonolysis experiments indicate that the aerosol concentration produced from the oxidation by O_3 is mainly made of organic acids. Furthermore, under the hypothesis that dimers and adducts have a low volatility, simulations show that the dimerization of multifunctional carboxylic acids play an important role in the SOA formation. However, our simulations have highlighted two important issues: first, the SOA yield measurements at different temperatures (290K-320K) indicate that the temperature dependence of the partitioning is much weaker than predicted. Secondly, the particle-phase concentration of volatile carbonyl products is negligible according to our model in contradiction with laboratory and field data. The temperature dependence adopted for the reactions of dimers and adducts, and for the vapour pressures of the condensables is of course questionable, but other processes favouring the condensation of carbonyl compounds should be considered like the oligomerization processes. Very recently several groups have identified products from the oxidation of isoprene in aerosol samples collected in forested areas (Claeys et al., 2004; Matsunaga et al., 2005). The presence of these products, among which some have a very high volatility, (e.g. glycoaldehyde, methylglyoxal) in the condensed phase might be due to these polymerization processes. These new observations con-

tradict past laboratory experiments which reported a negligible SOA formation from isoprene. It opens a debate on the suitability of the experimental set ups used to measure the SOA in laboratory and atmospheric conditions. If oligomerization reactions are confirmed to be of significant importance, the SOA production from biogenic sources should then be reevaluated by considering isoprene as a possible SOA precursor. In any case, an important conclusion of our work is that state-of-the-art model results based on the partitioning theory of Pankow cannot reproduce properly laboratory data without considering "non traditional" processes (e.g. dimerization, oligomerization reactions).

Even when considering dimerization, however, our model predicts a much lower potential for aerosol production for α-pinene than the mechanisms used in current global models. Box model simulations in typical atmospheric conditions show that the ozonolysis of α-pinene remains the privileged route for SOA production, through the production of multifunctional carboxylic acids. However, the oxidation by OH provides also a small fraction (around 30%) of the SOA concentration, mainly made of hydroxy hydroperoxides.

An innovative methodology has been developed to reduce in successive steps the gas phase oxidation/partitioning mechanism to a manageable size for global modeling. The reduced mechanism aims at reproducing the impact of α-pinene on inorganic compounds as well as the partitioning of the main chemical families and of the most important individual products. The reduced mechanism is designed for implementation in the IMAGES model in order to evaluate the global impact of α-pinene in the atmosphere. The dimerization of multifunctional carboxylic acids calculated to be effective in the atmosphere using the box model, will be more precisely evaluated using the global model.

Appendix A

Structure of α-pinene oxidation products

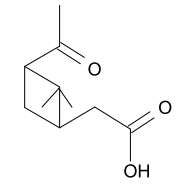

Pinonic Acid

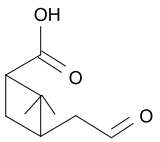

Pinalic Acid

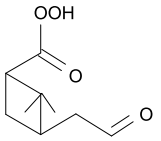

Perpinalic Acid

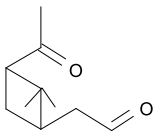

Pinonaldehyde

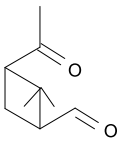

Norpinonaldehyde

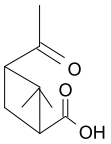

Norpinonic Acid

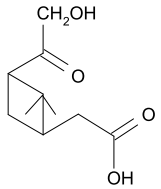

Hydroxypinonic Acid

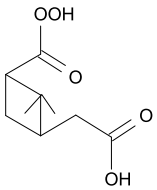

Pinic Acid

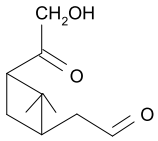

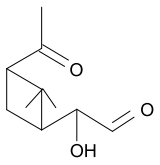

Hydroxypinonaldehydes & Isom.

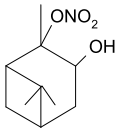

APINANO3

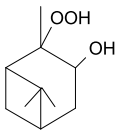

APINANOOH

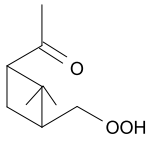

C96OOH

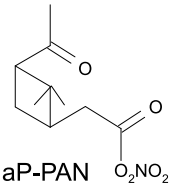

aP-PAN

Appendix B

List of the species and reactions of the reduced mechanism

Table B.1: Lumped and explicit species of the reduced mechanism. The self-reaction rates of the radicals and the vapour pressures of the products are also given.

Lumped radical	Class notation	k_{self}	Radical name	Class notation	k_{self}
OHAPIN2RO2	R2R	4.0E-13	APIN2OO2	R2O	1.0E-11
OHAPIN2HO2	R2H	2.0E-12	LXO2	R2R	4.0E-13
APIN3OO2	R3O	5.0E-14	APINCO3	RO3	1.5E-11
APIN1OO2	R1O	1.5E-11	LXO3	RO3	1.5E-11
Lumped species	Carbon number	Functionalities*			Vapour pressure at 298K (torr)
OHAPINONO2	10	1 OHs and 1 $\mathrm{ONO2s}$			9.7E-04
OHAPINOOH	10	1 OHs and 1 OOH			5.6E-05
APINONO2	10	2 carb and 1 $\mathrm{ONO2s}$			8.1E-04
APINOOH	10	2 carb and 1 OOH			3.6E-05
APINOH	10	1 carb and 1 OHs			4.5E-03
OHAPINOH	10	1 carb, 1 OHs and 1 OHt			9.2E-05
APINCHO	9	2 carb			2.6E-01
OXYPINALD	10	2 carb and 1 OHt			4.5E-03
APINPAN	10	1 carb and 1 PAN			4.6E-04
LXONO2	9	1 carb, 1 OHs and 1 $\mathrm{ONO2s}$			1.2E-04
LXOOH	9	1 carb, 1 OHs and 1 OOH			4.5E-05
LXOH	9	1 carb, 1 OHs and 1 OHs			5.2E-05
LXCHO	9	1 carb, 1 OHs and 1 carb			1.8E-03
LXPAN	9	1 carb, 1 OHs and 1 PAN			4.5E-05
LXCOOH	9	1 carb, 1 OHs and 1 COOH			2.5E-05
LXCOOOH	9	1 carb, 1 OHs and 1 COOH			2.5E-05
Explicit species	Structure				Vapour pressure at 298K (torr)
PINALD	Pinonaldehyde				2.4E-03
OXYPINONIC	Hydroxy pinonic acid				6.0E-07
PINIC	Pinic acid				1.3E-05
PINONIC	Pinonic acid				2.8E-04

* Notations refer to the functionalities as defined in Tab. 3.2, page 72: carb: carbonyl, OH: hydroxy, $\mathrm{ONO2}$: nitrate, PAN: peroxy acyl nitrate, OOH: hydroperoxide, COOH: carboxylic acid. The suffixes "p","s" and "t" refer to the degree of substitution of the carbon to which the functionality "OH" or "$\mathrm{ONO2}$" is attached.

Table B.2: Chemical reactions of the reduced mechanism and their associated kinetic rates

Reactions	Rates*
Gas-phase reactions	
APIN + OH → 0.22 OHAPIN2RO2 + 0.68 OHAPIN2HO2 + 0.10 APIN3OO2	1.21(-11)*exp(444/T)
APIN + O3 → 0.144 PINALD + 0.144 H2O2 + 0.396 APIN1OO2 + 0.132 APIN3OO2 + 0.728 OH + 0.2 APIN2OO2 + 0.064 PINONIC + 0.032 PINIC + 0.032 OXYPINONIC	1.01(-15)*exp(-732/T)
OHAPIN2RO2 + NO → 1.2 LXO2 + 0.3 LXO3 + NO2	0.79*2.54(-12)*exp(360/T)
OHAPIN2RO2 + NO → OHAPINONO2	0.21*2.54(-12)*exp(360/T)
OHAPIN2RO2 + NO3 → 1.2 LXO2 + 0.3 LXO3 + NO2	2.3E-12
OHAPIN2RO2 + HO2 → OHAPINOOH + O2	2.72(-13)*exp(1250/T)
OHAPIN2RO2 + OHAPIN2HO2 → 0.50 OHAPIN2HO2 + 0.70 OHAPINOH + 0.15 APINOH + 0.36 LXO2 + 0.09 LXO3 + 0.35 OXYPINALD	2.19E-12
OHAPIN2RO2 + OHAPIN2RO2 → 0.72 LXO2 + 0.18 LXO3 + 0.70 OXYPINALD + 0.70 OHAPINOH	4.00E-13
OHAPIN2RO2 + APIN1OO2 → 0.36 LXO2 + 0.09 LXO3 + 0.60 OXYPINALD + 0.35 OHAPINOH + 0.50 APIN1OO + 0.25 APINCHO	4.90E-12
OHAPIN2RO2 + CH3CO3 → CH3CO2 + 1.2 LXO2 + 0.3 LXO3	8.27E-12
OHAPIN2RO2 + CH3CO3 → CH3COOH + OXYPINALD	1.73E-12
OHAPIN2RO2 + LXO3 → 1.2 LXO2 + 0.3 LXO3	8.27E-12
OHAPIN2RO2 + LXO3 → OXYPINALD + LXCOOH	1.73E-12
OHAPIN2RO2 + LXO2 → 0.50 APIN1OO + 0.25 APINCHO + 0.60 OXYPINALD + 0.36 LXO2 + 0.09 LXO3 + 0.35 OHAPINOH	8.00E-13
OHAPIN2RO2 + CH3O2 → .40 CH3O + .30 CH2O + .30 CH3OH + 0.36 LXO2 + 0.09 LXO3 + 0.25 OHAPINOH + 0.25 OXYPINALD	8.00E-13
OHAPIN2HO2 + NO → 0.97 PINALD + 0.97 HO2 + 0.03 LXO2 + 0.03 CH2O + NO2	0.93*2.54(-12)*exp(360/T)
OHAPIN2HO2 + NO → OHAPINONO2	0.07*2.54(-12)*exp(360/T)
OHAPIN2HO2 + NO3 → 0.97 PINALD + 0.97 HO2 + 0.03 LXO2 + 0.03 CH2O + NO2	2.3E-12
OHAPIN2HO2 + HO2 → OHAPINOOH + O2	2.90(-13)*exp(1250/T)
OHAPIN2HO2 + OHAPIN2HO2 → 0.776 PINALD + 0.776 HO2 + 0.024 LXO2 + 0.024 CH2O + 0.60 OHAPINOH + 0.60 APINOH	3.00E-12
OHAPIN2HO2 + LXO3 → 0.97 PINALD + 0.97 HO2 + 0.03 LXO2 + 0.03 CH2O	8.27E-12

Chemical reactions of the reduced mechanism and kinetic rates and their associated kinetic rates (continued)

Reactions	Rates
OHAPIN2HO2 + LXO3 → APINOH + LXCOOH	1.73E-12
OHAPIN2HO2 + LXO2 → 0.485 PINALD + 0.485 HO2 + 0.015 LXO2 + 0.015 CH2O + 0.35 OHAPINOH + 0.15 APINOH + 0.15 LXOH + 0.35 LXCHO	2.19E-12
OHAPIN2HO2 + CH3O2 → 0.40 CH3O + 0.30 CH2O + 0.30 CH3OH + 0.485 PINALD + 0.485 HO2 + 0.015 LXO2 + 0.015 CH2O + 0.15 APINOH + 0.35 OHAPINOH	2.19E-12
OHAPIN2HO2 + CH3CO3 → CH3CO2 + 0.97 PINALD + 0.97 HO2 + 0.03 LXO2 + 0.03 CH2O	8.27E-12
OHAPIN2HO2 + CH3CO3 → CH3COOH + APINOH	1.73E-12
OHAPIN2HO2 + APIN1OO2 → 0.485 PINALD + 0.485 HO2 + 0.015 LXO2 + 0.015 CH2O + 0.15 APINOH + 0.35 OHAPINOH + 0.50 APIN1OO + 0.25 APINCHO + 0.25 OXYPINALD	1.34E-11
OHAPIN2HO2 + APIN3OO2 → 0.679 PINALD + 0.679 HO2 + 0.021 LXO2 + 0.021 CH2O + 0.30 OXYPINALD + 0.30 APINOH + 0.70 APIN3OO2	7.75E-13
APIN1OO2 + NO → CH2O + APINCO3 + NO2	0.86*2.54(-12)*exp(360/T)
APIN1OO2 + NO → APINONO2	0.14*2.54(-12)*exp(360/T)
APIN1OO2 + NO3 → CH2O + APINCO3 + NO2	2.3E-12
APIN1OO2 + HO2 → APINOOH	2.74(-13)*exp(1250/T)
APIN1OO2 + APIN1OO2 → 1.0 CH2O + APINCO3 + 0.50 APINCHO + 0.50 OXYPINALD	1.50E-11
APIN1OO2 + LXO3 → CH2O + APINCO3	8.27E-12
APIN1OO2 + LXO3 → APINCHO + LXCOOH	1.73E-12
APIN1OO2 + LXO2 → 0.50 CH2O + APINCO3 + 0.25 APINCHO + 0.25 OXYPINALD + 0.25 LXOH + 0.25 LXCHO	4.90E-12
APIN1OO2 + CH3O2 → .40 CH3O + .30 CH2O + .30 CH3OH + 0.50 CH2O + APINCO3 + 0.25 APINCHO + 0.25 OXYPINALD	4.90E-12
APIN1OO2 + CH3CO3 → CH3CO2 + CH2O + APINCO3	8.27E-12
APIN1OO2 + CH3CO3 → APINCHO + CH3COOH	1.73E-12
APINCO3 + NO → APIN3OO2 + NO2	6.70(-12)*exp(340/T)
APINCO3 + NO2 → APINPAN	$1.1*10^{-11}*(T/298)^{-1}$
APINCO3 + NO3 → APIN3OO2 + NO2	2.3E-12
APINCO3 + HO2 → PINONIC + O3	0.22*5.20(-13)*exp(983/T)
APINCO3 + HO2 → LXCOOOH + O2	0.78*5.20(-13)*exp(983/T)
APINCO3 + CH3O2 → APIN3OO2 + CH3O	8.27E-12
APINCO3 + CH3O2 → PINONIC + CH2O	1.73E-12
APINCO3 + CH3CO3 → CH3CO2 + APIN3OO2	1.70E-11
APINPAN → APINCO3 + NO2	2.80(16)*exp(-13580/T)

Chemical reactions of the reduced mechanism and kinetic rates and their associated kinetic rates (continued)

Reactions	Rates
APINR3O2 + NO → APINONO2	0.12*2.54(-12)*exp(360/T)
APINR3O2 + NO → 1.0 LXO2 + 0.224 acetone + 0.4 HO2 + 0.456 CH2O + 0.224 CH3COCHO + 0.320 OXYPINALD + 0.8 LXO3 + 0.12 APINCHO + NO2	0.88*2.54(-12)*exp(360/T)
APINR3O2 + NO3 → 1.0 LXO2 + 0.224 acetone + 0.4 HO2 + 0.456 CH2O + 0.224 CH3COCHO + 0.320 OXYPINALD + 0.8 LXO3 + 0.12 APINCHO + NO2	2.3E-12
APINR3O2 + HO2 → APINOOH + O2	2.74(-13)*exp(1250/T)
APIN2OO2 + NO → APINCHO + CO + HO2 + NO2	0.73*2.54(-12)*exp(360/T)
APIN2OO2 + NO → APINONO2	0.27*2.54(-12)*exp(360/T)
APIN2OO2 + NO3 → APINCHO + CO + HO2 + NO2	2.3E-12
APIN2OO2 + HO2 → APINOOH + O2	2.74(-13)*exp(1250/T)
APIN2OO2 + LXO2 → 0.50 APINCHO + 0.50 CO + 0.50 HO2 + 0.25 APINCHO + 0.25 OXYPINALD + 0.25 LXOH + 0.25 LXCHO	4.00E-12
APIN2OO2 + LXO3 → APINCHO + CO + HO2	8.27E-12
APIN2OO2 + LXO3 → APINCHO + LXCOOH	1.73E-12
APIN2OO2 + APIN2OO2 → APINCHO + CO + HO2 + 0.50 APINCHO + 0.50 OXYPINALD	1.00E-11
APIN2OO2 + APINCO3 → APIN3OO2 + APINCHO + CO + HO2	8.27E-12
APIN2OO2 + APINCO3 → PINONIC + APINCHO	1.73E-12
LXO2 + NO → NO2	0.89*2.54(-12)*exp(360/T)
LXO2 + NO → LXONO2	0.11*2.54(-12)*exp(360/T)
LXO2 + NO3 → NO2	2.3E-12
LXO2 + HO2 → LXOOH	2.72(-13)*exp(1250/T)
LXO2 + LXO2 → 0.50 LXOH + 0.50 LXCHO	2.00E-13
LXO2 + LXO3 →	8.27E-12
LXO2 + LXO3 → LXCHO + LXCOOH	1.73E-12
LXO3 + NO → NO2	6.70(-12)*exp(340/T)
LXO3 + NO2 → LXPAN	$1.1*10^{-11}(T/298)^{-1}$
LXO3 + NO3 → NO2	2.3E-12
LXO3 + HO2 → LXCOOH + O3	0.22*5.20(-13)*exp(983/T)
LXO3 + HO2 → LXCOOOH + O2	0.78*5.20(-13)*exp(983/T)
LXO3 + LXO3 →	8.5E-12
LXPAN → LXO3 + NO2	2.80(16)*exp(-13580/T)
Photodissociation reactions	
OHAPINONO2 + hv → 1.2 LXO2 + 0.3 LXO3 + NO2	J(Nitrates $C_{\geq 7}$)
APINONO2 + hv → 1.2 LXO2 + 0.3 LXO3 + NO2	J(Keto-nitrates $C_{\geq 7}$)
APINCHO + hv → 0.33 CH2CHCOCH3 + 1 LXCHO + 0.12 CH3CO3	

Chemical reactions of the reduced mechanism and kinetic rates and their associated kinetic rates (continued)

Reactions	Rates
+ 0.22 HO2 + 0.22 CO + 0.07 LXO3 + 0.35 LXO2	J(PINALD)
APINOOH + hv → OH + 1.2 LXO2 + 0.3 LXO3	J(ROOH)
OHAPINOOH + hv → OH + 1.2 LXO2 + 0.3 LXO3	J(ROOH)
OXYPINALD + hv → 1.2 LXO2 + 0.3 LXO3	J(PINALD)
APINPAN + hv → 0.8 APINCO3 + 0.8 NO2	
+ 0.2 APIN3OO2 + 0.2 NO3	J(PAN)
PINALD + hv → APIN2OO2 + CO + HO2	J(PINALD) (R2.40a)
PINALD + hv → 0.5 CH2CHCOCH3 + 1.5 LXCHO	J(PINALD) (R2.40b and R2.40c)
PINALD + hv → APIN3OO2 + CH3CO3	J(PINALD) (R2.40d)
LXPAN + hv → 0.8 NO2 + 0.2 N03	J(PAN)
LXOOH + hv →	J(ROOH)
LXCOOOH + hv →	J(RCOOOH)
LXCHO + hv →	J(PINALD)
LXONO2 + hv → NO2	J(Keto-nitrates $C_{\geq 7}$)
OH-oxidation of the primary products	
PINALD + OH → APINCO3 + H2O	2.2E-11
PINALD + OH → APIN3OO2 + H2O	5.0E-12
PINALD + OH → APIN2OO2 + H2O	8.0E-12
PINONIC + OH → 1.2 LXO2 + 0.3 LXO3	4.7E-12
PINIC + OH → 1.2 LXO2 + 0.3 LXO3	4.7E-12
OXYPINONIC + OH → 1.2 LXO2 + 0.3 LXO3	4.7E-12
OHAPINONO2 + OH → 1.2 LXO2 + 0.3 LXO3	3.5E-12
APINONO2 + OH → 1.2 LXO2 + 0.3 LXO3	8.0E-12
APINCHO + OH → 0.6 LXO2 + 0.9 LXO3	3.5E-11
APINOH + OH → 1.2 LXO2 + 0.3 LXO3	8.0E-12
OXYPINALD + OH → 0.6 LXO2 + 0.9 LXO3	2.0E-11
OHAPINOH + OH → 1.2 LXO2 + 0.3 LXO3	8.0E-12
APINOOH + OH → 1.2 LXO2 + 0.3 LXO3	8.0E-12
OHAPINOOH + OH → 1.2 LXO2 + 0.3 LXO3	7.2E-12
APINPAN + OH → 1.2 LXO2 + 0.3 LXO3	8.7E-12
LXOOH + OH →	8.0E-12
LXCOOH + OH →	8.0E-12
LXCOOOH + OH →	8.0E-12
LXOH + OH →	8.0E-12
LXCHO + OH →	2.0E-11
LXPAN + OH →	8.00E-12
LXONO2 + OH →	8.00E-12
Dimerization equilibrium	
PINONIC + PINONIC → PINONIC_PINONIC	$k_{dimer.}$

Chemical reactions of the reduced mechanism and kinetic rates and their associated kinetic rates (continued)

Reactions	Rates
PINONIC + PINIC → PINONIC_PINIC	$k_{dimer.}$
PINIC + PINIC → PINIC_PINIC	$k_{dimer.}$
PINONIC_PINONIC → PINONIC + PINONIC	$k_{diss.}$
PINONIC_PINIC → PINONIC + PINIC	$k_{diss.}$
PINIC_PINIC → PINIC + PINIC	$k_{diss.}$
Adsorption reactions	
PINONIC_PINONIC + aerosol → 3 aerosol + PINONIC_PINONICp	$k_{R3.2}$
PINONIC_PINIC + aerosol → 3 aerosol + PINONIC_PINICp	$k_{R3.2}$
PINIC_PINIC + aerosol → 3 aerosol + PINIC_PINICp	$k_{R3.2}$
PINONIC + aerosol → 2 aerosol + PINONICp	$k_{R3.2}$
PINIC + aerosol → 2 aerosol + PINICp	$k_{R3.2}$
OHAPINONO2 + aerosol → 2 aerosol + OHAPINONO2p	$k_{R3.2}$
APINONO2 + aerosol → 2 aerosol + APINONO2p	$k_{R3.2}$
OHAPINOH + aerosol → 2 aerosol + OHAPINOHp	$k_{R3.2}$
APINOOH + aerosol → 2 aerosol + APINOOHp	$k_{R3.2}$
OHAPINOOH + aerosol → 2 aerosol + OHAPINOOHp	$k_{R3.2}$
OXYPINONIC + aerosol → 2 aerosol + OXYPINONICp	$k_{R3.2}$
LXONO2C + aerosol → 2 aerosol + LXONO2Cp	$k_{R3.2}$
LXPANC + aerosol → 2 aerosol + LXPANCp	$k_{R3.2}$
LXOOH + aerosol → 2 aerosol + LXOOHp	$k_{R3.2}$
LXCOOH + aerosol → 2 aerosol + LXCOOHp	$k_{R3.2}$
LXCOOOH + aerosol → 2 aerosol + LXCOOOHp	$k_{R3.2}$
LXOH + aerosol → 2 aerosol + LXOHp	$k_{R3.2}$
LXCHO + aerosol → 2 aerosol + LXCHOp	$k_{R3.2}$
Desorption reactions	
PINONIC_PINONICp → - 2 aerosol + PINONIC_PINONIC	$k_{R3.3}$
PINONIC_PINICp → - 2 aerosol + PINONIC_PINIC	$k_{R3.3}$
PINIC_PINICp → - 2 aerosol + PINIC_PINIC	$k_{R3.3}$
PINICp → PINIC - aerosol	$k_{R3.3}$
PINONICp → PINONIC - aerosol	$k_{R3.3}$
OHAPINONO2p → OHAPINONO2 - aerosol	$k_{R3.3}$
APINONO2p → APINONO2 - aerosol	$k_{R3.3}$
OHAPINOHp → OHAPINOH - aerosol	$k_{R3.3}$
APINOOHp → APINOOH - aerosol	$k_{R3.3}$
OHAPINOOHp → OHAPINOOH - aerosol	$k_{R3.3}$
OXYPINONICp → OXYPINONIC - aerosol	$k_{R3.3}$
LXONO2C → LXONO2 - aerosol	$k_{R3.3}$
LXPANp → LXPAN - aerosol	$k_{R3.3}$
LXOOHp → LXOOH - aerosol	$k_{R3.3}$
LXCOOHp → LXCOOH - aerosol	$k_{R3.3}$

Chemical reactions of the reduced mechanism and kinetic rates and their associated kinetic rates (continued)

Reactions	Rates
LXCOOOHp → LXCOOOH - aerosol	$k_{R3.3}$
LXOHp → LXOH - aerosol	$k_{R3.3}$
LXCHOp → LXCHO - aerosol	$k_{R3.3}$

* rate units are cm^3 $molecule^{-1}$ s^{-1} for bimolecular reactions and s^{-1} for unimolecular reactions.

Bibliography

Alvarado, A., Arey, J., and Atkinson, R., Kinetics of the gas-phase reactions of OH and NO_3 radicals and O_3 with the monoterpene reaction products pinonaldehyde, caronaldehyde, and sabinaketone, J. Atmos. Chem., 31, 281–297, 1998.

Andreae, M. O., Climatic effects of changing atmospheric aerosol levels, In World Survey of Climatology, Vol. 16: Future Climates of the World, A. Henderson-Sellers (ed), Elsevier, Amsterdam, 1995.

Andreae, M. O. and Crutzen, P. J., Atmospheric aerosols: Biogeochemical sources and role in the atmospheric chemistry, Science, 276, 1052–1058, 1997.

Arey, J., Atkinson, R., and Aschmann, S. M., Product study of the gas-phase reactions of monoterpenes with the OH radical in the presence of NO_x, J. Geophys. Res., 95, 18539–18546, 1990.

Arey, J., Aschmann, S. M., Kwok, E. S. C., and Atkinson, R., Alkyl nitrate, hydroxyalkyl nitrate, and hydroxycarbonyl formation from NO_x-air photooxidations of C5–C8 *n*-alkanes, J. Phys. Chem., 105, 1020–1027, 2001.

Aschmann, S. M, Reissel, A., Atkinson, R., and Arey, J., Products of the gas phase reactions of the OH radical with α- and β-pinene in the presence of NO, J. Geophys. Res., 103, 25553–25561, 1998.

Asher, W. E., Pankow, J. F., Erdakos, G. B., and Seinfeld, J. H., Estimating the vapor pressures of multi-functional oxygen-containing organic compounds using group contribution methods, Atmos. Environ., 36, 1483–1498, 2002.

Atkinson, R., Lloyd, A. C., and Winges, L., An updated chemical mechanism for hydrocarbon/NO_x/SO_2 photooxidations suitable for inclusion in atmospheric simulation models, Atmos. Environ., 16, 1341–1355, 1982.

Atkinson, R., Gas-phase tropospheric chemistry of organic compounds, J. Phys. Chem. Ref. Data, Monograph, 2, 215, 1994.

Atkinson, R., Atmospheric chemistry of VOCs and NO_x, Atmos. Environ., 34, 2063–2101, 2000.

Atkinson, R., Baulch, D. L., Cox, R. A., Crowley, J. N., Hampson, R. F., Kerr, J. A., Rossi, M. J., and Troe, J., Summary of evaluated kinetic and photochemical data for atmospheric chemistry, 2003, IUPAC subcommittee on gas kinetic data evaluation for atmospheric chemistry, available on the subcommittee's website at http://www.iupac-kinetic.ch.cam.ac.uk, 2003.

Atkinson, R., Baulch, D. L., Cox, R. A., Crowley, J. N., Hampson, R. F., Hynes, R. G., Jenkin, M. E., Kerr, J. A., Rossi, M. J., and Troe, J., Summary of evaluated kinetic and photochemical data for atmospheric chemistry, 2004, IUPAC subcommittee on gas kinetic data evaluation for atmospheric chemistry, available on the subcommittee's website at http://www.iupac-kinetic.ch.cam.ac.uk, 2004.

Bacher, C., Tyndall, G. S., and Orlando, J. J., The atmospheric chemistry of glycolaldehyde, J. Atmos. Chem., 39, 171–189, 2001.

Baker, J., Aschmann, S. M., Arey, J., and Atkinson, R., Reaction of stabilized Criegee intermediates from gas-phase reactions with O_3 with selected alkenes, Intern. Jour. Chem. Kin., 34, 73–85, 2002.

Barnes, I., Becker, K. H., and Zhu, T., Near UV absorption spectra and photolysis products of difunctional organic nitrates, Possible importance as NO_x reservoirs, J. Atmos. Chem., 17, 353–373, 1993.

Bey, I., Aumont, B., and Toupance, G., A modeling study of the nighttime radical chemistry in the lower continental troposphere, 2. Origin and evolution of HO_x., J. Geophys. Res., 106, 9991–10001, 2001.

Bilde, M. and Pandis, S. N., Evaporation Rates and Vapor Pressures of Individual Aerosol Species Formed in the Atmospheric Oxidation of α- and β-pinene, Environ. Sci. Technol., 35, 3344–3349, 2001.

Bilde, M., Svenningsson B., Monster, J., and Rosenorn, T., Even-Odd Alternation of Evaporation Rates and Vapor Pressures of C3-C9 Dicarboxylic Acid Aerosols, Environ. Sci. Technol., 37, 1371–1378, 2003.

Billing, G. D. and Mikkelsen, K. V., Introduction to Molecular Dynamics and Chemical Kinetics, John Wiley and Sons, New York, 1996.

BIOVOC, Final report on the EU project on Degradation Mechanisms of Biogenic VOC "BIOVOC", Contract reference ENV-CT95-0059,Co-ordinator, Hjorth, J., JRC Ispra, 1998.

Bonn, B. and Moortgat, G. K., New particle formation during α- and β-pinene oxidation by O_3, OH and NO_3, and the influence of water vapour, particle size distribution studies, Atmos. Chem. Phys., 2, 183–196, 2002.

Bonn, B., von Kuhlmann, R., and Lawrence, M., G., High contribution of biogenic hydroperoxides to secondary organic aerosol formation, Geophys. Res. Lett., 31, L10108, doi:10.1029/2003GL019172, 2004.

Boyd, A. A., Nozière, B., and Lesclaux, R., Kinetic study of the allylperoxy radical self-reaction and reaction with HO_2, J. Chem. Soc., Faraday Trans., 92, 201–206, 1996a.

Boyd, A. A., Lesclaux, R., Jenkin, M. E., and Wallington, T. J., A spectroscopic, kinetic and product study of the $(CH_3)_2C(OH)CH_2O_2$ radical self reaction and reaction with HO_2, J. Phys. Chem., 100, 6594–6603, 1996b.

Boyd, A. A. and Lesclaux, R., The temperature dependence of the rate coefficients for β-hydroxyperoxy radical self reactions, Int. J. Chem. Kinet., 29, 323–331, 1997.

Boyd, A. A., Villenave, E., and Lesclaux, R., Structure-reactivity relationships for the self-reactions of linear secondary alkylperoxy radicals, An experimental investigation, Int. J. Chem. Kinet., 31, 37–46, 1999.

Boyd, A. A., Villenave, E., and Lesclaux, R., Self- and cross-reactions of β-hydroxyperoxy radicals of relevance to tropospheric monoterpene oxidation: structure-activity relationships for rate coefficients, Atmos. Environ., 37, 2751–2760, 2003.

Bowman, F. M., Odum, J. R., Seinfeld, J. H., and Pandis, S. N., Mathematical model for gas-particle partitioning of secondary organic aerosols, Atmos. Environ., 31, 3921–3931, 1997.

Brasseur, G. P., Hauglustaine, D. A., Walters, S., Rasch, P. J., and Müller, J.-F, MOZART, a global chemical transport model for ozone and related chemical tracers, 1, Model description. J. Geophys. Res., 103, 28265–28269, 1998.

Brasseur, G., Orlando, J., and Tyndall, G., Atmospheric Chemistry and Global Change, Oxford University Press, New York-Oxford, 1999.

Brockmann,K. J., Kriesche, V., Etzkom, T., Volkamer, R., and Wirtz, K., The European Photoreactor EUPHORE, A technical description, Proceedings of the EUROTRAC Symposium'96, Borell,P.M., Borell, P., Cvitas, T., Kdelly, K., and Seiler, W. (Eds.), 457–461, 1996.

Bruckmann, P. W. and Willner, H., Infrared Spectroscopic Study of Peroxyacetyl Nitrate (PAN) and Its Decomposition Products, Environ. Sci. Technol., 17, 352–357, 1983.

Canosa-Mas, C. E., Daele, V., King, M., Lopez, R., Percival, C. J., Wayne, R. P., Shallcross, D. E., and Pyle, J., Is the reaction between $CH_3C(O)O_2$ and NO_3 important in the night-time troposphere, J. Chem. Soc. Faraday Trans., 92, 2211–2222, 1996.

Carter, W. P. L., A detailed mechanism for the gas-phase atmospheric reactions of organic compounds, Atmos. Environ., 24, 481–518, 1990.

Chew, A. A. and Atkinson, R., OH radical formation yields from the gas-phase reactions of O_3 with alkenes and monoterpenes, J. Geophys. Res., 101, 28649–28653, 1996.

Christoffersen, T. S., Hjorth, J., Horie, O., Jensen, N. R., Kotzias, D., Molander, L. L., Neeb, P., Ruppert, L., Winterhalter, R., Virkkula, A., Wirtz, K., and Larsen, B., Cis-Pinic acid, a possible precurser for organic aerosol formation from ozonolysis of α-pinene, Atmos. Environ., 32, 1657–1661, 1998.

Chung, S. H. and Seinfeld J. H., Global distribution and climate forcing of carbonaceous aerosols, J. Geophys. Res., 107, 4407, doi:10.1029/2001JD001397, 2002.

Claeys, M., Graham, B., Vas, G., Wang, W., Vermeylen, R., Pashynska, V., Cafmeyer, J., Guyon, P., Andreae, M. O., Artaxo, P., and Maenhaut, W., Formation of Secondary Organic Aerosols Through Photooxidation of Isoprene, Science, 303, 1173–1176, 2004.

Czoschke, M. N., Jang, M., and Kamens, R. M., Effect of acidic seed on biogenic secondary organic aerosol growth, Atmos. Environ., 37, 4287–4299, 2003.

Damian-Iordache, V., Sandu, A., Potra, F. A., Carmichael, G. R., and Damian-Iordache, M., KPP-A symbolic preprocessor for chemical kinetics-User's guide, Center for Global and Regional Environmental Research, The University of Iowa, Internal report, 1995.

DeMore, W. B., Sander, S. P., Golden, D. M., Hampson, R. F., Kurylo, M. J., Howard, C. J., Ravishankara, A. R., Kolb, C. E., and Molina, M. J., Chemical kinetics and photochemical data for use in stratospheric modeling, JPL Publ., 97-4, Jet Propul. Lab., Pasadena, Calif., 1997.

Derwent, R. G., Collins, W. J., Jenkin, M. E., Johnson, C. E., and Stevenson, D. S., The Global Distribution of Secondary Particulate Matter in a 3-D Lagrangian Chemistry Transport Model, J. Atm. Chem., 44, 57–95, 2003.

Desai, J., Heicklen, J., Bahta, A., and Simonaitis, R., The photo-oxidation of i-C_3H_7CHO vapour, J. Photoch., 34, 137–164, 1986.

Elrod, M. J., Ranschaert, D. L., and Schneider, N. J., Direct kinetics study of the temperature dependence of the CH_2O branching channel for the CH_3O_2+HO_2 reaction, Int. J. Chem. Kinet., 33, 363–376, 2001.

Elterman, L., UV, Visible, and IR Attenuation for Altitudes to 50 km; AFCRL-68-0153, Bedford, MA, Air Force Cambridge Res. Lab., 1968.

Engineering Sciences Data Unit Ltd, Vapour pressures and critical points of liquids. Glycols and cyclic diols,item No 95002, Vol.2d(ii),ESDU international, London, 2001.

Fantechi, G., Atmospheric oxidation reactions of selected biogenic volatile organic compounds (BIOVOCs): A smog chamber study, Ph.D. Thesis, KULeuven, 1999.

Fantechi G., Vereecken L., and Peeters J., The OH-initiated atmospheric oxidation of pinonaldehyde: Detailed theoretical study and mechanism construction, Phys. Chem. Chem. Phys., 4, 5795–5805, 2002.

Finlayson-Pitts, B. J. and Pitts Jr., J. N., Chemistry of the upper and lower troposphere, 2nd ed., Academic Press Inc., New York, 1999.

Fischer R. G. and Ballschmiter K., Determination of vapor pressure, water solubility, gas-water partition coefficient P_{GW}, Henry's law constant, and octanol-water partition coefficient P_{OW} of 26 alkyl dinitrates, Chemosphere, 36, 2891–2901, 1998.

Fredenslund, A., Gmehling, J., and Rasmussen, P., Vapor-Liquid Equilibria Using UNIFAC: A Group Contribution Method. Elsevier, Amsterdam, 1977.

Fuller, E. N., Ensley, K., and Giddings, C. J., Diffusion of halogenated hydrocarbons in Helium, J. Phys. Chem., 73, 3679–3685, 1969.

Gallegos Saliner, A., Molecular quantum similarity in QSAR: Applications in computer-aided molecular design, Ph.D. thesis, University of Girona, Spain, 2004.

Gao, S., Ng, N. L., Keywood, M., Varutbangkul, V., Bahreini R., Nenes, A., He, J., Yoo, K. Y., Beauchamp, J. L., Hodyss, R. P., Flagan, R. C., and Seinfeld, J. H., Particle Phase Acidity and Oligomer Formation in Secondary Organic Aerosol, Environ. Sci. Technol., doi:10.1021/es049125k, 2004.

Gardner E. P., Sperry P. D., and Calvert, J. G., Photodecomposition of acrolein in O_2-N_2 mixtures, J. Phys. Chem., 91, 1922–1930, 1987.

Gierczak, T., Burkholder, J. B., Bauerle, S., and Ravishankara, A. R., Photochemistry of acetone under tropospheric conditions, Chem. Phys., 231, 229–244, 1998.

Glasius, M., Lahaniati, M., Calogirou, A., Di Bella, D., Jensen, N. R., Hjorth, J., Kotzias, D., and Larsen, B. R., Carboxylic Acids in Secondary Aerosols from Oxidation of Cyclic Monoterpenes by Ozone, Environ. Sci. Technol., 1001–1010, 2000.

Griffin, R. J., Cocker III, D. R., Flagan, R. C., and Seinfeld, J. H., Organic aerosol formation from the oxidation of biogenic hydrocarbons, J. Geophys. Res., 104, 3555–3567, 1999.

Griffin, R. J., Cocker III, D. R., Seinfeld, J. H., and Dabdub, D., Estimate of global atmospheric organic aerosol from oxidation of biogenic hydrocarbons, Geophys. Res. Lett., 26, 2721–2724, 1999.

Griffin, R. J., Dabdub, D., and Seinfeld, J. H., Secondary organic aerosol, 1. Atmospheric chemical mechanism for production of molecular constituents, J. Geophys. Res., 107, 4332, doi:10.1029/2001JD000541, 2002.

Griffin, R. J., Nguyen, K., Dabdub, D., and Seinfeld, J. H., A combined hydrophobic-hydrophilic module for predicting secondary organic aerosol formation, J. Atmos. Chem., 44, 171–190, 2003.

Griffin, R. J., Dabdub, D., and Seinfeld, J. H., Develoment and initial evaluation of a dynamic species-resolved model for gas phase chemistry ans size-resolved gas/particle partitioning associated with secondary aerosol formation, J. Geophys. Res., 110, D05304, doi:10.1029/2004JD005219, 2005.

Guenther, A., Hewitt, C. N., Erickson, D., Fall, R., Geron, C., Graedel, T., Harley, P., Klinger L., Lerdau, M., McKay, W. A., Pierce, T., Scholes, B., Steinbrecher, R., Tallamraju, R., Taylor, J., and Zimmerman, P., A global model of natural volatile organic compound emissions, J. Geophys. Res., 100, 8873–8892, 1995.

Hairer, E. and Wanner, G., Solving ordinary differential equations II. Stiff and differential-algebraic problems, Springer series in computational mathematics, Springer-Verlag, Berlin, 1990.

Hakola, H., Arey, J., Aschmann, S. M., and Atkinson, R., Product formation from the gas-phase reactions of OH radicals and O_3 with a series of monoterpenes, J. Atmos. Chem., 18, 75–102, 1994.

Hallquist M., Wängberg I., and Ljungström, E., Atmospheric fate of carbonyl oxidation products originating from α-pinene and Δ^3-carene: Determination of rate of reaction with OH and NO_3 radicals, UV absorption cross sections, and vapor pressure, Environ. Sci. Technol., 31, 3166–3172, 1997.

Hatakeyama, S., Izumi, K., Fukuyama, T., Akimoto, H., and Washida, N., Reactions of ozone with α-pinene and β-pinene in air: Yields of gaseous and particulate products, J. Geophys. Res., 94, 13013–13024, 1989.

Hatakeyama, S., Izumi, K., Fukuyama, T., Akimoto, H., and Washida, N., Reaction of OH with α-pinene and β-pinene in air: Estimate of global CO production from the atmospheric oxidation of terpenes, J. Geophys. Res., 96, 947–958, 1991.

Hermans, I., Müller, J. F., Nguyen, T. L., Jacobs, P. A., and Peeters J., Kinetics of alfa-hydroxy-alkylperoxyl radicals in oxidation processes. HO2*-initiated oxidation of ketones/aldehydes near the tropopause, J. Phys. Chem. A, 109, 4303–4311, 2005.

Hippler, M., Al-Janabi, F. A. H., and Pfab, J., Photodissociation of jet-cooled methyl and t-butyl nitrite near 380 nm, Chem. Phys. Lett., 192, 173–178, 1992.

Hoffmann, T., Odum, J. R., Bowman, F., Collins, D., Klockow, D., Flagan, R. C., and Seinfeld, J. H., Formation of organic aerosols from the oxidation of biogenic hydrocarbons, J. Atmos. Chem., 26, 189–222, 1997.

Hoffmann, T., Bandur, R., Marggraf, U., and Linscheid, M., Molecular composition of organic aerosols formed from α-pinene/O_3 reaction: Implications for new particle formation processes, J. Geophys. Res., 103, 25569–25578, 1998.

Horie, O. and Moortgat, G. K., Reactions of $CH_3C(O)O_2$ radicals with CH_3O_2 and HO_2 radicals between 263 and 333 K, J. Chem. Soc. Faraday Trans., 88, 3305–3312, 1992.

Houweling, S., Dentener, F., and Lelieveld., J., The impact of non-methane hydrocarbon compounds on tropospheric photochemistry, J. Geophys. Res., 103, 10673–10696, 1998.

HSDB (Hazardous Substances Data Bank), National Library of Medicine (NLM) Toxicology Data Network (TOXNET),2004, Available online at http://toxnet.nlm.nih.gov.

Iinuma, Y., Böge, O., Gnauk, T., and Herrmann, H., Aerosol-chamber study of the α-pinene/O_3 reaction: influence of particle acidity on aerosol yields and products, Atmos. Environ., 38, 761–773, 2004.

IPCC, Climate change 2001, The scientific basis, contribution of working group I to the third assessment report in the intergovernmental panel on climate change, edited by Houghton, J. T., Ding, Y., Griggs, D. J., Noguer, M., van der Linden, P. J., Dai, X., Maskell, K., and Johnson, C. A., Cambridge University Press, Cambridge, UK, 881, 2001.

Jang, M. and Kamens, R. M., Newly characterized products and composition of secondary aerosols from the reaction of α-pinene with ozone, Atmos. Environ., 33, 459–474, 1999.

Jang, M, Czoschke, N. M., Lee, S., and Kamens, R. M., Heterogeneous Atmospheric Aerosol Production by Acid-Catalyzed Particle-Phase Reactions, Science, 298, 814–8817, 2002.

Jang, M, Carroll, B., Chandramouli, B., and Kamens, R. M., Particle growth by acid-catalyzed heterogeneous reactions of organic carbonyls on preexisting aerosols, Environ. Sci. Technol., 37, 3828–3837, 2003.

Jenkin, M. E., Saunders, S. M., and Pilling, M. J., The tropospheric degradation of volatile organic compounds: A protocol for mechanism development, Atmos. Environ., 31, 81–104, 1997.

Jenkin, M. E., Boyd, A. A., and Lesclaux, R., Peroxy radical kinetics resulting from the OH-initiated oxidation of 1,3-butadiene, 2,3-dimethyl-1,3-butadiene and isoprene, J. Atmos. Chem., 29, 267–298, 1998.

Jenkin, M. E., Shallcross, D. E., and Harvey, J. N., Development and application of a possible mechanism for the generation of cis-pinic acid from the ozonolysis of α and β-pinene, Atmos. Environ., 34, 2837–2850, 2000.

Jenkin, M. E., Modelling the formation and composition of secondary organic aerosol from α-pinene and β-pinene ozonolysis using MCM v3, Atmos. Chem. Phys., 4, 1741–1757, 2004.

Jensen, T., Fredenslund, A., and Rasmussen, P., Pure-component vapor pressures using UNIFAC group contribution, Ind. and Eng. Chem., Fundamentals, 20, 239–246, 1981.

Joback, K. G. and Reid, R. C., Estimation of pure-component properties from group-contributions, Chem. Eng. and Com., 57,233–243, 1987.

Johnston, H. S., Davis, H. F., and Lee, Y. T., NO_3 Photolysis product channels: Quantum yields from observed energy thresholds, J. Phys. Chem., 100, 4713–4723, 1996.

Kalberer, M., Paulsen, D., Sax, M., Steinbacher, M., Dommen, J., Prevot, A.S.H., Fisseha, R., Weingartner, E., Frankevich, V., Zenobi, R., and Baltensperger, U., Identification of Polymers as Major Components of Atmospheric Organic Aerosols, Science, 303, 1659–1662, 2004.

Kamens, R., Jang, M., Chien C. J., and Leach K., Aerosol Formation from the Reaction of α-pinene and Ozone Using a Gas-Phase Kinetics-Aerosol Partitioning Model, Environ. Sci. Technol.,33,1430–1438, 1999.

Kamens, R. and Jaoui, M., Modeling Aerosol Formation from α-Pinene + NO_x in the Presence of Natural Sunlight Using Gas-Phase Kinetics and Gas-Particle Partitioning Theory, Environ. Sci. Technol., 35, 1394–1405, 2001.

Kanakidou, M., Tsigaridis, K., Dentener, F. J., and Crutzen, P. J., Human-activity-enhanced formation of organic aerosols by biogenic hydrocarbon oxidation, J. Geophys. Res., 105, 9243–9254, 2000.

Kanakidou, M. , Seinfeld, J. H., Pandis, S. N., Barnes, I., Dentener, F. J., Facchini, M. C., Van Dingenen, R., Ervens, B., Nenes, A., Nielsen, C. J., Swietlicki, E., Putaud, J. P., Balkanski, Y., Fuzzi, S., Horth, J., Moortgat, G. K., Winterhalter, R., Myhre, C. E. L., Tsigaridis, K., Vignati, E., Stephanou, E. G., and Wilson, J., Organic aerosol and global climate modelling: a review, J. Atmospheric Chemistry and Physics, 5, 1053–1123, 2005.

Kavouras, I. G., Mihalopoulos, N., and Stephanou, E. G., Formation of atmospheric particles from organic acids produced by forests, Nature, 395, 683–686, 1998.

Kesselmeier, J., Bode, K., Hofmann, U., Müller, H., Schäfer, L., Wolf, A., Ciccioli, P., Brancaleoni, E., Cecinato, A., Frattoni, M., Foster, P., Ferrari, C., Jacob, V., Fugit, J.L., Dutaur, L., Simon, V., and Torres, L., Emission of short chained organic acids, aldehydes, and monoterpenes, from Quercus ilex L. and Pinus pinea L. in relation to physiological activities, carbon budget and emission algorithms, Atmos. Environ., 31, Suppl. I, 119–134, 1997.

Knauth, P. and Sabbah, R., Energetics of intra- and intermolecular bonds in ω-alkanediols.II. Thermochemical study of 1,2-Ethanediol, 1,3-Propanediol, 1,4-Butanediol and 1,5-Pentanediol at 298.15 K, Struc. Chem., 1, 43–46, 1990a.

Knauth, P. and Sabbah, R., Energetics of intra- and intermolecular bonds in ω-alkanediols.III. Thermochemical study of 1,6-hexanediol, 1,7-heptanediol, 1,8-octanediol, 1,9-nonanediol, and 1,10-decanediol at 298,15 K, Canad. J. Chem., 68, 731–734,1990b.

Knauth, P. and Sabbah, R., Energetics of inter- and intramolecular bonds in Alkanediols.IV. The Thermochemical study of 1,2-Alkanediols at 298,15 K, Thermochimica Acta, 164, 145–152, 1990c.

Knight, G., Ravishankara, A. R., and Burkholder, J. B., UV absorption cross sections of HO_2NO_2 between 343 and 273 K, Phys. Chem. Chem. Phys., 4, 1432–1437, 2002.

Koch, S., Winterhalter, R., Uherek, E., Kolloff, A., Neeb, P., Moortgat, G. K., Formation of new particles in the gas-phase ozonolysis of monoterpenes, Atmos. Environ., 34, 4031–4042, 2000.

König, G., Brunda, M., Puxbaum, H., Hewitt, C. N., Duckham, S. C., and Rudolph, J., Relative contribution of oxygenated hydrocarbons to the total biogenic VOC emissions of selected mid-European agricultural and natural plant species, Atmos. Environ., 29, 861–874, 1995.

Kubátovátova, A., Vermeylen, R., Claeys, M., Cafmeyer, J., Maenhaut, W., Roberts, G., and Artaxo, P., Carbonaceous aerosol characterization in the Amazonian basin, Brazil: novel dicarboxylic acids and related compounds, Atmos. Environ., 34, 5037–5051, 2000.

Kuckelmann, U., Warscheid, B., and Hoffmann, T., On-line Characterization of Organic Aerosols Formed from Biogenic Precursors Using Atmospheric Pressure Chemical Ionization Mass Spectroscopy, Anal. Chem., 72, 1905–1912, 2000.

Kwok, E. S. C. and Atkinson, R., Estimation of hydroxyl radical reaction rate constants for gas-phase organic compounds using a structure-reactivity relationship: An update, Atmos. Environ., 29, 1685–1695, 1995.

Lack, D. A., Tie, X. X., Bofinger, N. D., Wiegand, A. N., and Madronich, S., Seasonal variability of secondary organic aerosol: A global modeling study, J. Geophys. Res., 109, D03203, doi:10.1029/2003JD003418.

Larsen, B. R., Di Bella, D., Glasius, M., Winterhalter, R., Jensen, N. R., and Hjorth, J., Gas-phase OH oxidation of monoterpenes: Gaseous and particulate products, J. Atmos. Chem., 38, 231–276, 2001.

Lelieveld, J. and Crutzen P. J., The Role of Clouds in Tropospheric Photochemistry, Jour. Atmos. Chem., 229–267, 1991.

Li, P., Ma, P. S., Yi, S. Z, Zhao, Z. G., and Cong, L. Z., A new Corresponding-States Group-Contribution method (CSGC) for estimating vapor pressures of pure compounds, Fluid Phase Equi., 101, 101–119, 1994.

Liao, H., Seinfeld, J. H., Adams, P. J., and Mickley, L. J., Global radiative forcing of coupled tropospheric ozone and aerosols in a unified general circulation model, J. Geophys. Res., 109, D16207, doi:10.1029/2003JD004456.

Librando, V., Tomaselli, G., and Tringali, G., OH-initiated oxidation of monoterpenes: Reaction of α-pinene, Annali di Chimica, 93, 407–413, 2003.

Lide, D. R., CRC Handbook of Chemistry and Physics, 82th edition, CRC Press, Boce Raton, Fla, 2001.

Liggio, J., Li, S-M., and McLaren, R., Heteorogeneous reactions of glyoxal on particulate matter: Identification of acetals and sulfate esters, Environ. Sci. Technol., 39, 1532–1542, 2005.

Lightfoot, P. D., Cox, R. A., Crowley, J. N., Destriau M., Hayman, G. D., Jenkin, M. E., Moortgat G. K., and Zabel F., Organic peroxy radicals: Kinetics, spectroscopy and tropospheric chemistry, Atmos. Environ., 26A, 1805–1961, 1992.

Liousse, C., Penner, J. E., Chuang, C., Walton, J. J., and Eddleman, H., A global three-dimensional study of carbonaceous aerosols, J. Geophys. Res., 101, 19411–19432, 1996.

Logan, J. A., Prather, M. J., Wolsy, S. C., and McElroy, M. B., Tropospheric chemistry: a global perspective, J. Geophys. Res. C:Oceans Atmos., 86, 7210–7254, 1981.

Madronich, S. and Calvert, J., The NCAR master mechanism of the gas phase chemistry-Version 2.0, Rep. NCAR/TN-333+STR, Natl. Cent. For Atmos. Res., Boulder, Colo., 1989.

Madronich, S. and Calvert, J. G., Permutation reactions of organic peroxy radicals in the troposphere, J. Geophys. Res., 95, 5697–5715, 1990.

Madronich, S. and Flocke, S., The role of solar radiation in atmospheric chemistry, Handbook of Environmental Chemistry, edited by Boule, P., Springer-Verlag, Heidelberg, 1998.

Makar, P. A., The estimation of organic gas vapour pressure, Atmos. Environ., 35, 961–974, 2001.

Marcolli, C., Luo, B., and Peter, T., Mixing of the Organic Aerosol Fractions, Liquids as the Thermodynamically Stable Phases, J. Phys. Chem. A, 108, 2216–2224, 2004.

Marrero, J. and Gani R., Group-contribution based estimation of pure component properties, Fluid Phase Equilibria, 183-184, 183–208, 2001.

Matsunaga, S. N., Wiedinmyer, C., Guenther, A. B., Orlando, J. J., Karl, T., Toohey, D. W., Greenberg, J. P., and Kajii, Y., Atmos. Chem. Phys. Discuss., 5, 11143–11156, 2005.

Molina, L. T. and Molina, M. J., Absolute absorption cross sections of ozone in the 185 to 350 nm wavelength range, J. Geophys. Res., 91, 14501–14508, 1986.

Morris, E. R. and Myers, T. C., User's Guide for the Urban Airshed Model. Volume I: User's Guide for the UAM (CB-IV), EPA-450/4-90-007A, U.S. Environmental Protection Agency, 1990.

Müller, J.-F. and Brasseur, G., IMAGES: A three-dimensional chemical transport model of the global troposphere, J. Geophys. Res., 100, 16445–16490, 1995.

Müller, J.-F. and Stavrakou, T., Inversion of CO and NO_x emissions using the adjoint of the IMAGES model, Atmospheric Chemistry and Physics, 5, 1157–1186, 2005.

Myrdal, P. B. and Yalkowsky, S. H, Estimating pure component vapor pressures of complex organic molecules, Ind. and Eng. Chem. Res., 36, 2494–2499, 1997.

Nielsen, T., Platz, J., Granby, K., Hansen, A. B., Skov, H., Egelov, A. H., Particulate organic nitrates: Sampling and night/day variation, Atmos. Environ., 32, 14/15, 2601–2608, 1998.

NIST Chemistry WebBook, NIST Standard Reference Database Number 69, National Institute of Standards and Technology, Gaithersburg MD, March 2003, http://webbook.nist.gov.

NOAA, U.S. Standard Atmosphere, National Oceanic and Atmospheric Administration, National Aeronautics and Space Administration, United States Air Force, Washington, D.C., 1976.

Nozière, B. and Barnes, I., Evidence for formation of a PAN analogue of pinonic structure and investigation of its thermal stability, J. Geophys. Res., 103, 25587–25597, 1998.

Nozière, B., Barnes, I., and Becker, K. H., Product study and mechanisms of the reactions of α-pinene and of pinonaldehyde with OH radicals, J. Geophys. Res., 104, 23645–23656, 1999a.

Nozière, B., Spittler, M., Ruppert, L., Pons, M., and Wirtz, K., Kinetics of the reactions of pinonaldehyde with OH radicals and with Cl atoms, Int. J. Chem. Kinet., 31, 291–301, 1999b.

Nozière, B. and Riemer, D. D., The chemical processing of gas-phase carbonyl compounds by sulfuric acid aerosols: 2,4-pentadione, Atmos. Environ., 37, 841–851, 2003.

Odum, J. R., Hoffmann, T., Bowman, F., Collins, D., Flagan, R. C., and Seinfeld, J. H., Gas/particle partitioning and secondary organic aerosol yields, Environ. Sci. Technol., 30, 2580–2585, 1996.

Odum, J. R., Jungkamp, T. P., Griffin, R. J., Forstner, H. J. L., Flagan, R. C., and Seinfeld, J. H., Aromatics, reformulated gasoline, and atmospheric organic aerosol formation, Environ. Sci. Technol., 31, 1890–1897, 1997.

Olsen, E. and Nielsen, F., Predicting Vapour Pressures of Organic Compounds from Their Chemical Structure for Classification According to the VOC-Directive and Risk Assessment in General, Molecules, 6, 370–389,2001.

Orlando, J. J., Nozière, B., Tyndall, G. S., Orzechowska, G. E., Paulson, S. E., and Rudich, Y., Product studies of the OH- and ozone-initiated oxidation of some monoterpenes, J. Geophys. Res., 105, 11561–11572, 2000.

Orlando, J. J. and Tyndall, G. S., Gas phase UV absorption spectra for peracetic acid, and for acetic acid monomers and dimers (248 K, 298 K), J. Photochem. and Photobiol., 157, 2–3, 161–166, 2003.

Pandis, S. N., Paulson, S. E., Seinfeld, J H., and Flagan, R. C., Aerosol formation in the photooxidation of isoprene and β-pinene, Atmos. Environ., 25, 997–1008, 1991.

Pandis, S. N., Harley, R. A., Cass, G. R., and Seinfeld, J. H., Secondary organic aerosol formation and transport, Atmos. Environ., 26A, 2269–2282, 1992.

Poling, B. E., Prausnitz, J. M., and O'Connell, J. P., The properties of gases and liquids, McGraw-Hill, New York, USA, 2001.

Pöschl, U., von Kuhlmann, R., Poisson, N., and Crutzen, P. J., Development and Intercomparison of Condensed Isoprene Oxidation Mechanisms for Global Atmospheric Modeling, J. Atmos. Chem., 37, 29–52, 2000.

Pun, B. K., Seigneur, C., Grosjean, D., and Seinfeld, J. H., Secondary organic aerosol: II. Thermodynamic model for gas/particle partitioning of molecular constituents, J. Geophys. Res., 107, D17, 4333, doi:10.1029/2001JD000542, 2002.

Pun, B. K., Wu, S.-Y., Seigneur C., Seinfeld, J. H., Griffin, R. J., and Pandis, S. N., Uncertainties in Modeling Secondary Organic Aerosols: Three-Dimensional Modeling Studies in Nashville/Western Tennessee, Environ. Sci. Technol., 37, 3647–3661, 2003.

Pankow, J. F., An absorption model of gas/particle partitioning of organic compounds in the atmosphere, Atmos. Environ., 28, 185–188, 1994a.

Pankow, J. F., An absorption model of gas/aerosol partitioning involved in the formation of secondary organic aerosol, Atmos. Environ., 28, 189–193, 1994b.

Paulson, S. E. and Seinfeld, J. H., Development and evaluation of a photooxidation mechanism for isoprene, J. Geophys. Res., 97, 20703–20715, 1992.

Paulson, S. E., Chung, M., Sen, A. D., Orzechowska, G., Measurement of OH radical formation from the reaction of ozone with several biogenic alkenes, J. Geophys. Res., 103, 25533–25539, 1998.

Peeters, J., Vereecken, L., and Fantechi, G., the detailed mechanism of the OH-initiated atmospheric oxidation of α-pinene: a theoretical study, Phys. Chem. Chem. Phys., 3, 5489–5504, 2001.

Peeters, J. and Vereecken, L., personal communication, 2005.

Prausnitz, J. M., Molecular Thermodynamics of Fluid-Phase Equilibria, Prentice-Hall, Englewoods Cliffs, 1969.

Raber, W. H. and Moortgat, G. K., Progress and problems in atmospheric chemistry, edited by Barker, J. R., Word Scientific Publ. Co., Singapore, 318–373, 1995.

Raes, F., Van Dingenen, R., Vignati, E., Wilson, J., Putaud, J.-P., Seinfeld, J. H., and Adams, P., Formation and cycling of aerosols in the global troposphere, Atmos. Environ., 34, 4215–4240, 2000.

Reissel, A., Harry, C., Aschmann, S. M., Atkinson, R., and Arey, J., Formation of acetone from the OH radical- and O_3-initiated reactions of a series of monoterpenes, J. Geophys. Res., 104, 13869–13879, 1999.

Rickard, A. R., Johnson, D., McGill, C. D., and Marston, G., OH yields in the gas-phase reactions of ozone with alkenes, J. Phys. Chem. A, 103, 7656–7664, 1999.

Rinne, J., Hakola, H., Laurila, T., and Rannik, Ü., Canopy scale monoterpene emissions of Pinus sylvestris dominated forests, Atmos. Environ., 34, 1099–1107, 2000.

Rosenorn, T., Monster, J., Svenningsson, B., and Bilde, M., Vapor pressures of C3-C9 Dicarboxylic Acid Aerosols, EGS - AGU - EUG Joint Assembly, Nice, France, April 2003.

Rowley, D. M., Lesclaux, R., Lightfoot, P. D., Hughes, K., Hurley, M. D., Rudy, S., and Wallington, T. J., Kinetic and mechanistic studies of the reaction of neopentylperoxy radicals with HO_2, J. Phys. Chem., 96, 7043–7048, 1992.

Ruppert, L., Becker, K. H., Nozière, B., and Spittler, M., Transport and Chemical Transformation in the Troposphere, Borrell, P. M., Borrell, P.,(Eds.), WIT Press, Southampton, UK, Vol. 1,63–68, Proceedings of EUROTRAC Symposium'98, 1999.

Sander, S. P., Friedl, R. R., DeMore, W. B., Golden, D. M., Kurylo, M. J., Hampson, R. F., Huie, R. E., Moortgat, G. K., Ravishankara, A. R., Kolb, C. E., and Molina, M. J., Chemical kinetics and photochemical data for use in stratospheric modeling Supplement to Evaluation 12: Update of Key Reactions, JPL Publ., 00–3, 2000.

Sanderson, M. G., Jones, C. D., Collins, W. J., Johnson, C. E., Derwent, R.G., Effect of climate change on isoprene emissions and surface ozone levels, Geophys. Res. Lett., 30, doi:10.1029/2003GL017642., 2003.

Saunders, S. M., Jenkin, M. E., Derwent, R. G., and Pilling, M. J., Protocol for the development of the Master Chemical Mechanism MCM v3 (Part A): Tropospheric degradation of non-aromatic volatile organic compounds, Atmos. Chem. Phys., 3, 161–180, 2003.

Schmidt, H., Derognat, C, Vautard, R., and Beekmann, M., A comparison of simulated and observed ozone mixing ratios for the summer of 1998 in western Europe, Atmos. Environ., 35, 6277–6297, 2001.

Schwarzenbach, R. P., Gschwend, P. M., Imboden, D. M., Environmental Organic Chemistry, Wiley-Interscience, New York, 1993.

Seinfeld, J. and Pandis, S. N., Atmospheric Chemistry and Physics, John Wiley and Sons, Inc. New York, 1998.

Seinfeld, J. H., Pankow, J. F., Organic atmospheric particulate material, Annu. Rev. Phys. Chem., 54, 121–140, 2003.

Singleton, D. L., Paraskevopoulos, G., and Irwin, R. S., UV Absorption Cross-Sections of the Monomer and Dimer of Formic Acid (302 K), J. Photochem., 37, 209–216, 1987.

Stroud, C. A., Makar, P. A., Michelangeli, D. V., Mozurkewich, M., Hastie, D. R., Barbu, A., and Humble, J., Simulating Organic Aerosol Formation during the Photooxidation of Toluene/NOx Mixtures: Comparing the Equilibrium and Kinetic Assumption, Environ. Sci. Technol., 38, 1471–1479, 2004.

Tadic, J., Juranic, I., and Moortgat, G. K., Pressure dependence of the photooxidation of selected carbonyl compounds in air: n-butanal and n-pentanal, J. Photoch. A, 143, 169–179, 2001a.

Tadic, J., Juranic, I., and Moortgat, G. K., Photooxidation of *n*-hexanal, Molecules, 6, 287–299, 2001b.

Tadic, J. M., Juranic, I. O., and Moortgat, G. K., Photooxidation of *n*-heptanal in air: Norrish type I and II processes and quantum yield total pressure dependency, J. Chem. Soc. Perkin Trans., 2, 135–140, 2002.

Talukdar, R. K., Burkholder, J. B., Hunter, M., Gilles, M. K., Roberts, J. M., and Ravishankara, A. R., Atmospheric fate of several alkyl nitrates, J. Chem. Soc. Faraday Trans., 93, 2797–2805, 1997.

Tolocka, M. P., Jang, M., Ginter, J. M., Cox, F. J., Kamens, R. M., and Johnston, M. V., Formation of Oligomers in Secondary Organic Aerosol, Environ. Sci. Technol., 38, 1428–1434, 2004.

Tomas, A. and Lesclaux, R., Self-reaction kinetics of the $(CH_3)_2CHC(O)O_2$ and $(CH_3)_3CC(O)O_2$ acylperoxy radicals between 275 and 363 K, Chem. Phys. Lett., 319, 521–528, 2000.

Tobias, H. J. and Ziemann, P. J., Thermal Desorption Mass Spectrometric Analysis of Organic Aerosol Formed from Reactions of 1-Tetradecene and O_3 in the Presence of Alcohols and Carboxylic Acids, Environ. Sci. Technol., 34, 2105–2115, 2000.

Tobias, H. J., Docherty, K. S., Beving, D. E., and Ziemann, P. J., Effect of Relative Humidity on the Chemical Composition of Secondary Organic Aerosol Formed from Reactions of 1-Tetradecene and O_3, Environ. Sci. Technol., 34,2116–2125, 2000.

Tsigaridis, K. and Kanakidou, M., Global modelling of secondary organic aerosol in the troposphere: a sensitivity analysis, Atmos. Chem. Phys., 3, 1849–1869, 2003.

Tu, C. H., Group-contribution method for the estimation of vapor pressures, Fluid Phase Equilibria, 99, 105–120, 1994.

Tyndall, G. S., Cox, R. A., Granier, C., Lesclaux, R., Moortgat, G. K., Pilling, M. J., Ravishankara, A. R., and Wallington, T. J., Atmospheric chemistry of small organic peroxy radicals, J. Geophys. Res., 106, 12157–12182, 2001.

Vanhees, I., Van Den Bergh, V., Shildermans, R., De Boer, R., Compernolle, F., and Vinckier, C., Determination of the oxidation products of the reaction between α-pinene and OH-radicals by high-performance liquid chromatography, J. Chromatogr. A, 915, 75–83, 2001.

Vereecken, L. and Peeters, J., Non-traditional (per)oxy ring-closure paths in the atmospheric oxidation of isoprene and monoterpenes, J. Phys. Chem. A., 108,5197–5204,2004.

Villenave, E. and Lesclaux, R., Kinetics and atmospheric implications of peroxy radical cross reactions involving the $CH_3C(O)O_2$ radical, J. Geophys. Res., 103, 25273–25285, 1998.

von Kuhlmann, R., Lawrence, M. G., Pöschl, U., and Crutzen, P. J., Sensitivities in global scale of modeling of isoprene, Atmos. Chem. Phys., 4, 1–17, 2004.

Wallens, S., Modélisation des émissions de composés organiques volatils par la végétation, Ph.D. thesis, Université Libre de Bruxelles, 2004.

Wang, Y., Jacob, D. J., and Logan, J., A., Global simulation of tropospheric O_3-NO_x-hydrocarbon chemistry. 3. Origin of tropospheric ozone and effects of nonmethane hydrocarbons, J. Geophys. Res., 103, 10757–10767, 1998.

Wang, K. Y. and Shallcross, D. E., Modelling terrestrial biogenic isoprene fluxes and their potential impact on global chemical species using a coupled LSM-CTM model, Atmos. Environ., 34, 2909–2925, 2000.

Warneck, P., Photodissociation of acetone in the troposphere: an algorithm for the quantum yield, Atmos. Environ., 35, 5773-5777, 2001.

Went, F. W., Blue hazes in the atmosphere, Nature, 187, 641–643, 1960.

Wiedinmyer, C., Guenther, A., Harley, P., Hewitt, C. N., Geron, C., Artaxo, P., Steinbrecher, R., and Rasmussen., R., Global organic emissions from vegetation, in Emissions of Atmospheric Trace Compounds, edited by Granier, C., Artaxo, P., and Reeves, C. E., Kluwer Academic Publishers, Dordrecht, The Netherlands, 2004.

Winterhalter, R., Neeb, P., Grossmann, D., Kolloff, A., Horie, O., and Moortgat, G. K., Products and mechanism of the gas phase reaction of ozone with β-pinene, J. Atmos. Chem., 35, 165–197, 2000.

Wisthaler A., Jensen, N. R., Winterhalter, R., Lindinger, W., and Hjorth, J., Measurements of acetone and other gas phase product yields from the OH-initiated oxidation of terpenes by proton-transfer reaction mass spectrometry (PTR-MS), Atmos. Environ., 35, 6181–6191, 2001.

Whitehouse, L. E., Tomlin, A. S., and Pilling, M. J., Systematic reduction of complex tropospheric chemical mechanisms, Part I: sensitivity and time-scale analyses, Atmos. Chem. Phys., 4, 2025–2056, 2004a.

Whitehouse, L. E., Tomlin, A. S., and Pilling, M. J., Systematic reduction of complex tropospheric chemical mechanisms, Part II: Lumping using a time-scale based approach, Atmos. Chem. Phys. , 4, 2057–2081, 2004b.

Whitten, C. Z., Hogo, H., and Killus, J. P., The carbon-bond mechanism: a condensed kinetic mechanism for photochemical smog, Envir. Sci. Technol., 14, 960–700, 1980.

World Health Organisation, Update and revision of the air quality guidelines for Europe, Report EUR/ICP/EHAZ9405/PB01, Meeting of the Working Group on "Classical" Air Pollutants, 11-14 October, Bilthoven, The Netherlands, 1994.

Yu, J., Cocker III, D. R., Griffin, R. J., Flagan, R. C., and Seinfeld, J. H., Gas-Phase Ozone Oxidation of Monoterpenes: Gaseous and Particulate Products, J. Atmos. Chem. 34, 207–258, 1999a.

Yu, J., Griffin, R. J., Cocker III, D. R., Flagan, R. C., Seinfeld, J. H., and Blanchard, P., Observations of gaseous and particulate products of monoterpenes oxidation in forest atmospheres, Geophys. Res. Lett., 26, 1145–1148, 1999b.